Development and application of lipidomics workflows:

from untargeted towards targeted enantioselective lipidomics

Dissertation

der Mathematisch-Naturwissenschaftlichen Fakultät

der Eberhard Karls Universität Tübingen

zur Erlangung des Grades eines

Doktors der Naturwissenschaften

(Dr. rer. nat.)

vorgelegt von

Carlos Calderón Castro

aus

Cartago, Costa Rica

Tübingen

2019

The research described in this thesis was conducted between October 1st 2015 and September 1st 2019 at the Institute of Pharmaceutical Sciences, Division Pharmaceutical (Bio)Analysis, Eberhard Karls Universität Tübingen under the supervision of Prof. Dr. Michael Lämmerhofer.

Gedruckt mit Genehmigung der Mathematisch-Naturwissenschaftlichen Fakultät der Eberhard Karls Universität Tübingen.

Tag der mündlichen Qualifikation:

10.12.2019

Dekan:

Prof. Dr. Wolfgang Rosenstiel

1. Berichterstatter:

Prof. Dr. Michael Lämmerhofer

2. Berichterstatter:

Prof. Dr. Stefan Laufer

Dedicated to my sisters Laura and Leidania, and to my nephews Jaden and Aaron.

ACKNOWLEDGEMENTS

First, I want to thank Prof. Dr. Michael Lämmerhofer for giving me the opportunity to do my thesis work in his laboratory and for his support in many different aspects of this experience in Germany. With his hard work, his good and novel ideas and his optimism he has inspired me to achieve the goals of this thesis work.

Thanks to Prof. Dr. Stefan Laufer, for agreeing to be my second supervisor in this doctoral thesis.

Thanks to Prof. Dr. Renato Murillo for being the person who encouraged me into the idea of doing a PhD and who pushed me towards this unforgettable and pleasant experience.

Thanks to Prof. Dr. Irmgard Merfort for welcoming me to Freiburg some years ago and for her motivation and help before and during this doctorate.

Thanks to Dr. Jeannie Horak and Dr. Stefan Neubauer, for supporting me with their helpful experience in analytical chemistry and for the interesting conversations we kept many times.

Thanks to Bernhard Drotleff and Dr. Jörg Schlotterbeck for introducing me into the world of mass spectrometry. Thanks for their valuable troubleshooting skills every time there were issues with the QTOF instrument. Special thanks to Bernhard for always being available to help in such a kind way despite having always a lot of work to do.

Thanks to my current colleagues Stefanie Bäurer, Malgorzata Cebo, Ece Aydin, Ryan Karongo, Christian Geibel, Marc Wolter, Kristina Dittrich, Simon Jaag, Peng Li and Feiyang Li, and to my previous colleagues Siyao Liu, Corinna Sanwald, Markus Höldrich, Ulrich Woiwode, Adrian Sievers-Engler and Aleksandra Zimmermann. To each of them my sincere thanks for all the experiences we have shared in the laboratory, conferences and social activities.

Thanks to the secretaries of our lab, Eveline Wachendorfer and Ingrid Straub, for their kind attention every time I was dealing with bureaucratic procedures in the lab and in the city.

I would like to thank all my friends and my family in Costa Rica for their unconditional support.

Thanks also to all my friends in Tübingen, but especially to Anu, Iti and Ash, who are without any doubt part of this achievement.

Thanks to the DAAD for the funding and organization of my stay in Tübingen, I really appreciated it. Thanks also to the University of Costa Rica for its partial funding of my PhD in Tübingen.

Thanks to Tübingen, such a beautiful city that will be always in my memories.

TABLE OF CONTENTS

ACKNOWLEDGEMENTS v

TABLE OF CONTENTS vii

ABBREVIATIONS xi

SUMMARY xv

ZUSAMMENFASSUNG xvii

LIST OF PUBLICATIONS xix

AUTHOR CONTRIBUTIONS xx

LIST OF POSTER PRESENTATIONS xxv

LIST OF ORAL PRESENTATIONS xxvi

INTRODUCTION 1

1 Lipids and lipid classes 1

1.1 Lipids 1

1.2 Biological importance of lipids 2

1.3 Classification of lipids 2

1.4 Description of studied lipid classes 3

2 Liquid chromatography of lipids 7

2.1 Reversed phase liquid chromatography 7

2.2 Normal phase liquid chromatography 8

2.3 Hydrophilic interaction liquid chromatography 8

2.4 Supercritical fluid chromatography 9

2.5 Comparison of LC systems 9

3 Mass spectrometry for lipids 12

3.1 MS instrumentation 12

3.2 MS experiments 16

3.3 Fragmentation pattern of studied lipid classes 22

4 Lipidomics 31
4.1 Sample preparation 31
4.2 Extraction 32
4.3 Sample analysis 34
4.4 Processing of data 36
5 Chiral lipidomics 39
5.1 Use of chiral chromatography 40
5.2 Case of short chain hydroxy fatty acids 40
AIM OF THE WORK 41
RESULTS AND DISCUSSION 42
6 Publication I. Comparison of lipid extraction protocols 42
6.1 Title 42
6.2 Abstract 43
6.3 Introduction 43
6.4 Materials and Methods 44
6.5 Results and discussion 48
6.6 Concluding remarks 56
6.7 Conflict of interest statement 57
6.8 Acknowledgements 57
6.9 Supplemental 58
7 Publication II. Lipid profiling of keratinocytes 65
7.1 Title 65
7.2 Abstract 66
7.3 Statement of significance of the study 66
7.4 Introduction 67
7.5 Materials and Methods 68

7.6 Results and discussion 71
7.7 Concluding remarks 78
7.8 Conflict of interest statement 78
7.9 Acknowledgements 79
7.10 Supplemental 79
8 Publication III. Chiral separation of 2-hydroxyglutaric acid 93
8.1 Title 93
8.2 Abstract 94
8.3 Introduction 94
8.4 Experimental 96
8.5 Results and discussion 97
8.6 Conclusions 106
8.7 Acknowledgements 107
8.8 Supplementary material 108
9 Publication IV. Chiral separation of short chain aliphatic hydroxycarboxylic acids 115
9.1 Title 115
9.2 Abstract 116
9.3 Introduction 116
9.4 Experimental 118
9.5 Results and discussion 120
9.6 Conclusions 127
9.7 Acknowledgements 127
9.8 Supplementary material 128
10 Publication V. Chiral separation of disease biomarkers 137
10.1 Title 137
10.2 Abstract 138

10.3 Introduction 138
10.4 Experimental 140
10.5 Results and discussion 141
10.6 Concluding remarks 146
10.7 Conflict of interest statement 147
10.8 Acknowledgements 147
10.9 Supplementary material 148
CONCLUDING REMARKS 157
REFERENCES 159
LIST OF FIGURES 183
LIST OF SUPPLEMENTARY FIGURES 187
LIST OF TABLES 190
LIST OF SUPPLEMENTARY TABLES 190
CURRICULUM VITAE 193

ABBREVIATIONS

AC	acylcarnitines
ACN	acetonitrile
BHT	butylated hydroxytoluene
BMP	bismonoacylglycerophosphate
CAD	charged aerosol detector
CE	cholesteryl ester
Cer	ceramide
Cer-NDS	ceramide non-hydroxyfatty acid-dihydrosphingosine
Cer-NS	ceramide non-hydroxyfatty acid-sphingosine
CID	collision-induced dissociation
CL	cardiolipin
CMA	citramalic acid
CSP	chiral stationary phase
DDA	data-dependent acquisition
DG	diacylglycerol
DGDG	digalactosyldiacylglycerol
DHA	4,7,10,13,16,19-docosahexaenoic acid
DIA	data-independent acquisition
DNA	deoxyribonucleic acid
EIC	extracted ion chromatogram
EM	electron multiplier
EP	extraction protocol
EPA	5,8,11,14,17-eicosapentaenoic acid
ESI	electrospray ionization
EtherPC	ether-linked phosphatidylcholine
EtherPE	ether-linked phosphatidylethanolamine
FA	fatty acyls, fatty acids
FTICR	Fourier-transform ion cyclotron resonance
GalCer	galactosyl ceramide
GL	glycerolipids
GluCer	glucosyl ceramide
GP	glycerophospholipids
2-HAA	2-hydroxyadipic acid
2-HBA	2-hydroxybutyric acid
2-HCA	2-hydroxycaproic acid
2-HDA	2-hydroxydecanoic acid
2-HDCA	2-hydroxydicarboxylic acid
HexCer	hexosylceramide
HexCer-NDS	hexosylceramide non-hydroxyfatty acid-dihydrosphingosine
HexCer-NS	hexosylceramide non-hydroxyfatty acid-sphingosine
2-HGA	2-hydroxyglutaric acid
2-HICA	2-hydroxyisocaproic
HILIC	hydrophilic interaction liquid chromatography

2-H-2-MBA	2-hydroxy-2-methylbutyric acid
2-H-3-MBA	2-hydroxy-3-methylbutyric acid
2-HMCA	2-hydroxymonocarboxylic acid
2-H-3-MPA	2-hydroxy-3-methylpentanoic acid
2-IMA	2-isopropylmalic acid
iMLF	intermediate molecular lipid species-selective fragment
IPA	isopropanol
IUPAC	International Union of Pure and Applied Chemistry
LA	lactic acid
LacCer	lactosyl ceramides
LC	liquid chromatography
LCF	lipid class-selective fragment
Lipid MAPS	Lipid Metabolites and Pathways Strategy
LMSD	Lipid MAPS Structure Database
LPA	lysophosphatidic acid
LPC	lysophophatidylcholine
LPE	lysophosphatidylethanolamine
LPG	lysophosphatidylglycerol
LPI	lysophosphatidylinositol
LPS	lysophosphatidylserine
LTQ	linear trap quadrupole
MA	malic acid
MDMS-SL	multidimensional MS-based shotgun lipidomics
MG	monoacylglycerol
MGDG	monogalactosyldiacylglycerol
MLF	molecular lipid species-selective fragment
MP	mobile phase
MS	mass spectrometry
MTBE	methyl tert-butyl ether
NEFA	non-esterified fatty acids
NLS	neutral loss scan
NMR	nuclear magnetic resonance
NPLC	normal phase liquid chromatography
OxFA	oxidized fatty acid
OxPC	oxidized phosphatidylcholine
OxPE	oxidized phosphatidylethanolamine
OxPG	oxidized phosphatidylglycerol
OxPI	oxidized phosphatidylinositol
OxPS	oxidized phosphatidylserine
PA	phosphatidic acid
PC	phophatidylcholine
PE	phosphatidylethanolamine
PG	phosphatidylglycerol
PI	phosphatidylinositol
PIA	product ion analysis

PIS	precursor ion scan
PK	polyketides
PR	prenol lipids
PRM	parallel reaction monitoring
PS	phosphatidylserine
PUFA	polyunsaturated fatty acids
QQQ	triple quadrupole
QTOF	quadrupole time of flight
RPLC	reversed phase liquid chromatography
S1P	Sphingosine-1-phosphate
SCHFA	short chain hydroxy fatty acids
SF	supercritical fluid
SFC	supercritical fluid chromatography
SIM	selected ion monitoring
SL	saccharolipids
SM	sphingomyelin
SP	sphingolipids, stationary phase
SQDG	sulfoquinovosyl diacylglycerol
SRM	selected reaction monitoring
ST	sterol lipids
SWATH	sequential window acquisition of all theoretical fragment ion mass spectra
TG	triacylglycerol
TIC	total ion current
TOF	time of flight
UHPLC	ultra-high performance liquid chromatography
WAX	weak anion-exchange

SUMMARY

Structure and function of lipids have been subject of intense studies for more than one century. However, during this time, the meaning of lipid has changed considerably, and nowadays lipids are defined as “small molecules derived from carbanion-based condensation of thioesters and/or by carbocation-based condensations of isoprene units”. The development of modern analytical techniques in the last decades led researchers to undertake the comprehensive analysis of lipids in biological systems, which has been defined as lipidomics.

Mass spectrometry (MS) has been the most important analytical tool for the exponential growth that lipidomics has achieved in the last twenty years. Two main approaches have been employed in MS: shotgun lipidomics (in which lipid extract is directly infused into the mass spectrometer without lipid separation) and liquid chromatography hyphenated to MS (LC-MS) based lipidomics (in which the lipid extract is first separated chromatographically before MS detection).

In this thesis, LC-MS based lipidomics studies were developed in order to determine proper conditions for analysis of as many lipid species as possible and with the most confident level of description.

In a first study, the performance of four extraction protocols was compared for the analysis of lipids in Hela cells. The comparison was based on performance parameters such as extraction recoveries of endogenous lipids and internal standards, precision, and complexity of the protocols. For the comparison two traditionally employed protocols, based on biphasic systems (chloroform -methanol (MeOH)-H_2O, known as Bligh & Dyer, and methyl *tert*-butyl ether (MTBE)-MeOH-H_2O, known as Matyash), and two novel protocols based on monophasic systems of isopropanol (IPA)-H_2O (IPA:H_2O 75:25 v/v and IPA:H_2O 90:10 v/v) were selected. The analysis of lipids after extraction was performed by reversed-phase ultra-high performance liquid chromatography (UHPLC) coupled to quadrupole-time of flight mass spectrometry (QTOF) via electrospray ionization (ESI) using MS/MS by data-independent acquisition in positive and negative polarity mode with sequential window acquisition of all theoretical fragment ion mass spectra (SWATH). Freely available software (MS-DIAL) was employed for the processing of the data. The selected performance parameters showed that extraction with IPA:H_2O 90:10 v/v performs similar to the Matyash protocol and better than Bligh & Dyer, with a protocol that is simpler and that can employ plastic labware instead of

glass. The use of IPA:H_2O 90:10 v/v simplifies the protocol for analysis of lipids in reversed phase LC-MS lipidomics studies.

In a second study, the optimized protocol with IPA:H_2O 90:10 v/v was employed to study the changes in the lipid profile of keratinocytes after treatment with the natural compound betulin, which has proven wound healing properties. Data from untargeted UHPLC-ESI-QTOF-MS/MS measurements of treated and control samples were subjected to a novel targeted data processing strategy for identification of lipids. This targeted data processing is based on the selection and analysis of a specific set of precursor and product ions for each lipid class and the corresponding comparison of their elution profiles not only for the lipid species but also for the whole lipid class in independent runs measured with opposite polarities. As a result of this analysis 440 out of 611 identified lipid species showed to be significantly regulated upon betulin treatment. Regulation can be described as a decrease in the concentration of cholesteryl esters and triacylglycerides and increase of glycerophospholipids, sphingolipids and diacylglycerides after the treatment with betulin.

Finally, a third study was focused on a particular group of fatty acids, which are called short chain hydroxy fatty acids (SCHFA). The presence of the hydroxyl group along the alkyl chain of SCHFA made them chiral. Some enantiomers of these SCHFA are linked to particular diseases and are potential biomarkers for diagnosis. In this study SCHFA were studied for their chiral separation by HPLC on a set of quinine- and quinidine-derived chiral stationary phases. MS compatible conditions for chiral separation of all studied SCHFA are analyzed and reported.

ZUSAMMENFASSUNG

Strukturen und Funktionen von Lipiden werden seit mehr als einem Jahrhundert intensiv untersucht. In dieser Zeit hat sich die Bedeutung von Lipiden jedoch erheblich geändert. Lipide werden heutzutage als "kleine Moleküle, die durch Kondensation von Thioestern auf Carbanionbasis und / oder durch Kondensation von Isopreneinheiten auf Carbokationbasis entstehen" definiert. Die Entwicklung moderner Analysetechniken der letzten Jahrzehnte veranlasste Forscherinnen und Forscher dazu eine umfassende Analytik von Lipiden in biologischen Systemen durchzuführen, welche schließlich als Lipidomik definiert wurde. Die Massenspektrometrie (MS) war seither das wichtigste analytische Instrument und zudem maßgeblich verantwortlich für das exponentielle Wachstum der Lipidomik in den letzten zwanzig Jahren. Im Allgemeinen werden zwei Hauptansätze in der MS verfolgt: Shotgun-Lipidomik (bei welcher der Lipidextrakt ohne Lipidtrennung direkt in das Massenspektrometer injiziert wird) und MS Lipidomik mittels Flüssigchromatographie Kopplung (LC-MS) (bei welcher der Lipidextrakt vor der MS-Detektion chromatographisch aufgetrennt wird).

In dieser Arbeit wurden LC-MS-basierte Lipidomik-Studien entwickelt, um geeignete Bedingungen für die Analyse möglichst vieler Lipidspezies zu ermitteln und dabei eine äußerst zuverlässliche Beschreibung der Lipide zu gewährleisten.

In einer ersten Studie wurden die Extraktionsausbeuten von vier Protokollen für die Analyse von Lipiden in Hela-Zellen verglichen. Der Vergleich basierte auf Parametern wie der Wiederfindung von endogenen Lipiden und internen Standards, sowie der Präzision und der Komplexität der jeweiligen Protokolle. Für den Vergleich wurden zwei klassische Protokolle, welche aus zweiphasigen Systemen (Chloroform-Methanol (MeOH) -H_2O, bekannt als Bligh & Dyer, und Methyl-tert-butylether (MTBE) -MeOH-H_2O, bekannt als Matyash) bestehen, und zwei neuartige Protokolle, die einphasige Systeme mit Isopropanol (IPA) -H_2O (IPA:H_2O 75:25 v/v und IPA:H_2O 90:10 v/v) bilden, ausgewählt. Nach der Extraktion erfolgte die Analyse der Lipide durch Umkehrphasen-Ultrahochleistungsflüssigchromatographie (UHPLC), gekoppelt mit Quadrupol-Flugzeit-MS (QTOF) und Elektrospray-Ionisation (ESI). Für die MS/MS Datenaufzeichnung bei positiver und negativer Polarität wurde eine datenunabhängige Akquisitionsmethode namens SWATH (engl.: sequential window acquisition of all theoretical fragment-ion spectra) verwendet.

Die Verarbeitung der Daten erfolgte über eine frei verfügbare Software (MS-DIAL). Über die zuvor definierten Parametern konnte gezeigt werden, dass die Extraktion mit IPA:H_2O 90:10 v/v vergleichbare Ergebnisse zu dem Protokoll von Matyash liefert und besser als die Extraktion nach Bligh & Dyer funktioniert. Zudem ist die auf IPA-basierende Extraktion einfacher und kann auch mit Kunststoff-Laborbehältern anstelle von Glas durchgeführt werden. Die Verwendung von IPA:H_2O 90:10 v/v vereinfacht demnach das Protokoll für die Analyse von Lipiden in Umkehrphasen-LC-MS Lipidomikstudien.

In einer zweiten Studie wurde das optimierte Protokoll (IPA:H_2O 90:10 v/v) angewendet, um die Veränderungen des Lipidprofils von Keratinozyten nach Behandlung mit dem Naturstoff Betulin zu untersuchen, der nachweislich wundheilende Eigenschaften aufweist. Daten aus nicht-zielgerichteten UHPLC-ESI-QTOF-MS/MS Messungen von behandelten Proben sowie von Kontrollproben wurden einer neuartigen, gezielten Datenverarbeitungstrategie zur Identifizierung von Lipiden unterzogen. Diese gezielte Datenverarbeitung basiert auf der Auswahl und Analyse eines spezifischen Satzes von Vorläufer- und Produktionen für jede Lipidklasse und dem entsprechenden Vergleich ihrer Elutionsprofile. Hierbei wurden nicht nur die einzelnen Lipidspezies, sondern auch Ergebnisse für die gesamte Lipidklasse aus unabhängigen Läufen beider Polaritäten berücksichtigt. Das Resultat dieser Analyse war, dass 440 von 611 identifizierten Lipidspezies bei Betulinbehandlung signifikant reguliert wurden. Die Regulation kann als eine Abnahme der Konzentration von Cholesterylestern und Triacylglyceriden bei gleichzeitiger Zunahme von Glycerophospholipiden, Sphingolipiden und Diacylglyceriden nach der Behandlung mit Betulin beschrieben werden.

Schließlich fokussierte sich eine dritte Studie auf eine bestimmte Gruppe von Fettsäuren, die kurzkettige Hydroxyfettsäuren (SCHFA) genannt werden. Durch die Anwesenheit der Hydroxylgruppe entlang der Alkylkette von SCHFA sind diese Analyte chiral. Einige Enantiomere dieser SCHFA werden mit bestimmten Krankheiten in Verbindung gebracht und sind potenzielle Biomarker bei der Diagnose. In dieser Studie wurde die chirale Trennung von SCHFA mittels HPLC an einer Reihe von auf Chinin und Chinidin aufbauenden, chiralen stationären Phasen untersucht. Zudem wurden MS-kompatible Bedingungen für die chirale Trennung aller untersuchten SCHFA analysiert und beschrieben.

LIST OF PUBLICATIONS

1. C. Calderón, C. Sanwald, J. Schlotterbeck, B. Drotleff, M. Lämmerhofer, Comparison of simple monophasic versus classical biphasic extraction protocols for comprehensive UHPLC-MS/MS lipidomic analysis of Hela cells, Anal. Chim. Acta. 1048 (2019) 66–74. doi:10.1016/j.aca.2018.10.035.

2. C. Calderón, L. Rubarth, M. Cebo, I. Merfort, M. Lämmerhofer, Lipid Atlas of Keratinocytes and Betulin Effects on its Lipidome Profiled by Comprehensive UHPLC-MS/MS With Data Independent Acquisition Using Targeted Data Processing, Proteomics. (2019) 1900113. doi:10.1002/pmic.201900113.

3. C. Calderón, J. Horak, M. Lämmerhofer, Chiral separation of 2-hydroxyglutaric acid on cinchonan carbamate based weak chiral anion exchangers by high-performance liquid chromatography, J. Chromatogr. A. 1467 (2016) 239–245. doi:10.1016/j.chroma.2016.05.042.

4. C. Calderón, M. Lämmerhofer, Chiral separation of short chain aliphatic hydroxycarboxylic acids on cinchonan carbamate-based weak chiral anion exchangers and zwitterionic chiral ion exchangers, J. Chromatogr. A. 1487 (2017) 194–200. doi:10.1016/j.chroma.2017.01.060.

5. C. Calderón, C. Santi, M. Lämmerhofer, Chiral separation of disease biomarkers with 2-hydroxycarboxylic acid structure, J. Sep. Sci. 41 (2018) 1224–1231. doi:10.1002/jssc.201701243.

AUTHOR CONTRIBUTIONS

Publication I

Comparison of simple monophasic versus classical biphasic extraction protocols for comprehensive UHPLC-MS/MS lipidomic analysis of Hela cells.

Carlos Calderón:

General idea generation

Sample preparation and analysis

Data processing and interpretation

Main writing of the manuscript

Corinna Sanwald:

Hela cell cultivation

Proofreading of the manuscript

Jörg Schlotterbeck:

Proofreading of the manuscript

Mass spectrometer maintenance

Bernhard Drotleff:

Advice on lipidomics profiling by SWATH-MS/MS

Proofreading of the manuscript

Mass spectrometer maintenance

Prof. Dr. Michael Lämmerhofer:

Generation, initiation, coordination and financing of the project

Discussion of results and interpretation

Correction and editing of the manuscript

Proofreading and final approval of the manuscript

Corresponding Author

Publication II

Lipid atlas of keratinocytes and betulin effects on its lipidome profiled by comprehensive UHPLC-MS/MS with data independent acquisition using targeted data processing

Carlos Calderón:

General idea generation

Sample preparation and analysis

Data processing and interpretation

Main writing of the manuscript

Lara Rubarth:

Keratinocytes cultivation

Malgorzata Cebo:

Proofreading of the manuscript

Discussion of results and interpretation

Irmgard Merfort:

Initiation of the project

Proofreading of the manuscript

Partial writing and editing of the manuscript

Discussion of results and interpretation

Prof. Dr. Michael Lämmerhofer:

Generation, initiation, coordination and financing of the project

Discussion of results and interpretation

Correction and editing of the manuscript

Proofreading and final approval of the manuscript

Corresponding Author

Publication III

Chiral Separation of 2-Hydroxyglutaric Acid on Cinchonan Carbamate based Weak Chiral Anion Exchangers by High-Performance Liquid Chromatography

Carlos Calderón:

General idea generation

Sample preparation and analysis

Data processing and interpretation

Main writing of the manuscript

Jeannie Horak:

Supervision of LC experiments

Proofreading of the manuscript

Discussion of results and interpretation

Prof. Dr. Michael Lämmerhofer:

Generation, initiation, coordination and financing of the project

Discussion of results and interpretation

Correction and editing of the manuscript

Proofreading and final approval of the manuscript

Corresponding Author

Publication IV

Chiral Separation of Short Chain Aliphatic Hydroxycarboxylic Acids on Cinchonan Carbamate Based Weak Chiral Anion Exchangers and Zwitterionic Chiral Ion Exchangers

Carlos Calderón:

General idea generation

Sample preparation and analysis

Data processing and interpretation

Main writing of the manuscript

Prof. Dr. Michael Lämmerhofer:

Generation, initiation, coordination and financing of the project

Discussion of results and interpretation

Correction and editing of the manuscript

Proofreading and final approval of the manuscript

Corresponding Author

Publication V

Chiral separation of disease biomarkers with 2-hydroxycarboxylic acid structure [#]

Carlos Calderón:

General idea generation

Sample preparation and analysis

Data processing and interpretation

Main writing of the manuscript

Cristina Santi:

Sample preparation and analysis

Prof. Dr. Michael Lämmerhofer:

Generation, initiation, coordination and financing of the project

Discussion of results and interpretation

Correction and editing of the manuscript

Proofreading and final approval of the manuscript

Corresponding Author

LIST OF POSTER PRESENTATIONS

- **(August 28th - September 1st 2016) 31st International Symposium on Chromatography (ISC 2016)**, Cork, Ireland

Poster title: Chiral Separation of 2-Hydroxyglutaric Acid on Cinchonan Carbamate based Weak Chiral Anion Exchangers by HPLC-Charged Aerosol Detection

Carlos Calderón, Jeannie Horak, Michael Lämmerhofer

- **(September 19th - 22nd 2017) 23rd International Symposium on Separation Sciences (ISSS 2017)** Vienna, Austria.

Poster title: Chiral Separation of Short Chain Aliphatic Hydroxycarboxylic Acids on Cinchona Carbamate-Based Weak Chiral Anion Exchangers and Zwitterionic Chiral Ion Exchangers

Carlos Calderón, Michael Lämmerhofer

- **(February 21st -23rd, 2018) Irseer Naturstofftage**, Kloster Irsee, Germany

Poster title: The triterpene betulin and its influence on the lipid profile in primary keratinocytes

Carlos Calderón, Lara Rubarth, Irmgard Merfort, Michael Lämmerhofer

- **(September 23rd – 27th, 2018)** ***32nd International Symposium on Chromatography ISC 2018,*** Cannes-Mandelieu, France

Poster title: Study on Extraction Protocols for UHPLC-ESI-MS/MS-Based Lipidomic Analysis of Hela Cells

Carlos Calderón, Michael Lämmerhofer

- **(July 16th – 20th, 2019)** ***48th International Symposium on High-Performance Liquid Phase Separations and Related Techniques*****,** Milan, Italy.

Poster title: Comprehensive UHPLC-MS/MS lipidomics profiling to study effects of betulin on keratinocytes

Carlos Calderón, Lara Rubarth, Malgorzata Cebo, Irmgard Merfort, Michael Lämmerhofer

Awarded with a Poster Prize

LIST OF ORAL PRESENTATIONS

- **(March 27th – 29th, 2019)** ***DPhG Doktorandentagung 2019,*** Darmstadt, Germany

Presentation: Monophasic versus biphasic lipid extraction protocols for comprehensive UHPLC-MS/MS based lipidomics profiling of cell cultures

Carlos Calderón, Michael Lämmerhofer

INTRODUCTION

1 Lipids and lipid classes

1.1 Lipids

Lipid is a concept that appeared more than one hundred years ago and that has evolved trough words like lipine, lipin, lipoid or lipide, which were having a more restricted meaning. However, there is not yet a widely accepted definition [1]. According to IUPAC, lipids are described as "a loosely defined term for substances of biological origin that are soluble in nonpolar solvents"[2]. This definition, given in terms of solubility, brings many inconsistencies when we consider the solubility of some polar compounds, which are nowadays classified as lipids. Precisely, with the goal of encouraging a comprehensive classification of lipids, Lipid Metabolites and Pathways Strategy (Lipid MAPS), a consortium created by lipid chemists, defined lipids as "hydrophobic or amphipathic small molecules which are originated entirely or partially by carbanion-based condensation of thioesters and/or by carbocation-based condensations of isoprene units" [3].

Christie and Han also proposed an interesting definition considering the nature of substances which are nowadays studied and analyzed as lipids: "Lipids are fatty acids and their derivatives, and substances related biosynthetically or functionally to these compounds"[4].

Table 1.1. Summary of the Major Functions of Individual Lipid Classes

Cellular functions	Lipid classes
Membrane structural component	PC, PE, PI, PS, PG, PA, SM, CL, cholesterol, cerebroside (e.g., GalCer and GluCer), glycolipids, ST, gangliosides, etc.
Energy storage and metabolism	NEFA, TG, DG, MG, acyl CoA, acylcarnitine, etc.
Signaling	All lysolipids, DG, MG, acyl CoA, acylcarnitine, NEFA, eicosanoids and other oxidized FA, ceramide, sphingosine, S1P, psychosine, steroids, *N*-acyl ethanolamine, etc.
Other special functions	Plasmalogen (*antioxidant*), acylcarnitine (*transport*), CL (*respiration*), PS (*cofactors*, *substrate of PE synthesis*), etc.

Table reproduced with permission from [1]. PC: phosphatidylcholines, PE: phosphatidylethanolamine, PI: phosphatidylinositol, PS: phophatidylserine, PG: phosphatidylglycerol, PA: phosphatidic acid, SM: sphingomyelin, CL: cardiolipin, NEFA: Non-esterified fatty acids, TG: triacylglycerides, DG: diacylglycerides, MG: monoacylglycerides, S1P: sphingosine 1-phosphate, GalCer: galactosyl ceramide, GluCer: glucosylceramide, ST: sterols

1.2 Biological importance of lipids

Lipids are recognized as key component of many vital biological processes in living beings. Some of the principal functions of lipids in cells are: energy storage, structural integrity of cells and membranes and signaling [5–7]. More details about the role of some of the most well-known lipid classes are described in Table 1.1.

1.3 Classification of lipids

As mentioned before, one of the main goals of the consortium Lipid MAPS, was to establish a comprehensive classification of lipids. Thus, the lipid classification system introduced by Lipid MAPS consists of eight lipid categories which are having their own subclassification. These categories are fatty acyls (FA), Glycerolipids (GL), Glycerophospholipids (GP), Sphingolipids (SP), Sterol lipids (ST), Prenol lipids (PR), Saccharolipids (SL) and Polyketides (PK) [3,8,9]. The nomenclature proposed by Lipid MAPS has been widely accepted and supported with a rich feedback from lipid researchers worldwide [8].

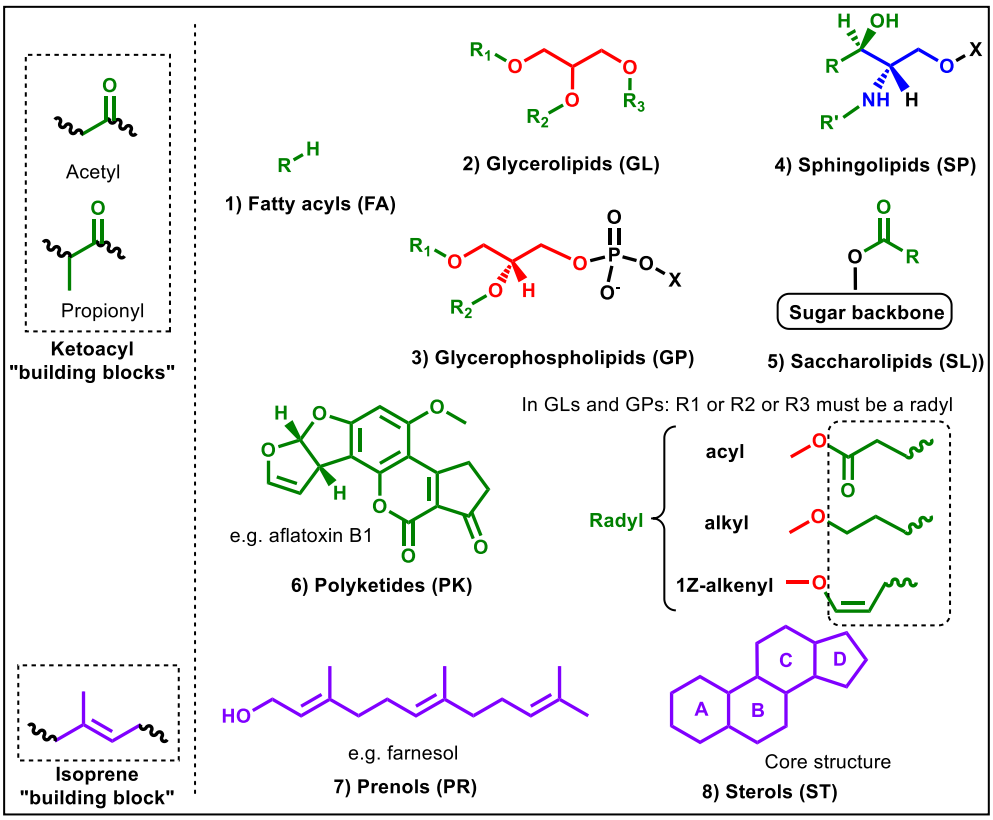

Figure 1.1. Skeleton of the 8 lipid categories defined by Lipid MAPS. In glycerolipids and glycerophospholipids at least one of R1, R2 or R3 has to be a radyl group.

Figure 1.1 shows the basic structures of the lipid categories defined by the classification system of Lipid MAPS. This classification system is based on the concept of two fundamental building blocks: ketoacyl groups and isoprene groups [9]. Ketoacyl groups are the main building blocks,

by different metabolic pathways, of fatty acyls and polyketides. Fatty acyls, in general, and fatty acids (a specific class of fatty acyls), in particular, are the main constituents of more complex lipids such as glycerolipids, glycerophospholipids, sphingolipids and saccharolipids. Isoprene groups (dimethylallyl pyrophosphate and isopentenyl pyrophosphate) are the main building blocks of prenols and sterols. Cholesterol esters, a class of sterols, are a good example of lipids, where the two kinds of building blocks (ketoacyls and isoprenes) are present.

In the cases of glycerolipids and glycerophospholipids, at least one radyl chain has to be attached to the glycerol moiety in order to be classified in that category. Radyl is a term used to describe the three different possibilities in which hydrocarbon chains are linked to the glycerol moiety. These three possibilities are acyl, alkyl or 1Z-alkenyl substituents (see Figure 1.1).

Lipid MAPS possesses also the biggest database for lipid structures (Lipid MAPS Structure Database, LMSD), with more than 43000 structures to the date (available online at https://www.lipidmaps.org/). All the structures included in LMSD are strictly classified and labeled with a unique 12 characters code (14 characters for a few lipid classes), which include information about the database (2 characters), lipid category (2 characters), lipid class (2 characters), lipid subclass (2 characters) and unique ID within the lipid subclass (4 characters). Figure 1.2 shows the distribution of lipid structures contained in LMSD, classified by categories.

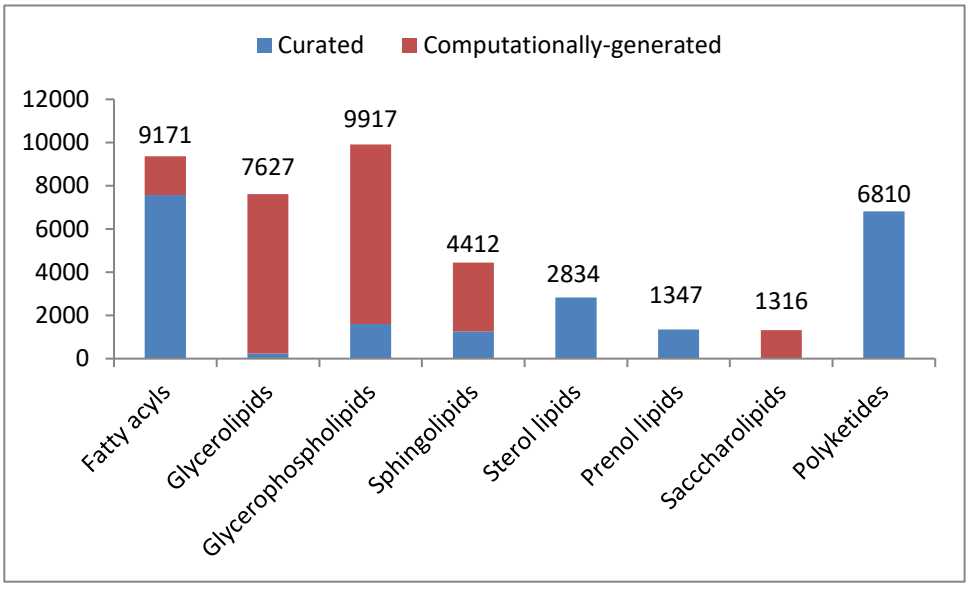

Figure 1.2. Distributions of structures available in LMSD. Updated 10.10.2019 from http://www.lipidmaps.org/ [8]

1.4 Description of studied lipid classes

As mentioned before, each lipid category has its own subclassification, which can be very complex. However, there are, in each lipid category, some classes or subclasses that are commonly studied because they are the most abundant ones or because of their biological importance. Here some of the most important ones are described.

1.4.1 Fatty acyls

The main class of the fatty acyls are the fatty acids, because they are also building blocks of some other lipid categories. Saturated and unsaturated fatty acids with straight hydrocarbon chain are the most commonly found in nature. However, modifications including branched-chain fatty acids or the presence of heteroatoms attached to the main carbon chain also exist.

In animal tissues, fatty acids can vary from 14 to 24 carbons but in some cases the range can be from 2 to 36 or more carbons. In some microorganisms 80 or more carbons are possible while in higher plants the range is more limited [4]. Table 1.2 shows the list of most common fatty acids. Odd-chain fatty acids are mainly produced by some microorganisms but are also present in low concentration in animal tissues. They are produced via propionyl coenzyme A or after alpha-oxidation of fatty acids.

Table 1.2. Names and designations of most common fatty acids.

Common name	Systematic name	Shorthand designation[1]
Butyric	**butanoic**	**4:0**
Caproic	**hexanoic**	**6:0**
Caprylic	**octanoic**	**8:0**
Capric	**decanoic**	**10:0**
Lauric	**dodecanoic**	**12:0**
Myristic	**tetradecanoic**	**14:0**
Palmitic	**hexadecanoic**	**16:0**
Stearic	**octadecanoic**	**18:0**
Arachidic	**eicosanoic**	**20:0**
Palmitoleic	**9-hexadecenoic**	**16:1 (n-7)**
Oleic	**9-octadecenoic**	**18:1 (n-9)**
Elaidic	***trans*-9-octadecenoic**	**18:1**
Cis-vaccenic	**11-octadecenoic**	**18:1 (n-7)**
Linoleic	**9,12-octadecadienoic**	**18:2 (n-6)**
α –linolenic	**9,12,15-octadecatrienoic**	**18:3 (n-3)**
γ –linolenic	**6,9,12-octadecatrienoic**	**18:3 (n-6)**
dihomo-γ –linolenic	**8,11,14-eicosatrienoic**	**20:3 (n-6)**
Arachidonic	**5,8,11,14-eicosatetraenoic**	**20:4 (n-6)**
EPA	**5,8,11,14,17-eicosapentaenoic**	**20:5 (n-3)**
	7,10,13,16,19-docosapentaenoic	**22:5 (n-3)**
DHA	**4,7,10,13,16,19-docosahexaenoic**	**22:6 (n-3)**

Reproduced with permission from Christie and Han, 2010 [4]. 1 Format of notation suggested according to Liebisch *et al.* [10].

Some special classes of fatty acyls are octadecanoids, eicosanoids and docosanoids which are fatty acids with multiple functional groups the designation of which is based on the number of

carbons of the biosynthetic precursor: jasmonic acid (18 carbons), arachidonic acid (20 carbons) and docosahexanoic acid (22 carbons), respectively. Subclasses of the eicosanoids are for example prostaglandins, leukotrienes and thromboxanes.

Fatty alcohols, fatty aldehydes, fatty esters, fatty ethers and fatty amides are also classes belonging to the fatty acyl category. An important family of fatty esters are the carnitine esters (acyl carnitines, AC). They are well-known for being involved in the transport of fatty acids into mitochondria [11].

1.4.2 Glycerolipids

Glycerolipids are defined because of the presence of glycerol moiety in their structure. One, two or three radyl substituents can be attached to the glycerol moiety. Acyl groups are the most common substituents leading to the lipid classes monoacylglycerides (MG), diacylglycerides (DG) and triacylglycerides (TG), respectively.

1.4.3 Glycerophospholipids

Glycerophospholipids contain at least one phospho group and one radyl chain attached to the glycerol moiety. Figure 1.3 shows the backbone structure of the most common glycerophopholipids. The presence of different substituents linked to the phospho group defines different lipid classes. If one of the radyl groups (R1 or R2) is lacking, the prefix lyso is used for the lipid class (e.g. Lysophophosphatidylcholine, LPC)

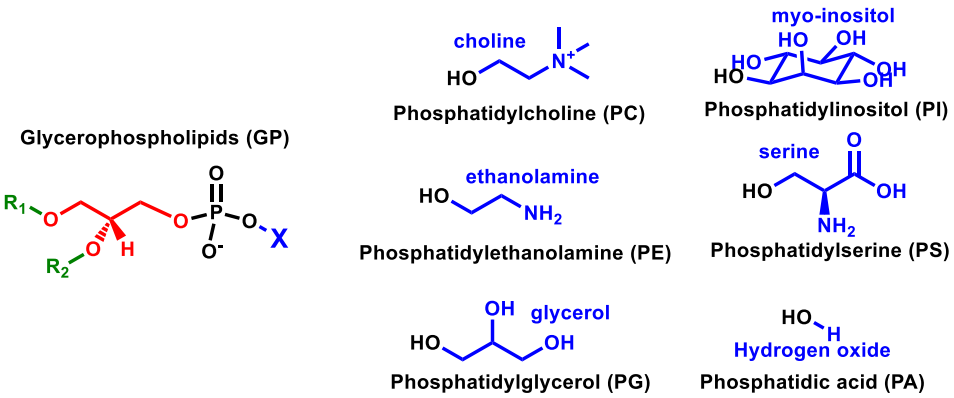

Figure 1.3. Structure of main glycerophospholipid classes

1.4.4 Sphingolipids

Sphingolipids are defined by the presence of a sphingoid base in their structure. This sphingoid base is synthesized in cells from a long chain fatty acyl-CoA (commonly palmitoyl CoA) and the amino acid serine. Some of the most important sphingolipid classes are ceramides (Cer),

phosphosphingolipids and glycoshingolipids. Within the phosphosphingolipids, the subclass sphingomyelin is the most abundant in mammalian cells.

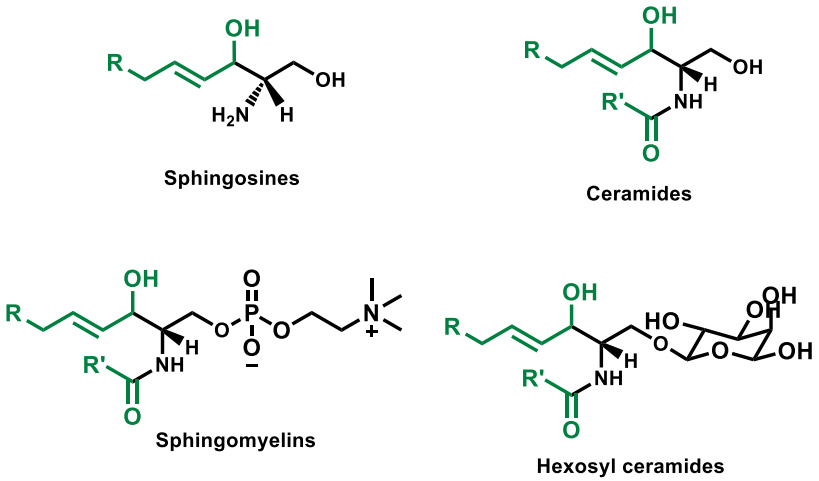

Figure 1.4. Common structures of sphingolipids

1.4.5 Sterols

Sterols possess a core structure, which consists of four fused rings (perhydro-cyclopentaphenanthrene) (see Figure 1.1). Some of the main lipid classes in this category are cholesterol and derivatives, steroid hormones, secosteroids, bile acids, amongst others. Cholesterol esters (CEs) are some of the most studied sterols in mammals. Cholesterol and its derivatives is one of the major classes of membrane lipids.

2 Liquid chromatography of lipids

Considering the wide polarity range that lipids possess, liquid chromatography (LC) represents a very useful tool for their analysis since it is possible to separate lipid classes or lipid species according to their physicochemical properties. Also, LC enables the concentration of lipids for further analysis [12].The three most important LC configurations for analysis of lipid extracts are reversed phase LC (RPLC), normal phase LC (NPLC) and hydrophilic interaction LC (HILIC). In 2014, Cajka *et al.* published a review with the analysis of 185 lipidomics publications from the last decade (2004-2014). Figure 2.1A, shows the percentage of studies, from that selected group, that were using each type of LC configuration [12]. Figure 2.1B-C also shows the polarity and MS instruments employed in those studies.

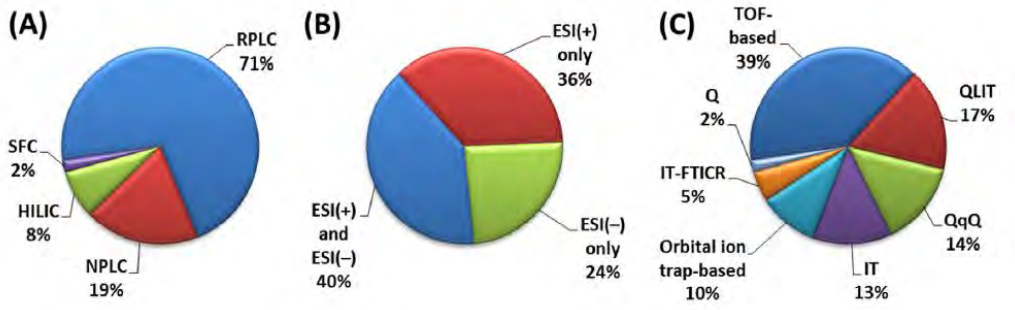

Figure 2.1. Use of different chromatographic and mass spectrometric systems in lipidomics analysis. Reproduced with permission from [12].

2.1 Reversed phase liquid chromatography

RPLC is the type of LC most widely used for analysis of lipids. This technique is based on partition mechanism of the solutes into the stationary phase in accordance to their hydrophobicity [13]. In RPLC, the stationary phase (SP) is apolar and consists of silica particles which are functionalized with hydrocarbon chains (C30, C18, C8) or other groups like cyano, phenyl and alkyl chain with polar embedded group. Among these, the ones functionalized with C18, are the most employed. The mobile phase (MP) is polar and consists of water and water-miscible organic solvents (methanol, acetonitrile, isopropanol). In general, the mechanism for retention is described as hydrophobic interaction between the solutes and SP. When lipids are loaded into the column, and mobile phase contains some amount of water, the driving force for the retention of analytes in the hydrophobic SP comes mainly from an increase in entropy of the system rather than from intermolecular interactions [13]. Release of lipids from the SP occurs when the organic solvent content is increased in the MP.

In RPLC, lipid species with more and longer radyl chains elute later from the LC column. In the same way, lipid species with saturated radyl chains elute later than the corresponding ones with polyunsaturated radyl chains.

The use of mobile phase additives improves RPLC separation and detection of lipids, especially when it is coupled to MS detection. The most common additives are ammonium formate, and ammonium acetate (in concentrations from 5 to 10 mM) or their corresponding acids, formic acid and acetic acid (in typical concentration ranging from 0.05 to 0.1%) [13].

2.2 Normal phase liquid chromatography

NPLC separates analytes based on the polarity of their headgroups. The SP is polar and consists of silica or polar functionalized silica, and the MP consists of apolar solvents, like hexane or heptane, and a relatively more polar solvent miscible with it, like chloroform or isopropanol. Additives are usually acetic acid and ammonium acetate in low concentrations. In NPLC, the retention of analytes is based on the adsorption of polar groups of the molecule on the SP whereas apolar tails of lipids play a minor role leading to lipid class separations [13].

NPLC has the disadvantage that polar eluent fraction binds strongly to the SP which is not easily exchanged and leads to longer equilibration times. Furthermore, even traces of water will be strongly attached to the SP resulting in low reproducibility and must be carefully avoided.

Another disadvantage is the low suitability of the mobile phase for electrospray ionization (ESI), since apolar solvent reduce ionization efficiency. Thus, dopant or post column mixing are often required [13].

2.3 Hydrophilic interaction liquid chromatography

HILIC is a variant of NPLC. The SP is generally silica or polar functionalized silica like in NPLC and the MP is based on ACN-water mixtures, rich in ACN while other water-miscible organic solvents like MeOH, IPA, MTBE play no significant role. Unlike NPLC, HILIC uses normally between 5 and 40 % content of water in the MP , and requires at least 2% of water to maintain an enriched layer of water on the SP [12]. Additives like ammonium formate and ammonium acetate allow to control the pH and ionic strength of the MP [1].

In HILIC, analytes are separated based on their partition between the MP and the water layer on the SP. However, once in the aqueous layer, analytes may interact with functional groups of the SP as well leading to a mixed partition-adsorption mechanism [13].

In a similar way to NPLC, HILIC enables a separation of lipids based on their polarities. In comparison to NPLC, HILIC gives better reproducibility and robustness and it is more compatible with MS analysis [12].

2.4 Supercritical fluid chromatography

Supercritical fluid chromatography (SFC) is a kind of chromatography which employs supercritical fluids (SF) or subcritical fluids as a mobile phase. Despite many substances have proven to have a good performance as SFs, CO_2 is practically the only one used as mobile phase. The reasons for that are: it is inert, critical pressure and temperature are relatively easy to achieve (31 °C and 74 bar), it is nonflammable, it is cheap and it is environmentally friendly [14,15].

Considering that fluidized CO_2 is a solvent with similar polarity to hexane, SFC was often considered only as an alternative for NPLC. However, eluotropic strength of CO_2 can be modified with additives, which makes possible to use also reversed-phase type materials [14].

Some of the advantages of SFC over other chromatographic techniques are due to the low viscosity and high-diffusion coefficients of the MP. This allows the use of elevated linear velocities and to obtain highly efficient separations [16]. SFC based lipidomics leads to lipid class separation. It has the advantage over HILIC that also neutral lipids such as TGs and CEs are retained and can be analyzed while neutral lipids elute with or very close to t0 in HILIC.

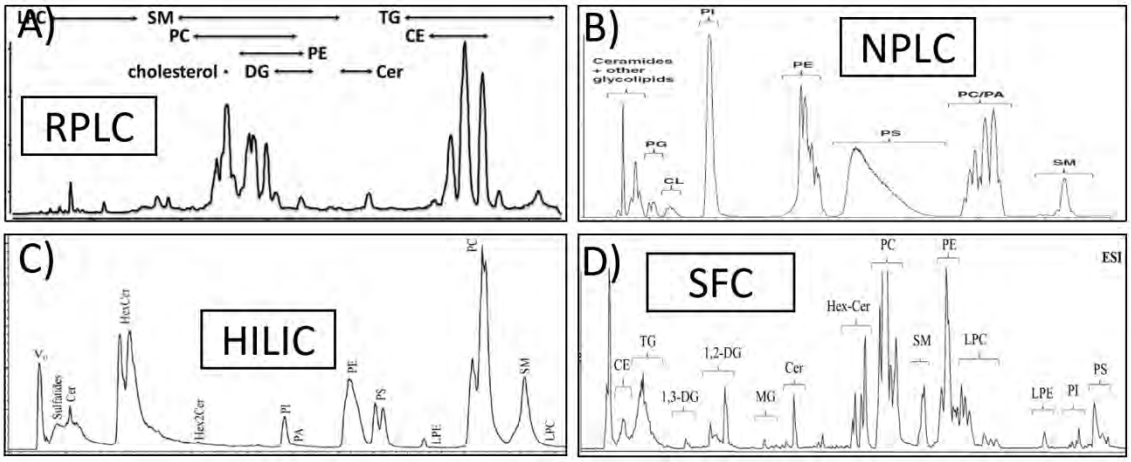

Figure 2.2. Elution profile of lipid extracts in four different LC configurations RPLC, NPLC, HILIC and SFC (in normal phase mode). All figures are reproduced with permission in the following manner: RPLC from [17], HILIC from [18], NPLC from [19] and SFC from [20].

2.5 Comparison of LC systems

Figure 2.2 shows the separation profile of 4 different lipid extracts by using different kinds of chromatography. As can be seen NPLC, HILIC and SFC (in NP mode) allow the separation of

different lipid classes while in RPLC, many lipid classes elute at the same time. Despite of this, the strength of RPLC resides in their capacity to separate lipid species from the same lipid class.

Since NPLC and HILIC have the capability of separating lipid classes and RPLC has the capability to separate lipid species based on the hydrophobicity of their fatty acyl chains, it has been common to observe approaches where a lipid class is first separated, via selective extraction, NPLC or HILIC, and then analyzed by RPLC for separation of lipid species. 2D LC, in an offline or online mode, has been employed for this purpose [21–24]. However, with the development of instrumentation and stationary phases, and specially with the introduction of UHPLC, many researchers have replaced the sequential NPLC-RPLC for a RP-UHPLC lipid separation [25–28].

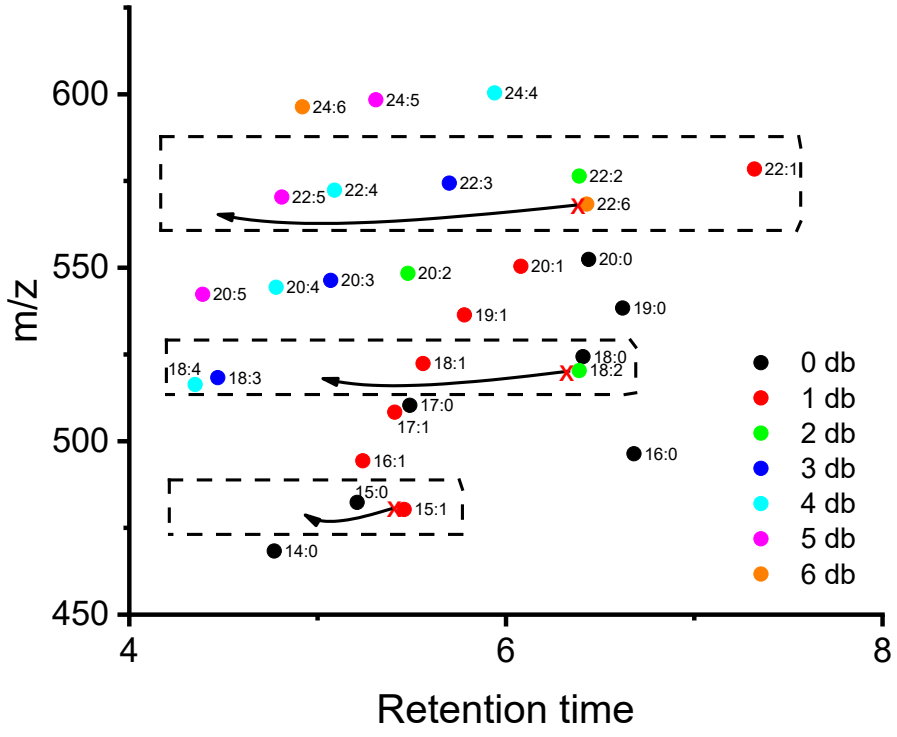

Figure 2.3. Peak spotting plot for LPCs identified in a previous publication according to the number of double bonds. Reference is Yamada *et al.* [29]. db: double bonds. For series of 15, 18 and 22 carbons, one irregularity is marked with a red X and the expected retention time is showed with an arrow. These irregularities are most likely misidentifications.

The retention behavior of different lipid classes in RPLC is an aspect that has been well described in terms of length and number of double bonds of the radyl chains [30–32]. This information is very useful and has a lot of potential on the identification of lipid species, since some misidentifications can be easily recognized by inspecting the elution profiles of the lipid species. However, there are publications where RPLC-MS is employed for analysis of lipids and

identification is only based on MS information leaving aside the rich chromatographic information. Figure 2.3 shows a peak spotting plot (in terms of retention time and m/z) of the lysophosphatidylcholines (LPC) species identified in a RPLC-MS lipidomic study published in 2013 [29]. Identification was done in this case with an automated lipid identification software with no LC information taking into consideration. Identified species were reported with their corresponding m/z values and retention time, and for illustrative purposes Figure 2.3 has been elaborated here. As can be seen in this figure, there are a few clear inconsistent identifications.

3 Mass spectrometry for lipids

Mass spectrometry is a technique dedicated to separate and analyze ions based on their mass to charge ratio (m/z) [33]. The principle of MS can be described in three simple steps [1]:

- Formation of molecular ions and/or corresponding fragment ions
- Separation of precursor ions or fragment ions by their m/z
- Measurement of each ion abundancy.

3.1 MS instrumentation

Some standard components of a mass spectrometer are an ion source, a mass analyzer system, a detector, and a data processing system (Figure 3.1).

In a first step, the sample is introduced into the ion source through an inlet or from a previous separation interface such as LC or GC, analytes are then vaporized and ionized. Once in the analyzer, ions in the gas phase are separated according to their m/z values and finally detected.

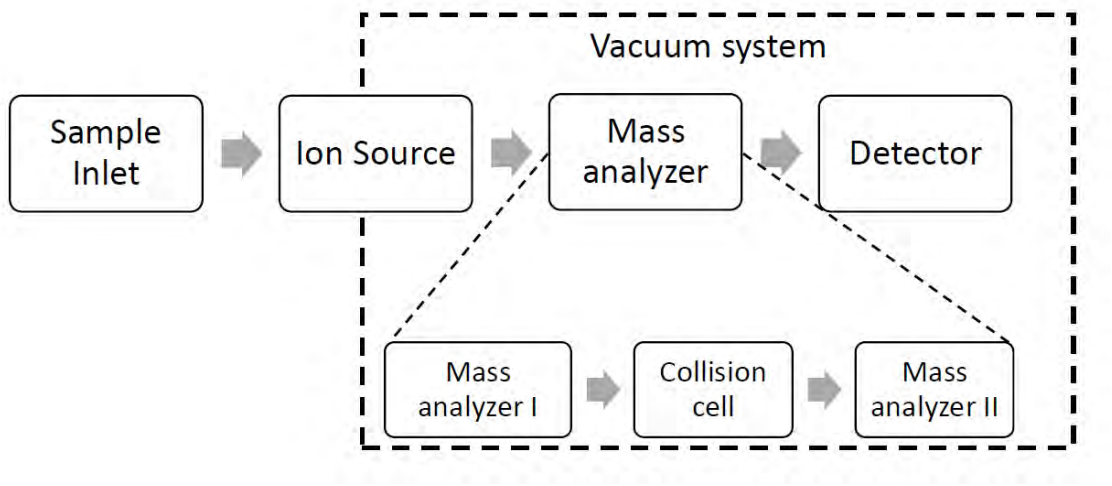

Figure 3.1. Schematic diagram of a mass spectrometer. Reproduced with permission from [1].

3.1.1 Ion Source

The ion source is the device where ions are generated. These ion sources are mainly defined for the ionization method employed [34]. An illustrative diagram has been published by Gross [33] (See Figure 3.2), which classifies the most important developed ion sources according to the hardness of the technique and the main type of analytes for what is was developed. Currently, electrospray ionization (ESI) is the most important technique used to generate molecular lipid ions in MS [6]. Details of this technique will be described below.

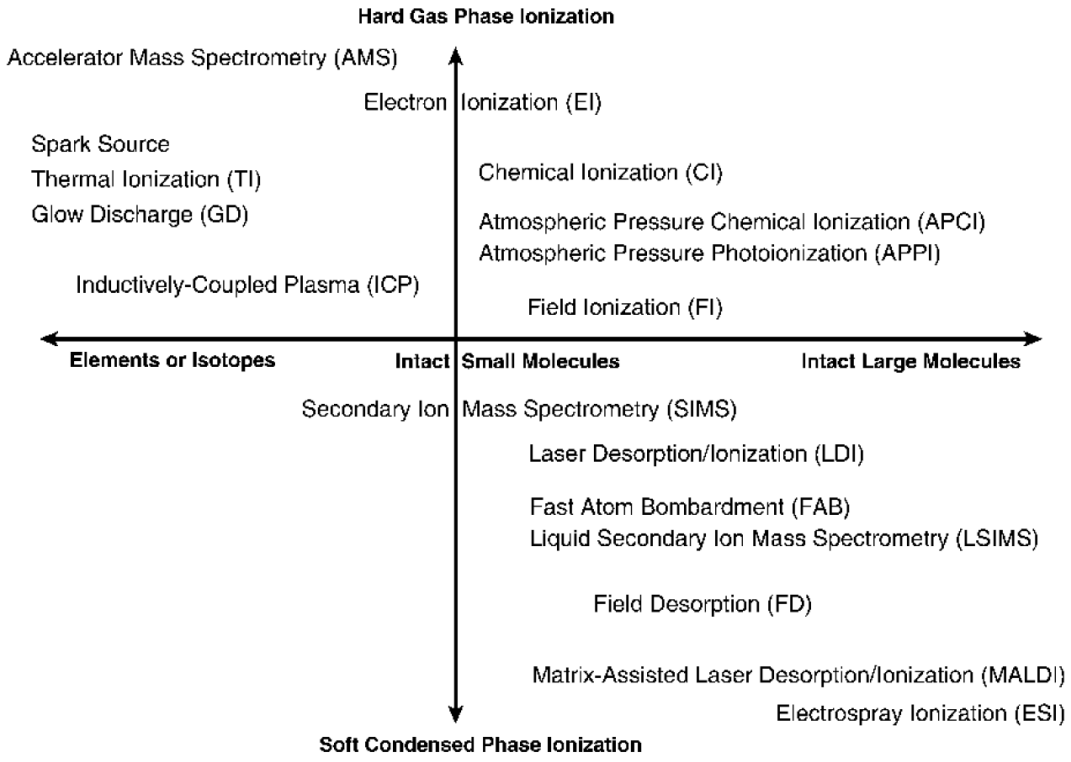

Figure 3.2. Ionization technique employed in MS, classified according to their application and estimated relative hardness of softness. Reproduced with permission from [33].

3.1.1.1 Electrospray ionization (ESI)

In ESI, sprayed small droplets are formed inside the ionization chamber. An applied high voltage provokes that sprayed aerosol droplets carry net charges. These droplets are exposed to high temperature, which leads to evaporation of the solvent and size reduction of droplets. Once multiple charges in the droplets get closer because of the size reduction, Rayleigh limit is reached and Coulomb fission is undergone [33]. Figure 3.3 shows a diagram of the ionization process in ESI.

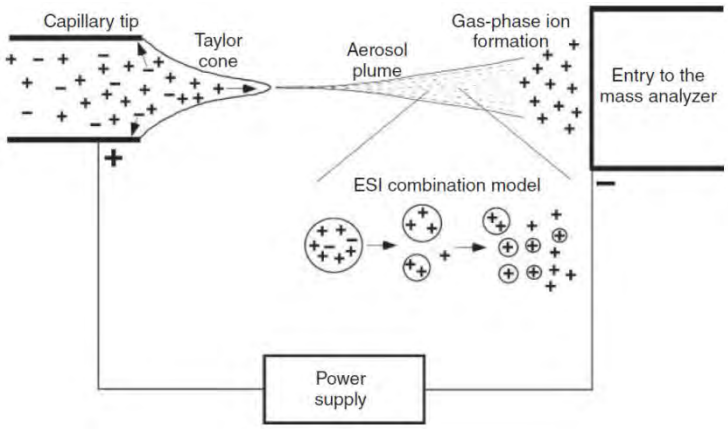

Figure 3.3. Schematic diagram of the principle of electrospray ionization. Reproduced with permission from Han, 2016. [1].

ESI can be adapted to a broad range of flow rates and solvents in the MP. In ESI, even neutral lipids can form adducts with small cations and anions. Therefore, almost all nonvolatile lipids can be ionized [1]. Some of the advantages of ESI, are that the sensitivity of ESI-MS for lipid analysis is remarkably high in comparison to other approaches, the linear dynamic relationship between an ion peak intensity and concentration of the compound is very wide and the reproducibility is good [1].

3.1.2 Mass analyzer

Once ions are generated in the ion source, they are transferred to the analyzer to be separated based on their m/z. During the last century, mass spectrometers based on different principles have been introduced. Mass resolution is probably the most important feature regarding MS instruments, and this has made a division line between low resolution (LR-) and high resolution (HR-) instruments. However, other features like sensitivity, acquisition speed, maintenance costs and price, are also very important. Furthermore, the possibility to combine two or more instruments (hybrid MS instruments) in one device, normally one LR-MS with one HR-MS instrument have opened a set of possibilities and approaches for analysis of metabolites. Table 3.1 shows a comparison of some features of most common mass analyzers. In the following section, we will describe some of the features of quadrupole and TOF analyzer, which give origin to the QTOF instrument, one of the most employed instruments nowadays for analysis of lipids and is the kind of the main instrument employed in this work.

Table 3.1. Comparison of the features of some common mass analyzers:

Mass analyzer	Mass resolution[a]	Mass accuracy (ppm)	Sensitivity	Identification	Quantification
LTQ (LIT)	2000	100-500	Good	++	+
QQQ	1000	100-1500	High	+	+++
TOF/TOF-TOF	10,000-40,000	<5	High	++	++
QTOF	10,000-60,000	<5	High	++	+++
Orbitrap	100,000-800,000	<3	Medium	+++	++
FTICR	>1,000,000	<1-2	Medium	+++	++

Reproduced with permission from Wang *et al.* [35]. [a]Mass resolution at full width half maximum. LTQ: linear trap quadrupole, QQQ: triple quadrupole, TOF: Time of flight, FTICR: Fourier-transform ion cyclotron resonance

3.1.2.1 Quadrupole

The principle of quadrupole is based on the use of oscillating electrical fields to selectively stabilize the trajectory of ions crossing the analyzer. At a specific time point only ions within a

specific range of m/z values (usually around 1 Da window) can cross the analyzer while the rest collide with the quadrupoles and are discarded. The potentials on the rods of the quadrupole can be changed rapidly, in a way that a new window of m/z values are able to cross the analyzer. In this manner, ions can be selected and detected.

Quadrupole is a low-resolution instrument. However, the combination with a second quadrupole gives a wide versatility to the instrument. This combination includes an extra quadrupole in between which is employed as a collision cell (see Figure 3.1). In this way precursor ions coming from the first quadrupole can be selected and fragmented in the collision cell and their product ions can be analyzed in the second quadrupole analyzer. These instruments are known as triple quadrupoles (QQQ) and they are especially used for quantitative purposes in targeted lipidomic analysis [35]. MS and MS/MS experiments that can be performed in a triple quadrupole are described in section 3.2.

3.1.2.2 Time of flight (TOF)

Time of flight (TOF) analyzer measures the time required for ions to fly through a drift tube. Because same potential is applied to the ions at the entrance of the drift tube it is possible to establish a correlation between the time required to cross the tube and their m/z. An equation for conservation of energy, from potential energy to kinetic energy is expressed as

$$zeV = \frac{mv^2}{2}$$

where z is the number of charges of the ion, e is the charge of electron, V is the potential applied to the ions, m is the mass of the ion and v is its velocity. v can be expressed as the ratio between the distance of the drift tube (d) and the time required to cross it (t), which leads to

$$\frac{m}{z} = 2eV\left(\frac{t}{d}\right)^2$$

establishing the relationship between m/z and t.

TOF analyzers can reach mass resolutions in the range of 10,000-40,000 and have acquisition speed in the range of ms (typically 50 Hz equivalent to 50 spectra per s). Their relative cost can be described from low to middle. Hybrid TOF instruments with quadrupoles (QTOF) offer nowadays the possibility of obtaining product ion spectra, with high resolution at a high speed. This is especially useful in untargeted analysis of lipids, where data from many species and many samples are recorded and afterwards analyzed in order to describe qualitatively and quantitatively the lipidome of the samples.

3.1.3 Detector

The detector is the last component of the mass spectrometer. This component works by recording an induced charge or a current produced when an ion passes by or hits a surface [1]. The most employed detectors are electron multipliers [1]. Table 3.2 shows a comparison of the most common detector principles employed in MS.

Table 3.2 Comparison of commonly used detectors:

Detector Type	Advantages	Trade-Offs
Faraday cup	Robustness, stable sensitivity, and good for measuring ion transmission	Low amplification (∼10)
Scintillation counter	Extremely robust, long lifetime (>5 yrs), good sensitivity (∼10^6)	Sensitive to light
Electron multiplier (EM)	Fast response, good sensitivity (∼10^6)	Short lifetime (1–2 yrs)
High-energy dynodes w/EM	Increased sensitivity for measuring high mass	May shorten lifetime of EM
Array	Fast response, good sensitivity, simultaneous detection	Low resolution (∼0.2 amu), expensive, short lifetime (<1 yr)
FT-MS (Orbitrap)	Mass analyzer serves as the detector of high resolution	Used only for the specific instruments

Reproduced with permission from [1].

3.2 MS experiments

Figure 3.4 shows a scheme for classification of MS experiments which have been distributed in three main different categories: 1) single MS, 2) Tandem MS, and 3) Combined single + tandem MS experiments. The main function of the analyzer(s) in single and tandem MS experiments is also described in Table 3.3.

3.2.1 Single MS experiments

Single MS experiments are performed by using only one analyzer. In tandem mass spectrometers it implies that only one spectrometer keeps working while the other one works in a transmission mode. For example, in a triple quadrupole single MS experiment can be performed either in the Q1 or Q3 quadrupole.

3.2.1.1 Survey Scan

In this experiment all precursor ions are scanned in one analyzer of the MS instrument. This experiment allows to have an overview of all ions generated at a certain time point in the source of the spectrometer. Depending on the resolution and accuracy of the instrument, molecular formula of precursor ions can be determined. Also, isotopic pattern of the ions can be observed.

Figure 3.4. Scheme for classification of MS experiments. [1] In Ion trap instruments it is possible to perform MS^n experiments, it means that fragment ions can be isolated and further fragmented with a new PIA or SRM experiment [2] QTRAP instruments have some further specific scan modes [3] In high resolution instruments as QTOF and QOrbitrap, this experiment is described as Parallel Reaction Monitoring (PRM).

3.2.1.2 Selected ion monitoring (SIM)

In SIM, a narrow window of m/z values are selected and monitored [36]. In a quadrupole instrument a SIM experiment takes shorter time than a survey scan and therefore it can be convenient to save some time by monitoring only m/z values of interest, instead of a whole range. On the other hand, it is also possible to measure a single ion over the same (i.e. longer) time which results in enhanced sensitivity. The spectrum of a SIM experiment is quite simple since only a short m/z window is being monitored (normally 1 Da). In LC-MS, a SIM chromatogram shows the total current produced by the traced m/z values through the whole run. This trace is very useful for quantitation purposes since height and area of peaks can be compared with those of standard solutions of analytes. In high resolution instruments such as TOF, with a high acquisition speed, it is more practical to measure a Survey Scan, since a SIM chromatogram for a particular m/z value can be obtained from the Survey Scan as extracted ion chromatograms (EIC).

3.2.2 MS/MS experiments for analysis of lipids

MS/MS experiments can be performed when two or more analyzers are coupled or when there is the possibility of tandem MS in time in the same analyzer, as in the case of ion trap. For these tandem MS experiments, precursor ions reach the first analyzers where they are filtered, after that, ions are transferred to a collision cell where energy is applied in order to generate fragments which are filtered in the second analyzer.

Table 3.3 Comparison among scan modes in mass spectrometry:

Experiment	Mass Analyzer 1 (precursor ions)	Collision Cell	Mass analyzer 2 (fragment ions)	Application
Survey scan	Scanning	-	-	
SIM	Selecting	-	-	
Product ion analysis	Selecting	Precursor ions are broken into fragment ions	Scanning	To obtain structural information about the precursor ions
PIS	Scanning		Selecting	To detect the analytes yielding an identical fragment ion after CID
NLS	Scanning		Scanning	To detect the analytes losing a common neutral fragment after CID
SRM	Selecting		Selecting	To monitor a particular CID reaction

Reproduced and modified with permission from [1].

3.2.2.1 Product Ion analysis

In this experiment precursor ions are selected by its m/z in a first analyzer, then their fragmentation is induced in a collision cell and their fragments are scanned in a second analyzer. For this experiment the user should know which precursor ions have to be analyzed (except in combined MS + MS/MS workflows, see 3.2.3).

3.2.2.2 Selected reaction monitoring/Multiple reaction monitoring (SRM/MRM)

For this experiment, both analyzers are set to filter a specific m/z value. SRM is performed mainly in low resolution instruments: triple quadrupole or quadrupole ion trap. This is a targeted approach since the identity of species to be analyzed and their corresponding fragmentation pattern must be known previously. This is the most typical experiment for quantitation of metabolites, because of the short time required for the experiment and the good selectivity

given by the filtration of a precursor and its fragment ion. Normally, the experiment is performed in LC-MS, where an SRM chromatogram allows to monitor the elution (as a chromatographic peak) of analytes that produce the preselected precursor and fragment ion. Areas and heights of peaks generated after the elution of metabolites are used for quantitation after comparison with its corresponding standards.

Recently, an approach called Parallel reaction monitoring (PRM; also called HR-MRM) has been implemented in QTOF and QOrbitrap instruments, and has been compared with SRMs [37]. However, PRM is a PIA experiment rather than an SRM experiment, since it filters a precursor ion and all its fragments are analyzed. Thus, in LC-MS a PRM experiment not only allows the identification of metabolites, since high resolution m/z values of fragments are determined, but also quantification, since "SRM chromatograms" can be reconstructed from the measured data.

3.2.2.3 Precursor ion scan (PIS) and Neutral loss scan (NLS)

PIS and NLS will be explained and analyzed together because their applicability is very similar.

In PIS, fixed m/z window is selected in the second analyzer, while the first one scans precursor ions which give this fragment (product) ion. In this way, only when a precursor ion produces a fragment with the specific m/z value, a signal is detected. In NLS both analyzers are scanning at the same time, with a predetermined offset of m/z values between the two analyzers, then only when precursor and product ion are fulfilling this offset a signal will be recorded.

PIS and NLS are typical integrated experiments in triple quadrupoles and Qtrap instruments. QTOF machines can acquire multiple PIS, but not NLS [38].

PIS and NLS are specially used for untargeted analysis of specific lipid classes in lipidomics, because these lipid classes have a typical fragmentation pattern where a specific neutral fragment is lost (e.g. loss of 87 in PS) or a typical fragment ion is produced (e.g. 184 in PC). A drawback of this method is that only one PIS or NLS can be performed at the time which means that only one lipid class is normally studied at the time [38].

These experiments are specially applied in shotgun lipidomics [39–41] (See 4.3.1.1). However also applications have been reported for LC-MS lipidomics studies [42–44].

Figure 3.5 shows the spectra of a rat myocardial lipid extract which is analyzed with PIS and NLS experiments. In this example an ion with m/z 885.7 is having a signal in the precursor ion scan experiments corresponding to characteristics fragments of inositol phosphate and fatty acyls 18:0 and 20:4.

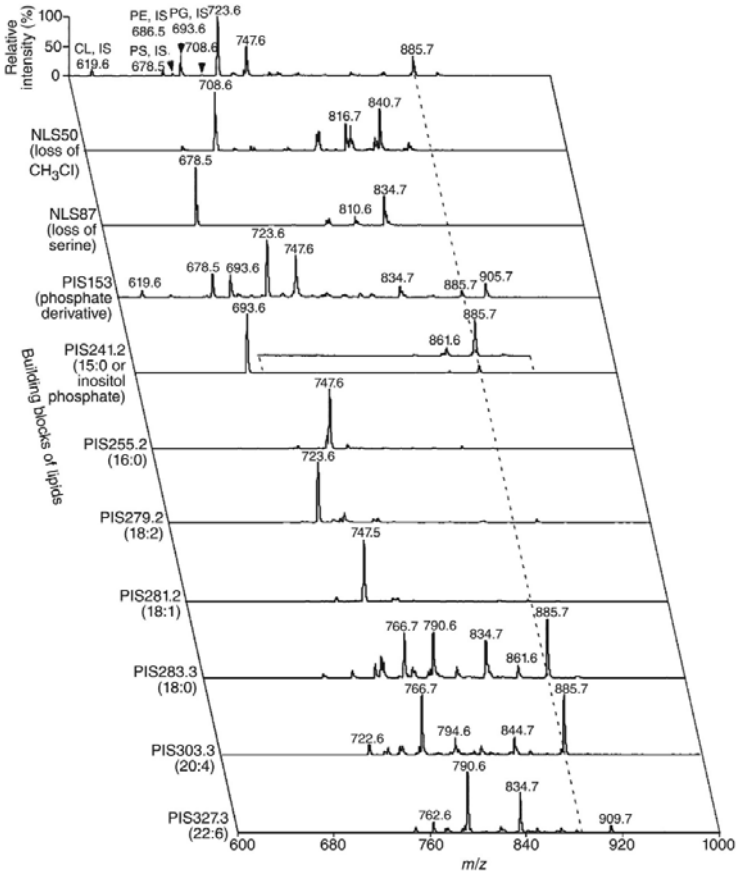

Figure 3.5. Corresponding spectra of different PIS and NLS experiments of a rat myocardial lipid extract. Reproduced with permission from [35].

Table 3.4 shows the list of most common PIS and NLS experiments employed for the analysis of specific lipid classes.

3.2.3 Combined MS + MS/MS workflows

This kind of workflow consists of at least two different experiments. In all the cases these experiments include a first MS experiment (usually a Survey Scan) and at least a second MS/MS experiment (usually Product ion analysis).

These approaches are especially useful for untargeted analysis of metabolites where MS/MS information is required for identification of compounds but the identity of species in the sample is unknown. Considering the complexity of the approach, HR-MS instruments are commonly employed for performing these kind of experiments.

3.2.3.1 Data dependent acquisition (DDA)

Data dependent acquisition (DDA) receives its name because the second (MS/MS) experiment is defined by a list of criteria which are applied to the results of the first experiment. Generally, a Survey Scan experiment is performed in a first stage and precursor ions detected are immediately analyzed for deciding, based on set criteria, which of them will be triggered for an

MS/MS experiment. This selection is normally based on the intensity of detected precursor ions but also it is possible to establish lists of m/z values which will be included or excluded automatically for the MS/MS experiment [45].

A disadvantage of DDA is that MS/MS chromatograms, which are oftentimes more selective and/or more sensitive cannot be extracted because full MS/MS data sets are not available.

Table 3.4. Example of some PIS and NLS experiments applied in ESI–MS/MS analysis of lipids.

Lipid class(es) analyzed	Polarity	Scan mode
PC, LysoPC, SM	Positive	PIS of 184^{+}
PE and LysoPE	Positive	NLS of 141
PA, PG and LysoPG	Negative	PIS of 153^{-}
PI	Negative	PIS of 241^{-}
PS	Negative	NLS of 87
SQDG	Negative	PIS of 225^{-}
MGDG	Positive	PIS of 243^{+}
DGDG	Positive	PIS of 243^{+}
PC, SM	Negative	PIS of 168^{-}
PE	Negative	PIS of 195^{-}
PS	Negative	NLS of 185
PG	Positive	NLS of 189
Cer	Positive	PIS of 264^{+}
CE	Positive	PIS of 369^{+}

Modified from references [6,39,46].

3.2.3.2 Data Independent acquisition (DIA)

In data independent acquisition (DIA) the second experiment is completely defined before the measurement of the sample and is totally independent of the results from the first experiment. There are three well known possibilities of this approach. In all of them a MS scan experiment is initially measured, and successive MS/MS experiments are executed afterwards.

DIA is a good strategy for acquiring comprehensively MS and MS/MS data over an entire range of m/z values [47]. In this manner retrospective analysis of the data can be done once new databases are created or new algorithms for identification of lipids are developed without need for remeasuring samples.

3.2.3.2.1 MS^{All}

In this approach, hundreds or thousands of MS/MS experiments (PIA) are acquired in order to obtain MS/MS fragmentation of all the precursor ions within certain m/z range (e.g. 100-1500 Da). Thus, PIA experiments are designed by filtering a narrow m/z window at the time, normally 1 Da, and obtaining its product ion spectra. This experiment is only used in shotgun lipidomics because of the large cycle time required (a few minutes, Figure 3.6A)) [48,49].

3.2.3.2.2 MS^E or all ion fragmentation (AIF)

In this approach, all the precursor ions are selected at the same time for a PIA experiment. MS^E is normally used in LC-MS analysis in which in each MS cycle two experiments are performed, one MS survey scan at low collision energy, leading to no fragmentation, followed by a full scan at high collision energy, leading to fragmentation and corresponding to an MS/MS experiment with broad band precursor isolation. Depending on the complexity of the sample and the performance of the LC separation the MS/MS spectra can be very complex. It requires a deconvolution step to determine which product ions belong to each precursor ion (Figure 3.6B).

3.2.3.2.3 SWATH

SWATH represents a middle point between the last two approaches, since here the MS/MS experiments consist of multiple PIA for precursor ions from selected sequential m/z windows. Size can be adjusted for each window. As in the case of MS^E, SWATH is usually employed in LC-MS analysis and also requires a deconvolution process to determine which product ions correspond to each precursor ion. This deconvolution step is less complex in SWATH since precursor ions are split and fragmented in groups and not all at the same time. Figure 3.6 shows a relative comparison in term of time and design of experiments for MS^{All}, MS^E and SWATH. As it can be seen, MS^{ALL} requires a much larger number of experiments, which takes more time but allow to have simpler MS/MS spectra, MS^E is faster but MS/MS spectra are quite more complex (composite spectra), whereas SWATH is also fast (cycle time around 1 s) and MS/MS spectra are less complex than MS^E. Also, in SWATH experiments the background noise is filtered more efficiently leading to higher sensitivity [50].

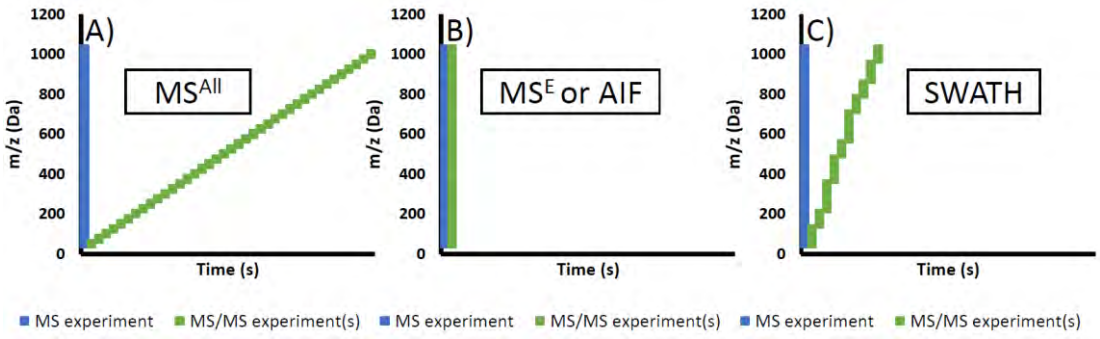

Figure 3.6. Schematic representation of DIA experiments A) MS^{All}, B) MS^E and C) SWATH

3.3 Fragmentation pattern of studied lipid classes

Ionization of lipids occurs by many different mechanisms. In ESI, the polar headgroups of most lipid classes play a key role for ionization and therefore fragmentation patterns can be linked to each lipid class.

Some lipid classes ionize significantly in both polarities while other ones can ionize only under one polarity. In the cases where the lipid ionizes in both polarities possibilities for identification increase considerably. In most instances, the formation of ions involves attachment of charging species such as H^+, NH_4^+ or alkali metal (Na^+, Li^+) in positive polarity and attachment of $HCOO^-$, CH_3COO^-, Cl^- or the loss of H^+, in negative polarity. Table 3.5 shows the adducts most commonly observed during ESI of each lipid class.

In tandem MS, each of these adducted forms has unique behavior that provides information relevant to the structural features of the lipid. The following description about fragmentation pattern of some of the most studied lipid classes will be done considering the employment of ESI sources and CID.

Table 3.5. Molecular species formed during electrospray ionization of lipids.

Lipid class	Positive mode	Negative mode
LPC, PC	$[M + H]^+$, $[M + Na]^+$	$[M–H]^–$, $[M + HCOO]^–$, $[M + CH_3COO]^–$
LPE, PE	$[M + H]^+$, $[M + Na]^+$	$[M–H]^–$
PG	$[M + H]^+$, $[M + NH_4]^+$, $[M + Na]^+$	$[M–H]^–$
PI	$[M + H]^+$, $[M + NH_4]^+$, $[M + Na]^+$	$[M–H]^–$
PS	$[M + H]^+$	$[M–H]^–$
PA		$[M–H]^–$
CE	$[M + NH_4]^+$, $[M + Na]^+$	
SM	$[M + H]^+$	$[M + HCOO]^–$, $[M + CH_3COO]^–$
Cholesterol	$[M–H_2O+H]^+$	
MG, DG, TG	$[M + NH_4]^+$, $[M + Na]^+$	
MGDG, DGDG, SQDG	$[M + NH_4]^+$, $[M + Na]^+$	$[M–H]^–$
Fatty acids		$[M–H]^–$
CL	$[M + H]^+$, $[M + NH_4]^+$, $[M + Na]^+$	$[M–H]^–$, $[M–2H]^{2–}$
Cer, GluCer, LacCer	$[M + H]^+$, $[M + NH_4]^+$, $[M + Na]^+$	$[M–H]^–$, $[M + HCOO]^–$, $[M + CH_3COO]^–$

Reproduced with permission from [12,51]. MGDG: monogalactosyldiacylglycerol, DGDG: digalactosyldiacylglycerol, SQDG: sulfoquinovosyl diacylglycerol

3.3.1 Fatty acyls

3.3.1.1 Fatty acids

Fatty acids are analyzed in negative mode. Under typical mobile phase conditions carboxylate anions $[M-H]^-$ are formed and analyzed. For saturated fatty acids fragmentation by CID yields typically only the product ion $[M-H_2O-H]^-$.

Considerably more fragments can be obtained for polyunsaturated carboxylate anions, which may give information about the position of double bonds. For polyunsaturated fatty acids, for example, $[M-CO_2-H]^-$ is typically yielded [11].

3.3.1.2 Acyl carnitines

Acyl carnitines are analyzed in positive mode. The tandem mass spectra of ACs are characterized by the presence of high abundant m/z 85 which is explained as the result of two neutral losses. The first one is the neutral loss of fatty acid and the second one the loss of trimethylamine. The fragment produced by direct neutral loss of trimethylamine can also be observed (see Figure 3.7).

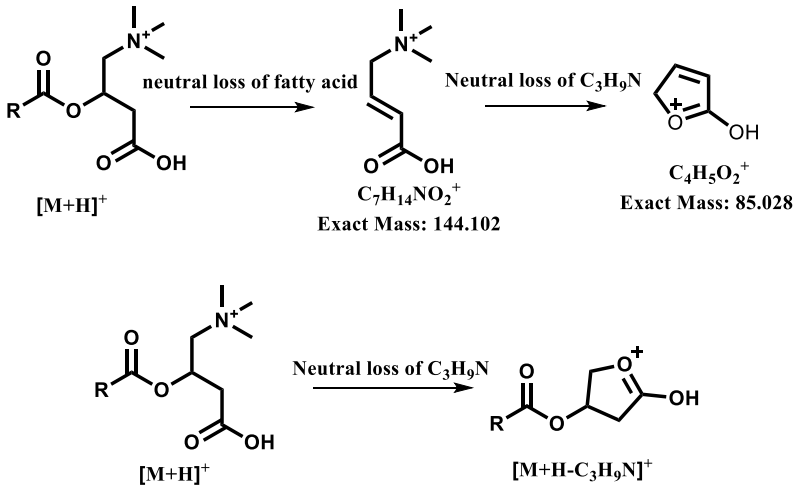

Figure 3.7. Common fragments of acyl carnitines in positive mode

3.3.2 Glycerolipids

Glycerolipids are, with a few exceptions, neutral lipids. Therefore, their characterization is made somewhat more challenging. In most of the cases, the formation of ions for glycerolipids requires the attachment of species like H^+, NH_4^+ or an alkali metal such as Na^+ or Li^+. Therefore, fragmentation studies of glycerolipids are mainly performed in positive mode.

3.3.2.1 Triacylglycerol (TG)

Fragmentation of ammonium adduct of TG yields a product ion spectrum consisting of $[M+H]^+$ and diglyceride-like product ions for each of the unique fatty acyls attached to the glycerol moiety. Figure 3.8 shows the most common fragments observed after CID of TG, which correspond to neutral losses of ammonia and neutral losses of the three acyl chains [11,52–54].

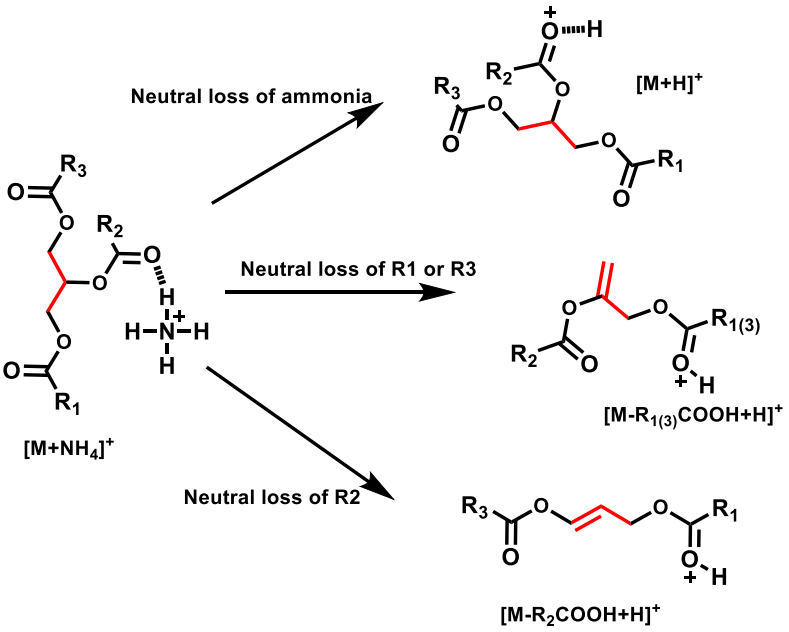

Figure 3.8. Typical product ions of TGs

3.3.2.2 Diacylglycerol (DG)

In the case of DG similar losses to the ones described for TG occur. One additional product ion corresponding to the loss of water and ammonia (loss of 35 Da) is present (Figure 3.9) [11,52–54].

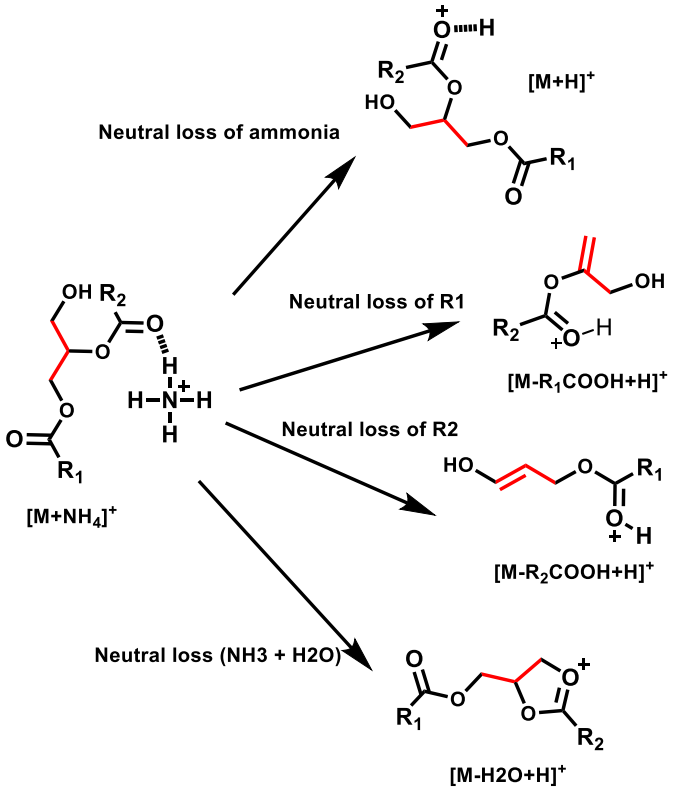

Figure 3.9. Typical product ions of DGs

3.3.2.3 Monoacylglycerol (MG)

Collisional activation in the case of MG leads to the corresponding acylium ion of carboxylate (see Figure 3.10) [11].

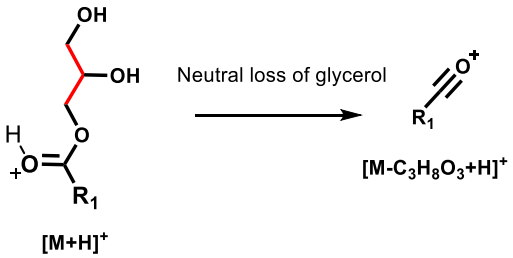

Figure 3.10. Acylium product ion of carboxylate in MGs

3.3.3 Glycerophospholipids

Glycerophospholipid are characterized by the presence of a phospho group esterified to the *sn3* position of glycerol moiety. Different groups attached to the phospho group produce different lipid classes. The phospho group in combination with this substituent is called headgroup and it determines the characteristics of the spectrum for that lipid class [1].

ESI ionization forms both positive and negative molecular species $[M+H]^+$ and $[M-H]^-$ for most glycerophospholipids. However the abundance of these ions in positive and negative mode depends strongly on the corresponding headgroup [11,55].

The decomposition of the positive ion species reveals information typically about the polar headgroup since each of the phospholipid classes specifically decompose to unique product ions. Analysis of product ions generated by CID of $[M-H]^-$ gives information about the radyl groups [11,55].

3.3.3.1 Analysis of positive ions for phospholipids

The most abundant product ion for GP, in positive mode, is obtained after the cleavage of phosphoester bond from the glycerol moiety. This process can produce two results: the case where the net positive charge is located in the polar phosphorylated headgroup and the diglyceride-like fragment is neutral, as it occurs in PCs with the typical fragment with m/z 184.07 (phosphocholine), or a second possibility where diglyceride-like fragment is charged and the polar headgroup is neutral, as it occurs in PE, PS, PG, PI and PA, with typical neutral losses of 141, 185, 172, 260 and 96 Da, respectively (see Figure 3.11) [55].

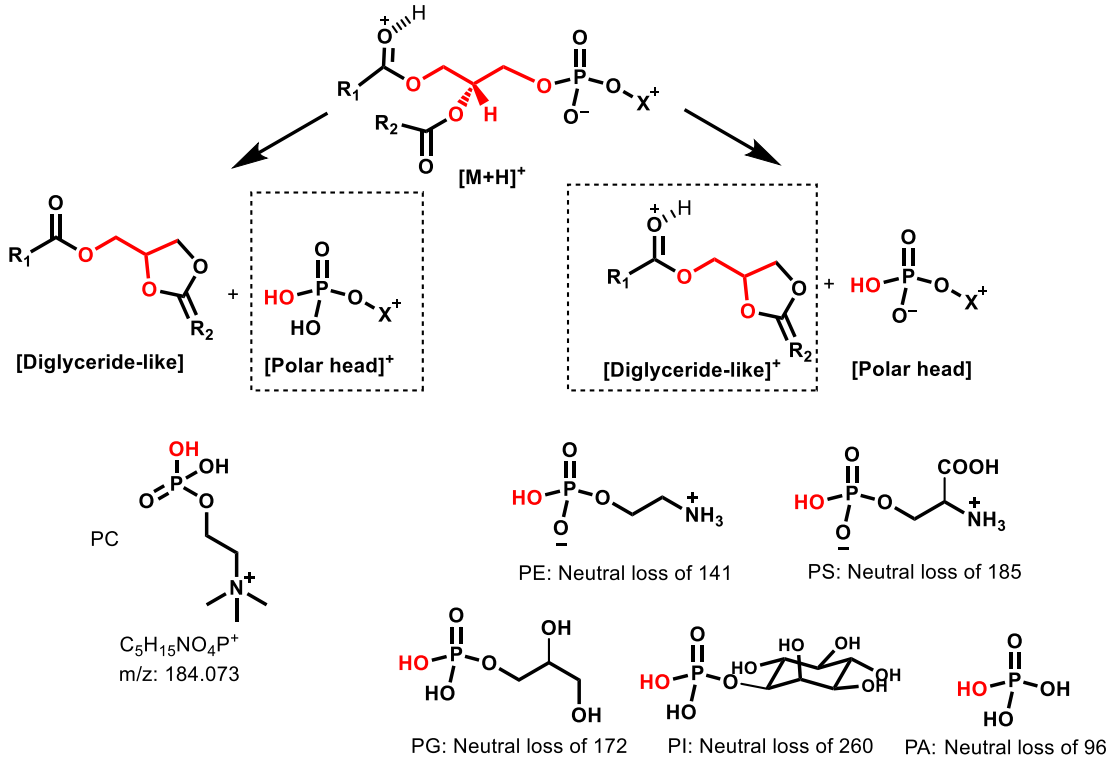

Figure 3.11. Loss of polar headgroups for $[M+H]^+$ ions of glycerophospholipids

3.3.3.2 Analysis of negative ions for phospholipids

Negative $[M-H]^-$ or adducts are common for glycerophospholipids. In the case of PC, negative ions are originated from an adduct ion with acetate, formate, chloride or other anionic adduct. This anionic group can produce a demethylation reaction forming methyl acetate, methyl formate, methylchloride or other. This means that an abundant product ion $[M-15]^-$, corresponding to the loss of methyl, is present in the spectrum of PCs. For further fragmentation, this product ion $[M-15]^-$ of PC behaves similar to the $[M-H]^-$ precursor ions of the other phospholipids [55].

The most prominent fragment ions formed after collisional activation of [M-H]- (or [M-15]- for PC) are derived from the fatty acyl ester groups as carboxylate anions (Figure 3.12). In another process, anionic phosphate can attack a 2-acyl proton in either *sn1* or *sn2* ester moiety to yield the loss of a neutral ketene (Figure 3.13). A third kind of fragment, observed in tandem spectra of [M-H]-, occurs after neutral loss of fatty acids at position *sn1* or *sn2* (Figure 3.14) [11,56,57].

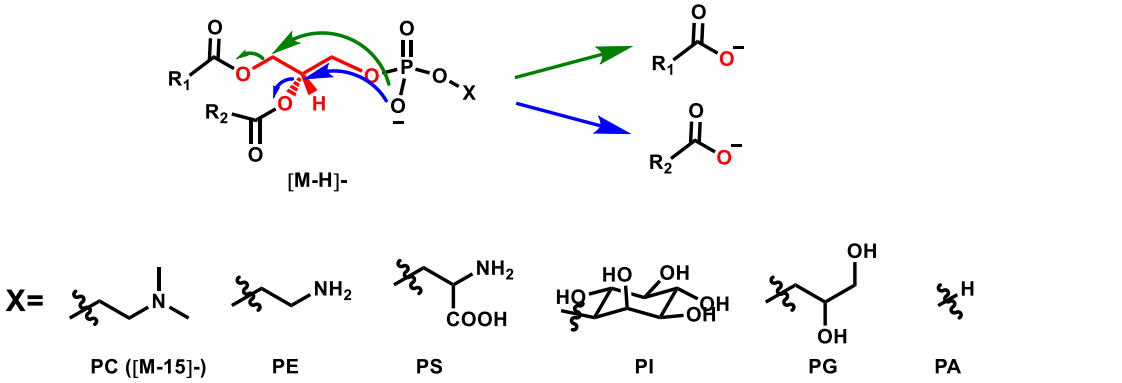

Figure 3.12. Mechanism for formation of carboxylate anions from [M-H]- of phospholipids.

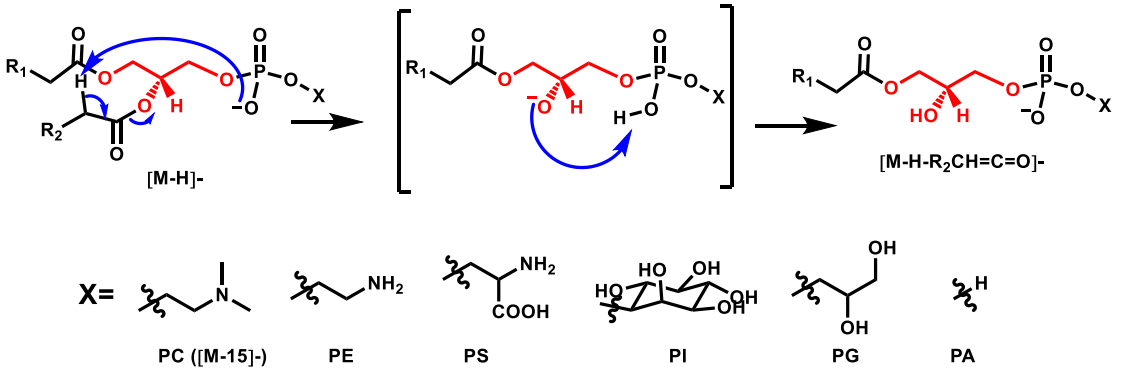

Figure 3.13. Mechanism for loss of neutral ketenes (RxCH=C=O) from [M-H]- of phospholipids

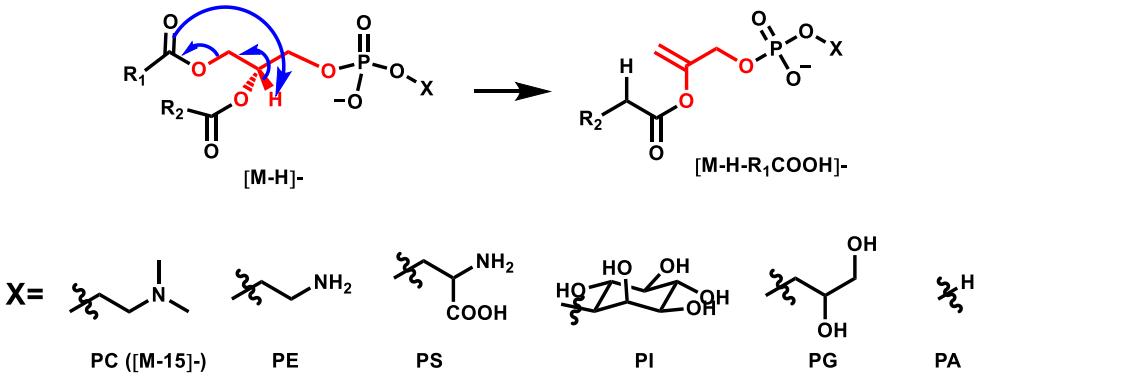

Figure 3.14. Mechanism for loss of R_xCOOH from [M-H]- of phospholipids.

In addition to the product ions described for the different phospholipids, there are some of them, which are particular for some lipid classes. For example, in the case of PS a neutral loss of serine residue forms an ion identical to that of phosphatidic acid which is very prominent, and it is described as $[M-H-87]^-$ [11,56,57].

3.3.4 Sphingolipids

Sphingolipids are a major category of lipids which contain a long-chain sphingoid base, such as sphingosine or sphinganine, as a structural unit. Here, fragmentation patterns of three of the most important classes of sphingolipids will be discussed [11,52–54].

3.3.4.1 Ceramides

Ceramides form both positive ($[M+H]^+$) and negative ($[M-H]^-$) molecular ions easily. The most abundant product ion formed after CID of $[M+H]^+$ corresponds to cleavage of amide bond and loss of one or two molecules of water, which produces the ions called N' and N'', respectively. Additionally, ceramides produce fragment ionsdue to the loss of one or two molecules of water. Another interesting fragment ion corresponds to the loss of water followed by the loss of a neutral formaldehyde molecule (See Figure 3.15) [11,52–54].

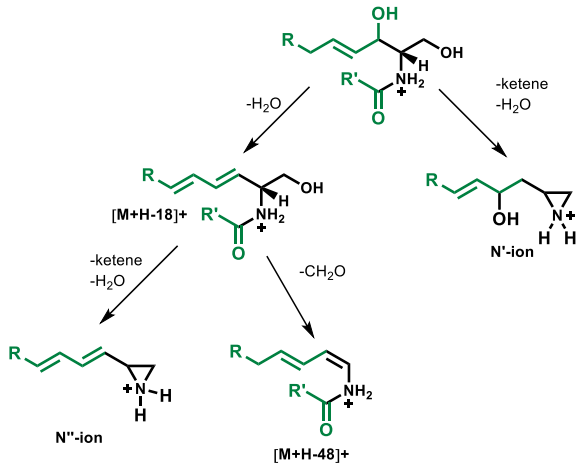

Figure 3.15. Common fragments after CID of $[M+H]^+$ of ceramides

CID of negative ions $[M-H]^-$ of ceramides yields a few product ions which are described with specific alphabetic letters. These fragments, represented in Figure 3.16, allow to confirm not only the length of sphingoid base but also the *N*-acyl chain.

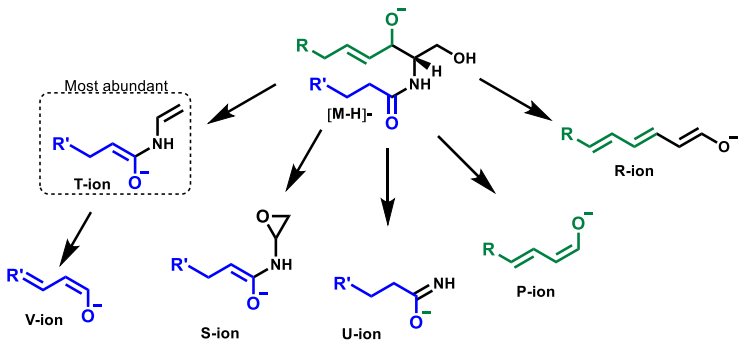

Figure 3.16. Common fragments after CID of $[M-H]^-$ of ceramides

3.3.4.2 Sphingomyelins

As in the case of PC, CID of $[M+H]^+$ of sphingomyelins is dominated by the m/z 184, which corresponds to the loss of positively charged phosphocholine. In ESI negative mode, SM form adducts with formate, acetate or chloride, which drive the loss of a methyl group and the corresponding [M-15]- product ion. Collisional activation of $[M-15]^-$ yields a product ion at m/z

168 and m/z 79 corresponding to the formation of *N*-dimethylaminoethylphosphate and HPO_3^- [11,52–54].

3.3.4.3 Hexosylceramides

Fragmentation of hexosylceramides shows similarities with that of ceramides. Figure 3.17 shows the most common product ions observed after CID of $[M-H]^-$ of hexosylceramides [11,52–54].

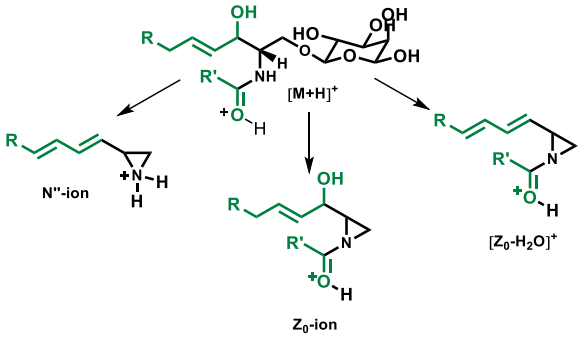

Figure 3.17. Common fragments after CID of $[M+H]^+$ of hexosylceramides

3.3.5 Sterols

3.3.5.1 Cholesteryl esters

CE lipids form charged adducts with NH_4^+ or Na^+ dependent on the abundance of these cations in the electrospray solvent. CID of $[M+NH_4]^+$ generates a spectrum which is dominated by the product ion with m/z 369 which corresponds to the cholestene cation, which is also common after CID of cholesterol [11]. As in the case of glycerolipids, fragmentation studies for CE are mainly performed in positive mode.

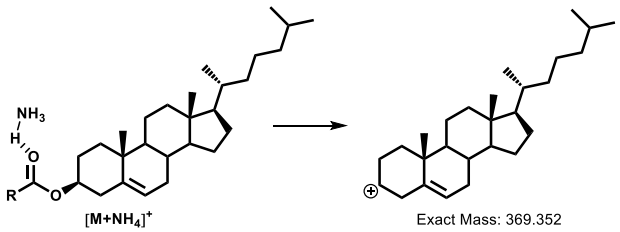

Figure 3.18. Common fragment after CID of $[M+NH_4]^+$ of cholesteryl esters

4 Lipidomics

Lipidomics is defined as the "comprehensive characterization of lipids in biological systems" [58]. In fact the concept of lipidome appeared in literature before and it was described as "the entire collection of chemically distinct lipid species in a cell, an organ, or a biological system" [59]. It is estimated that the lipidome can consist of over 100 000 unique structures [60]. General workflows for lipidomic analysis consist of sample preparation, extraction, measurement and data processing.

4.1 Sample preparation

Sample preparation is a key step in lipid analysis and it is responsible for most of the variability of results. For the sample preparation protocol, it is important to consider the approach for analysis of lipids that will be employed afterwards. Thus, for example, the presence of contaminants is more critical in shotgun lipidomics than in LC-MS approaches, since this could produce a higher ion suppression effect in direct infusion. In the case of LC-MS based approaches, different elution times for contaminants and analytes of interest reduce the effect of their presence [1,61].

For the sampling process, it is important to avoid contamination of other materials in the sample of interest (e.g. presence of blood in tissue samples). Also, it is very important to consider which kind of normalizer will be used for the sample. Typical normalizers are wet weight, dry weight, cell counting, protein content, DNA content or creatinine content, etc [62].

In current analysis methods, the amount of sample required is relatively small, therefore, special care must be taken to ensure that the used amount of sample is representative to the entire source material. Typical amount of samples used for lipidomics analysis are 1-100 mg of wet tissue, a million of cells (with exceptions for small sized cells), 5-500 µL of plasma [51].

It is recommended to extract samples as soon as possible, to avoid changes during storage. Yang *et al.* [63], for example, have demonstrated how storage of plasma samples, at 4 °C during 24 h, is enough to produce significant changes in the concentration of some lipids (see Figure 4.1). If storage is required, samples must be frozen rapidly with dry ice or liquid nitrogen and stored in glass container at -20 °C or lower temperature, under nitrogen atmosphere [5,61,64,65].

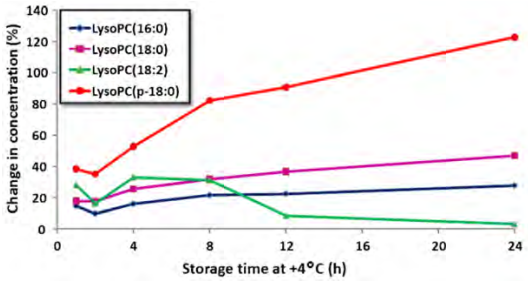

Figure 4.1. Change in the level of LPCs, from plasma samples extracted at different time points after storage at 4 °C. Reproduced from [51,63].

Hydrolysis and autoxidation of lipids should be kept under control during the whole analysis workflow. Lipolytic enzymes, for example can hydrolyze lipids during prolonged storage at −20 °C, therefore it is suggested to homogenize and extract tissue samples at the lowest temperature applicable [66]. Acidic pH can also effect hydrolysis of fatty acid residues [66] and because of that only in particular cases, addition of acids is considered an alternative for improving extraction of some lipid classes. In the case of autoxidation, the contact with the air, especially for lipid extracts, must be avoided. Handling under nitrogen atmosphere and the addition of antioxidants such as butylated hydroxytoluene (BHT) are recommended [61].

4.2 Extraction

Many aspects must be considered while designing a lipid EP. As shown before, lipids can be very diverse in terms of polarity and EPs cover only a portion of all lipid classes. Therefore, the choice of a solvent for lipid extraction determines which kind of lipids will be mainly recovered from the sample [58].

The type of sample and the location of the lipids in the sample can be also critical since some lipids have some association with proteins and polysaccharides in some parts of the cell. The interaction between lipids and those components can be in the form of van der Waals' forces, hydrogen bonds or ionic bonds [1].

4.2.1 Biphasic extraction protocols

Most widely employed protocols for extractions of lipids have been based on biphasic systems. The strategy has been to employ a ternary mixture of solvents for extraction. After that, additional amount of the two solvent with higher difference in polarity are added in order to create a biphasic system, which contains the extracted lipids in the organic layer, while the rest of components in the sample remains in the aqueous layer.

4.2.1.1 Extraction with $CHCl_3$

Two EPs with the system chloroform-methanol-water ($CHCl_3$-MeOH-H_2O), were introduced in 1950s and they have been used extensively as "gold standards" methods for extraction of lipids. These two methods, known as Folch [67] and Bligh & Dyer [68], possess together more than 80 000 citations to date.

In the case of the Folch protocol, it is based on the use of a mixture of chloroform/methanol (2:1, v/v) for extraction of lipids, then water or 0.9% NaCl is added to wash the solvent extract.

In the Bligh and Dyer protocol, chloroform/methanol/H_2O (1:1:0.9, v/v/v) is used for extraction.

Some disadvantages of these protocols include the use of chloroform, which is very toxic and difficulty for collecting the chloroform extract from the bottom layer, which cause some contamination of the lipid extract.

4.2.1.2 Extraction with hexane

A less toxic alternative with hexane-isopropanol-water (Hexane-IPA-H_2O) was proposed in 1978 by Hara *et al*. [69]. However, in many comparisons the recoveries for polar lipid classes with this EP showed to be low.

4.2.1.3 Extraction with MTBE

An EP with the system MTBE-methanol-water (MTBE-MeOH-H_2O) [70] was introduced in 2008 and it has become popular because in comparison to the protocols with $CHCl_3$, they have similar or even better performance, the extraction is easier and the solvents are less toxic.

MTBE method employs a ratio MTBE/methanol/water 5:1.5:1.45, (v/v/v). This method has the advantage that, at the moment of the phase separation, the organic layer is located in the top, which makes its removal and automation easier. A drawback is that the MTBE phase contains a significant amount water which can cause carry-over problems.

4.2.1.4 Extraction with BUME

A protocol with the mixture butanol-MeOH-H_2O was proposed in 2012 [71]. This method is called BUME because of the organic solvents present in the extraction mixture. The method showed similar or better recoveries than Folch method for specified lipid classes. This method has also the advantage that organic phase after the extraction is located in the top layer, as in the case of MTBE extraction.

4.2.2 Monophasic extraction protocols

Biphasic systems offer the advantage of eliminating polar interferences in the aqueous layer, which can interfere with the performance of the techniques for analyzing the lipids. However, when LC-MS and especially RPLC-MS approaches are employed, polar impurities can be separated during elution and the use of monophasic systems are an alternative for lipid extraction.

Some monophasic mixtures like $CHCl_3$:MeOH (2:1 v/v) [72,73] and 1-butanol/methanol (1:1 v/v) [74] have been reported for lipidomics studies on plasma samples, and $CHCl_3$:MeOH (1:2 v/v) has been used for sphingolipids analysis in mammalian cells [75,76]. In all the cases good recoveries have been reported.

4.2.2.1 Case of isopropanol

Aqueous isopropanol is another case of monophasic mixture which has been used for extraction of lipids, particularly on microalgae [77]. As mentioned previously isopropanol has also been used in the system hexane-isopropanol-water for extraction of lipids [58,74,78–83], reporting low recoveries for some lipid classes. However, it must be indicated that in this ternary system, two phases are present and the organic layer (employed for the analysis of lipids) is composed mainly of hexane and only a small portion of isopropanol. It means that most of the isopropanol is discarded as part of the aqueous layer.

4.3 Sample analysis

4.3.1 MS based lipidomics approaches

Mass spectrometry with ESI source is undoubtedly the most important analytical tool for analysis of lipids. There are, within MS, two different approaches for the measurement of samples. These two main approaches are differentiated in the form how lipid extract solutions are introduced in the mass spectrometer. The first approach is direct infusion, also known as shotgun lipidomics, and the second one is LC-MS based lipidomics which incorporates the use of LC for the analysis [1]. To date these two approaches have similar popularity.

4.3.1.1 Shotgun lipidomics

In shotgun lipidomics, the lipid extract is continuously injected, at a fixed flow rate, to the ESI source and ionization occurs while keeping constant the concentration of lipids [35]. One of the disadvantages in general for shotgun lipidomics is that in-source fragmentations may compromise the analysis for certain lipid classes [84]. There are three main approaches for

shotgun lipidomics, which are defined as tandem MS, high resolution MS-based and multidimensional MS-based shotgun lipidomics [85].

4.3.1.1.1 Tandem MS shotgun lipidomics

Conventional shotgun lipidomics is performed by tandem MS analysis of lipid classes using PIS and NLS experiments with low resolution instruments. Advantages of this kind of shotgun lipidomics include simplicity, efficiency, ease of management, and less expensive instrumentation [35]. However, some disadvantages of this approach are among others that the detection in some specific experiments (PIS or NLS) is not entirely specific for the lipid class of interest, the presence of isobaric lipid species limits identification, the fatty acyl (FA) substituents of lipid species are not identified and some irregularities in detection are not easily recognized during and after the experiments [35].

4.3.1.1.2 High resolution MS-based shotgun lipidomics

With the development of MS instruments and the improvements in sensitivity, resolution and accuracy, new possibilities of shotgun lipidomics were also implemented. One possibility has been high mass accuracy/resolution multi-PIS (or NLS) shotgun lipidomics [85–88] and the other one is the use of DDA and DIA (such as MS^{All}), which are supported by the development of software able to process the information from full MS scans and product ion spectra [89].

4.3.1.1.3 Multidimensional MS-based shotgun lipidomics

A last alternative has been called multidimensional MS-based shotgun lipidomics (MDMS-SL), which involves more than MS. This approach is based on the chemical and physical properties of each lipid class. For example, derivatization and selective extraction for specific lipid classes are some of the strategies included here.

4.3.1.2 LC-MS based lipidomics

LC-MS includes a separation step, which allows to reduce the complexity of the lipid mixture that is reaching the MS-source at any time. Also, new information in terms of retention can be used for identification of lipid species and finally low abundant species can be better analyzed since ion suppression is lower.

Most common MS experiments employed in LC-MS lipidomics are SRM (MRM), which is especially used for targeted quantification. Untargeted approaches with LC-MS employ high resolution instruments with combined experiments such as DDA and DIA (MS^E and SWATH).

As mentioned before, compared to direct infusion systems, HPLC uses retention time to increase specificity for lipid identification, but it complicates quantitation, because matrix effects and solvent composition are unique in each point of the chromatographic run and standardization is difficult [90].

4.3.2 NMR based analysis of lipids

NMR has been an important tool for analysis of lipids. It possesses some advantages in comparison to MS approaches, like nondestructive sample analysis, the possibility of direct quantitation, high reproducibility, possibility to obtain molecular dynamics information [5,91].

However, also some disadvantages like the low sensitivity and higher complexity of NMR spectra, due to overlapped signals, have to be mentioned [92].

^{1}H-, ^{13}C-, and ^{31}P-NMR and the corresponding 2D experiments are especially employed for structural analysis of lipids, but also for quantitative purposes [93].

In general, NMR represents a complementary tool to MS for analysis of lipids.

4.4 Processing of data

Depending on the strategy employed for lipid analysis, the processing of the data has different grades of complexity. Here, a brief description of the steps required for processing of untargeted data, obtained after LC-MS analysis with DIA (MS^E or SWATH) will be discussed.

A first step consists of filtering and feature detection, with data obtained from the MS Survey Scan. In this step, a list of recorded m/z values for ions that exceed a determined intensity threshold is obtained for each sample. These features, described by their retention time, m/z value and signal intensity, can be further analyzed and compared between different samples. In order to compare them, an alignment step is required previously. Since the retention time and m/z values measured for the same ionic species in deferent samples are not exactly the same, the alignment checks, within defined tolerances, which ones correspond to the same lipid.

The comparison of features from different samples is performed on the intensity values. However, these values must be normalized. The idea of normalization is to control unwanted systematic deviations produced by factors during measurements or sample-preparation steps [12,51,64,94].

4.4.1 Deconvolution

As explained before, when a PIA experiment is performed, precursor ions within a window of m/z values, are filtered and transferred to a collision cell, where fragmentation occurs.

Generated product ions are analyzed afterwards in a second analyzer. The complexity of the obtained product ion spectra depends on the amount of different precursor ions selected in the first analyzer, which is directly related with the size of the employed m/z window. The usefulness of the experiment resides here in the capacity to connect information of precursor and fragment ions, it means in determining which fragments are coming from each precursor ion. If this is accomplished, identification of species can be done with information of product ions but also more selective quantitative information can be obtained from product ions. In LC-MS, a deconvolution process is applied for achieving this goal. The principle of the deconvolution is to analyze the elution profile of precursor ions (from the survey scan experiment) and fragment ions (from the corresponding PIA experiment), to determine their relationship. A similarity score for the elution profiles is calculated and when a threshold is reached, a fragment ion is assigned to the corresponding precursor ion. Cases where two or more species have total coelution cannot be solved with this algorithm. Also, it is challenging the analysis of common product ions coming from coeluting species, especially for the low abundant ones. Figure 4.2 illustrates the process of deconvolution.

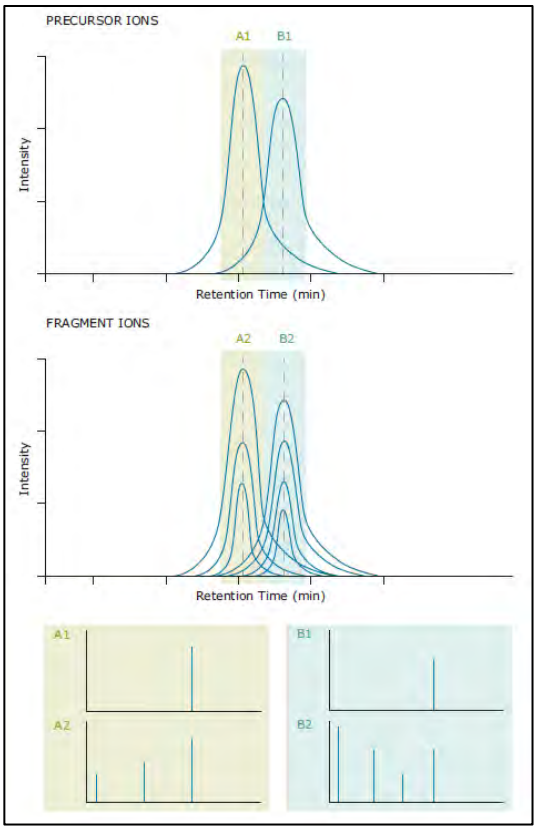

Figure 4.2. Example of deconvolution in cases of chromatographic coelutions. By courtesy of Waters GmbH [95]

4.4.2 Identification

Until now, it has been explained how to make a comparison of a feature, described in terms of m/z and retention time, based on its intensity. However, the most meaningful part comes in the

moment that is possible to describe that feature as a metabolite. For helping with this identification, different kinds of information can be collected and analyzed. The first and most powerful filter correspond to m/z of the precursor ion [96], which can remove up to 99.9% of the false candidates [96], and together with an analysis of the isotopic pattern allow to determine the formula of the molecular species. Retention time obtained from LC run can be very useful. In the case of NPLC or HILIC, the lipid class can be automatically determined. In the case of RPLC, elution pattern can be very useful for confirmation of identifications. However, it is through MS/MS spectra, that most of the identification can be done [5]. For this, proper deconvolution is required (see Figure 4.2). In the case of lipids, it was described in section 3.3, that most of the lipid classes have specific fragmentation patterns that allow to identify different components in the structure [94]. With proper knowledge, analysis of product ion spectra can lead to the identification, however, this labor is time consuming and requires a lot of expertise. Experimental and in silico lipid spectra databases have been created and algorithms have been developed for the comparison of experimental and stored product ion spectra [27,97].

With the use of MS/MS, the lipid class, length of carbon chains, and number of double bonds in each radyl chain can be annotated. Positions of double bond and position of *sn* in glycerol moiety are difficult to distinguish by MS/MS. Therefore, structures are usually reported at this lower level of annotation [12].

5 Chiral lipidomics

Considering the wide variety of cellular function in which lipids participate, it is important to determine their molecular structure as accurate as possible [98].

As it has been described above, MS techniques allow to obtain a lot of information in this regard. Figure 5.1 shows for example the level of identification that can be reached with information supplied by MS and MS/MS experiments [99].

It is important to highlight that proper guidelines have been established for the identification process in order to avoid misannotation of lipids [10,65,100].

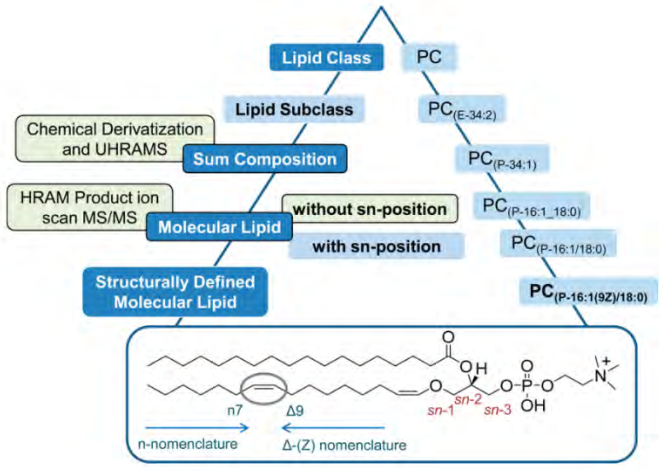

Figure 5.1. Hierarchy of lipid identification and characterization. Reproduced with permission from [99]

Nevertheless, MS suffers limitations to distinguish between structural isomers. There is often incomplete information to decide when the mass spectral signals correspond to a single molecule or isomeric mixture [60]. Some of the specific limitations concern the position of each radyl esterified to the glycerol backbone (*sn* position), the position of the double bond within the fatty acyl chains and stereochemistry of the double bonds (E/Z) or other functionalized carbons (R/S) [98].

Different approaches have been reported in order to solve those issues. However, these approaches are time consuming, require normally abundant amount of sample and they can be done only in targeted approaches for a small amount of samples. Therefore, they are not available for high-throughput lipidomic analyses [98].

Silver-ion chromatography for example has been used in the separation of double-bound isomers, cis- and trans-isomers, or regioisomers of TG, since they form weak complexes with the silver ions in the SP [12].

5.1 Use of chiral chromatography

Chiral chromatography has been specially employed in lipidomics for the analysis of chiral isomers of eicosanoids, MG and DG [1].

Eicosanoids are compounds produced after oxidation of polyunsaturated fatty acids (PUFA). It has been demonstrated that these compounds play an important role in many biological processes in renal, reproductive and cardiovascular systems [101].

The oxidation of PUFAs can be done in organisms via enzymatic or non-enzymatic reactions with oxygen reactive species. In the case of enzymatic oxidation almost pure enantiomers are usually obtained, whereas in the case of oxidation with free radicals racemic mixtures are commonly produced. For this reason, oxygenated PUFA derived from non-enzymatically reactions are used as biomarkers of oxidative stress and tissue damage [101].

Because of the involvement of these oxygenated PUFA in biological processes and because their biological activity is mostly linked to one specific enantiomer, chiral stationary phases (CSP) have been developed and employed for their analysis.

Polysaccharide-based CSPs have been especially used in this regard, they have good chiral recognition towards oxygenated PUFAs. Additionally these CSPs are compatible with normal- and reversed-phase elution modes [101].

5.2 Case of short chain hydroxy fatty acids

Short chain hydroxy fatty acids (SCHFA) are a relatively small group of fatty acids, which contain less than 10 carbons with one hydroxyl group along the chain. The presence of the hydroxyl substituent in the alkyl chain generates in most of the cases a stereogenic center and hence the occurrence of enantiomers.

Some SCHFA are known for their relationship with particular human diseases, some of them inherited metabolic disorders. Therefore, the analysis of these small lipids has become an important issue in areas such as biochemistry and clinical chemistry.

The enantioseparation of SCHFA is challenging in chiral chromatography since it is difficult to establish enough interaction points between chiral selector and surroundings of the stereogenic center [102].

AIM OF THE WORK

The general aim of this thesis was to develop improvements in methodologies for analysis of lipids.

In a first study, the goal was to evaluate the most critical steps in an LC-MS lipidomic workflow. In this regard sample preparation and particularly extraction protocols are critical because they have high incidence in the variability of results and because they determine the main classes of lipids that will be analyzed. The proposal was then to evaluate four lipid extraction protocols in terms of lipid recoveries, precision of results and complexity of protocols, in order to determine proper conditions for lipidomic analysis of Hela cells.

In a second study, the goal was to evaluate and describe the changes on lipid profile of keratinocytes after the treatment with the compound betulin, which has proven wound healing effects. A challenge in this approach was the development of a strategy for data processing, especially for increasing the number of high confidence identifications while avoiding misidentifications that are common when some software packages are employed.

In a third study, the goal was to develop targeted methodologies for enantioseparation of short chain hydroxy fatty acids (SCHFA). In this regard a list of chiral SCHFA involved in critical biological processes but especially with inherited diseases, was identified. The idea was to evaluate a set of quinine- and quinidine- chiral stationary phases in order to obtain baseline resolution with chromatographic conditions that are compatible with MS analysis for the chiral analysis of SCHFA.

RESULTS AND DISCUSSION

6 Publication I. Comparison of lipid extraction protocols

6.1 Title

Comparison of simple monophasic versus classical biphasic extraction protocols for comprehensive UHPLC-MS/MS lipidomic analysis of Hela cells

Carlos Calderón[1], Corinna Sanwald[1], Jörg Schlotterbeck[1], Bernhard Drotleff[1], Michael Lämmerhofer[1]*

[1]Institute of Pharmaceutical Sciences, Pharmaceutical (Bio-)Analysis, University of Tübingen, Auf der Morgenstelle 8, 72076 Tübingen, Germany

Reprinted with permission from Analytica Chimica Acta, Volume 1048, Pages 66-74,

DOI: 10.1016/j.aca.2018.10.035

Copyright (2018) Elsevier B.V.

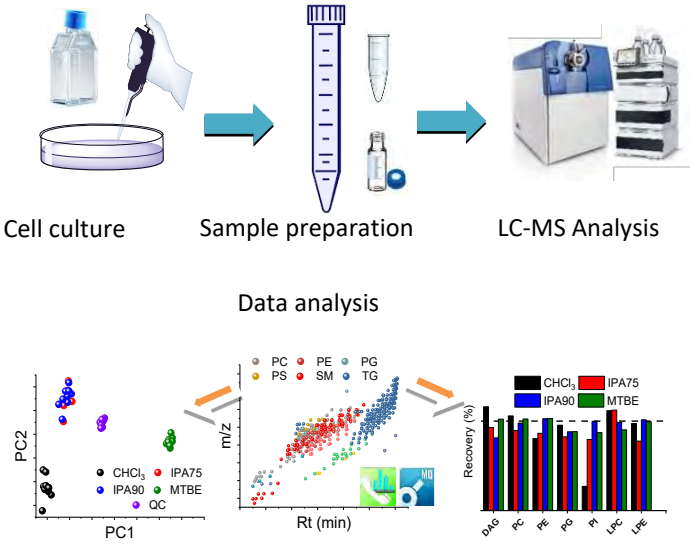

6.2 Abstract

In this study, two monophasic isopropanol-water mixtures (IPA:H_2O 75:25 v/v and IPA:H_2O 90:10 v/v) were compared with traditionally employed biphasic methods of Bligh & Dyer and Matyash *et al*. as extraction systems for lipidomics analysis in Hela cells. Samples were analyzed by UHPLC-ESI-QTOF-MS/MS in positive and negative mode using sequential window acquisition of all theoretical fragment ion spectra (SWATH) and a relatively new software (MS-DIAL) was employed for the processing of the data which includes detection of peaks, MS/MS spectra deconvolution, identification of detected lipids and alignment of peaks through the analyzed samples.

The studied performance parameters such as precision, recoveries of isotopically labeled internal standards and endogenous lipids, number of extracted lipids, and complexity of employed procedure showed that extraction with IPA:H_2O 90:10 v/v performs similar to the Matyash protocol and better than Bligh & Dyer as well as IPA:H_2O 75:25 v/v. However, less complex monophasic protocol which is simpler to implement and can be executed in plastic rather than glass, make the monophasic IPA:H_2O 90:10 v/v protocol an excellent alternative to the classical biphasic protocols for reversed phase LC-MS lipidomics studies.

6.3 Introduction

Liquid chromatography-mass spectrometry (LC-MS) has become the most widely used analytical tool for lipidomics analysis in the last few years [7,85,103,104]. Despite many reported publications on this topic, there is no consensus about the most adequate protocol to follow. One of the most critical points is the sample preparation and therefore the choice of a solvent or solvent mixture for the lipid extraction, since this will determine which lipid classes are mostly recovered from the sample [58]. Extractions with the system chloroform-methanol-water ($CHCl_3$-MeOH-H_2O), at specific ratios, were introduced more than six decades ago, with the pioneering works of Folch [67] and Bligh & Dyer [68], and have frequently been described as "gold standards" [28,70,81,103,105–107]. Hexane-isopropanol-water (Hexane-IPA-H_2O) was proposed in 1978 by Hara *et al*. as a less toxic option [69]. However, its performance in terms of wide coverage of distinct lipid classes is modest [80,82,83]. Recently, two methods using methyl *tert*-butyl ether-methanol-water (MTBE-MeOH-H_2O) [70] and butanol-MeOH-H_2O [71] were introduced and they have become popular because of their similar or even better performance, less tedious procedure for preparing the samples and less toxicity with respect to the chloroform mixtures.

Solvent mixtures have been suggested for lipid extraction after considering that most of the biological samples are composed of some amount of water and that the lipids are mainly soluble in organic solvents. Thus, the strategy for extractions of lipids has traditionally been based on two steps, a first one where a miscible solvent mixture (considering the water present in the sample) is added to the sample, which allows good interaction between solvent and sample matrix, and a second one where more aqueous or organic solvent or both are added to the original mixture in order to create a biphasic system which separates the extracted lipids, in the organic layer, from the rest of the sample, in the aqueous layer. However, considering that nowadays many workflows for lipidomics analysis include a reversed phase liquid chromatographic separation and polar interferences elute in the first minutes of the separation, the use of a biphasic system is not strictly required [61]. In 2017 Jurowski *et al.* [61] reviewed the use of some monophasic mixtures for lipidomics studies. Among the cited examples are $CHCl_3$:MeOH (2:1 v/v) [72,73], 1-butanol/methanol (1:1 v/v) [74] for plasma samples, $CHCl_3$:MeOH (1:2 v/v) for sphingolipids analysis in mammalian cells [75,76] and aqueous isopropanol for extraction of lipids on microalgae [77]. In 2014, Sarafian *et al*. [108] published a study showing a monophasic mixture IPA-H_2O as a good choice for lipid extraction of plasma samples with good recoveries for most of the lipid classes.

In this study, we evaluated the performance of monophasic isopropanol extraction in comparison to biphasic extraction protocols (EPs) in detail for lipid extraction from Hela Cells. No information about the suitability of this monophasic EP for mammalian cells and how it compares to classical EPs was available. Thus, two IPA-H_2O mixtures (75:25 v/v and 90:10 v/v) were compared with the biphasic extraction systems: $CHCl_3$-MeOH-H_2O (2:2:1.8 v/v/v, Bligh & Dyer) [68] and MTBE:MeOH:H_2O (10:3:2.5, v/v/v, Matyash) [70], which currently are two of the most widely employed protocols for lipid analysis [81–83,106,109–112].

6.4 Materials and Methods

6.4.1 Materials

Mobile phases were prepared with solvents of LC-MS grade. Methanol (MeOH), acetonitrile (ACN) and isopropanol (IPA) were supplied by Roth (Karlsruhe, Germany). As additive, formic acid (FA, 98%) was obtained by Carl Roth (Karlsruhe, Germany) and ammonium formate was purchased from Sigma–Aldrich (Steinheim, Germany). Water was purified by a water filtration system from Elga (High Wycombe, United Kingdom).

Solvents for extraction were of HPLC grade: chloroform ($CHCl_3$, ≥ 99.8%) and tert-butyl methyl ether (MTBE, anhydrous, 99.8%) from Sigma-Aldrich.

SPLASH™ Lipidomix® solution containing the following isotopically labeled internal standards (ILIS): 15:0-18:1(d7) PC, 15:0-18:1(d7) PE, 15:0-18:1(d7) PS, 15:0-18:1(d7) PG, 15:0-18:1(d7) PI, 15:0-18:1(d7) PA, 18:1(d7) LPC, 18:1(d7) LPE, 18:1(d7) Chol Ester, 18:1(d7) MG, 15:0-18:1(d7) DG, 15:0-18:1(d7)-15:0 TG, 18:1(d9) SM, Cholesterol (d7) was obtained from Avanti Polar Lipids (Alabama, USA) (See Suppl. Table 6.1 for more information about internal standards).

6.4.2 Cell culture

The human cervical cancer HeLa cells adapted to serum free conditions (AC free, ECACC 08011102) were grown in T75-flask and EX-CELL HeLa serum free media (Sigma Aldrich) supplemented with 2 mM L-glutamine (Sigma Aldrich), until they reached a density of around 2-3 x 10^6 cells/mL. Afterwards they were transferred to 50 mL falcon tubes and centrifuged for 5 min at 700 rcf, before the supernatant was discarded. The cell pellet was resuspended in 15 mL ice-cold Dulbecco's Phosphate Buffered Saline (PBS, Sigma Aldrich) for washing and centrifuged again for 5 min at 700 rcf. The washing was repeated twice and after the last resuspension cells were counted in triplicate with a hemocytometer. According to the mean of the counted cells, aliquots containing approximately 8 x 10^5 cells were transferred randomly to 15 mL falcon tubes (for extraction with isopropanol mixtures) and 15 mL glass tubes (for extractions with $CHCl_3$ and MTBE). Samples were centrifuged at 700 rcf for 5 min and the pellets were stored at -80 ºC until extraction.

6.4.3 Extraction protocols

Extraction solvents were kept on ice before their addition to the samples. For each EP, 10 samples (pellets containing 8 x 10^5 cells) were extracted. In order to estimate the recovery of some lipid classes, 5 of these samples were spiked before the extraction with 100 µL of 5 % v/v SPLASH Lipidomix solution in methanol and were resuspended with 100 µL MeOH before the LC-MS measurement (pre-extraction spiking). For the other 5 samples 100 µL of MeOH were added before the extraction and they were resuspended with 100 µL of 5 % v/v SPLASH Lipidomix solution before the LC-MS measurement (post-extraction spiking). Recoveries were calculated as ratio of average intensities for internal standards in the pre-extraction and post extraction spiked samples.

6.4.3.1 Extraction with MTBE:MeOH:H_2O (10:3:2.5, v/v/v, "MTBE")

This EP was based on Matyash *et al.* [70]. Either methanol or solution of 5% SPLASH Lipidomix in MeOH (100 µL) was added to the pellet. Then 1.4 mL of methanol and 5 mL of MTBE were added. Vortexing (30 s), ultrasonication (2 min) and vortexing (30 s) cycle was applied to disrupt the pellet. Samples were incubated on ice while shaking (500 rpm, 60 min). After the extraction,

1.25 mL of H_2O was added and samples were incubated on ice for another 10 min. Afterwards, centrifugation at 3500 rcf for 10 min was applied and the upper layer was transferred to a glass tube. Samples were dried in an evaporator (Genevac EZ-2; Warminster, Pennsylvania, USA) for 10 hours under nitrogen protection. The lipid extract was resuspended in 100 µL of either methanol or solution of 5% SPLASH Lipidomix while sonication (2 min) and vortexing (30 s) were applied. Centrifugation at 3500 rcf for 10 min was applied and the supernatant was transferred to vials for MS-measurements. During the last step, 10 µL aliquot of each sample were transferred to a separate vial to prepare a pooled QC sample.

6.4.3.2 Extraction with IPA:H_2O (75:25 v/v, "IPA75")

Either methanol or solution of 5% SPLASH Lipidomix in MeOH (100 µL) was added to the pellet. Then 5.0 mL of IPA:H_2O (75:25 v/v) were added. Vortexing (30 s), ultrasonication (2 min) and vortexing (30 s) cycle was applied to disrupt the pellet. Samples were incubated on ice while shaking (500 rpm, 60 min). After the extraction, centrifugation at 3500 rcf for 10 min was applied and supernatant was transferred to a 15 mL falcon tube. Samples were dried in an evaporator for 10 hours under nitrogen protection. The lipid extract was resuspended in 100 µL of either methanol or solution of 5% SPLASH Lipidomix while sonication (2 min) and vortexing (30 s) were applied. Centrifugation at 3500 rcf for 10 min was applied and the supernatant was transferred to vials for MS-measurements. During the last step, 10 µL aliquot of each sample were transferred to a separate vial to prepare a pooled QC sample.

6.4.3.3 Extraction with IPA:H_2O (90:10 v/v, "IPA90")

As described before for extraction with IPA75, only that IPA:H_2O (90:10 v/v) was used instead of IPA:H_2O (75:25 v/v).

6.4.3.4 Extraction with $CHCl_3$-MeOH-H_2O (2:2:1.8 v/v/v, "$CHCl_3$")

This EP was based on Bligh & Dyer [68]. Either methanol or solution of 5% SPLASH Lipidomix in MeOH (100 µL) was added to the pellet. Then, 0.8 mL of H_2O, 1.90 mL of MeOH and 1.0 mL of $CHCl_3$ were added. Vortexing (30 s), ultrasonication (2 min) and vortexing (30 s) cycle was applied to disrupt the pellet. Samples were incubated on ice while shaking (500 rpm, 60 min). After the extraction 1.0 mL $CHCl_3$ and 1.0 mL of H_2O were added and samples were incubated on ice for another 10 min. Afterwards, centrifugation at 3500 rcf for 10 min was applied and the upper layer was transferred to a glass tube. Samples were dried in an evaporator for 10 hours under nitrogen protection. The lipid extract was resuspended in 100 µL of either methanol or solution of 5% SPLASH Lipidomix while sonication (2 min) and vortexing (30 s) were applied. Centrifugation at 3500 rcf for 10 min was applied and the supernatant was transferred to vials

for MS-measurements. During the last step, 10 µL aliquot of each sample were transferred to a separate vial to prepare a pooled QC sample.

6.4.3.5 Blank extractions for all extraction protocols

Seven blank extraction replicates for each EP were performed following the same steps indicated above, only that extraction solvents were added to empty falcon or glass tubes. For further analysis, an additional IPA90 blank EP (also 7 replicates) was performed replacing plasticware with glassware. The results from these blank samples were used to correct the result from the cell extractions.

6.4.3.6 Extractions without internal standards

One cell extract for each EP was prepared following the same steps described before, but no ILIS were added. These samples were used to validate assay specificity for internal standards i.e. to check that no significant signals are present at m/z and retention times corresponding to the ILIS. For all EPs no signals i.e. no interferences were found.

6.4.4 LC-MS measurement

All analyses were performed on an Agilent 1290 Series UHPLC instrument (Agilent, Waldbronn, Germany) coupled to a Sciex TripleTOF 5600+ mass spectrometer (Sciex, Concord, Ontario; Canada). Duospray ion source for ESI in positive and negative ion mode was used. Sample injections were done in randomized order with a Pal HTC-XS autosampler from CTC (Zwingen, Switzerland). QC samples were run at the beginning of the sequence, during the sequence (every five samples) and at the end of the sequence.

Chromatographic separation was performed according to conditions published by Tsugawa *et al.* [113] in order to enable retention time scoring for peak identification with MS-Dial software. Briefly an Acquity UPLC CSH C18 Column, 130Å, 1.7 µm, 2.1 mm X 100 mm with an Acquity UPLC CSH C18 VanGuard Pre-column, 130Å, 1.7 µm, 2.1 mm X 5 mm (Waters, Eschborn, Germany) was used. The mobile phase was composed of 10 mM ammonium formate and 0.1 % formic acid in A) 60:40 ACN:H_2O (v/v) and B) 90:10 (v/v) IPA:ACN. The following gradient profile was used: 0.00 min, 15 % B; 2.00 min, 30 % B; 2.50 min, 48 % B; 11.00 min, 82 % B; 11.50 min, 99 % B; 12.00 min, 99 % B; 12.10 min, 15 % B, 15.00 min, 15 % B. Flow rate was 600 µL/min and column temperature was 65 °C. The injection volumes were 3 µL and 5 µL for positive and negative mode, respectively.

The following MS-settings of the mass spectrometer were used: Curtain gas (CUR) 35 psi, nebulizer gas (GS1) 60 psi, drying gas (GS2) 60 psi, ion-spray voltage floating (ISVF) +5500 V in

positive and -4500 V in negative mode, source temperature (T) 350°C, collision energy 45 V, collision energy spread 15 V, declustering potential (DP) 80 V, mass range m/z 50 – 1250 in ESI (+) and 50 – 1050 in ESI (-), and RF Transmission (RF) m/z 40: 50 % and m/z 120: 50 %. An external mass calibration was performed every five samples (see Suppl. Table 6.2).

MS data was obtained by using sequential window acquisition of all theoretical fragment ion spectra (SWATH) [114,115], after optimizing Q1 windows size (See Suppl. Table 6.3) with Swath Tuner software [116].

6.4.5 MS data processing

MS-Dial software (RIKEN, version 3.06) [113] was used to process the MS data (see parameters in Suppl. Table 6.4). This included detection of peaks, MS^2 data deconvolution, compound identification and alignment of peaks through all the samples. For identification a cut off value of 80% was selected: This value is based on 6 different similarity scores: 1 for retention time, 1 for m/z, 1 for isotopic pattern and 3 for MS/MS (dot product, dot product reversed and presence). An important condition established in MS-Dial was that a peak was selected for alignment only when it was present in at least 51% of the samples of one EP. Features which were relatively close (m/z difference less than 0.03 Da and retention time difference less than 0.1 min) in the alignment file of MS-Dial were visually inspected in order to determine if they are effectively corresponding to more than one feature, otherwise the repeated feature was removed. List of aligned peaks from MS-Dial were further evaluated with Multiquant 3.0 (Sciex). Intensities were processed for principal component analysis (PCA) with MarkerView (Sciex) and exported to Excel for statistical analysis. A feature was considered for comparison between the different EPs when it was present in at least 90 % of the samples of one EP having a CV less than 30% for the 10 extraction replicates of that protocol. Furthermore blank extraction samples were used to exclude features that have m/z difference less than 0.01 Da, retention time difference less than 0.5 min and fold change less than 5 between the cell extraction and blank extraction replicates (List of detected features in extraction blanks are in Appendix D).

Peaks corresponding to internal standards were removed from MS-Dial detected features and were analyzed directly with Multiquant to evaluate the recoveries.

6.5 Results and discussion

In order to compare the different EPs some modifications were introduced to the originally published protocols. Thus, extraction volumes were modified to be as similar as possible for all EPs while keeping the solvent ratios for each EP as they were published. Variables like temperature, vortexing time, vortexing intensity, centrifugation time and centrifugation speed

were kept the same for all EPs. For the same reason no re-extractions were done for any of the EPs. The solvent evaporation step was performed overnight to save time and it was kept at 10 hours even when the time required for the evaporation of each solvent ranges from less than 3 hours, in the case for $CHCl_3$ and MTBE, to approximately 6 hours, in the case of IPA75. Thus, all the extracts were kept under nitrogen atmosphere until resuspension to minimize possible oxidation of lipids.

6.5.1 Chromatograms and principal component analysis (PCA)

Total ion chromatograms (TICs) in positive and negative mode for extracted samples with different EPs (Figure 6.1) show a very similar profile with only some slight differences, especially during the first minutes. After processing the data with MS-Dial and Multiquant, peak intensities for detected features were analyzed by PCA (Figure 6.2). Score plots with the first two principal components, in both ESI (+) and ESI (-) mode (Figure 6.2A, 2C), show a clear separation between the samples extracted with each protocol, except for extractions with isopropanol 75% and isopropanol 90%, which are overlapped. This result indicates that the detected features and their corresponding intensities show significant alterations between the different EPs. Loadings plots, with the first two principal components, are shown in Figure 6.2B and 2D, for positive and negative mode respectively (for a better visualization, unknown features and lipid classes with less than five identified features were excluded from each loadings plot). In Figure 6.2B it is possible to note influences of some lipid classes to the shown differentiation of EPs in Figure 6.2A, for example LPE are oriented in the direction of $CHCl_3$ and PGs are oriented in the direction of the EPs IPA75 and IPA90, which means that those lipid classes are better extracted with the mentioned EPs. In the same manner, in Figure 6.2D, LPCs and LPEs are oriented in the same direction of the EP $CHCl_3$ and Cers are oriented in the direction of the EPs IPA75 and IPA90.

Table 6.1. Description of processed features with MS-Dial and Multiquant softwares

	ESI (+)					ESI (-)				
Description	**Total**	**$CHCl_3$**	**IPA75**	**IPA90**	**MTBE**	**Total**	**$CHCl_3$**	**IPA75**	**IPA90**	**MTBE**
Detected features in MS-Dial [1]	**1872**	904	893	928	1038	**1541**	708	674	718	1015
Detected features after processing with Multiquant[2]	**1382**	1110	1054	1118	1183	**1074**	824	759	771	906
Detected features after correction with blanks	**1167**	991 (85 %)	955 (82 %)	1003 (86 %)	985 (84 %)	**842**	777 (92 %)	713 (85 %)	725 (86 %)	701 (83 %)
Identified features	292	289 (99 %)	285 (97.6 %)	290 (99.3 %)	291 (99.7 %)	206	205 (99.5 %)	201 (97.6 %)	205 (99.5 %)	200 (97.1 %)
• **SM**	**29**	29	28	29	29	**22**	22	22	22	22
• **PG**	**6**	6	5	6	6	**10**	10	10	10	10
• **PE**	**29**	29	29	29	29	**55**	55	54	55	55
• **PC**	**88**	88	88	87	87	**43**	43	43	43	43
• **LPE**	**7**	7	7	7	7	**22**	22	20	22	20
• **LPC**	**4**	4	4	4	4	**11**	11	11	11	10
• **Cer-NS**	**12**	12	10	12	12	**6**	6	6	6	6
• **Cer-NDS**	**5**	5	5	5	5	**2**	2	2	2	2
• **TG**	**92**	89	89	91	92					
• **HexCer-NS**	**3**	3	3	3	3	**1**	1	1	1	1
• **DG**	**12**	12	12	12	12					
• **CE**	**2**	2	2	2	2					
• **BMP**	**3**	3	3	3	3					
• **PS**						**1**	1	1	1	1
• **PI**						**11**	11	10	11	11
• **OxPS**						**1**	1	1	1	1
• **OxPG**						**1**	1	1	1	1
• **OxPE**						**6**	6	5	5	5
• **OxPC**						**3**	3	3	3	3
• **LPI**						**2**	2	2	2	2
• **LPG**						**2**	2	2	2	2
• **HexCer-NDS**						**5**	5	5	5	5
• **FA**						**2**	1	2	2	0

[1] present in at least 51 % of samples of one group. [2] present in at least 90 % of samples of one EP having a CV < 30%

6.5.2 Number of detected features

Table 6.1 and Figure 6.3 show the numbers and distribution of features detected in ESI (+) and ESI (-) for the EPs (Specific data about detected features can be observed in Appendix B). Features list obtained after processing with MS-Dial was reprocessed with Multiquant. In this manner we are combining the capabilities of MS-Dial for recognizing features and the identification of approximately 15 % of them with the capabilities of Multiquant for a more controlled integration, making it easier to determine whether a feature is present or not in a

group of samples. After the processing with Multiquant and the feature filtration (only those features which are present in at least 90 % of the samples of one EP and have a CV less than 30 % for the replicates of that EP were selected) the number of features was reduced from 1872 to 1382 in ESI (+) and from 1541 to 1024 in ESI (-) but the number of features which were found with each EP was higher (See Table 6.1). Similar procedures with MS-Dial and Multiquant were applied to blank extraction replicates and peak exclusion lists were used to filter only the features coming from the cell pellets (1167 features in ESI (+) and 842 features in ESI (-)). In terms of the total number of detected features, all extractions protocols show similar performance in ESI (+) (maximum difference is 4 % between IPA90 and IPA75) and a slight greater amount is obtained with $CHCl_3$ in ESI (-) (difference of 9 % respect to the MTBE protocol). Venn diagrams in Figure 6.3 show the distribution of detected features in ESI (+) and ESI (-) modes. It is possible to see that 72 % of the features in ESI (+) and 77% in negative mode were detected with all EPs. In ESI (+) the amount of features that can be exclusively extracted with each EP is very similar (6.7 % with $CHCl_3$, 5.7 % in common with IPA75 and IPA90 and 5.1% with MTBE).

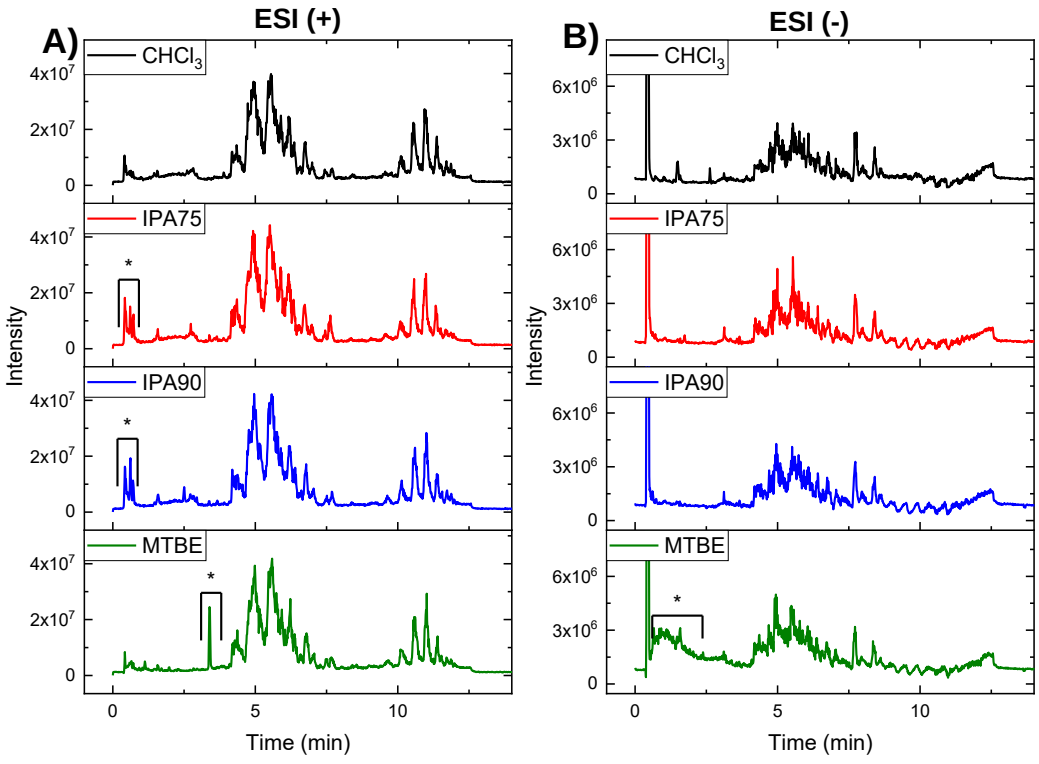

Figure 6.1. Representative TICs for samples extracted with four different EPs using A) ESI (+) and B) ESI (-) mode. Asterixes indicate major differences between the chromatograms.

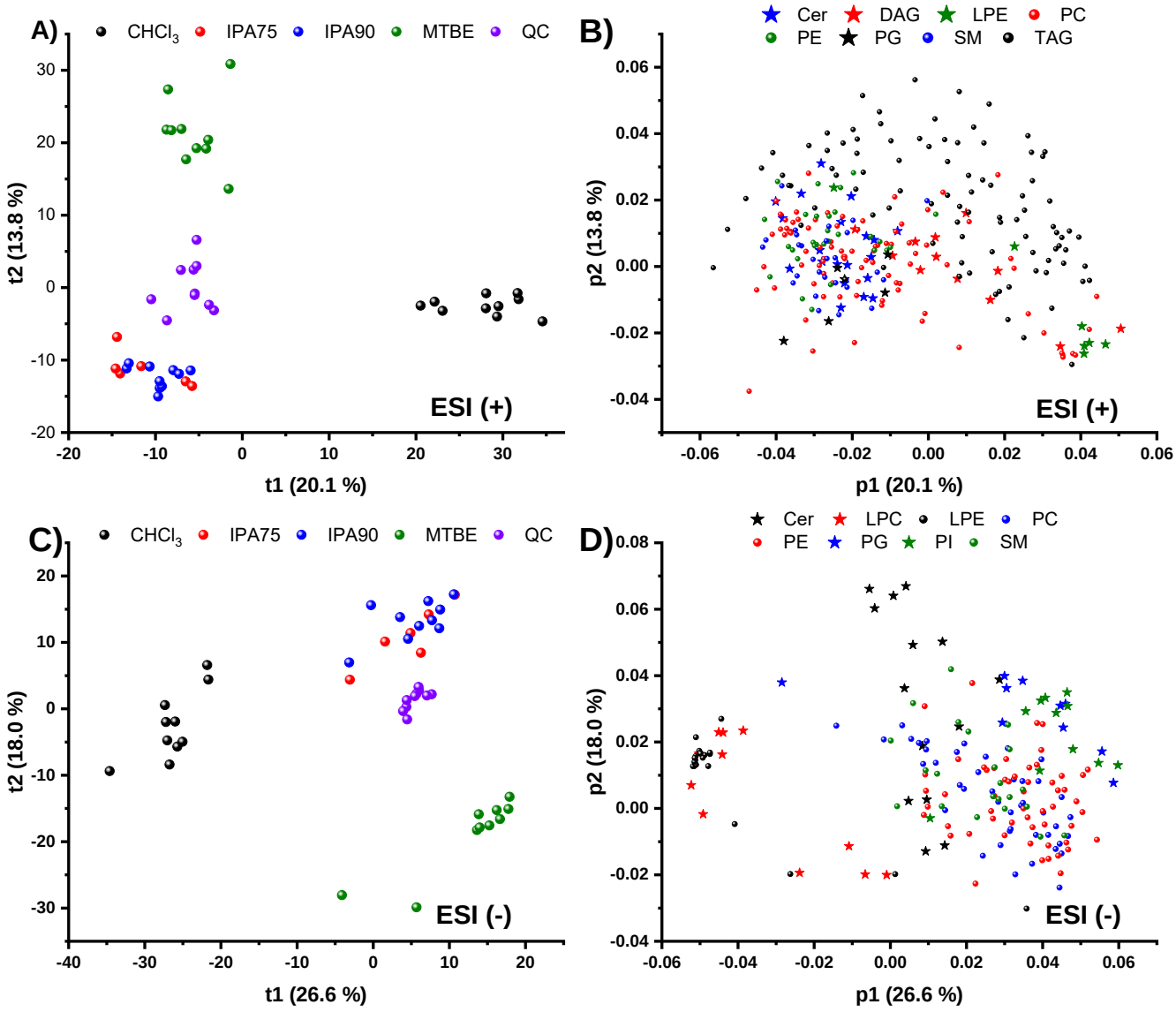

Figure 6.2. PCA plots for intensities of detected features. A) Scores plot in ESI (+), B) Loadings plot including only lipid classes with more than 5 identified features ESI (+) C) Scores plot in ESI (-), D) Loadings plot including only lipid classes with more than 5 identified features ESI (-)

In ESI (-), $CHCl_3$ protocol extracts exclusively 9.7 % of total detected features in comparison to 3.4 % of MTBE and 2.6 % of IPA75 and IPA90 (in common). These features detected with only one of the specific EP (or two of them in the case of IPA75 and IPA90) correspond to not identified features which are spread through the whole studied range of m/z and retention time and for this reason no specific lipid class can be assigned to them.

6.5.3 Identified lipids and relative recovery of endogenous lipids

Table 6.1 also shows the distribution of lipids identified with each EP (Specific data about identified features can be observed in Appendix C). Only IPA75 and MTBE extraction allowed the

identification of a few less features (2% less in each mode for IPA75 and 2% less in negative mode for MTBE), it means that in terms of the number of identified features the four studied EPs have similar performance. However, Figure 6.2B and 2D, already showed that even when similar number of lipids where detected with each EP, their intensities were significantly different for some lipid classes.

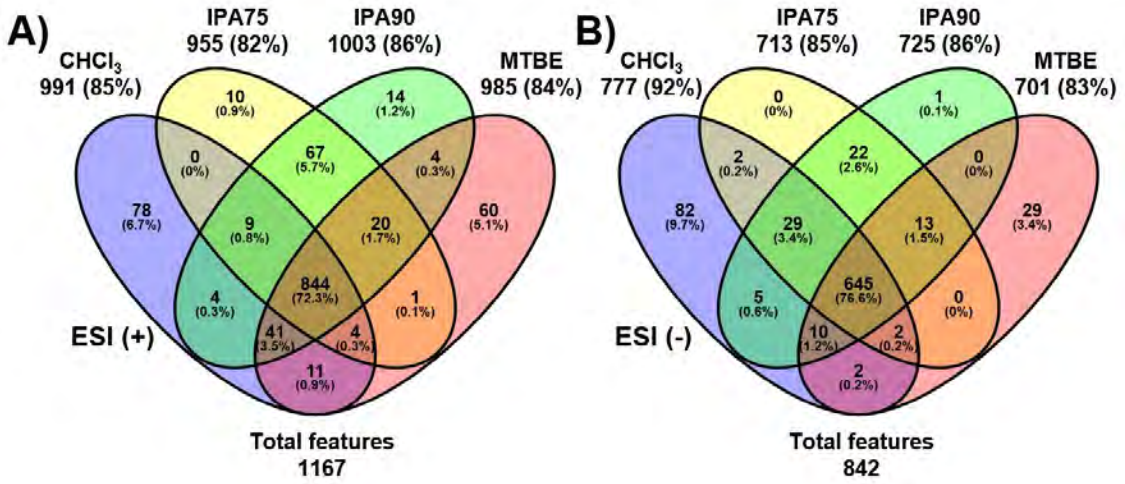

Figure 6.3. Venn diagrams showing the distribution of detected features with each EP and their overlapping selectivities. A) Results from ESI (+) and B) ESI (-) modes.

In order to describe the relative ability of each EP to extract a particular lipid class, a relative recovery of endogenous extracted lipids was calculated using IPA90 as a reference. Thus, the average intensity of each identified lipid extracted with $CHCl_3$, IPA75 and MTBE was normalized with respect to the average intensity of the same lipid after extraction with IPA90. Afterwards, the normalized values were averaged for the lipids belonging to the same lipid class (Figure 6.4, Suppl. Table 6.5). The results show similar intensities for some lipid classes independently of which protocol was employed. However, in some other cases significant differences are noted. In ESI (-) mode, for example, significantly lower intensities were obtained for polar lipids LPG, LPI, PG, PI, PS and FA when $CHCl_3$ and MTBE extractions were employed. Also, higher intensities are achieved for LPE and LPC with $CHCl_3$ protocol while lower ones are obtained with IPA75 and MTBE. This higher recovery for LPC and LPE with $CHCl_3$ has to be further investigated considering that these are two of the most polar lipid classes and it is expected that polar mixtures IPA:H_2O can extract better these substances, as it has been indicated previously [108].

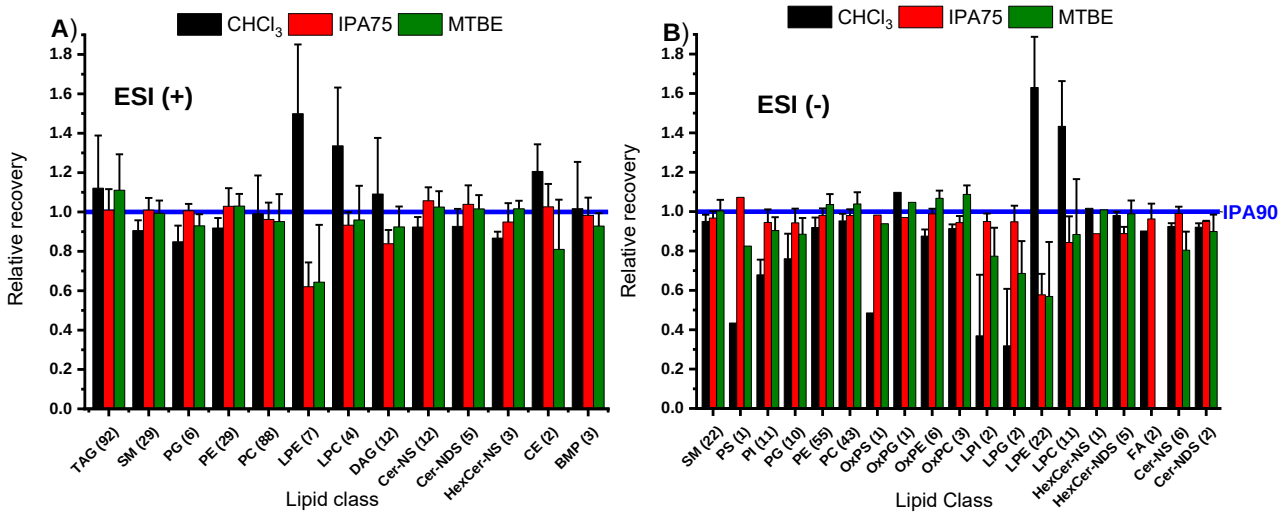

Figure 6.4. Relative lipid class recoveries of endogenous lipids obtained with different EPs and using IPA90 as a reference. A) Results from ESI (+) and B) ESI (-) modes. Numbers in parenthesis indicate the number of identified lipids from each lipid class that were normalized and averaged.

6.5.4 Lipid recovery of internal standards

To determine the absolute recovery of lipid classes with each EP, pre-extraction and post-extraction spiking of the samples with a mixture of ILIS was performed. Figure 6.5 and Suppl. Table 6.6.

show the % recovery for each ILIS. As an average MTBE and IPA90 have the best performance. In the case of $CHCl_3$, its performance is significantly higher than other protocols for the recovery of TG. IPA75 shows recoveries in most of the cases lower than the ones that can be reached with IPA90. $CHCl_3$ protocols shows significantly lower recoveries for polar lipid classes PA, PI and PS.

Here, it is important to highlight that beside the fact that ILIS were added to the pellet just before the addition of extraction solvent, which means they have less interaction with cellular matrix and more direct contact with extraction solvent than endogenous lipids, a good correlation was observed for the recoveries that were calculated with the ILIS in comparison with the relative recoveries of endogenous lipids described in section 3.3. Only exception for this finding was the anomalous mentioned case of LPEs and LPCs.

Also, good correlation was observed between the obtained recoveries and reported results by Sarafian *et al.* [108] in plasma samples after extraction with isopropanol and relative comparison with protocols based on MTBE (Matyash) and $CHCl_3$ (Bligh and Dyer, Folch). However, only recovery of odd-chained internal standards was reported at that moment and no comparison with endogenous lipids was done.

Higher recoveries obtained with IPA90 respect to IPA75, especially for the most abundant lipid classes are also in good concordance with comparison done by Yao *et al.* [77] in microalgae and

soybeans, where aqueous isopropanol mixtures with 88 % and 95 % of isopropanol yielded higher oil extraction efficiency than mixtures with 50 % and 70 % isopropanol.

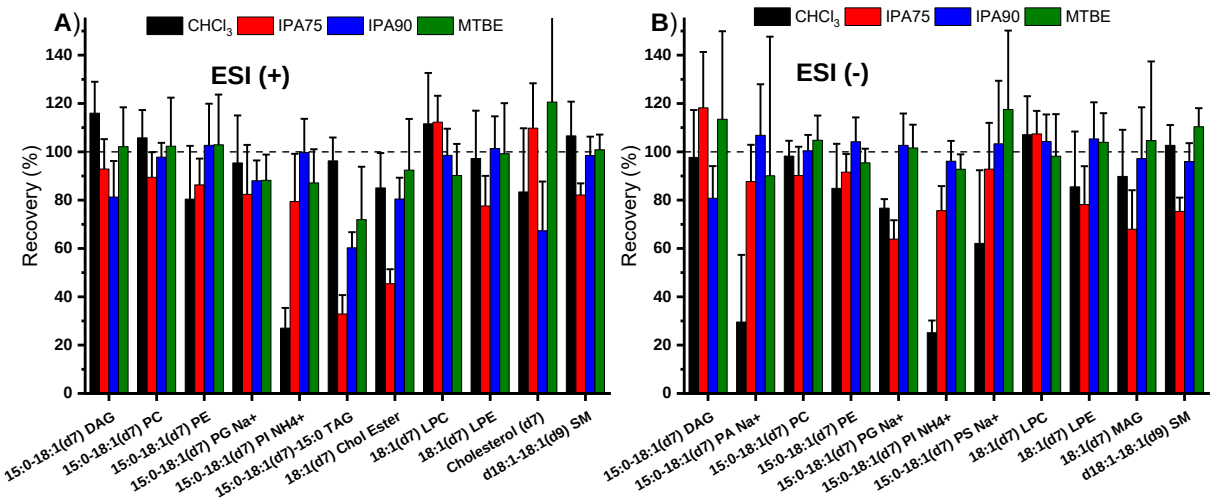

Figure 6.5. Recoveries of isotopically labeled internal standards after pre and post-extraction spiking. A) Results from ESI (+) and B) ESI (-) modes.

6.5.5 Precision

For a comparison of precisions obtained with the EPs, CV % for each detected feature was calculated. A profile of the CVs for the features that were found with each EP (1167 features in ESI (+) and 842 features in ESI (-), Figure 6.3) is shown in Figure 6.6 and Suppl. Table 6.7. For features detected in ESI (+), CV profiles show to be very similar having a maximum CV % bin from 10 to 15% and around 80 % of the features with CV less than 30 % independently of the employed EP. For features detected with ESI (-), IPA75 and IPA90 have a maximum CV bin from 5 to 10 %, while $CHCl_3$ and MTBE have a maximum CV bin from 10 to 15 %. All EPs have more than 90% of detected features with a CV below 30%.

6.5.6 Protocol complexity

Many publications have already made emphasis about the advantage of using EPs where the organic layer is the upper phase (as in MTBE protocol) and not the lower one (as in $CHCl_3$ protocol) of a two-phase partitioning system. The reason for this is the more tedious removal of the lipid containing organic phase when this one is in the bottom, especially because a layer of protein is located between the organic and aqueous layer. In the case of tested EPs IPA75 and IPA90, the fact of having a monophasic mixture makes this process even easier because only a separation of the supernatant from the solid residue is required. A possible disadvantage of employing monophasic mixtures for extraction rely on the presence of salts as part of the extract. However, in reversed phase LC-MS this is not necessarily a problem because these salts elute during the first minutes of chromatographic run. As part of this research, QC samples run

at the beginning, in between and at the end of measured sequences in ESI (+) and ESI (-), did not show significant differences in terms of intensity (see Suppl. Figure 6.1).

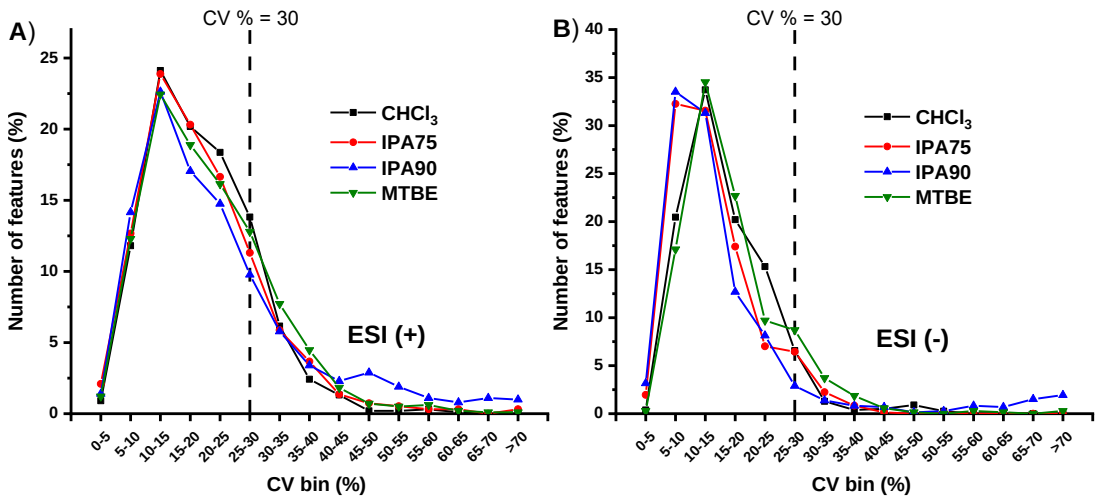

Figure 6.6. Distribution of CVs (%) obtained for precision evaluation of peak intensities of features detected in all four EPs. A) Results from ESI (+) (1167 analyzed features) and B) ESI (-) modes (842 analyzed features).

Another advantage for IPA75 and IPA90 extractions, is that they are compatible with plasticware, which does not happen with MTBE and $CHCl_3$. In our study, extraction blanks were performed to remove those features which are not coming from cell pellets (lists of features detected in extractions blanks are in Appendix D). Additionally, an extra extraction blank for IPA90 using glassware, yielded a higher amount of detected features than the corresponding one using plasticware (See Suppl. Figure 6.2 and Suppl. Figure 6.3). This higher amount of detected features could be related with the cleaning process employed for the glass tubes. Therefore, in the case that glassware is employed for these extractions, either new glassware has to be utilized for each new extraction, which is very expensive or a very strict cleaning protocol has to be employed, which will demand extra time and make the process more tedious. Consequently, it can be said that the EPs IPA75 and IPA90, employing plasticware, are less time consuming, cheaper and easy to automatize.

6.6 Concluding remarks

After comparison of the performance for extraction of lipids, it is possible to conclude that there was no significant difference with the number of identified lipids with each EP. In terms of recoveries for different lipid classes, extraction with IPA90 showed similar results as MTBE for most of the lipid classes, better results than $CHCl_3$ for the more polar lipid classes and better results than IPA75 for the less polar lipid classes. Precision with IPA mixtures showed to be slightly better in ESI (-) and similar in ESI (+) than the precision obtained with MTBE and $CHCl_3$.

In terms of complexity, monophasic extractions with IPA offered a simpler, less time consuming and cheaper protocol. Also, MS signal intensities did not show any decrease after samples extracted with IPA:H_2O mixtures were measured, which could be corroborated with the reproducibility of measured intensities for QC samples through the whole study. Considering all these aspects, extraction with IPA90 represents an excellent alternative as a solvent for developing reversed-phase LC-MS lipidomics studies.

6.7 Conflict of interest statement

None

6.8 Acknowledgements

C.C. is grateful to the DAAD for a doctoral fellowship (DAAD no. 57129429). We are grateful to the “Struktur- und Innovationsfonds für die Forschung (SI-BW)” by the regional government of Baden-Württemberg (Ministry of Science, Research and Arts) and the German Science Foundation (DFG no. INST 37/821-1 FUGG) for financial support of infrastructure.

6.9 Supplemental

Suppl. Table 6.1. Information about internal standards of the SPLASH™ Lipidomix® Mass Spec Standard (in MeOH)

Mixture Components	Target Conc. (µg/mL)
15:0-18:1(d7) PC	160
15:0-18:1(d7) PE	5
15:0-18:1(d7) PS	5
15:0-18:1(d7) PG	30
15:0-18:1(d7) PI	10
15:0-18:1(d7) PA	7
18:1(d7) LPC	25
18:1(d7) LPE	5
18:1(d7) Chol Ester	350
18:1(d7) MG	2
15:0-18:1(d7) DG	10
15:0-18:1(d7)-15:0 TG	55
18:1(d9) SM	30
Cholesterol (d7)	100

Suppl. Table 6.2. m/z values of sodium acetate clusters used for external calibration of QTOF

ESI+ (m/z)	ESI- (m/z)
104.99230	141.01693
351.00152	223.02000
433.00459	305.02307
515.00767	387.02615
597.01074	469.02922
679.01381	551.03230
761.01689	633.03537
843.01996	715.03844
1007.02611	797.04152
1089.02918	879.04459
	961.04767
	1043.05074

Suppl. Table 6.3. Information about design of MS experiments

Experiment	MS Type	Accumulation time (ms)	Pos mode		Neg mode	
			Min m/z	Max m/z	Min m/z	Max m/z
MS	SCAN	80	50	1250	50	1050
MS/MS	SWATH 1	31	50.0	214.6	50.0	342.2
MS/MS	SWATH 2	31	213.6	281.8	341.2	453.6
MS/MS	SWATH 3	31	280.8	390.7	452.6	480.8
MS/MS	SWATH 4	31	389.7	480.4	479.8	507.8
MS/MS	SWATH 5	31	479.4	509	506.8	532.3
MS/MS	SWATH 6	31	508	536.5	531.3	566.8
MS/MS	SWATH 7	31	535.5	610.6	565.8	617.4
MS/MS	SWATH 8	31	609.6	677.1	616.4	687.1
MS/MS	SWATH 9	31	676.1	709.0	686.1	715.0
MS/MS	SWATH 10	31	708.0	735.1	714.0	744.1
MS/MS	SWATH 11	31	734.1	759.1	743.1	755.1
MS/MS	SWATH 12	31	758.1	773.1	754.1	776.0
MS/MS	SWATH 13	31	772.1	790.2	775.0	794.6
MS/MS	SWATH 14	31	789.2	811.2	793.6	807.6
MS/MS	SWATH 15	31	810.2	827.2	806.6	830.3
MS/MS	SWATH 16	31	826.2	856.2	829.3	840.1
MS/MS	SWATH 17	31	855.2	884.3	839.1	859.2
MS/MS	SWATH 18	31	883.3	915.9	858.2	889.1
MS/MS	SWATH 19	31	914.9	983.7	888.1	924.6
MS/MS	SWATH 20	31	982.7	1250.0	923.6	1050.0

Suppl. Table 6.4. Parameters used for processing of data with MS-Dial in negative and positive mode

Mode	POSITIVE	NEGATIVE
Data collection parameters		
Retention time begin	0.5	0.5
Retention time end	13	13
Mass range begin	50	50
Mass range end	1250	1050
Centroid parameters		
MS1 tolerance	0.01	0.01
MS2 tolerance	0.025	0.025
Peak detection-based	TRUE	TRUE
Isotope recognition		
Maximum charged number	2	2
Data processing		
Number of threads	4	3
Peak detection parameters		
Smoothing method	LinearWeightedMovingAverage	LinearWeightedMovingAverage
Smoothing level	3	3
Minimum peak width	5	5
Minimum peak height	3000	1000
Peak spotting parameters		
Mass slice width	0.1	0.1
Exclusion mass list (mass & tolerance)		
Deconvolution parameters		
Peak consideration	Both	Both
Sigma window value	0.5	0.5
Exclude after precursor	TRUE	TRUE
MSP file and MS/MS identification setting		
MSP file	MSDIAL-LipidDBs-VS35-FiehnO.lbm	MSDIAL-LipidDBs-VS35-FiehnO.lbm
Retention time tolerance	0.5	0.5
Accurate mass tolerance (MS1)	0.01	0.01
Accurate mass tolerance (MS2)	0.05	0.05
Identification score cut off	80	80
Text file and post identification (retention time and accurate mass based) setting		
Text file	IS_PostIdentification_Pos.txt	IS_PostIdentification_Neg.txt
Retention time tolerance	0.1	0.1
Accurate mass tolerance	0.01	0.01
Identification score cut off	85	85
Advanced setting for identification		
Relative abundance cut off	0	0
Top candidate report	TRUE	TRUE
Adduct ion setting		
	[M+H]+, [M+NH4]+, [M+Na]+	[M-H]-, [M-H2O-H]-, [M+Cl]-, [M+FA-H]-
Alignment parameters setting		
Reference file	QC-5.abf	QC-05.abf
Retention time tolerance	0.05	0.05
MS1 tolerance	0.015	0.015
Retention time factor	0.5	0.5
MS1 factor	0.5	0.5
Peak count filter	0	0
N% detected in at least one group	51	51
QC at least filter	FALSE	FALSE
Tracking of isotopic labels	FALSE	FALSE

Suppl. Table 6.5. Relative recoveries of endogenous lipids extracted with $CHCl_3$, IPA75 and MTBE EPs respect to IPA90 EP. Each identified lipid was normalized with the corresponding intensity detected by using IPA90 EP. Then all the values from lipids belonging to the same lipid class were averaged and their standard deviation was calculated.

ESI (+)				ESI (-)			
Lipid class[1]	**$CHCl_3$[2]**	**IPA75[2]**	**MTBE[2]**	**Lipid class[1]**	**$CHCl_3$[2]**	**IPA75[2]**	**MTBE[2]**
TAG (92)	1.12 (0.13)	1.01 (0.05)	1.11 (0.09)	**SM (22)**	0.95 (0.02)	0.97 (0.02)	1 (0.03)
SM (29)	0.91 (0.03)	1.01 (0.03)	0.99 (0.03)	**PS (1)**	0.43	1.07	0.82
PG (6)	0.85 (0.04)	1.01 (0.02)	0.93 (0.03)	**PI (11)**	0.68 (0.04)	0.94 (0.03)	0.9 (0.03)
PE (29)	0.92 (0.03)	1.03 (0.05)	1.03 (0.03)	**PG (10)**	0.76 (0.06)	0.94 (0.04)	0.88 (0.04)
PC (88)	0.99 (0.1)	0.96 (0.04)	0.95 (0.07)	**PE (55)**	0.92 (0.03)	0.98 (0.02)	1.04 (0.03)
LPE (7)	1.5 (0.18)	0.62 (0.06)	0.64 (0.15)	**PC (43)**	0.95 (0.02)	0.98 (0.02)	1.04 (0.03)
LPC (4)	1.34 (0.15)	0.93 (0.03)	0.96 (0.09)	**OxPS (1)**	0.49	0.98	0.94
HexCer-NS (3)	0.87 (0.02)	0.95 (0.05)	1.02 (0.02)	**OxPG (1)**	1.1	0.97	1.05
DAG (12)	1.09 (0.14)	0.84 (0.03)	0.92 (0.05)	**OxPE (6)**	0.88 (0.02)	0.99 (0.01)	1.07 (0.02)
Cer-NS (12)	0.92 (0.03)	1.06 (0.03)	1.02 (0.04)	**OxPC (3)**	0.91 (0.01)	0.94 (0.02)	1.09 (0.02)
Cer-NDS (5)	0.93 (0.04)	1.04 (0.05)	1.02 (0.03)	**LPI (2)**	0.37 (0.16)	0.95 (0.02)	0.77 (0.07)
CE (2)	1.21 (0.07)	1.03 (0.06)	0.81 (0.13)	**LPG (2)**	0.32 (0.14)	0.95 (0.04)	0.69 (0.08)
BMP (3)	1.02 (0.12)	0.98 (0.05)	0.93 (0.03)	**LPE (22)**	1.63 (0.13)	0.58 (0.05)	0.57 (0.14)
				LPC (11)	1.43 (0.11)	0.84 (0.07)	0.88 (0.14)
				HexCer-NS (1)	1.02	0.89	1.01
				HexCer-NDS (5)	0.98 (0.01)	0.89 (0.02)	0.99 (0.03)
				FA (2)	0.9	0.96 (0.04)	
				Cer-NS (6)	0.92 (0.01)	0.99 (0.02)	0.8 (0.05)
				Cer-NDS (2)	0.92 (0.01)	0.95	0.9 (0.04)
Average	1.05	0.96	0.95	Average	0.87	0.93	0.87

[1]In parenthesis it is indicated the number of lipids identified in each lipid class, [2]Values in parenthesis are standard deviations for relative recoveries of lipids belonging to the same lipid class.

Suppl. Table 6.6. Recoveries of isotopically labeled internal standards after pre-extraction and post-extraction spiking

Mode	ESI (+)				ESI (-)			
Isotopically labeled internal standard	**$CHCl_3$**	**IPA75**	**IPA90**	**MTBE**	**$CHCl_3$**	**IPA75**	**IPA90**	**MTBE**
15:0-18:1(d7) DAG	116 (13)	93 (12)	81 (15)	102 (16)	98 (20)	118 (23)	81 (13)	113 (36)
15:0-18:1(d7) PA Na+					30 (28)	88 (15)	107 (21)	90 (58)
15:0-18:1(d7) PC	106 (12)	89 (10)	98 (6)	102 (20)	98 (6)	90 (12)	100 (7)	105 (10)
15:0-18:1(d7) PE	80 (22)	86 (11)	103 (17)	103 (21)	85 (18)	92 (8)	104 (10)	95 (6)
15:0-18:1(d7) PG Na+	95 (20)	82 (20)	88 (8)	88 (11)	77 (4)	64 (8)	103 (13)	102 (10)
15:0-18:1(d7) PI NH4+	27 (8)	79 (20)	100 (14)	87 (14)	25 (5)	76 (10)	96 (8)	93 (6)
15:0-18:1(d7) PS Na+					62 (30)	93 (19)	103 (26)	118 (33)
15:0-18:1(d7)-15:0 TAG	96 (10)	33 (8)	60 (6)	72 (22)				
18:1(d7) Chol Ester	85 (14)	45 (6)	80 (9)	92 (21)				
18:1(d7) LPC	112 (21)	112 (11)	99 (11)	90 (13)	107 (16)	107 (10)	104 (11)	98 (17)
18:1(d7) LPE	97 (20)	78 (12)	101 (13)	99 (21)	85 (23)	78 (16)	105 (15)	104 (12)
18:1(d7) MAG	83 (96)	86 (37)	91 (32)	85 (66)	90 (19)	68 (16)	97 (21)	105 (33)
Cholesterol (d7)	83 (26)	110 (19)	67 (20)	121 (58)				
d18:1-18:1(d9) SM	107 (14)	82 (5)	99 (8)	101 (6)	103 (8)	75 (6)	96 (8)	110 (8)
Average	88	80	90	95	78	86	100	103

[1]Values in parenthesis are standard deviations of absolute recoveries of ILIS

Suppl. Table 6.7. Distribution of CVs (%) obtained for precision evaluation of peak intensities of features detected in all four EPs.

	% of features falling in the respective category							
	ESI (+)				**ESI (-)**			
CV bin(%)	CHCl3	IPA75	IPA90	MTBE	CHCl3	IPA75	IPA90	MTBE
0-5	0.9	2.1	1.4	1.2	0.4	2.0	3.2	0.3
5-10	11.8	12.7	14.2	12.3	20.5	32.3	33.5	17.1
10-15	24.1	23.9	22.6	22.4	33.7	31.6	31.3	34.5
15-20	20.2	20.3	17.0	18.9	20.2	17.4	12.7	22.7
20-25	18.4	16.6	14.8	16.1	15.3	7.0	8.1	9.7
25-30	13.8	11.3	9.8	12.8	6.6	6.5	2.9	8.7
30-35	6.2	5.9	5.8	7.7	1.3	2.2	1.4	3.7
35-40	2.4	3.7	3.4	4.5	0.4	0.8	0.8	1.9
40-45	1.3	1.4	2.3	1.8	0.5	0.1	0.7	0.6
45-50	0.2	0.7	2.9	0.7	0.9	0.0	0.1	0.1
50-55	0.2	0.5	1.9	0.5	0.3	0.1	0.3	0.0
55-60	0.3	0.3	1.1	0.6	0.0	0.0	0.8	0.3
60-65	0.1	0.3	0.8	0.2	0.0	0.0	0.7	0.1
65-70	0.0	0.0	1.1	0.1	0.0	0.0	1.5	0.0
>70	0.1	0.3	1.0	0.1	0.0	0.0	1.9	0.3
Total	**100.0**	**100.0**	**100.0**	**100.0**	**100.0**	**100.0**	**100.0**	**100.0**

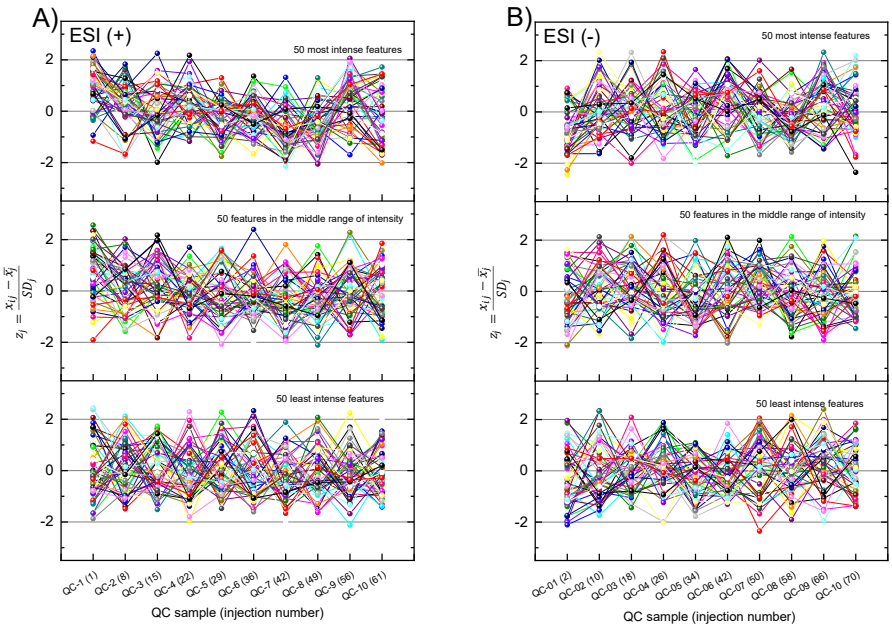

Suppl. Figure 6.1. Z values for selected features (based on their intensity) in QC samples through the run sequence in A) ESI (+) and B) ESI (-). The number in parenthesis for each QC sample is the position of that QC in the sequence of injected samples. SD means standard deviation

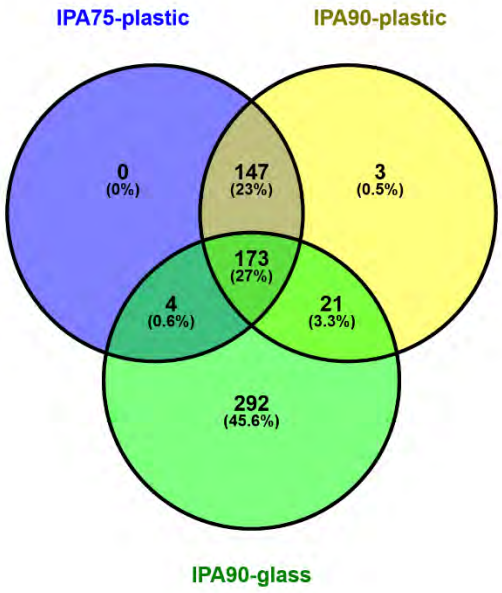

Suppl. Figure 6.2. Venn diagram showing the distribution of detected features with blanks for EPs of IPA75 using plasticware, IPA90 using plasticware and IPA 90 using glassware in ESI (+).

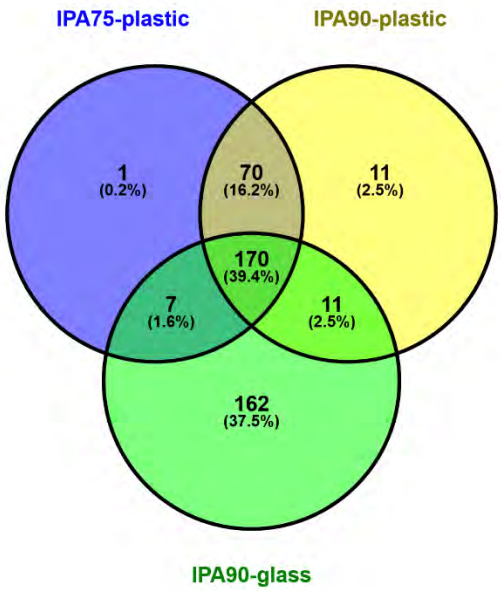

Suppl. Figure 6.3. Venn diagram showing the distribution of detected features with blanks for EPs of IPA75 using plasticware, IPA90 using plasticware and IPA 90 using glassware in ESI (-).

7 Publication II. Lipid profiling of keratinocytes

7.1 Title

Lipid atlas of keratinocytes and betulin effects on its lipidome profiled by comprehensive UHPLC-MS/MS with data independent acquisition using targeted data processing

Carlos Calderón[1], Lara Rubarth[2], Malgorzata Cebo[1], Irmgard Merfort[2], Michael Lämmerhofer[1]*

[1]Institute of Pharmaceutical Sciences, Pharmaceutical (Bio-)Analysis, University of Tübingen, Auf der Morgenstelle 8, 72076 Tübingen, Germany

[2]Institute of Pharmaceutical Sciences, Department of Pharmaceutical Biology and Biotechnology, University of Freiburg, 79104 Freiburg, Germany

Reprinted with permission from Proteomics, in Press

DOI: 10.1002/pmic.201900113

Copyright (2019) WILEY-VCH Verlag GmbH & Co. KGaA

7.2 Abstract

Betulin is a pentacyclic triterpene with demonstrated healing properties in mid-dermal wounds. A few earlier studies have provided insights into the wound healing effects on the molecular level. However, there are still questions left on the molecular targets of betulin. Therefore, we have undertaken a pharmacolipidomics analysis of betulin in human immortalized keratinocytes to monitor alterations in the lipid profiles induced by treatment with betulin.

For this purpose, lipid extracts of keratinocytes treated with betulin and untreated controls were comprehensively analyzed by an untargeted UHPLC-ESI-QTOF-MS/MS lipidomics profiling workflow using data-independent acquisition (DIA). Targeted data processing allowed the identification of 611 lipid species from 21 different lipid classes. Statistical analysis of the identified lipids show significant changes in 440 lipid species which can be described as down-regulation of cholesteryl esters and triacylglycerides and up-regulation of glycerophospholipids, sphingolipids and diacylglycerides.

Additionally, some other signals corresponding to triterpenes were found in the betulin group and suggested that betulin is incorporated (in the membrane) and metabolized in keratinocytes.

7.3 Statement of significance of the study

In this study we performed a comprehensive description of the lipidome of human immortalized keratinocytes and its changes after the treatment with betulin. Data processing was based on a target list of lipids. Our identification approach combines information from precursor and product ions obtained from analyses in both polarities under same chromatographic conditions and from elution patterns in reversed phase-LC of each lipid class. Cholesteryl esters (CEs) with very long fatty acid chains (up to 36 carbons) were detected and may serve as depot to support the synthesis of ceramides that play an important role in the skin barrier function. Significant changes of CEs (down regulated) upon betulin treatment as many other lipid classes are described. Results also suggest that betulin is incorporated and metabolized in the keratinocytes.

7.4 Introduction

Betulin, a pentacyclic triterpene, was shown to exert a variety of different biological effects including anticancer, antiinflammatory, antifungal or antiviral activities[117,118]. Interestingly, in 2016 a birch bark preparation (Episalvan®) which contains betulin to around 80% has been approved by the European Medicines Agency (EMA) for the treatment of partial-thickness skin wounds. Studies on the molecular level with betulin have been conducted which explain the clinically proven wound healing effects[119–121]. Betulin influences the inflammatory and the new tissue formation phase in the wound healing process. It enhances the migration of keratinocytes and stimulates their differentiation. However, it has not yet been clarified whether or in which way the lipophilic betulin may act on cell membranes, permeate membranes to enter the cell or have an impact on the lipid profile of the cell. Up to now, it has only been proven with erythrocytes that betulin can replace cholesterol in the membranes leading to alterations of their membrane shapes[122].

In the case of skin, two of its most important barrier functions are the barrier to the movement of water and electrolytes and the barrier against invasive and toxic microbes[123]. Lipids are considered important players in the maintenance of these two functions, and ceramides, cholesterol and free fatty acids are particularly enriched in stratum corneum (SC), the outer layer of the epidermis[124–126], where keratinocytes show their last step of differentiation.

Specific studies on murine keratinocytes, normal human keratinocytes or immortalized human keratinocytes showed a correlation between their lipid content and their state of differentiation. Analysis of lipid classes content by densitometry after HPTLC and fatty acid profiling by GC after derivatization were performed for that purpose[127–131]. More recently, lipidomics studies in keratinocytes have been performed to elucidate the effect of some factors like narrow band ultraviolet B[131], allergen and irritant compounds[132], dioxin[133], radical generator[134] and a glycolytic inhibitor[26].

From a methodological perspective, lipidomics profiling of biological samples is nowadays achieved by either targeted or untargeted approaches[51,64,135,136]. Untargeted assays are based on high-resolution mass spectrometry using direct infusion with FTICR- or Orbitrap-MS (shotgun lipidomics)[137,138] or employing UHPLC-MS/MS (with QTOF or QOrbitrap) in data-dependent acquisition (DDA) or data-independent acquisition (DIA) mode. UHPLC-MS/MS with DIA[47] offers the possibility to acquire MS and MS/MS data comprehensively over the entire chromatogram and across all samples. It allows uncompromised retrospective data processing so that the measurements represent a digital map of the lipid phenotype of the biological sample. Data processing of untargeted lipidomics data can be quite elaborate and a number of

distinct procedures have been proposed for DIA data including software tools like MS-DIAL[113] or Lipid-Pro[139] which allow automated identification by matching *in silico* or experimental databases besides some general tools to process lipidomics data. Typical approaches for metabolite identification include a first filtering step based on matching of a precursor ion *m/z* and a second step based on similarity scores with MS/MS databases[96]. Also, scores for isotopic pattern similarity and retention time (in case of LC-MS) have been implemented as part of some identification algorithms[113].

In this work, we employ a targeted data processing approach on untargeted lipidomics data generated by DIA with SWATH in order to determine significant changes in human immortalized keratinocytes after treatment with betulin. For identification of lipid species we performed an approach which combines the analysis of specific fragments for each lipid class, the matching of retention times for identification in positive and negative mode and the analysis of retention time for a particular species within the retention time pattern of the whole lipid class.

7.5 Materials and Methods

7.5.1 Materials

Methanol (MeOH), acetonitrile (ACN) and isopropanol (IPA), all LC-MS quality and formic acid (FA, 98%) were purchased from Roth (Karlsruhe, Germany). Ammonium formate was obtained from Sigma Aldrich (Steinheim, Germany). Water was purified by in-house Elga purification system (High Wycombe, United Kingdom).

Isotopically labelled internal standards (ILIS) were purchased from Avanti Polar Lipids (Alabama, USA) as a ready to use mixture: SPLASH™ Lipidomix® solution (See Table A1 for more information about ILIS). Odd-chained lipid standards LPC 17:1 and PC 17:0-20:4 were obtained from Avanti Polar Lipids. Lupeol, betulinic acid and erythrodiol standards were obtained from Sigma Aldrich.

Keratinocyte serum-free growth medium, supplements (recombinant human epidermal growth factor rhEGF, bovine pituitary extract BPE), 0.05% trypsin/EDTA (w/v) were bought from Thermo Fischer Scientific (Waltham, MA, USA); penicillin–streptomycin was obtained from Roche (Mannheim, Germany). Betulin was a gift from Birken AG, Niefern-Öschelbronn, Germany. A 10 mM stock solution of betulin was prepared in DMSO.

7.5.2 Cell culture and lipid extraction

Human immortalized keratinocytes were kindly provided from Prof. Dr. L. Bruckner-Tuderman, Department of Dermatology, Medical Center, University of Freiburg. Human immortalized keratinocytes were cultivated in Keratinocyte SFM supplemented with rhEGF, BPE and 1 % v/v

penicillin/streptomycin at 5 % CO_2 and 37 °C. Cells were split when they reached a confluency of 80 %. Passage 3 or 4 were used. Cells were plated in 20 Petri dishes (10 cm^2, 1 x 10^6 cells/ per dish) and cultivated for 4 days in 10 mL of the above mentioned medium for adherence. 10 dishes were incubated with 1.95 µM betulin (10 µL of the 1.95 mM stock solution in DMSO) for 8 hrs prior to removal of the medium and the remaining ones were used as control. Control samples were treated with 10 µL DMSO. The concentration of 1.95 µM of betulin was used, as this concentration has shown effects in our previous studies on the molecular wound healing effect[120]. On day 4, cells were incubated with 3 mL of trypsin (0.05 %) at 37°C. After 5 min cells were washed by adding 7 mL medium. The suspension was transferred into 15 mL falcon tubes and centrifuged for 5 min at 4°C and 1.200 rpm, respectively. The supernatant was withdrawn and the remaining cell pellets were washed and then frozen at -20°C in the falcon tubes until extraction.

Lipid extraction was performed with IPA:H_2O (90:10 v/v) as described previously [140] (See details of EP in Supplementary text A1).

7.5.3 LC-MS measurement

Analyses were performed by Agilent 1290 Series UHPLC instrument (Agilent, Waldbronn, Germany) coupled to Sciex TripleTOF 5600+ MS (Sciex, Concord, Ontario; Canada) with duospray source and Pal HTC-XS autosampler from CTC (Zwingen, Switzerland). Positive and negative ESI ionization were used in separate LC-MS runs with the same chromatographic separation conditions as described previously [113,140]. Briefly: Acquity UPLC CSH C18 (130Å, 1.7 µm, 2.1 mm X 100 mm) column was utilized with Acquity UPLC CSH C18 VanGuard pre-column (130Å, 1.7 µm, 2.1 mm X 5 mm) (Waters, Eschborn, Germany). The mobile phase was composed of 10 mM ammonium formate and 0.1 % formic acid dissolved in 60:40 ACN:H_2O (v/v) (A) and 90:10 (v/v) IPA:ACN (B). Further details on LC gradient elution conditions and MS parameters can be found in Supplementary text A2.

MS/MS data were obtained by data independent acquisition (DIA) using sequential window acquisition of all theoretical fragment ion mass spectra (SWATH)[114,115]. Q1 window sizes (See Table A3) were optimized with SwathTuner software[116] based on a QC sample.

7.5.4 Lipid identification

A lipid list was prepared and the target lipids were first searched and identified in a QC sample (pool of an aliquot of all study samples and injected after every 5th sample). Lipid classes were analyzed one by one. Notation of identified lipid species and fragment ions was done according to detailed rules proposed by Liebisch *et al.*[10] and Pauling *et al.*[100]. Thus, lipids were

annotated at the “lipid species level” (e.g. PC 34:2) or “molecular lipid species level” (e.g. PC 16:1-18:1) depending on analyzed fragments, which were of three different types: lipid class-selective fragment (LCF) (e.g. PC(184)), intermediate molecular lipid species-selective fragment (iMLF) (e.g. -PE O-(141)) and molecular lipid species-selective fragments (MLFs) (e.g. FA 18:1(+C3H6O2)), whose definitions given by Pauling *et al.* [100], are copied in Supplementary text A3 (note, no distinction between alkyl ether (O-) and alk-1-enyl ether (P-) lipids was made in this work). For the identification (see Figure 7.1) a set of characteristic ions for each lipid class was selected and their m/z values were obtained from LipidBlast database[27,97]. Each set consisted of the most intense adduct ion in the TOF MS scan as well as the most intensive LCF or iMLF in the corresponding SWATH experiment, in both ESI (+) and ESI (-) (See list of fragments for each lipid class in Suppl. Table 7.4). EICs (of selected ions for each lipid) were compared by using PeakView (Sciex) in order to determine whether the lipid was present or not in the QC sample. For some of the lipid classes, also EICs of MLFs were analyzed to identify fatty acyl chains in the lipid species. Additionally, peak spotting maps of retention time versus precursor ion m/z of each identified lipid were generated for each lipid class.

7.5.5 Lipid comparison and quantitation

Precursor and selected fragment ions of identified lipids were analyzed through the whole set of samples with Multiquant 3.0 (Sciex, for integration parameters see Table A5). Peak apex intensities were exported for statistical analysis. Intensities were normalized with corresponding intensities (from TOF MS scan) of standard PC 17:0-20:4, which was added with the resuspension solvent after extraction and prior to LC-MS measurement. Concentrations for each lipid species were estimated, based on its normalized intensity and the response factor of ILIS from the corresponding lipid class. For those lipid classes with no internal standard added before extraction, a standard addition curve was prepared with QC sample. Response factors to estimate concentrations were obtained from the slope of standard addition curves (see Table A6).

Reported concentrations of a lipid species are an average of its corresponding estimated concentrations from ESI (+) and ESI (-), and from precursor and fragment ion traces.

7.5.6 Statistics

Normalized intensities of precursor and product ions from positive and negative mode were combined and hypothesis testing was done in R statistical language (https://cran.r-project.org) using the non-parametric Mann-Whitney-U-test (obtaining a p-value for each studied trace) and

correction for multiple hypothesis testing adjusting a false discovery rate of <0.05 according to the approach proposed by Storey[141] (results reported as q-values).

7.6 Results and discussion

7.6.1 Lipid identification

Identification of lipid species in QC samples was performed by analyzing EICs of specific precursor and product ions for each lipid class in TOF MS and SWATH, acquired in ESI (+) and ESI (-) using the same LC separation. Figure 7.1 shows an example comprising the following steps for identification of lipid species.

Table A4 summarizes the list of precursor and fragment (product) ions selected for the identification of lipids from each lipid class. For each lipid class, the most abundant precursor ion in ESI-TOF-MS, positive and negative polarity, and the most intense LCF or iMLF in SWATH (positive or negative or both) were employed to identify all the lipids at the “lipid species level”. In total, 611 lipids from 21 lipid classes were identified at this level in QC samples and their distribution is shown in Suppl. Figure 7.1.

EICs of precursor ions and LCF or iMLF for species of the same lipid class with equal number of carbons and different number of unsaturations (e.g. PE O-36:1 and PE O-36:2, see Figure 7.1C) show that their chromatographic separation is achieved by the employed LC method.

Additional analysis of MLF allowed us to identify around 70% of the lipids at the “molecular lipid species level” (see Table B1) but also showed that in most cases a (partial) co-elution of lipid species (isomers) with the same number of carbons and unsaturations is occurring. For example, analysis of possible MLFs “FA x:y(+C3H6O2)” for PE O-36:2 showed the co-elution of PE O-18:1-18:1, PE O-16:1-20:1 and PE O-18:2-18:0. Therefore, we decided to keep the annotation of lipids that were identified at the “molecular lipid species level”, but quantitative comparison was done at the “lipid species level” because of the better S/N obtained from EICs of precursor ions, LCFs and iMLFs.

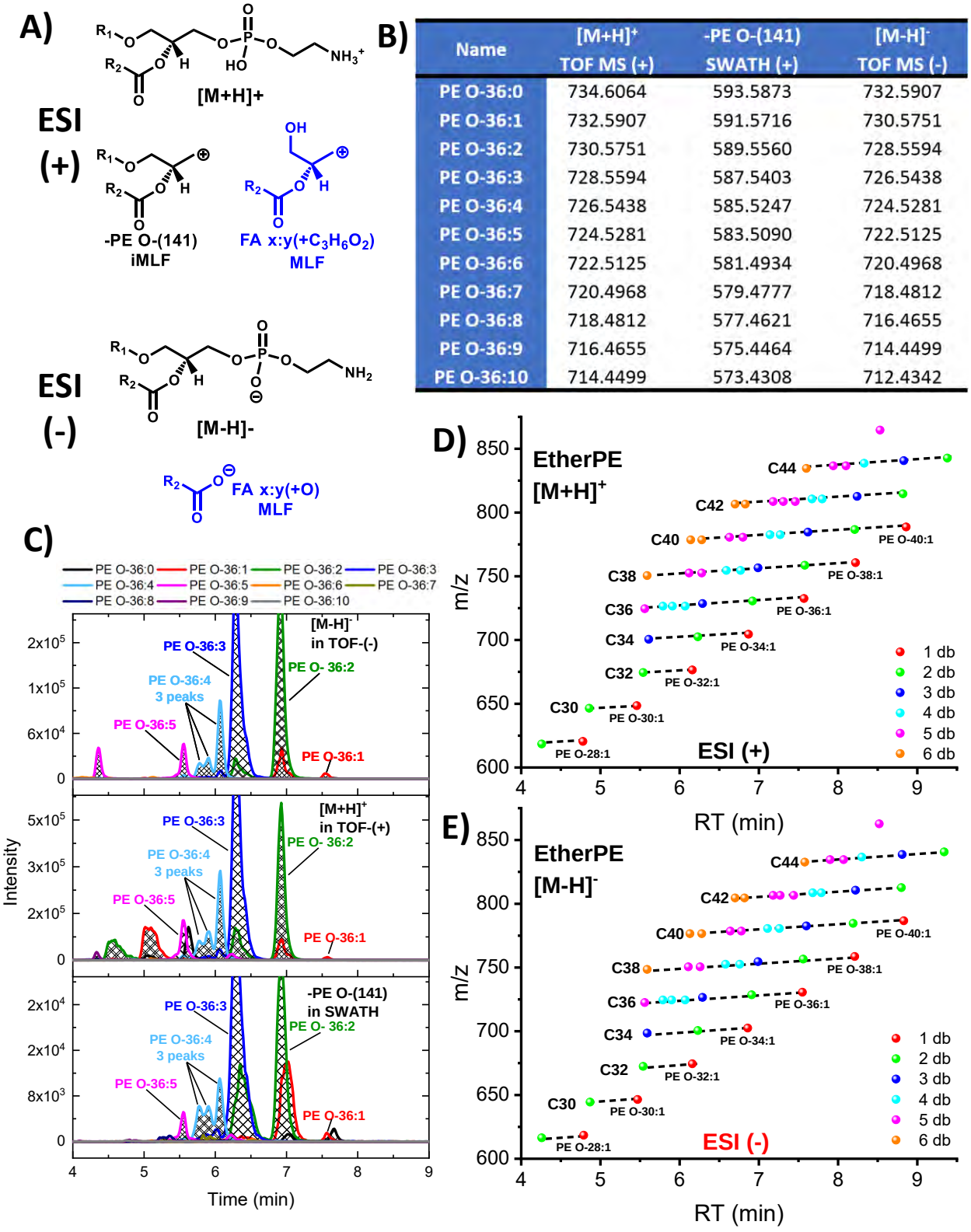

Name	[M+H]+ TOF MS (+)	-PE O-(141) SWATH (+)	[M-H]- TOF MS (-)
PE O-36:0	734.6064	593.5873	732.5907
PE O-36:1	732.5907	591.5716	730.5751
PE O-36:2	730.5751	589.5560	728.5594
PE O-36:3	728.5594	587.5403	726.5438
PE O-36:4	726.5438	585.5247	724.5281
PE O-36:5	724.5281	583.5090	722.5125
PE O-36:6	722.5125	581.4934	720.4968
PE O-36:7	720.4968	579.4777	718.4812
PE O-36:8	718.4812	577.4621	716.4655
PE O-36:9	716.4655	575.4464	714.4499
PE O-36:10	714.4499	573.4308	712.4342

Figure 7.1. Scheme for lipid identification process. Briefly, A) a specific set of fragments for each lipid class was selected, B) *m/z* values from selected ions were obtained from LipidBlast database, C) EICs of selected ions were obtained and compared in corresponding TOF MS ESI (-) (top), TOF MS ESI (+) (middle) and SWATH (MS/MS) ESI (+) (bottom) experiments to determine which lipids are present in the sample, D) spotting maps for precursor ions of lipids identified, from the same lipid class, with ESI (+) and E) ESI (-) were plotted to check for possible misidentifications

In those cases, in which lipid species of the same class with the same number of carbons and unsaturations were chromatographically separated, individual species were analyzed and annotated with an extra Arabic number (e.g. PE O-36:4 (1) at 6.07 min, PE O-36:4 (2) at 5.91 min and PE O-36:4 (3) at 5.79 min, see Figure 7.1C).

From Suppl. Figure 7.2 the distribution of MS data (precursor ions, LCFs and iMLFs) from different polarities and acquisition modes that were used for identification of lipids at the "lipid species level" and the subsequent comparison can be depicted. Thus, in 58% of the cases, identification was done by MS data measured in ESI (+) and ESI (-), while in the remaining 42% identification was done with measurement of only one polarity. This means that 58% of the lipids have an additional level of confidence for their identification by the other ionization mode since their presence was confirmed with the same retention time (± 3s) by separate chromatographic runs with distinct polarities. For the 42 % of lipid species identified with only one polarity, 32 % are in the ESI (+) mode which comprises mainly the analysis of ACs, CEs, TGs and DGs and 10 % are in the ESI (-) which corresponds mainly to the analysis of FAs and LPGs.

As part of the identification process, peak spotting maps were plotted for each lipid class in order to check the distribution of identified lipids in terms of *m/z* and retention time (See Figure 7.1D-E for case of ether PE and Suppl. Figure 7.3 or Suppl. Figure 7.4 for other lipid classes). In this manner, it is possible to observe very well-defined elution patterns for lipids of the same class depending on the total number of carbons and unsaturations. These elution patterns have been well described previously for reversed phase LC separations[31] and are commonly utilized in LC-MS lipidomics studies. However, this additional confirmative information, on the other hand, is also frequently neglected. We suggest elution patterns to be analyzed when LC-MS lipidomics studies are performed because they increase the confidence for identifications and can be used as an alert for checking possible misidentifications. On the other hand, scores for retention time similarities with databases have been included as part of some identifications algorithms [113]. However, this comparison only establishes a comparison between the lipid, which has to be identified, and the reference in the database without taking into account the retention time of species from the same lipid class, which have been already identified.

7.6.2 Presence of long fatty acyl chains

A first glance into the identified lipid species, especially those ones with only one fatty acyl chain, allows a good overview of the fatty acyl composition present in the studied sample. In the case of CE, it was interesting to observe the presence of an extended range of fatty acyl chains from CE 16:1 to CE 36:7. Figure A5 shows the distribution in terms of intensity for CEs identified in keratinocytes. Cholesteryl esters with long chain fatty acids have been suggested as a depot for

long chain fatty acids in human secretions [142]. This function may also apply for keratinocytes. Here, long fatty acyl chains in CE could be important for the synthesis of Cers and HexCers with long fatty acyl side chains, which play an important role in the skin barrier [143].

7.6.3 Concentration of lipid species

ILIS from different lipid classes which were added to each sample before lipid extraction were used to estimate concentrations of lipid species in control samples, which are reported in Table B1. The total sum for each lipid class was calculated as µg of each lipid class per million of cells. Figure 7.2 shows the mass percentage of each lipid class with respect to the total amount of lipid. A comparison to previously reported estimations on lipid concentrations in keratinocytes [127–131] cannot be done in a straightforward manner because of methodological differences like extraction protocol, analytical technique for detection or lipid classes included in each particular study. However, most of the estimated percentages for the lipid classes content seem to be similar and only the percentage of CEs obtained in our study (22 %) seems to be considerably higher than previously reported values, which were less than 10 % in all the cases.

7.6.4 Comparison of lipid classes after betulin treatment

Characteristic precursor and fragment ion (LCFs and iMLFs) intensities from TOF MS and SWATH experiments, respectively, were compared for each lipid species from betulin (B1 to B10) and control samples (C1 to C10). The coefficients of variation of the signal intensities for each of these ion traces (MS and MS/MS) both in control and betulin-treated groups including measurement and biological variance was in average around 15 % (See Suppl. Figure 7.6 and Suppl. Table 7.7). The mere measurement variance was significantly less and close to 100% of the features showed a CV<30%.

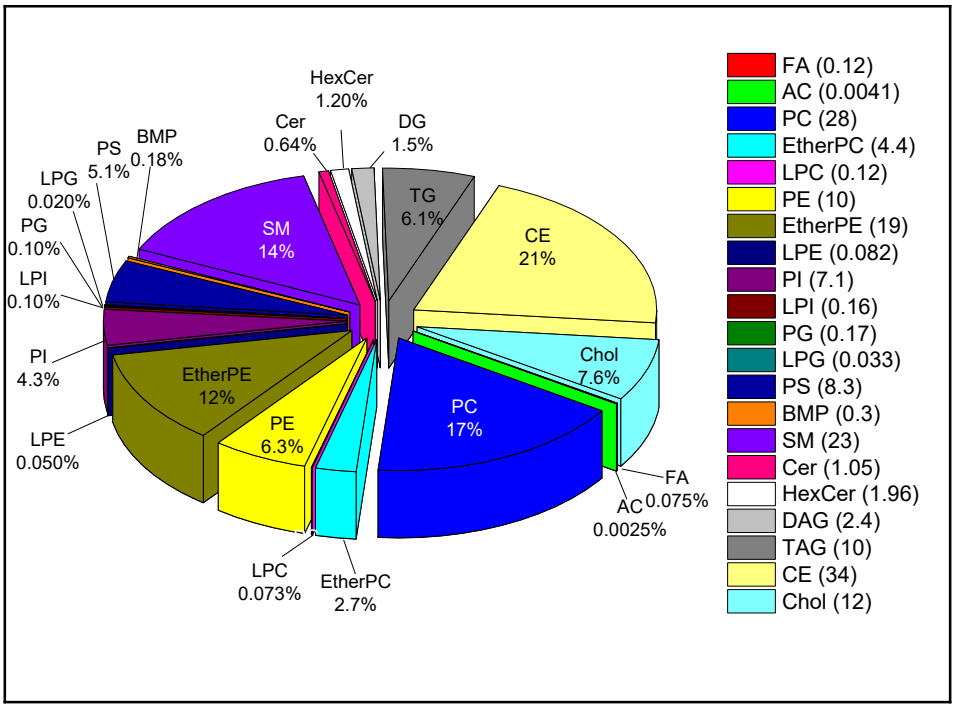

Figure 7.2. Mass percentage distribution of analyzed lipid classes in keratinocytes (Control group). Numbers in parenthesis are the quantities of lipids (μg/million cells, corresponding to pg/cell) determined in each class.

Non-parametric Mann-Whitney-U test and a correction for false discovery rate were employed to determine statistically significant differences[141]. Table B1 shows the values of the fold change between betulin versus control group and corresponding q-values for each monitored signal (1294 in total, see Table B4) of all 611 identified lipids. In general, similar FCs and q-values were obtained for the same lipid species regardless whether they were analyzed on precursor or fragment ion level in ESI (+) or ESI (-) being indicative for the good assay specificity. Out of 611 identified lipids, 440 turned out to be significantly different ($q<0.05$). Relative intensities (as Z-scores) of significantly changed lipids are shown in Figure 7.3. It can be observed that even when some differences are present between samples of the same group (B1-B4 compared to B5-B10), significant changes in the lipid profile of keratinocytes occur after treatment with betulin in certain lipid classes. Thus, all significantly altered triacylglycerides (TGs) and cholesteryl esters (CEs) are down-regulated while the opposite occurs for glycerophospholipids, sphingolipids and diacylglycerides.

A volcano plot for the 611 identified species (Figure 7.4) describes in more detail the significance for the down-regulation or up-regulation of some species (values of $\log_{10}$FC and $\log_2(q)$ can be found in Table B2). For example, as mentioned before TGs and CEs are down-regulated in

samples treated with betulin, however, the FC observed for CEs is more pronounced (< 0.67 for most of them while in the case of TGs the FC is between 0.67 and 1.0). On the other side of the volcano plot, it is possible to see that the rest of studied lipid classes show a clear up-regulation and few species from some of these lipid classes are more significantly up-regulated (FC > 1.5 see Table B3). Up-regulation of acyl carnitines (AC) can be highlighted here considering that four of them are included in the 10 most up-regulated species with a FC > 2.0.

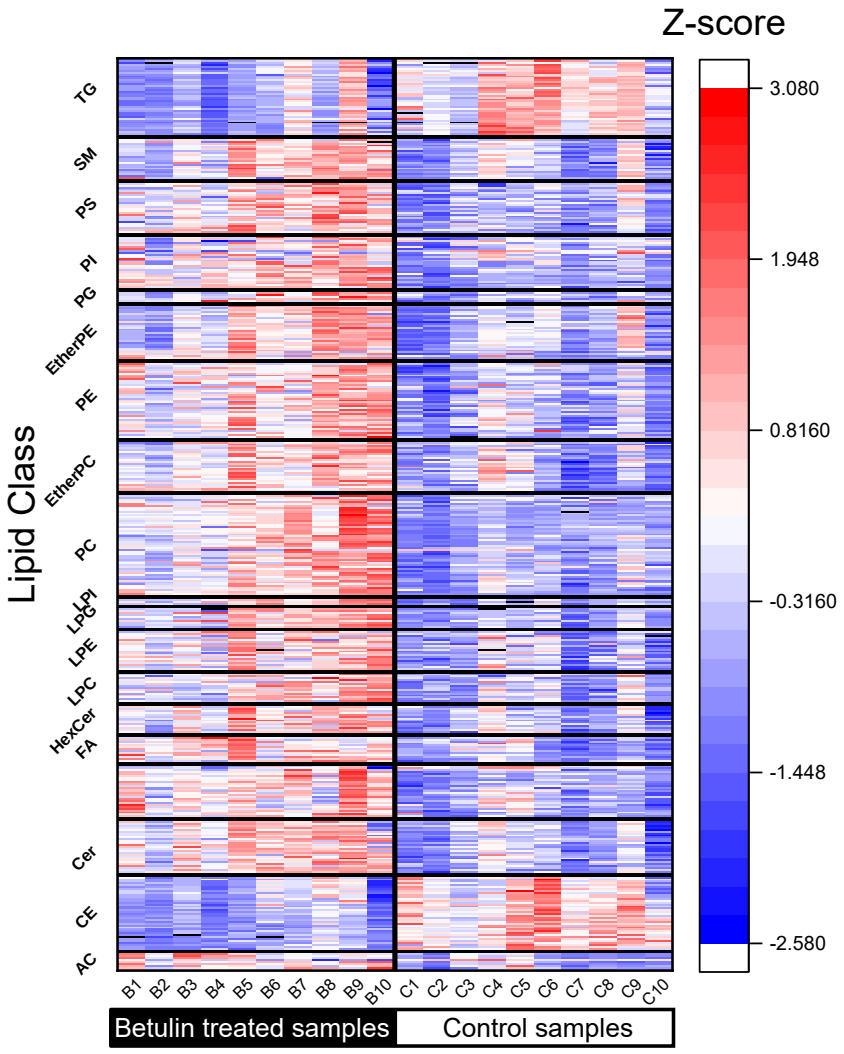

Figure 7.3. Heatmap for comparison of relative intensities of 440 lipids, identified in human immortalized keratinocytes, which showed a significant change (correction for false discovery rate after Mann-Whitney-U test, q-value < 0.05) after treatment with betulin (1.95 µM).

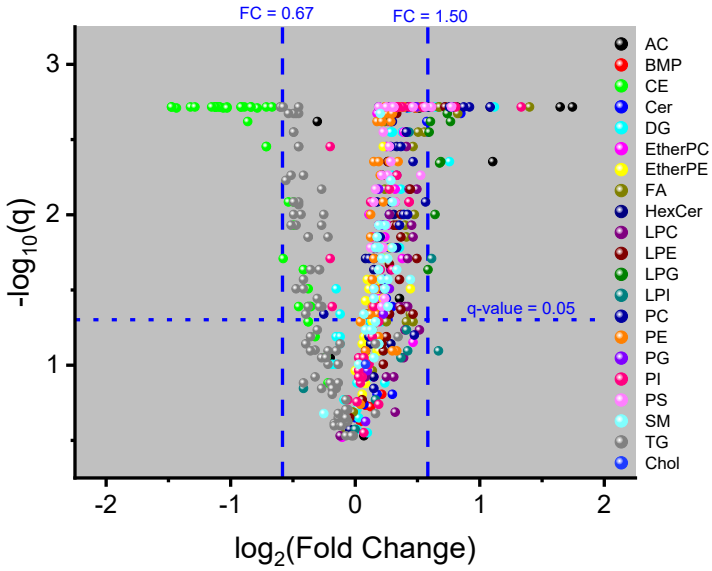

Figure 7.4. Volcano plot for 611 identified lipid species whose intensity was compared between betulin-treated keratinocytes versus control keratinocytes.

Interestingly, most of the up-regulated lipid classes are components of phospholipids and sphingolipids which are essential structural membrane constituents and play an important role in barrier functions of the skin. Here, up-regulation of Cers (e.g. Cer d18:0/24:0, Cer d18:0/24:1) with long chain fatty acids by betulin serve special interest. These lipids are known to be synthesized intracellularly by keratinocytes. They are transported in specialized vesicles to the stratum corneum where they are an important part of the intercellular lipid lamellae forming the water permeability barrier[123,143–145]. The up-regulation of ceramides with long chain fatty acids by betulin may contribute to explain our recent finding that a betulin containing formulation promotes the formation of the skin barrier shown in the *ex-vivo* porcine wound healing model [120]. The down-regulation of (long chain acyl) cholesteryl esters may be an indication for a metabolic remodeling for the above purpose. Our comprehensive study about the influence of betulin on the lipidome of keratinocytes may also support new fields of application, such as treatment of atopic dermatitis, as it was reported that this skin disease is combined with a decrease of long chain fatty acid Cers [126].

7.6.5 Betulin and betulin-related metabolites in treated keratinocytes

In addition to the identified lipid species, some other signals were independently found to be differently abundant in the two sample groups, betulin-treated and control. For example, betulin and some related compounds were detected in the lipid extracts of the betulin-treated samples although the betulin solution was removed after incubation and the keratinocytes washed

before analysis. *m/z*-values and retention times of these peaks are summarized in Table A8. Combined information for adducts eluted at the same retention time and in different polarities allowed the determination of five molecular formulas of compounds, present in the extracts, corresponding to triterpenes.

In order to determine if these signals originate from the betulin solution used for treatment of keratinocytes, standard solutions of betulin and other triterpenes (see chemical structures in Suppl. Figure 7.7) were analyzed by the same method (see Suppl. Table 7.9).

Suppl. Figure 7.8 shows intensities of analyzed signals in samples treated with betulin, control samples and standard solution of betulin. As shown, two compounds, which were found in samples treated with betulin, were present in the betulin standard solution and were identified as betulin (eluted a 2.39 min) and betulinic acid (eluted at 2.64 min). This means that betulin and the impurity betulinic acid, either remained absorbed to the surface of keratinocytes despite washing steps after treatment or more likely, that betulin was incorporated into the lipid membrane of the keratinocytes and extracted with the organic solvents, which is worthwhile to be further investigated. The other three compounds, which have an increased intensity in treated samples compared to the control ones and are not present in the standard solution of betulin, were annotated as “betulin isomer”, “betulin loss of O” and “betulinic acid loss of CH2”. These compounds could correspond to metabolites of betulin produced in the keratinocytes. Future experiments should be undertaken to clarify in which way these metabolites arise.

7.7 Concluding remarks

The presented untargeted lipidomics approach with targeted data processing enables a detailed characterization of the lipidome in keratinocytes and can detect significant differences after “drug” treatment, shown by the natural product betulin. In total, 611 lipids were identified at the “lipid species level” and 440 of them showed to be significantly changed. Changes can be described in terms of lipid classes. Thus, CEs and TGs are significantly down-regulated in betulin treated samples and glycerophospholipids, sphingolipids and diacylglycerides are up-regulated.

Additionally, the presence of betulin in extracts of keratinocytes (previously treated with betulin and washed) indicate that betulin may be incorporated into the membrane of keratinocytes. The presence of other triterpenes in betulin treated samples and absent in control samples could mean that betulin is metabolized in the keratinocytes.

7.8 Conflict of interest statement

None

7.9 Acknowledgements

We are grateful to Prof. Dr. L. Bruckner-Tuderman, Department of Dermatology, Medical Center, University of Freiburg for providing us with human immortalized keratinocytes.

CC is grateful to the DAAD (DAAD no. 57129429) and University of Costa Rica for financial support of his PhD.

7.10 Supplemental

Supplementary text 1. Lipid extraction

Extraction solvents were cooled down for at least 20 min on ice before their addition to samples. Lipid extraction was performed with IPA:H_2O (90:10 v/v) as described previously [140]. Briefly, a 5% (v/v) SPLASH Lipidomix solution was prepared in MeOH and then 50 µL of the diluted solution was added to the cell pellet. Next, 4.95 mL of IPA:H_2O (90:10 v/v) were added. Samples were vortexed (30 s), sonicated (2 min) and vortexed again (30 s) to disrupt the pellet. Incubation on ice was continued on a shaker for 1h (500 rpm, 60 min). Samples were centrifuged (3500 rcf, 10 min) and the supernatant was transferred to 15 mL falcon tubes. Samples were dried in an evaporator (Genevac EZ-2; Warminster, Pennsylvania, USA) for 10 hours under nitrogen protection. Dried extract was resuspended in 100 µL of methanol containing odd-chained lipid standards LPC 17:1 and PC 17:0-20:4 at 500 ng/mL and 125 ng/mL, respectively. Sonication (2 min) and vortexing (30 s) were applied to ensure that lipids were not stuck to the surface of the extraction container. Then, samples were centrifuged (3500 rcf, 10 min) and the supernatant was transferred to vials for LC-MS measurements. Quality control (QC) sample was prepared by pooling together 15 µL aliquot of each sample. Samples were measured randomly and QC samples were run at the beginning, at the end and every fifth sample during the sequence.

Supplementary text 2. Details about LC-MS measurement

The gradient profile was as follows: 0.0 min, 15 % B; 2.0 min, 30 % B; 2.5 min, 48 % B; 11.0 min, 82 % B; 11.5 min, 99 % B; 12.0 min, 99 % B; 12.1 min, 15 % B, 15.0 min, 15 % B. Flow rate was equal to 600 µL/min and column was kept at 65 °C. The injection volume was 3 µL for positive mode and 5 µL for negative mode.

MS settings were used as follows: Curtain gas (CUR) 35 psi, nebulizer gas (GS1) 60 psi, drying gas (GS2) 60 psi, ion-spray voltage floating (ISVF) +5500 V in positive and -4500 V in negative mode, source temperature (T) 350°C, collision energy (CE) 45 V, collision energy spread (CES) 15 V, declustering potential (DP) 80 V, mass range m/z 50 – 1250 in ESI (+) and 50 – 1050 in ESI (-), and RF Transmission (RF) m/z 40: 50 % and m/z 120: 50 %.

An external mass calibration was performed during the sequence every five samples (see list of m/z values for calibration in Table A2).

Supplementary text 3. Definitions of some lipid fragment types

The notation of fragment ions in our document have been done in accordance to the open access document "Proposal for a common nomenclature for fragment ions in mass spectra of lipids" by Pauling *et al.* [100]. In order to facilitate the reading of our document we have copied here some important definitions, given in the mentioned document.

> "LCFs (lipid class-selective fragments) which are characterized by the properties that they can be both neutral and charged, are released from all lipid molecules belonging to the same lipid class and have identical mass, and they do not contain a hydrocarbon chain. Thus, LCFs provide information about structural attributes that are common to all molecules of a particular lipid class (e.g. a head group of a glycerophospholipid). Of note, masses of certain LCFs are not unique given that molecules from other lipid classes can release LCFs with identical masses (e.g. *m/z* 184.0733 can be released from LPC, PC, PC O-, SM species). Moreover, LCFs can only be used to identify lipid molecules at the "lipid species level" (e.g. PC 36:6)".
>
> "MLFs (molecular lipid species-specific fragments) which are characterized by the properties that they can be both neutral and charged, and contain only one hydrocarbon chain with variations in the number of carbon atoms, double bonds and hydroxyl groups. Depending on the lipid class and category, these hydrocarbon chains can be classified as FA, alkanol and alkenol (i.e. plasmanyl and plasmenyl groups, respectively), LCB and sterol moieties. MLFs can be used to identify lipid molecules at the "molecular lipid species level" (e.g. PC 18:3-13:3)".
>
> "iMLFs (intermediate molecular lipid species-selective fragments) which are characterized by the properties that they can be both neutral and charged, and contain two or more hydrocarbon chains that depending on the lipid class can be composites of FA, alkanol, alkenol, LCB and sterol moieties. As for LCFs, iMLFs can only be used to identify intact lipid molecules at the "lipid species level" (e.g. PE 36:2)."

Suppl. Table 7.1. Information about internal standards of the SPLASH™ Lipidomix® Mass Spec Standard (in MeOH)

Mixture Components	Original concentration (µg/mL)	Concentration after resuspension for MS analysis (µmol/mL)
15:0-18:1(d7) DAG	9.40	8.0E-04
15:0-18:1(d7) PA	7.40	5.5E-04
15:0-18:1(d7) PC	160.70	1.1E-02
15:0-18:1(d7) PE	5.70	4.0E-04
15:0-18:1(d7) PG	29.10	2.0E-03
15:0-18:1(d7) PI	9.10	5.5E-04
15:0-18:1(d7) PS	4.20	2.8E-04
15:0-18:1(d7)-15:0 TAG	57.30	3.5E-03
18:1(d7) Chol Ester	356.10	2.7E-02
18:1(d7) LPC	25.50	2.4E-03
18:1(d7) LPE	5.30	5.4E-04
18:1(d7) MAG	2.00	2.8E-04
Cholesterol (d7)	98.40	1.3E-02
d18:1-18:1(d9) SM	30.90	2.1E-03

Suppl. Table 7.2. m/z values of sodium acetate clusters used for external calibration of QTOF

ESI+ (m/z)	ESI- (m/z)
104.99230	141.01693
351.00152	223.02000
433.00459	305.02307
515.00767	387.02615
597.01074	469.02922
679.01381	551.03230
761.01689	633.03537
843.01996	715.03844
1007.02611	797.04152
1089.02918	879.04459
	961.04767
	1043.05074

Suppl. Table 7.3. Information about design of MS and MS/MS experiments

Experiment	MS Type	Accumulation time (ms)	Pos mode		Neg mode	
			Min m/z	Max m/z	Min m/z	Max m/z
MS	SCAN	80	50	1250	50	1050
MS/MS	SWATH 1	31	50.0	214.6	50.0	342.2
MS/MS	SWATH 2	31	213.6	281.8	341.2	453.6
MS/MS	SWATH 3	31	280.8	390.7	452.6	480.8
MS/MS	SWATH 4	31	389.7	480.4	479.8	507.8
MS/MS	SWATH 5	31	479.4	509	506.8	532.3
MS/MS	SWATH 6	31	508	536.5	531.3	566.8
MS/MS	SWATH 7	31	535.5	610.6	565.8	617.4
MS/MS	SWATH 8	31	609.6	677.1	616.4	687.1
MS/MS	SWATH 9	31	676.1	709.0	686.1	715.0
MS/MS	SWATH 10	31	708.0	735.1	714.0	744.1
MS/MS	SWATH 11	31	734.1	759.1	743.1	755.1
MS/MS	SWATH 12	31	758.1	773.1	754.1	776.0
MS/MS	SWATH 13	31	772.1	790.2	775.0	794.6
MS/MS	SWATH 14	31	789.2	811.2	793.6	807.6
MS/MS	SWATH 15	31	810.2	827.2	806.6	830.3
MS/MS	SWATH 16	31	826.2	856.2	829.3	840.1
MS/MS	SWATH 17	31	855.2	884.3	839.1	859.2
MS/MS	SWATH 18	31	883.3	915.9	858.2	889.1
MS/MS	SWATH 19	31	914.9	983.7	888.1	924.6
MS/MS	SWATH 20	31	982.7	1250.0	923.6	1050.0

Suppl. Table 7.4. Selected precursor and fragments ions for identification of each lipid class in ESI (+) and ESI (-)

Lipid class	ESI (+)			ESI (-)		
	Precursor ion TOF-MS scan	LCF or iMLF	Molecular lipid species-specific fragments (MLF)	Precursor ion TOF-MS scan	LCF or iML	Molecular lipid species-specific fragments (MLF)
FA				[FA x:y-H]- [M-H]-		
AC	[AC x:y + H]+ [M]+	AC(85) [C4H5O2]+				
CE	[SE 27:1/x:y+NH4]+ [M+NH4]+	ST 27:1(-H) Sterol Fragment				
LPC	[LPC x:y+H]+ [M+H]+	PC(184) [C5H15NO4P]+		[LPC x:y+HCOO]- [M+HCOO]-	-LPC(60) [M-CH3]-	FA1 x:y(+O)/FA2 x:y(+O) SN1/SN2
LPE	[LPE x:y+H]+ [M+H]+	FA x:y(+C3H6O2) [M-C2H8NO4P]+		[LPE x:y-H]- [M-H]-		FA1 x:y(+O)/FA2 x:y(+O) SN1/SN2
LPI	[LPI x:y+NH4]+ [M+NH4]+			[LPI x:y-H]- [M-H]-	LPI(241) [Inositol Phosphate-H2O]- LPI(315) NL of SN1/SN2+H2O	FA1 x:y(+O)/FA2 x:y(+O) SN1/SN2
LPG				[LPG x:y-H]- [M-H]-		FA1 x:y(+O)/FA2 x:y(+O) SN1/SN2
BMP	[BMP x:y+NH4]+ [M+NH4]+		FA1 x:y(+C3H6O2) [SN1+C3H5O]+ FA2 x:y(+C3H6O2) [SN2+C3H5O]+			
Cer	[Cer x:y;z+H]+ [M+H]+		LCB x:y;z(-H3O2) [Sph-2H2O+H]+ FA x:y(+H3N) [FAA+H]+	[Cer x:y;z+HCOO]- [M+HCOO]-		FA x:y(+C2H3N) [FA+NCCO-O-3H]-
HexCer	[HexCer x:y;z+H]+ [M+H]+		LCB x:y;z(-H3O2) [Sph-2H2O+H]+	[HexCer x:y;z+HCOO]- [M+HCOO]-		
PC	[PC x:y+H]+ [M+H]+	PC(184) [C5H15NO4P]+		[PC x:y+HCOO]- [M+HCOO]-	-PC(60) [M-CH3]-	FA1 x:y(+O) and FA2 x:y(+O) SN1 and SN2
EtherPC	[PC O-x:y+H]+ [M+H]+	PC(184) [C5H15NO4P]+		[PC O-x:y+HCOO]- [M+HCOO]-	-PC O-(60) [M-CH3]-	FA2 x:y(+O) SN2
PE	[PE x:y+H]+ [M+H]+	-PE O-(141) [M+H-C2H8NO4P]+		[PE x:y-H]- [M-H]-		FA1 x:y(+O) and FA2 x:y(+O) SN1 and SN2
EtherPE	[PE O-x:y+H]+ [M+H]+	-PE O-(141) [M+H-C2H8NO4P]+	FA x:y(+C3H6O2) NL of C2H8NO4P+SN1	[PE O-x:y-H]- [M-H]-		FA2 x:y(+O) SN2
PI	[PI x:y+NH4]+ [M+NH4]+	-PI(277) [M-C6H12O9P]+		[PI x:-H]- [M-H]-		FA1 x:y(+O) and FA2 x:y(+O) SN1 and SN2
PG	[PG x:y+NH4]+ [M+NH4]+	-PG(189) [M-C3H8O6P]+		[PG x:y-H]- [M-H]-		FA1 x:y(+O) and FA2 x:y(+O) SN1 and SN2
PS	[PS x:y+H]+ [M+H]+	-PS(185) [M+H-C3H8NO6P]+		[PS x:y-H]- [M-H]-	-PS(87) NL of C3H5NO2	FA1 x:y(+O) and FA2 x:y(+O) SN1 and SN2
SM	[SM x:y;z +H]+ [M+H]+	PC(184) [C5H15NO4P]+		[SM x:y;z+HCOO]- [M+HCOO]-	-SM(60) [M-CH3]-	
DG	[DG x:y+NH4]+ [M+NH4]+		-FA1(+OH) and -FA2(+OH) SN1 and SN2 acyl loss			
TG	[TG x:y+NH4]+ [M+NH4]+		-FA1(+OH), -FA2(+OH) and -FA3(+OH) SN1, SN2 and SN3 acyl loss			
Chol	[SE 27:1-OH]+ [M-H2O+H]+					

Notes: LCF, Lipid class-selective fragments; iMLF, intermediate molecular lipid species-selective fragment. In black the recommended notation according to Pauling *et al.* [100] and in red the original notation from LipidBlast database[97] are given. x: number of carbons, y: number of double bonds, z: number of OH groups in the long chain base and acyl moiety.

Suppl. Table 7.5. Parameter for integration of peaks in Multiquant 3.0

MultiQuant parameter	Value	Unit
Gaussian Smooth With	1.0	points
RT Half Window	3	Sec
Min. Peak Width	5	Points
Min Peak Height	50	Cps
Noise Percentage	40	%
Baseline Sub. Window	2.00	Min
Peak Splitting	1	Point

Suppl. Table 7.6. Quantitation method for each analyzed lipid class

Lipid class	Standard	Quantitation method
FA	Arachidonic acid-d8	7 points standard addition
	alpha-Linolenic acid-d14	
AC	C18:1 Carnitine	7 points standard addition
CE	18:1(d7) Chol Ester	1 point calibration
LPC	18:1(d7) LPC	1 point calibration
LPE	18:1(d7) LPE	1 point calibration
LPI	15:0-18:1(d7) PI	1 point calibration
LPG	15:0-18:1(d7) PG	1 point calibration
BMP	18:1-18:1 BMP	7 points standard addition
Cer	Ceramide d18:1/18:0	7 points standard addition
HexCer	Glucosyl(ß) Ceramide (d18:1/17:0)	7 points standard addition
PC	15:0-18:1(d7) PC	1 point calibration
EtherPC	15:0-18:1(d7) PC	1 point calibration
PE	15:0-18:1(d7) PE	1 point calibration
EtherPE	15:0-18:1(d7) PE	1 point calibration
PI	15:0-18:1(d7) PI	1 point calibration
PG	15:0-18:1(d7) PG	1 point calibration
PS	15:0-18:1(d7) PS	1 point calibration
SM	d18:1-18:1(d9) SM	1 point calibration
DG	15:0-18:1(d7) DAG	1 point calibration
TG	15:0-18:1(d7)-15:0 TAG	1 point calibration
Chol	Cholesterol (d7)	1 point calibration

Suppl. Table 7.7. Distribution of coefficient of variations (CVs, %) for 1293 analyzed traces (of 610 identified lipid species) in each group of samples (See Suppl. Figure 3.6)

CV bin (%)	Samples treated with betulin N = 10	Control samples N = 10	QC 10 injections
	Amount of traces		
0-5	0	1	36
5-10	205	164	576
10-15	402	510	383
15-20	280	267	153
20-25	171	153	90
25-30	110	102	44
30-35	69	50	8
35-40	30	32	3
40-45	10	8	0
45-50	6	2	0
50-55	5	1	0
55-60	3	1	0
60-65	1	0	0
65-70	0	0	0
>70	1	2	0
Total	**1293**	**1293**	**1293**

Suppl. Table 7.8. List of detected peaks in extract of keratinocytes with a significant FC for comparison between betulin and control group, which were analyzed as betulin related metabolites

Number	Analysis	RT	Measured m/z	Assigned formula	Exact mass	Error (ppm)	Assigned adduct	Neutral formula	Assigned compound
1	ESI (+)	2.39	425.3781	C30H49O	425.3778	1	[M-H2O+H]+	C30H50O2	Betulin
			443.3883	C30H51O2	443.3884	0	[M+H]+		
			460.4143	C30H54NO2	460.4149	-1	[M+NH4]+		
	ESI (-)	2.39	487.3783	C31H51O4	487.3793	-2	[M+FA-H]-		
2	ESI (+)	2.64	457.3690	C30H49O3	457.3676	3	[M+H]+	C30H48O3	Betulinic acid
			474.3945	C30H52NO3	474.3942	1	[M+NH4]+		
	ESI (-)	2.64	455.3540	C30H47O3	455.3531	2	[M-H]-		
			911.7160	C60H95O6	911.7134	3	[2M-H]-		
3	ESI (+)	3.7	425.3784	C30H49O	425.3778	1	[M-H2O+H]+	C30H50O2	Betulin isomer
			460.4156	C30H54NO2	460.4149	1	[M+NH4]+		
4	ESI (-)	3.75	441.3360	C29H45O3	441.3374	-3	[M-H]-	C29H46O3	Betulinic acid loss of CH2
5	ESI (+)	5.2	444.4191	C30H54NO	444.4200	-2	[M+NH4]+	C30H50O	Betulin loss of O
			409.3817	C30H49	409.3829	-3	[M-H2O+H]+		

Suppl. Table 7.9. Retention times for standards of betulin and some other related compounds

Standard (0.195 mM)	Assigned formula	Analyzed adducts	Measured m/z	Exact m/z	Error (ppm)	Mode	Retention time (min)
Betulin	C30H50O2	[M-H2O+H]+	425.377	425.3778	-2	ESI (+)	2.39
		[M+H]+	443.3877	443.3884	-1		
		[M+NH4]+	460.4142	460.4149	-2		
		[M+FA-H]-	487.3776	487.3793	-3	ESI (-)	
Betulinic acid	C30H48O3	[M+H]+	457.3679	457.3676	1	ESI (+)	2.64
		[M+NH4]+	474.3945	474.3942	1		
		[M-H]-	455.3519	455.3531	-3	ESI (-)	
Erythrodiol	C30H50O2	[M-H2O+H]+	425.3775	425.3778	-1	ESI (+)	2.83
		[M+H]+	443.389	443.3884	1		
		[M+NH4]+	460.4154	460.4149	1		
		[M+FA-H]-	487.3774	487.3793	-4	ESI (-)	
Lupeol	C30H50O	[M-H2O+H]+	409.3818	409.3829	-3	ESI (+)	5.03
		[M+H]+	427.3925	427.3935	-2		
		[M+NH4]+	444.4187	444.4200	-3		
		[M+FA-H]-	471.3828	471.3844	-3	ESI (-)	5.03

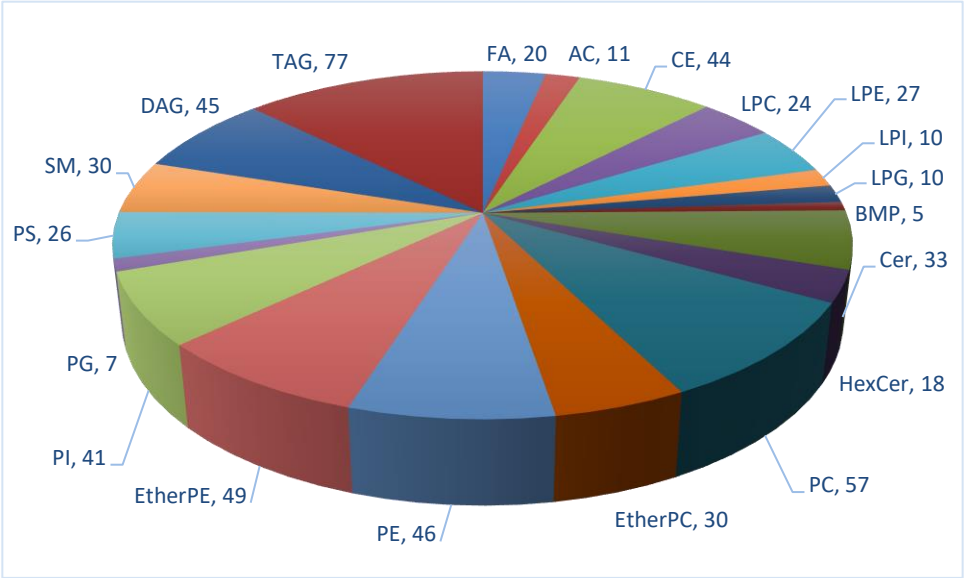

Suppl. Figure 7.1. Distribution of 611 identified lipids in QC samples according to their lipid class with number of identified lipids for each class.

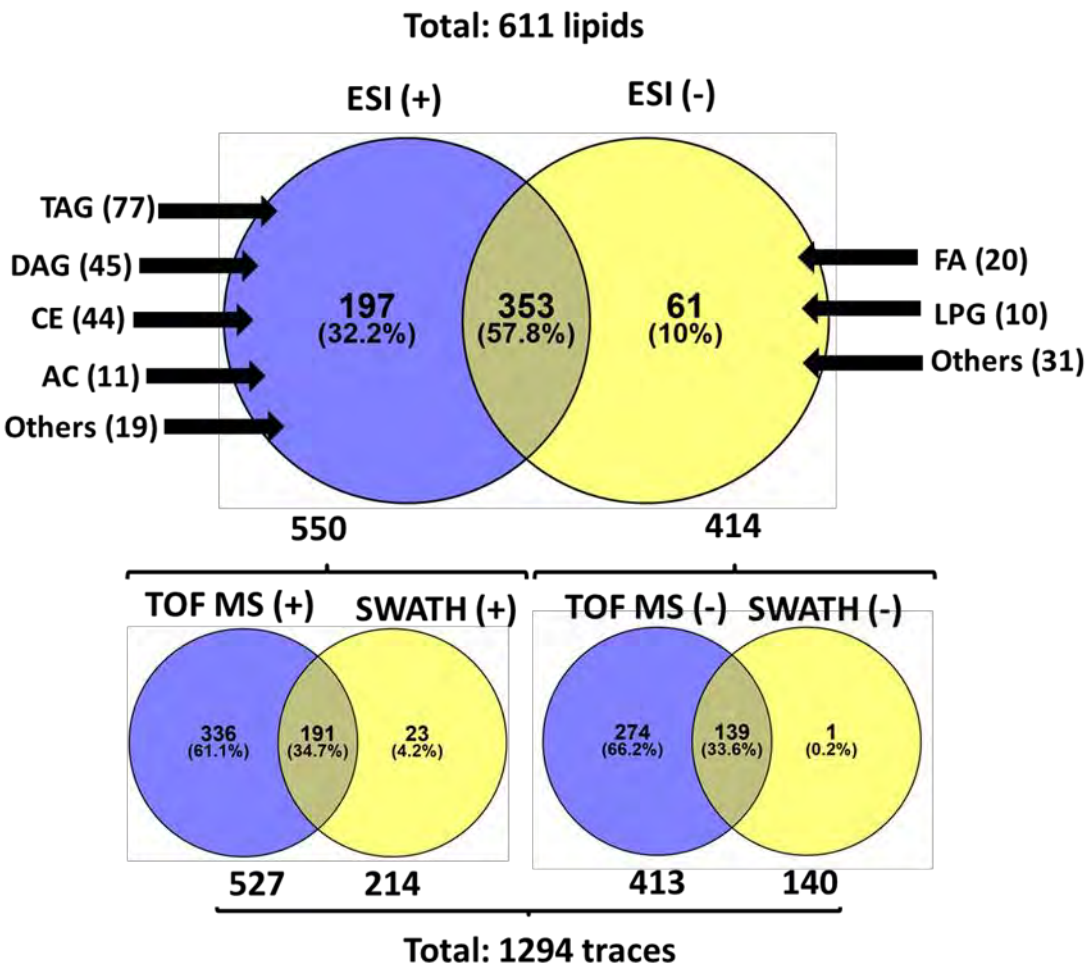

Suppl. Figure 7.2. Venn diagram showing the number of lipids identified in each ion mode and the distribution MS data used for identification of lipids in QC samples of keratinocytes.

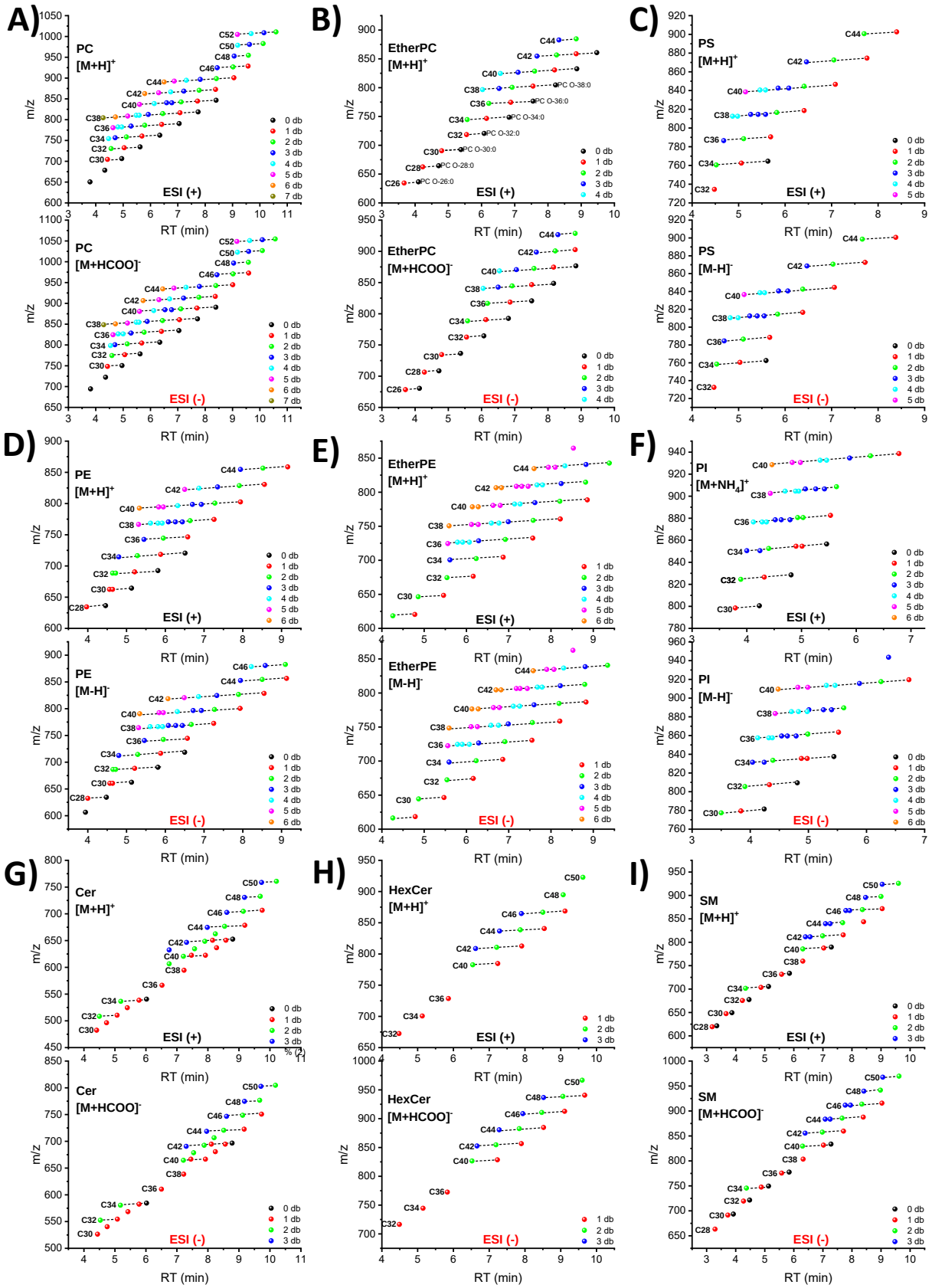

Suppl. Figure 7.3. Spot maps m/z versus retention time for specific adducts of lipid classes in TOF MS analyzed in the ESI (+) and ESI (-). Colored series correspond to different number of unsaturation, db: amount of double bonds.

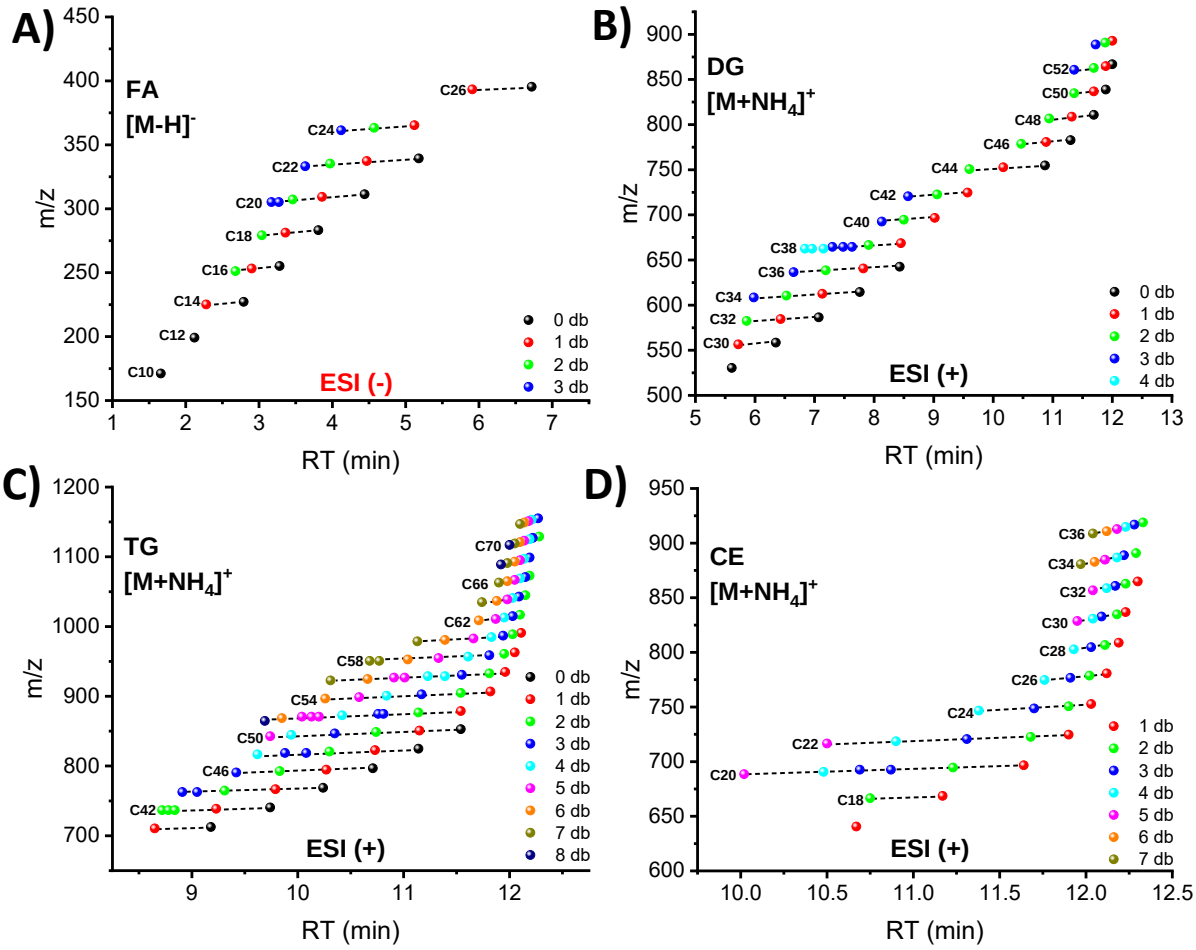

Suppl. Figure 7.4. Spot maps m/z versus retention time for specific adducts of lipid classes in TOF MS analysis either in the ESI (+) or ESI (-). Colored series correspond to different number of unsaturation, db: amount of double bonds.

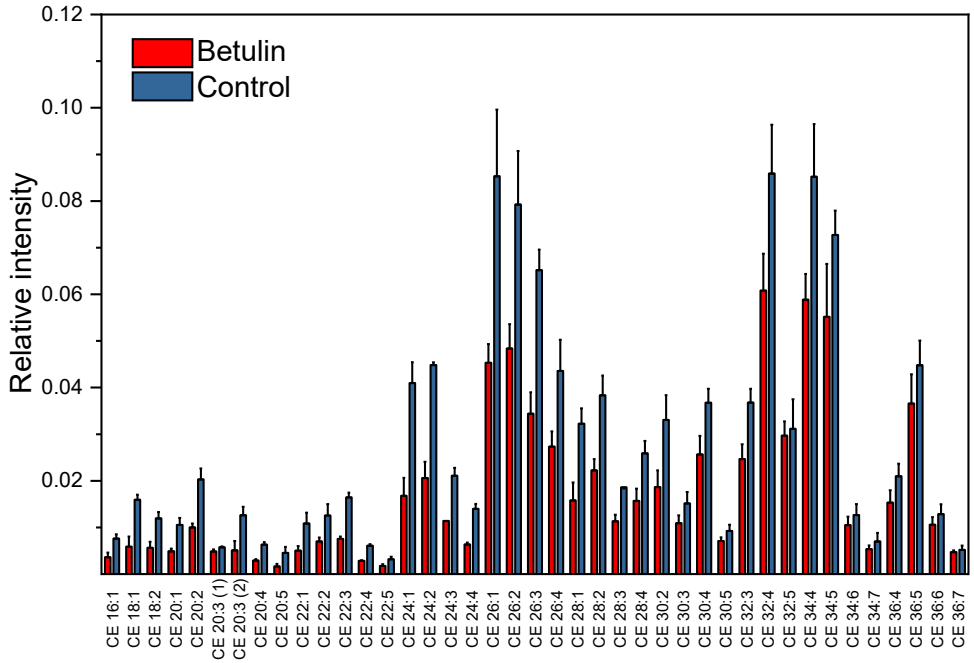

Suppl. Figure 7.5. Relative intensities of CEs identified in betulin and control groups. CEs with fatty acyl chains from 16:1 to 36:7 are present. Bar represents median and error bars standard error

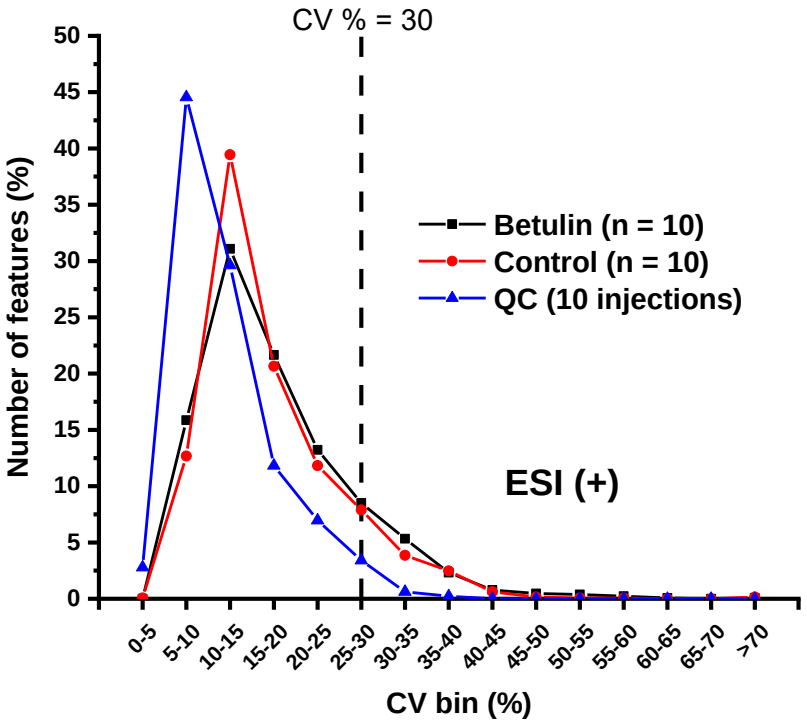

Suppl. Figure 7.6. Distribution of coefficient of variations (CVs, %) for 1293 analyzed traces (of 610 identified lipid species) in each group of samples, (See values in Table A6).

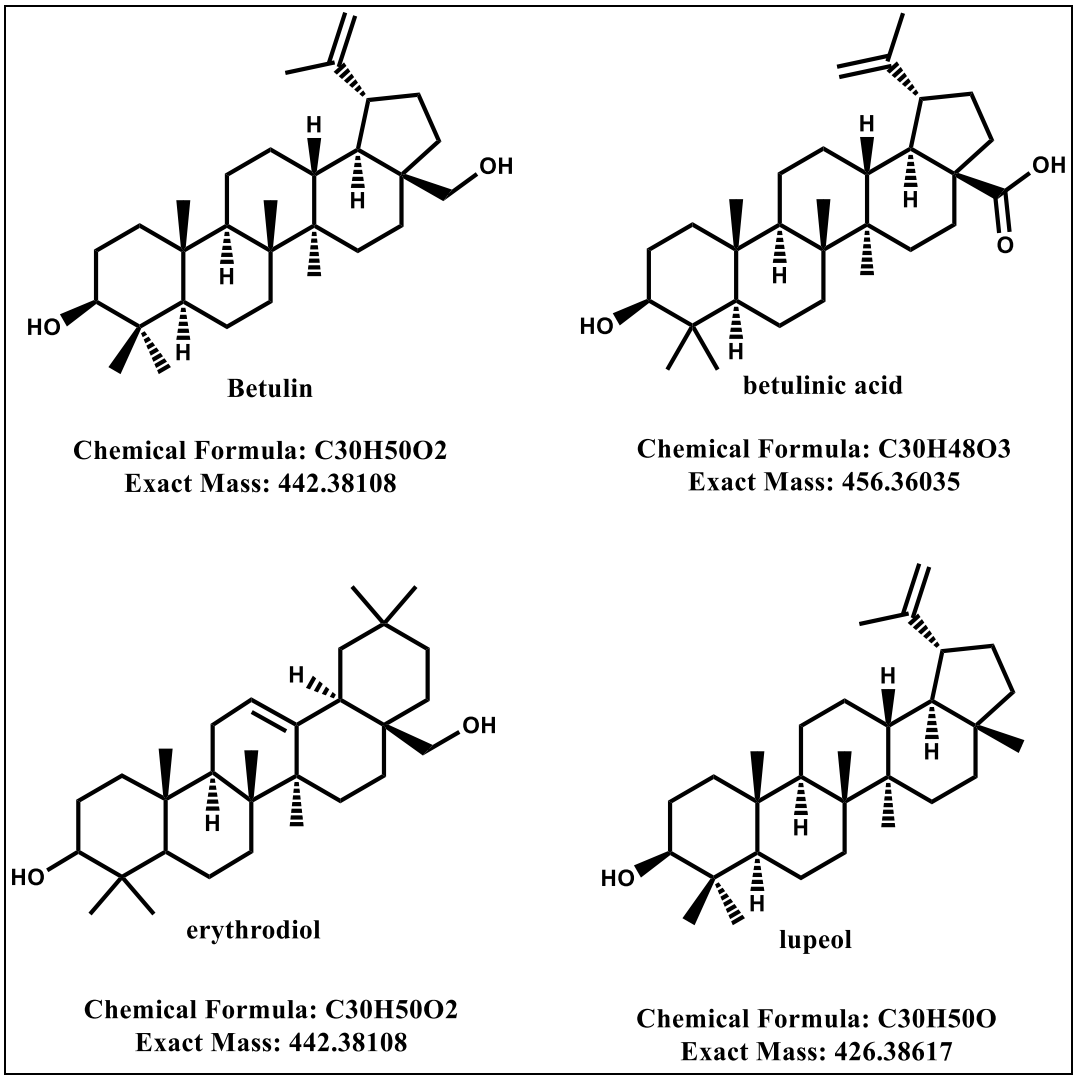

Suppl. Figure 7.7. Chemical structure of betulin and related compounds betulinic acid, erythrodiol and lupeol

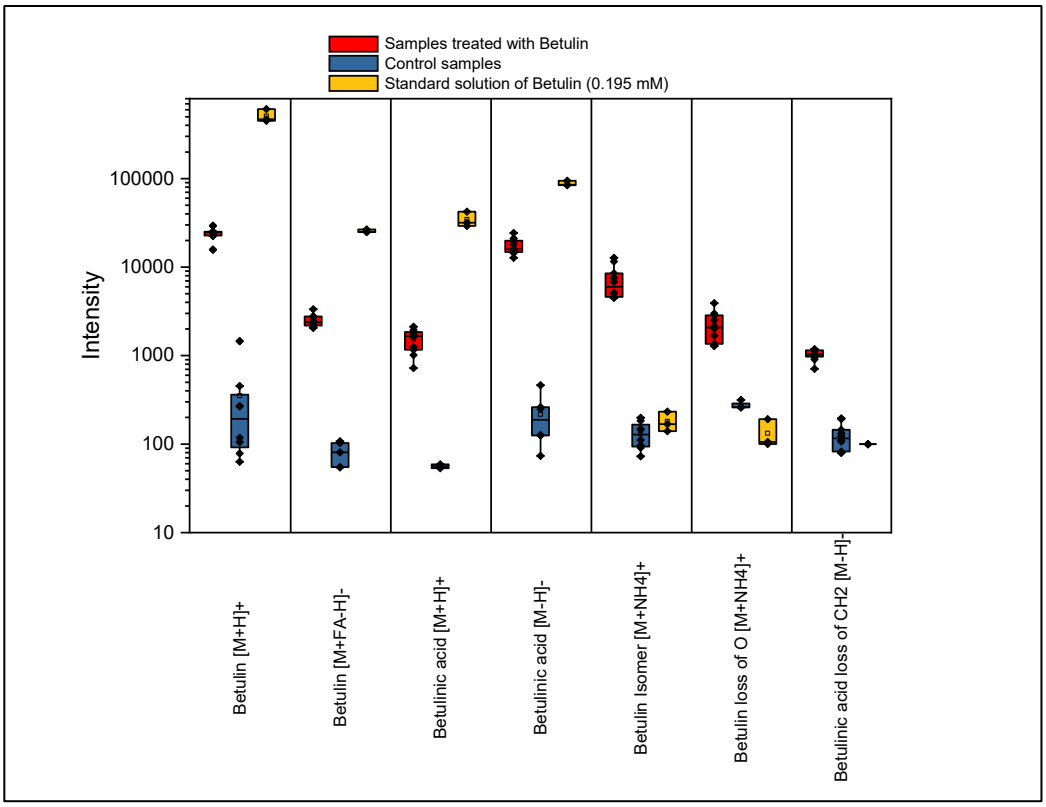

Suppl. Figure 7.8. Absolute intensities of some triterpenes signals observed in lipid extract of keratinocytes

8 Publication III. Chiral separation of 2-hydroxyglutaric acid

8.1 Title

Chiral Separation of 2-Hydroxyglutaric Acid on Cinchonan Carbamate based Weak Chiral Anion Exchangers by High-Performance Liquid Chromatography

Carlos Calderón [1], Jeannie Horak [1], Michael Lämmerhofer [1] *

[1] Institute of Pharmaceutical Sciences, Pharmaceutical (Bio-)Analysis, University of Tübingen, Auf der Morgenstelle 8, 72076 Tübingen, Germany

Reprinted with permission from Journal of Chromatography A, Volume 1467, Pages 239-245,

DOI: 10.1016/j.chroma.2016.05.042

Copyright (2016) Elsevier B.V.

8.2 Abstract

D- and L-2-Hydroxyglutaric acid (D- and L-2-HG, respectively) are metabolites related to some diseases (2-hydroxyglutaric aciduria, cancer), which make their identification and analysis crucially important for diagnostic purposes. Chiral stationary phases (CSP) based on *tert*-butylcarbamoyl-quinine and -quinidine (Chiralpak QN-AX and QD-AX), and the corresponding zwitterionic derivatives (Chiralpak ZWIX(+) and Chiralpak ZWIX(-)) were employed in a weak anion-exchange mechanism to perform the enantiomer separation of D- and L-2-HG without derivatization.

QD-AX CSP showed the most promising separation and therefore optimization of eluent, additives, and temperature, required for the baseline separation of solutes was carried out. Depending on experimental conditions resolution values ranged up to 2.0 with run times < 20 min and MS-compatible conditions. Inversion on the elution order of D- and L-2-HG was possible by using the pseudo-enantiomeric QN-AX CSP.

8.3 Introduction

2-Hydroxyglutaric acid is a clinically relevant chiral metabolite existing in two enantiomeric forms, i.e. D-2-HG and L-2-HG (Figure 8.1a). Generally, their concentrations in humans are relatively low, with intracellular levels in normal cells below 0.1 mM [146]. However, high concentrations of these compounds have been identified in some patients, who suffer of particular diseases.

The best known of these diseases are D-2-hydroxyglutaric aciduria and L-2-hydroxyglutaric aciduria, which are reported for the first time in 1977 [147,148] and 1980 [149], respectively. Since then, multiple reports of both types of diseases have been published [150,151,160–163,152–159]. Also, cases of combined D,L-2-hydroxyglutaric aciduria have been reported [164].

The clinical phenotype of patients with D-2-hydroxyglutaric aciduria includes epilepsy, hypotonia and psychomotor retardation [156]. The clinical phenotype of patients with L-2-hydroxyglutaric aciduria is characterized mainly by developmental delay, epilepsy and cerebellar ataxia [156].

More recently, high concentrations of D-2-HG have been identified in cancer cells, including gliomas, glioblastomas and acute myelogenous leukemia (AML), with mutations of the enzymes isocitrate dehydrogenase 1 (IDH1) and isocitrate dehydrogenase 2 (IDH2) [158,165].

Mutated IDH enzymes reduce the compound 2-oxoglutarate (2-OG) to D-2-HG, considered an oncometabolite (or cancer-causing metabolite). 2-OG is a tricarboxylic acid (TCA) cycle intermediate and an essential cofactor for many enzymes [146]. The levels of D-2-HG in IDH mutant tumors can be extremely elevated, ranging from 1 mM to as high as 30 mM, hence being 10 to 300 times higher than the normal values [146].

Due to the clinical importance of D-2-HG and L-2-HG, different methodologies have been developed in order to identify and quantify their concentration in biological fluids enantioselectively. Indirect gas chromatographic enantiomer analysis using precolumn derivatization with 2-(-)-butanol as chiral derivatizing agent (CDA) for esterification and *O*-acetylation with acetic anhydride [148,149,153] or with (S)-(+)-3-methyl-2-butanol for carboxyl group derivatization and O-trifluoroacetylation [163] have been proposed. Some reports described direct GC enantiomer separation methods with achiral derivatization, e.g. with ethyl chloroformate, and subsequent analysis on cyclodextrin-based enantioselective columns [161,166]. A number of studies also reported indirect LC-enantiomer separation of 2-HG, e.g. after derivatization with diacetyl-L-tartaric anhydride [160], or with *N*-(p-toluenesulfonyl)-L-phenylalanyl chloride [167]. Only a few studies used direct liquid chromatographic enantiomer separation. In one study, D-2-hydroxyglutarate dehydrogenase activity was measured in cell homogenates derived from D-2-hydroxyglutaric aciduria patients using enantioselective ligand-exchange LC with D-penicilamine-based CSP and 2 mM Cu(II) acetate in water-MeOH (90:10; v/v) as eluent [168]. This method showed excellent enantioselectivity but the Cu(II) ions in the eluent prevent its hyphenation to MS. In another study, enantiomeric separation of D- and L-2-HG was achieved by HPLC-MS using a ristocetin A glycopeptide antibiotic silica gel bonded column [162]. Last but not least, the enantioselective determination of D-2-HG in urine samples by using enantioselective membrane electrodes based on vancomycin and teicoplanin is worth to be mentioned [159].

In this study, a screening of the capability of four different chiral stationary phases (Figure 8.1b) for the separation of the enantiomers D- and L-2-HG is performed. Conditions for the separation without derivatization are optimized by using HPLC-MS compatible conditions. This allows a straightforward translation of the procedure obtained in this work to a MS related platform in a subsequent step for the analysis of biologically relevant samples such as from cancer patients using a HPLC-MS/MS approach.

8.4 Experimental

8.4.1 Materials

All solvents used were of HPLC grade. Acetonitrile (ACN) was purchased from Panreac (Barcelona, Spain), methanol (MeOH) was obtained from VWR (Vienna, Austria), ethanol (EtOH) was obtained from Sigma–Aldrich (Munich, Germany) and 1-propanol (PrOH) from Merck (Darmstadt, Germany). The employed water was purified by a water filtration system from Elga Veolia (Paris, France). Formic acid (FA) was supplied by Roth (Karlsruhe, Germany). Acetic acid (AcOH), ammonia in methanol (NH_3), diethylamine (DEA) and triethylamine (TEA) were obtained from Sigma–Aldrich (Munich, Germany).

The racemic mixture D,L-2-hydroxyglutaric acid sodium salt and the enantiomerically pure compound L-2-hydroxyglutaric acid sodium salt were purchased from Sigma–Aldrich. The enantiomer elution order was assessed by injection of single enantiomer and/or non-racemic mixtures. The analytes were dissolved in water or methanol at approximate concentrations of 1.0 mg/mL.

8.4.2 Instrumentation and chromatographic method

All chromatographic measurements were performed on a 1100 Series HPLC from Agilent Technologies (Waldbronn, Germany) consisting of a solvent degasser, a binary pump, an autosampler, a column thermostat and a UV–VIS detector. The HPLC system was connected to a Corona® Charged Aerosol Detector, CAD® from ESA Biosciences Inc., (Chelmsford, U.S.A.). The nitrogen flow of the CAD was adjusted to 35 psi. Data acquisition and analysis were done with ChemStation chromatographic data software from Agilent Technologies. The void volumes of the columns were determined by injecting a solution of 10% acetone in MeOH with detection at 280 nm.

Four different chiral stationary phases were employed in this study: a Chiralpak ZWIX(+) column (150 x 4 mm ID, 3 µm particle size), a Chiralpak ZWIX(-) column (150 x 4 mm ID, 3 µm particle size), a Chiralpak QD-AX (150 x 4 mm, 5 µm) and a Chiralpak QN-AX (150 x 4 mm ID, 5 µm particle size) from Chiral Technologies Europe (Illkirch, France).

The columns were conditioned with the selected mobile phase at a flow rate of 1.0 mL/min for at least 30 min, before performing analysis. Unless otherwise stated, the column temperature was kept at 25°C.

8.5 Results and discussion

8.5.1 Column screening and elution order

Chiralpak ZWIX(+) and ZWIX(-) as well as Chiralpak QD-AX and QN-AX correspond to chiral zwitterionic ion-exchangers and chiral anion exchangers, respectively, based on carbamoylated cinchona alkaloid derivatives as illustrated in Figure 8.1b. In the case of the chiral zwitterionic (ZWIX) selectors, successful separation of chiral acids [169], chiral bases [170,171] and zwitterionic chiral species [169,172,173] have been reported. Chiral weak anion-exchange (WAX) selectors have been employed for the chiral separation of amino acids derivatives [174–176], acids [177] and peptides [178]. Although many chiral acidic compounds have been successfully separated using both types of selectors, it should be pointed out that in most of these cases, the acidic compounds corresponded to structures in which not only the acid motif but also other functional groups were present as supportive interaction sites with the chiral selectors (SO). This includes in particular aromatic rings for π-π-interaction and amide or carbamate moieties with hydrogen donor-acceptor groups for H-bonding or dipole-dipole stacking. The lack of such interaction sites with strong directional nature makes the separation of enantiomers in the case of simpler molecules, like aliphatic hydroxy alkanoic acids, more difficult. The hydroxyl group can freely rotate so that the H-donor is less directed. Hydroxyl groups are furthermore strongly solvated in polar solvents such as water, which renders them less available for interaction with the chiral selector. In spite of these difficulties, lactic acid enantiomer separation has been reported by using QN-AX and QD-AX columns [179] and some 3-hydroxycarboxylic acids have been separated by using ZWIX(+) and ZWIX(-) columns using a polar organic elution mode [180]. Different ratios of ACN-MeOH were used in those cases for the elution of analytes, and normally formic acid or acetic acid as additives (the dissociation products of which represent counterions) were employed to increase the elution strength. In 2-HG another unfavorable structural feature is present in the analyte. The second carboxylic acid group increases the effective charge number which causes stronger retention. Furthermore, it may compete with the α-carboxylic acid for interaction at the anion-exchanger site which leads to a mixture of distinct binding states, a situation that is often accompanied by a decrease in enantioselectivity [181]. All these aspects make method development for 2-HG rather challenging.

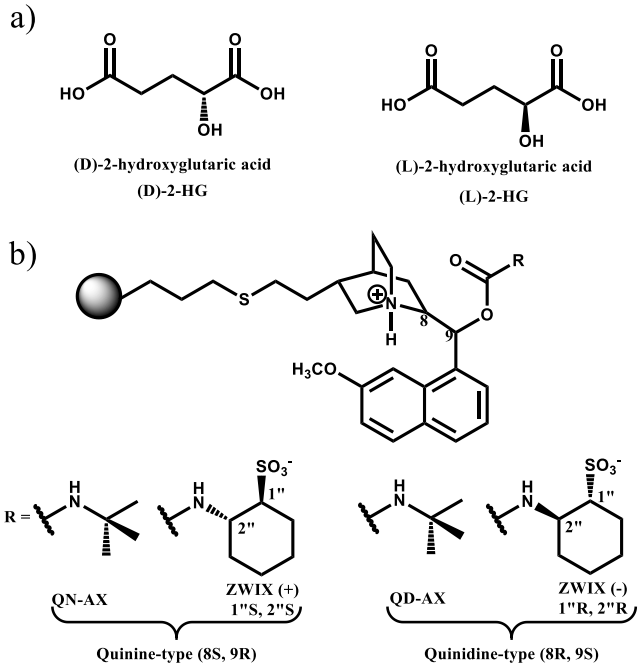

Figure 8.1. a) Enantiomers of 2-HG-, D-2-hydroxyglutaric acid and L-2-hydroxyglutaric acid, b) Chiral stationary phases tested in this study: Chiralpak QN-AX and QD-AX as well as Chiralpak ZWIX(+) and ZWIX(-)

This raises the question for availability of a generic screening experiment, which can be utilized to figure out reasonable starting conditions for a systematic optimization. The column supplier typically suggests following a decision tree. However, this may need a couple of experiments until useful starting conditions are identified. We herein propose gradient elution, which is quite uncommon in enantiomer separation, as a generic screening run [182]. Considering the different retention capacities that ZWIX and WAX selectors possess, gradient elution was tested to approximate the conditions required for the elution of D- and L-2-HG. In a first approach, an ACN:MeOH ratio of 75:25 (v/v) was maintained constant and formic acid, constituting the competing acid additive, was increased from 0 to 90 mM in 30 min (acid additive gradient). As expected, 2-HG enantiomers were stronger retained on the WAX columns due to the intramolecular counterion effect [169]that sulfonic acid groups (see Figure 8.1b.) exert in case of ZWIX selectors (Figure 8.2, Suppl. Table 8.1). The sulfonic acid group is present in the chiral selector molecule in equimolar quantities to the anion-exchanger site at which 2-HG binds and contributes to the displacement of the analyte. Thus, the concentration of the displacer (competing acid) in the mobile phase can be lower or in other words the analyte elutes at lower retention factors as compared to the corresponding chiral anion-exchanger which lacks such intramolecular counterion effect. A slight separation was observed under tested conditions with ZWIX(+) (R_S = 0.13) and no resolution with ZWIX(-) columns, while an almost baseline separation was achieved using QD-AX (R_S = 1.35) and QN-AX (R_S = 1.11) columns (Figure 8.2, Suppl. Table

8.2). Due to successful enantiomer separations with the chiral WAX columns, it was of interest to determine the elution order of D- and L-2-HG and more importantly if this elution order can be inversed by exchanging a QD-AX for a QN-AX column. Injection of pure L-2-HG enantiomer solution showed indeed an inversion in the elution order; D-2-HG is eluted first on the QD-AX column and L-2-HG is eluted first on the QN-AX column (Figure 8.2). It is a characteristic feature of quinine and quinidine carbamate selectors that are actually diastereomeric to each other but behave experimentally like pseudo-enantiomers. Other CSPs derived from natural chiral pool such as Chirobiotic phases do not offer such a possibility. This enables elution of the minor enantiomer ahead of the major enantiomer peak which is advantageous for the accuracy of the method and can be sometimes helpful for validation purposes.

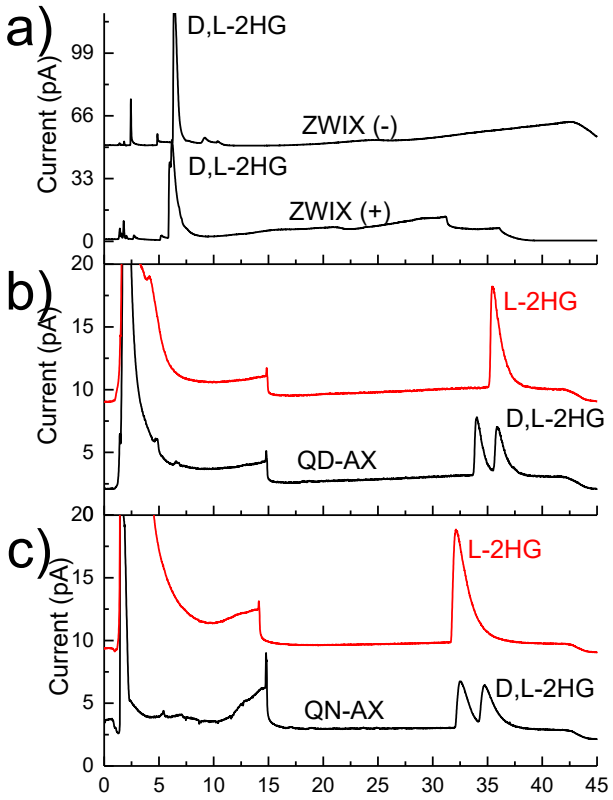

Figure 8.2. Generic gradient elution screening runs for a mixture of D- and L-2-HG, and pure enantiomer L-2-HG using a) ZWIX (+) and ZWIX (-), b) QD-AX and c) QN-AX column. Eluent: A: ACN:MeOH (75:25;v/v), B: ACN:MeOH (75:25; v/v) with 90 mM FA; gradient profile, 0-100% B in 30 min; flow rate, 1.0 mL/min; column temperature, 25 °C. Note that system peaks are due to sodium in the sample (Na^+-salt of analyte was used as sample) and aqueous sample matrix significantly deviating from eluent composition. Na^+ is eluted at about t_0 on the QD-AX column while it is retained on the ZWIX(+) column.

In order to obtain more information about the separation of D- and L-2-HG and to possibly establish an even more generic screening method for chiral ion-exchanger columns, a second mixed polar modifier-acid additive gradient was tested by changing the composition of the bulk solvent from MeOH:ACN (5:95; v/v) to MeOH:ACN (100:0; v/v) and increasing at the same time

the concentration of formic acid from 10 to 90 mM. MeOH has higher elution strength than ACN and higher additive concentrations in channel B also promote elution. With such a mixed gradient it is easier to identify reasonable MeOH and formic acid concentrations for isocratic runs. Only ZWIX(+) and QD-AX were tested in this case because it was previously observed that their behavior is similar to the corresponding ZWIX(-) and QN-AX columns, respectively. Only slight separation with the ZWIX(+) column (R_S = 0.19) and a partial separation with the QD-AX column (R_S = 0.99) was achieved (see Suppl. Figure 8.2, Suppl. Table 8.2). Considering the conditions under which D- and L-2-HG were eluted, and reducing the strength of channel B at that moment by about 20 %, QD-AX column with initial isocratic conditions composed of ACN:MeOH (30:70; v/v) with 60 mM formic acid, flow rate 1.0 mL/min and temperature 25 °C were derived as starting choice for further isocratic optimization.

8.5.2 Effect of ACN-MeOH ratio

In previous screening runs it was assumed that in the employed polar organic mode the protic MeOH has stronger elution strength than the aprotic ACN owing to its competing effect for hydrogen bonding with the analyte enantiomers. In order to verify this and optimize the ratio of these two solvents, the influence of four different ACN and MeOH ratios was examined while keeping the formic acid concentration fixed at 60 mM (see Figure 8.3). As expected, a clear decrease of the retention was observed with higher concentrations of methanol. It exhibits favorable solvation capabilities of the polar analyte due to H-donor and H-acceptor properties as opposed to ACN which is a non-protic solvent with H-acceptor capabilities only. Selectivity values remain practically constant when the MeOH content was increased, while resolution showed at the beginning almost no change, when the MeOH content was varied from 100 % to 75 %. It was then observed, that the resolution improved when less MeOH was employed (see Figure 8.3 and Suppl. Table 8.3). This improvement in resolution with lower MeOH content can be explained by the fact that MeOH strongly interacts with the analytes, interfering thereby significantly with the interaction between selector and selectand (SO-SA), as explained above. In a previous study [176], it was shown for a group of chiral acids that an increase of the percentage of acetonitrile (in an ACN:MeOH mixture) has a negative effect on resolution, which is opposite to the situation in the present case. However, in that study the chiral acids contained aromatic motifs which can interact with ACN molecules thus interfering with π-π interactions between selector and selectand.

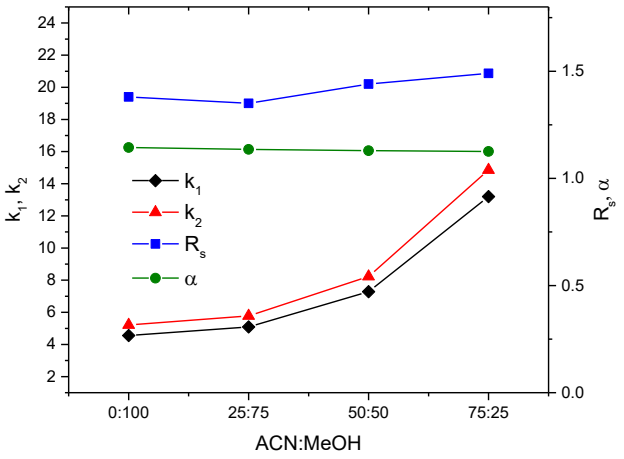

Figure 8.3. Effect of ACN:MeOH ratios on the chromatographic parameters of the separation of D- and L-2-HG. Eluent: ACN:MeOH at different ratios (v/v) at constant FA concentration of 60 mM; flow rate, 1.0 mL/min; column temperature, 25 °C.

It can be pointed out from this experiment that even MeOH at 100 % with 60 mM FA can be used as eluent obtaining an almost baseline separation (R_s = 1.39) with retention times lower than 10 minutes (Suppl. Figure 8.3 and Suppl. Table 8.3).

8.5.3 Effect of alcohol-type

MeOH is the most common protic solvent in polar organic mode while other types of alcohol are rarely investigated. Since resolution was slightly below baseline separation, also other alcohols, such as EtOH and n-PrOH, were tested, as polar modifiers, for their capability to yield slightly higher resolutions keeping the concentration of formic acid at 60 mM. Higher retention with decrease in polarity and a slight increase of separation factors were observed in the order MeOH < EtOH < n-PrOH. Yet, resolution decreased in this order due to less favorable mass transfer properties and lower chromatographic efficiencies of longer chain alcohols (see Figure 8.4a and Suppl. Table 8.4).

8.5.4 Effect of water content

2-HG with two carboxylic groups and its α-hydroxyl functionality is a very hydrophilic compound. For solubility reason, aqueous conditions could be of advantage. A series of experiments were therefore envisaged in which methanol was replaced by water as polar co-solvent, thus ending up in a hydroorganic elution mode (HILIC or RP-type depending on percentage of water). As can be seen in Suppl. Figure 8.5, retention significantly decreased with increase of water content. Simultaneously, enantioselectivity declined and was lost at about 25% aqueous fraction. This stands in agreement with former findings for hydroxyalkanoic acid enantiomer separations on chiral ion-exchangers and can be explained by the unfavorable desolvation characteristics of the

analyte in aqueous solvents [179,180]. Note that 1-2% (v/v) of water are in contrast tolerated (e.g. R_s=1.28 with ACN:MeOH:H_2O (49.5:49.5:1; v/v) + FA 60 mM and 1.27 without water i.e. ACN:MeOH (50:50; v/v) + FA 60 mM), and may be used for solubility reasons of very polar analytes in the eluent. Yet herein, further experiments were performed in the polar organic mode with non-aqueous conditions.

8.5.5 Effect of amines

Amines as mobile phase additives can participate as co-ions in the anion-exchange (AX) mechanism. It has been indicated in a previous study [176] that a strong decrease on retention of acidic compounds can be observed when amines are included in the eluent as co-ions in AX separations, emphasizing that elution strength increases in the order NH_3<DEA<TEA. Nonetheless, another study indicates that there is practically no effect on chromatographic parameters when changing the type of co-ion for a ZWIX selector used in AX mode [183].

For earlier separation of D,L-2-HG a slight peak tailing was observed. It was therefore attempted to overcome this detrimental effect by addition of co-ions to the mobile phase. NH_3, DEA and TEA, which differ in their degree of alkylation and basicity, were investigated to determine their effect on retention and resolution of D,L-2-HG. Each amine was added to the mobile phase at a concentration of 10 mM while the concentration of FA was maintained at 60 mM.

Suppl. Table 8.5 summarizes the results obtained and corresponding chromatograms are shown in Figure 8.4b. Oppositely to the results of above indicated study [176], elution strength increases in the order TEA<DEA<NH_3, and furthermore, elution is slightly faster when no amine is added to the mobile phase. This minor effect can originate from shifts in deprotonation equilibria of D,L-2-HG which is a stronger acid than formic acid. With addition of amines, the fraction of dissociated 2-HG increases with increased basicity of the additive. More deprotonated D,L-2-HG can produce stronger SO-SA interactions and therefore enhance retention.

Unfortunately, a decrease in resolution was observed when the degree of alkyl substitution of the amine is increased and there was no favorable effect on peak shape with amine additives. Since the incorporation of a co-ion does not represent any practical advantage for the separation of D,L-2-HG, it was decided not to include it as a component of the mobile phase.

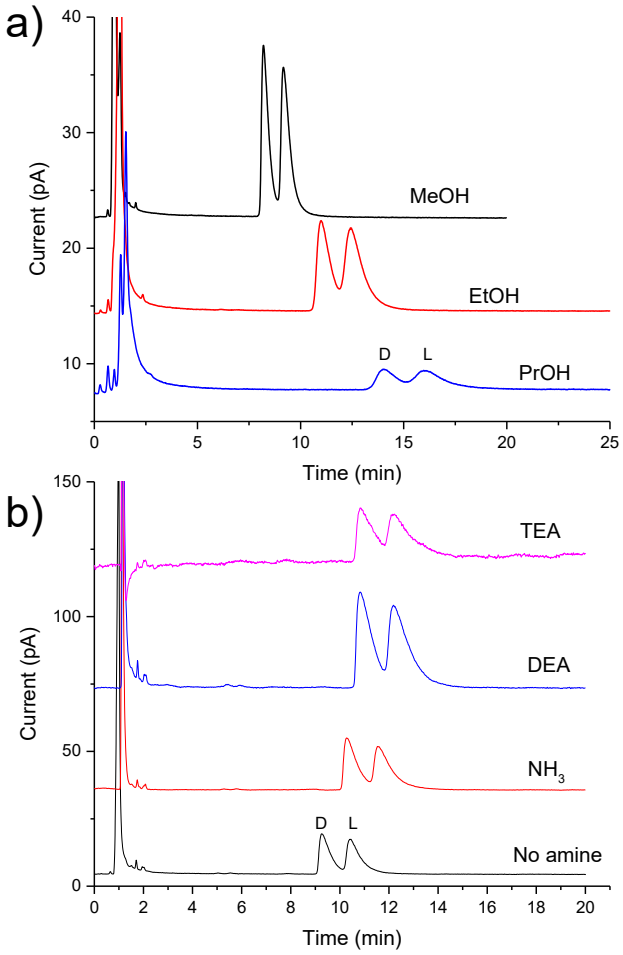

Figure 8.4. Chromatographic runs for a mixture of D- and L-2-HG with a) different types of alcohols, and b) different types of co-ions (ammonia, NH_3; DEA, diethylamine; TEA, triethylamine) in the mobile phase. a) Eluent: alcohol 100 % (v/v) with 60 mM FA; flow rate, 1.0 mL/min; column temperature, 25 °C, and b) Eluent: 100 % MeOH (v/v) containing 60 mM FA and 10 mM amine; flow rate, 1.0 mL/min; column temperature, 25 °C.

8.5.6 Effect of additive concentration

Modification of the acid additive concentration in the eluent represents a convenient way to adjust retention on chiral ion-exchange systems. Thus, after having established the general mobile phase composition for isocratic elution, the influence of formic acid concentration (ranging from 30 to 90 mM) was investigated. The solvent system ACN:MeOH (30:70; v/v) was selected as a compromise between higher resolution and faster elution.

As expected, a significant decrease on retention was observed when higher concentrations of formic acid were used (Figure 8.5 and Suppl. Table 8.6). This trend in retention is clearly consistent with an anion-exchange retention mechanism, which has been previously described [176,184,185]. Practically, no change in enantioselectivity and only a small decrease in resolution were observed when the FA concentration was increased. In this case, a compromise has to be found between the quality of the required separation and the needed time for analysis. A baseline separation is possible when the concentration of FA is below 50 mM. Interestingly, it

was also observed during this experiment that the peak area and therefore the sensitivity of the CAD were increased when higher concentrations of FA were employed (Suppl. Figure 8.7c).

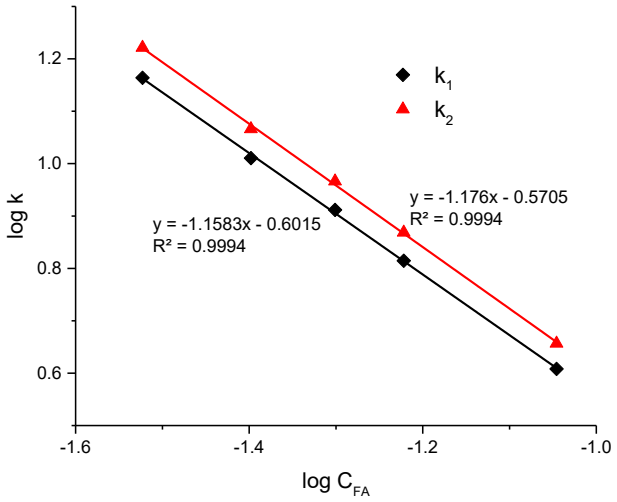

Figure 8.5. Effect of FA concentrations in accordance to the stoichiometric displacement model. Column: QD-AX; Eluent: ACN:MeOH (30:70;v/v) with different concentrations of FA; flow rate, 1.0 mL/min; column temperature, 25 °C.

Additional chromatographic runs were performed with 100 % MeOH as eluent and changing the concentration of FA (data not shown). This change allowed us to reduce the chromatographic run times while the resolution did not change significantly. When the FA concentration was 40 mM, a R_s = 1.47 i.e. baseline separation was achieved. For that reason, these conditions were used for further optimization of flow rate and column temperature.

Besides FA, AcOH was also tested as a displacer for the separation of D and L-2-HG (data not shown). However, even with an AcOH concentration as high as 150 mM, elution of analytes was not observed within 90 min, and for that reason further experiments with this acid additive that has a weaker net elution strength were not performed.

8.5.7 Effect of Temperature

The effect of column temperature on the separation was also studied as one of the last influential factors to be examined because its effect, at least on some chromatographic parameters ($k_{1,2}$, α, $N_{1,2}$), is to some extent predictable on QD-AX and QN-AX columns. So far, with very few exemptions [186,187], adsorption and separation processes were found to be enthalpically driven, and expected for the present case as well. This implies that retention and separation factors decrease with increasing temperature, while plate numbers increase upon raising the temperature. Nonetheless, the resultant optimum of resolution has to be studied on a case-to-case basis.

Five different temperatures were used in the range from 10°C to 40°C using 100% MeOH with 40 mM FA as eluent. The temperature effect can be analyzed in terms of the Van´t Hoff equation in accordance to eq. 1,

$$lnk = -\frac{\Delta H^\circ}{RT} + \frac{\Delta S^\circ}{R} + ln\phi \quad (1)$$

wherein Δ*H*° and Δ*S*° are standard enthalpy and entropy changes upon adsorption, *R* is the universal gas constant, *T* the absolute temperature in *K*, and ϕ is the phase ratio. The corresponding relationship for the separation factors α is described by eq. 2

$$ln\alpha = -\frac{\Delta\Delta H^\circ}{RT} + \frac{\Delta\Delta S^\circ}{R} \quad (2)$$

wherein ΔΔ*H*° and ΔΔ*S*° are differential standard enthalpy and entropy changes between the two corresponding enantiomers. At this point it has to be emphasized that these thermodynamic parameters are macroscopic entities representing averages over adsorption at distinct sites[181,188].

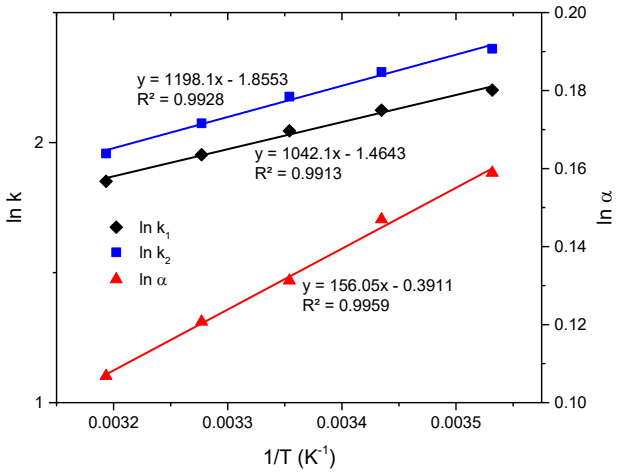

Figure 8.6. Temperature dependence of retention and separation factors as illustrated by Van't Hoff plots. Eluent: 100 % MeOH containing 40 mM FA, flow rate: 1.0 mL/min.

Figure 8.6 shows the corresponding Van´t Hoff plots and according to equation 2, estimated negative values for ΔΔH°(-1.297 ± 0.048 kJ mol-1) and ΔΔS° (-3.25 ± 0.16 J mol-1 K-1) permit to establish that the enantioseparation of D- and L-2-HG on QD-AX column is an enthalpically driven process.. Over the tested temperature range both enantioselectivity and resolution showed a clear trend with higher values the lower the temperature (Suppl. Figure 8.8b and Suppl. Table 8.7).

8.5.8 Effect of flow rate

Chiral separations of acidic compounds on chiral anion-exchangers are typically characterized by a relatively slow mass transfer term due to multi-point attachment of solutes on the sorbent surface and slow desorption kinetics. This is quite common for chiral separations on CSPs which exhibit therefore a steep C-term branch in H/u-curves. This behavior is found for 2-HG as well (Suppl. Figure 8.9b). Upon decrease of the flow rate by a factor of 2 from 1 mL/min to 0.5 mL/min, the plate height is decreased by a factor of about 1.2. Although this translates into a gain in R_s by a square root of only 1.2 (gain in R_s by factor of ca. 1.1), this is significant but comes at the expense of longer run times (factor 2) (see Suppl. Figure 8.9c and Suppl. Table 8.8).

8.5.9 Multi-criteria decision making

The above stated experiments clearly indicated with which conditions a separation of 2-HG enantiomers can be achieved. However, some of these separations require long run times. To optimize both R_S and run times Pareto-optimality plots were constructed by plotting R_s vs inverse of run time (Figure 8.7). From this plot it is straightforward to select acceptable conditions. Pareto optimal points are indicated in blue. Beyond their boundary to the right no other conditions were tested, which give better results i.e. higher resolution at shorter run times.

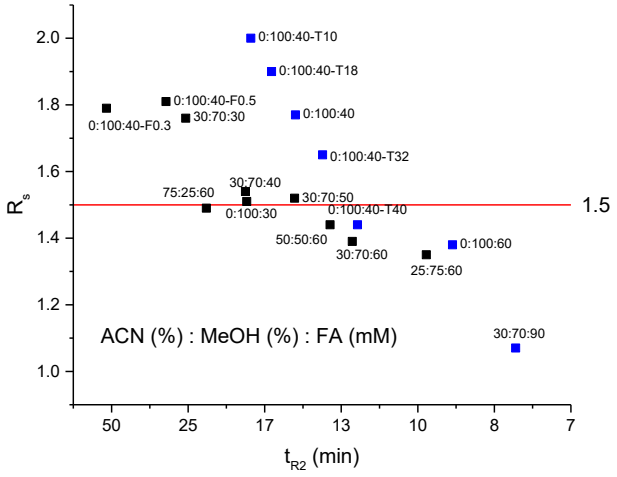

Figure 8.7. Plot of resolution versus inverse of retention time for second peak, obtained during different chromatographic runs. Pareto optimal points in blue. Labels mean eluent composition % of ACN:% of MeOH: FA concentration (mM). F means flow (mL/min) and T means column temperature (°C). If not stated otherwise temperature was 25 °C and flow rate was 1.0 mL/min. Note, run time (tR2) was plotted in inverse scale because a smaller value is advantageous. Users can easily find the best compromise between resolution and speed of analysis.

8.6 Conclusions

Enantioseparation of underivatized D,L-2-HG was successfully achieved on a Chiralpak QD-AX column, operating in accordance to an anion-exchange mechanism. Full baseline separation was

accomplished with a mobile phase composed of MeOH with 40 mM FA, at a flow rate of 1.0 mL/min and at a column temperature of 10°C.

The elution order of enantiomers was determined on QD-AX and QN-AX columns showing an inversion of elution order by exchanging these columns confirming their pseudo-enantiomeric behavior. This represents an important advantage when the minor enantiomer must be analyzed in the presence of the major one. Such systematic reversal of the elution order is not possible with Ristocetin-based Chirobiotic R [162], also previously suggested for 2-HG enantiomer separation by LC. Compared to chiral ligand exchange systems, which are typically endowed with Cu(II) ions in the mobile phase and therefore incompatible with MS detection, the current enantioselective anion-exchange LC process has the advantage of providing fully MS-compatible elution conditions. Thus, it can be concluded that the here presented chromatographic procedure represents currently the first choice for 2-HG enantiomer separation by LC-MS.

8.7 Acknowledgements

We are grateful for financial support by the “Struktur- und Innovationsfonds für die Forschung (SI-BW)” by the regional government of Baden-Württemberg (Ministry of Science, Research and Arts). C.C. gratefully acknowledges financial support through a scholarship from the German Academic Exchange Programme (DAAD no. 57129429).

8.8 Supplementary material

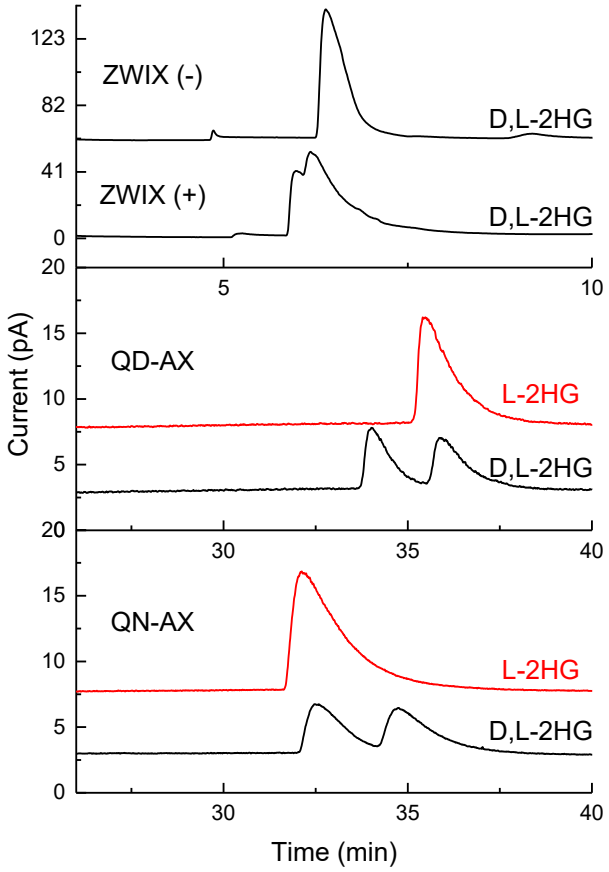

Suppl. Figure 8.1. Generic gradient elution screening runs for a mixture of D- and L-2-HG, and pure enantiomer L-2-HG using different cinchona alkaloid-derived chiral ion-exchanger CSPs. Eluent: A: ACN:MeOH (75:25;v/v), B: ACN:MeOH (75:25; v/v) with 90 mM FA; gradient profile, 0-100% B in 30 min; flow rate, 1.0 mL/min; column temperature, 25 °C. Note that system peaks are due to sodium in the sample (Na^+-salt of analyte was used as sample) and aqueous sample matrix significantly deviating from eluent composition. Na^+ is eluted at about t_0 on the QD-AX column while it is retained on the ZWIX(+) column.

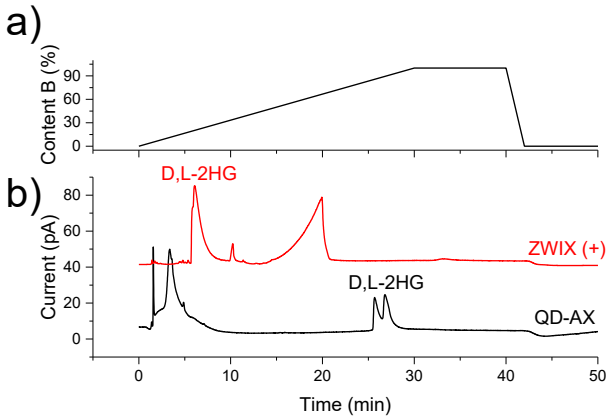

Suppl. Figure 8.2. a) Gradient profile and corresponding b) mixed polar modifier-acid additive gradient screening runs for a mixture of D- and L-2-HG, using ZWIX(+) and QD-AX columns. Eluent: A: ACN:MeOH (95:5; v/v) with 10 mM FA, B: MeOH with 90 mM FA; gradient profile, 0-100% B in 30 min; flow rate, 1.0 mL/min, temperature: 25 °C. Note that system peaks are due to sodium in the sample (Na^+-salt of analyte was used as sample) and aqueous sample matrix significantly deviating from eluent composition. Na^+ is eluted at about t_0 on the QD-AX column while it is retained on the ZWIX(+) column.

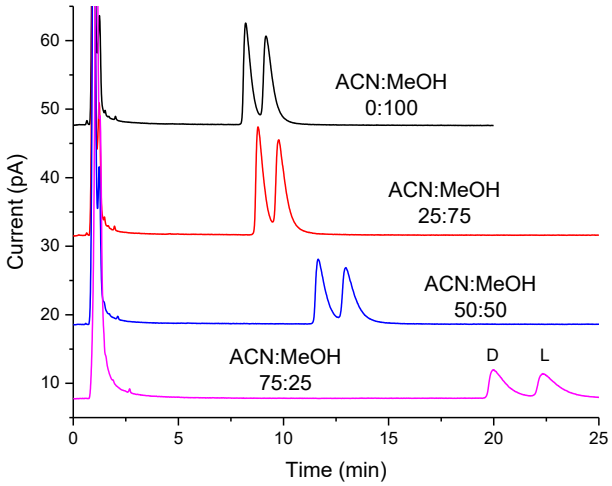

Suppl. Figure 8.3. Chromatographic runs for a mixture of D- and L-2-HG at different ratios of ACN:MeOH. Eluent: ACN:MeOH at different ratios (v/v) at constant FA concentration of 60 mM; flow rate, 1.0 mL/min; column temperature, 25 °C.

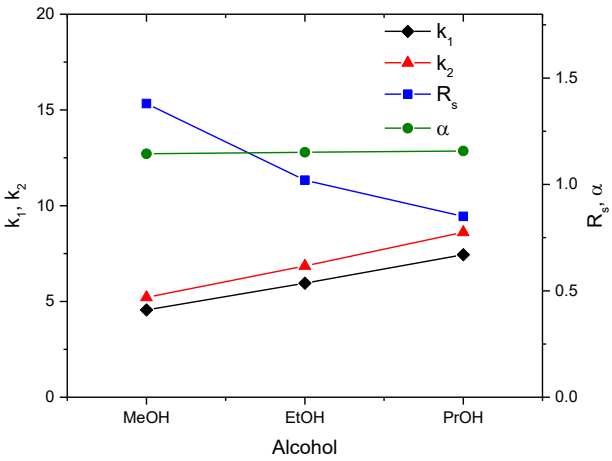

Suppl. Figure 8.4. Effect of different types of alcohols on the chromatographic parameters. Eluent: alcohol 100 % (v/v) with 60 mM FA; flow rate, 1.0 mL/min; column temperature, 25 °C.

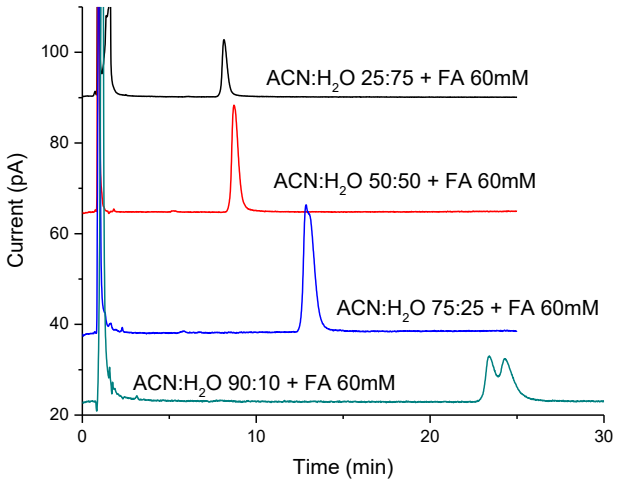

Suppl. Figure 8.5. Chromatographic runs for a mixture of D- and L-2-HG at different ratios of ACN:H_2O. Eluent: ACN:H_2O at different ratios (v/v) at constant concentration of 60 mM FA; flow rate, 1.0 mL/min; column temperature, 25 °C.

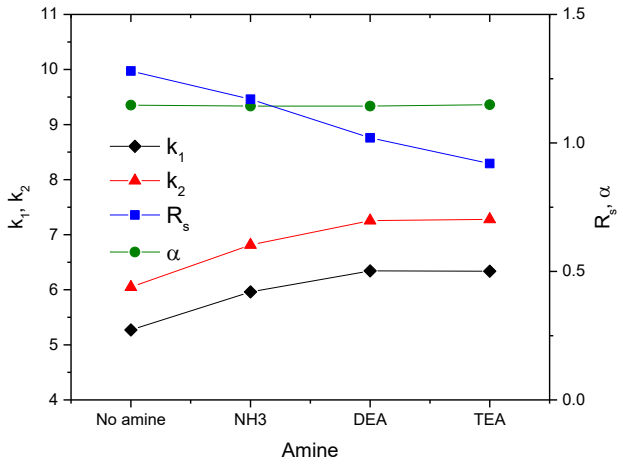

Suppl. Figure 8.6. Effect of different types of co-ions (ammonia, NH_3; DEA, diethylamine; TEA, triethylamine) in the mobile phase on the chromatographic parameters. Eluent: 100 % MeOH (v/v) containing 60 mM FA and 10 mM amine; flow rate, 1.0 mL/min; column temperature, 25 °C.

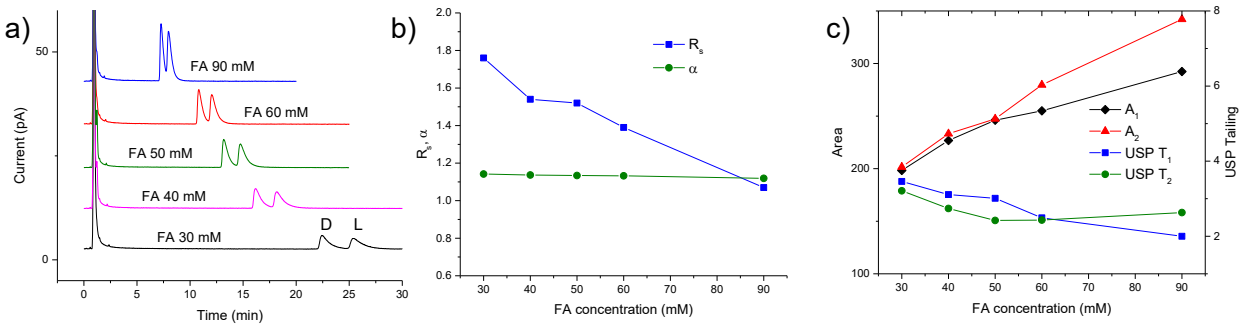

Suppl. Figure 8.7. a) Chromatographic runs for a mixture of D- and L-2-HG at different FA concentrations using QD-AX column, b) corresponding resolution and selectivity plots and c) peak area and USP tailing plots. Eluent: ACN:MeOH (30:70;v/v) with different concentrations of FA; flow rate, 1.0 mL/min; column temperature, 25 °C.

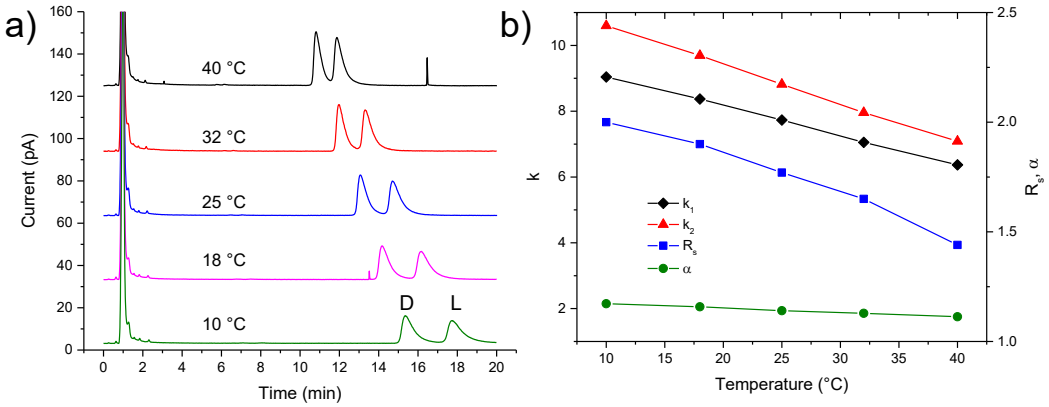

Suppl. Figure 8.8. a) Chromatographic runs for a mixture of D- and L-2-HG, at different temperatures, b) corresponding plots of chromatographic parameters. Eluent: 100 % MeOH containing 40 mM FA, flow rate: 1,0 mL/min.

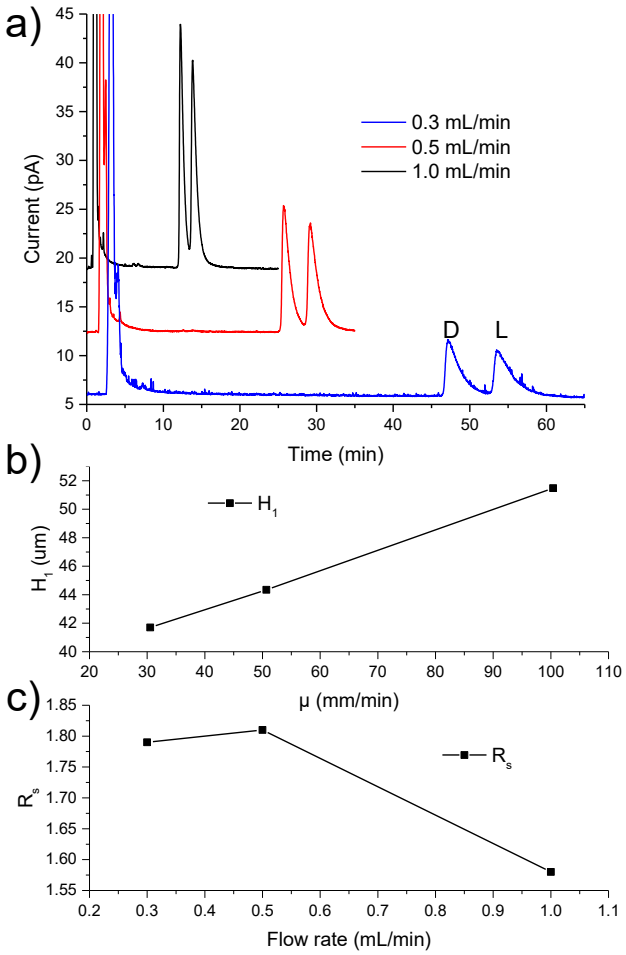

Suppl. Figure 8.9. a) Chromatographic runs for a mixture of D- and L-2-HG, at different flow rates, and b), c) corresponding plots of chromatographic parameters. Eluent: MeOH 100 % with 40 mM FA; temperature, 25 ° C.

Suppl. Table 8.1. Chromatographic parameters obtained for the separations of D- and L-2-HG in the counterion gradient elution screening runs on the four different CSPs.

Column	t_R 1 [min]	t_R 2 [min]	k^*_1	k^*_2	α^*	N^*_1	N^*_2	R_S
ZWIX (+)	6.108	6.180	3.01	3.06	1.02	4782	1027	0.13
ZWIX (-)	6.387	6.387	3.36	3.36	1.00	1695		0.00
QD-AX	34.017	35.873	23.30	24.62	1.06	12343	8810	1.35
QD-AX	35.479		24.34			8018		
QN-AX	32.472	34.736	22.11	23.72	1.07	4661	4148	1.11
QN-AX	32.119		21.86			3048		

Chromatographic conditions: Eluent: A: ACN:MeOH (75:25;v/v), B: ACN:MeOH (75:25; v/v) with 90 mM FA; gradient profile, 0-100% B in 30 min; flow rate, 1.0 mL/min; column temperature, 25 °C. k*, α* and N* represent apparent values

Suppl. Table 8.2. Chromatographic parameters obtained during the mixed polar modifier-counterion gradient elution separation of D- and L-2-HG with QD-AX and ZWIX(+) column.

Column	t_R 1 [min]	t_R 2 [min]	k^*_1	k^*_2	α^*	N^*_1	N^*_2	R_S
QD-AX	25.685	26.792	17.28	18.07	1.05	9486	8433	0.99
ZWIX (+)	5.917	6.080	2.77	2.88	1.04	5266	300	0.19

Eluent: A: ACN:MeOH (95:5; v/v) with 10 mM FA, B: MeOH with 90 mM FA; gradient profile, 0-100% B in 30 min; flow rate: 1.0 mL/min, temperature: 25 °C. k*, α* and N* represent apparent values

Suppl. Table 8.3. Chromatographic parameters obtained for the separations of D- and L-2-HG at different ACN:MeOH ratios.

ACN:MeOH (v/v)	tR_1 [min]	tR_2 [min]	k_1	k_2	α	N_1	N_2	R_S
0:100	8.200	9.168	4.56	5.21	1.14	2738	2261	1.38
25:75	8.787	9.781	5.09	5.78	1.14	2829	2351	1.35
50:50	11.647	12.971	7.28	8.23	1.13	3107	2698	1.44
75:25	20.008	22.342	13.20	14.86	1.13	3222	2713	1.49

Eluent: ACN:MeOH at different % (v/v) ratios with 60 mM FA, flow rate: 1.0 mL/min; column temperature: 25 °C.

Suppl. Table 8.4. Chromatographic parameters obtained for the separation of D- and L-2-HG by employing different types of alcohol

Polar modifier	tR_1 [min]	tR_2 [min]	k_1	k_2	α	N_1	N_2	R_S
MeOH	8.200	9.168	4.56	5.21	1.14	2738	2261	1.38
EtOH	10.994	12.418	5.95	6.85	1.15	1304	999	1.02
PrOH	14.025	15.967	7.44	8.61	1.16	839	588	0.85

Eluent: 100% alcohol with 60 mM FA, flow rate, 1.0 mL/min; column temperature, 25 °C.

Suppl. Table 8.5. Chromatographic parameters obtained for the separation of D- and L-2-HG by employing different types of amines as co-ions

Amine	tR_1 [min]	tR_2 [min]	k_1	k_2	α	N_1	N_2	R_S
-	9.256	10.402	5.27	6.05	1.15	2003	1866	1.28
NH_3	10.274	11.535	5.96	6.82	1.14	1770	1523	1.17
DEA	10.840	12.184	6.34	7.25	1.14	1397	1095	1.02
TEA	10.830	12.221	6.34	7.28	1.15	1037	857	0.92

Eluent: 100% MeOH with 60 mM FA and 10 mM amine, flow rate, 1.0 mL/min; column temperature, 25 °C.

Suppl. Table 8.6. Chromatographic parameters obtained for the separation of D- and L-2-HG at different concentrations of formic acid.

FA conc [mM]	t_{R1} [min]	t_{R2} [min]	k_1	k_2	α	N_1	N_2	R_S
30	22.413	25.391	14.59	16.66	1.14	3855	2751	1.76
40	16.169	18.181	10.24	11.64	1.14	3027	2585	1.54
50	13.172	14.745	8.16	9.25	1.13	3180	2710	1.52
60	10.824	12.065	6.53	7.39	1.13	2941	2399	1.39
90	7.270	7.963	4.06	4.54	1.12	2643	1947	1.07

Eluent: ACN:MeOH (30:70;v/v) with different concentrations of FA; flow rate, 1.0 mL/min; column temperature, 25 °C.

Suppl. Table 8.7. Chromatographic parameters obtained during the separation of D- and L-2-HG at different temperatures.

Temperature [°C]	t_{R1} [min]	t_{R2} [min]	k_1	k_2	α	N_1	N_2	R_S
10	15.353	17.734	9.04	10.6	1.17	3171	3035	2.00
18	14.176	16.181	8.37	9.69	1.16	3528	3186	1.90
25	13.072	14.696	7.73	8.82	1.14	3851	3572	1.77
32	11.966	13.311	7.05	7.96	1.13	4064	3676	1.65
40	10.816	11.870	6.37	7.09	1.11	4179	3582	1.44

Eluent: 100 % MeOH with 40 mM FA; flow rate, 1.0 mL/min; column temperature, 25 °C.

Suppl. Table 8.8. Chromatographic parameters obtained during the separation of D- and L-2-HG at different flow rates

Flow (mL/min)	t_{R1} [min]	t_{R2} [min]	k_1	k_2	α	N_1	N_2	R_S
1.0	12.218	13.827	7.18	8.26	1.15	2914	2383	1.58
0.5	25.686	29.206	7.68	8.87	1.15	3382	3076	1.81
0.3	47.117	53.502	8.59	9.89	1.15	3597	2874	1.79

Eluent: 100 % MeOH with 40 mM FA; flow rate, 1.0 mL/min; column temperature, 25 °C.

9 Publication IV. Chiral separation of short chain aliphatic hydroxycarboxylic acids

9.1 Title

Chiral Separation of Short Chain Aliphatic Hydroxycarboxylic Acids on Cinchonan Carbamate Based Weak Chiral Anion Exchangers and Zwitterionic Chiral Ion Exchangers

Carlos Calderón[1], Michael Lämmerhofer[1]*

[1]Institute of Pharmaceutical Sciences, Pharmaceutical (Bio-)Analysis, University of Tübingen, Auf der Morgenstelle 8, 72076 Tübingen, Germany

Reprinted with permission from Journal of Chromatography A, Volume 1487, Pages 194-200,

DOI: 10.1016/j.chroma.2017.01.060

Copyright (2017) Elsevier B.V.

9.2 Abstract

Chiral short chain aliphatic hydrocarboxylic acids (HCAs) are common compounds being part of different biological processes. In order to control and understand these processes is of pivotal importance to determine the identity of the involved enantiomer or their enantiomeric ratio. In this study the capacity of quinine- and quinidine-derived chiral stationary phases to perform the enantioseparation of eight chiral HCAs (tartaric acid, isocitric acid, malic acid, glyceric acid, 2-hydroxyglutaric acid, 2-hydroxybutyric acid, lactic acid and 3-hydroxybutyric acid) was evaluated. MS-compatible conditions consisting of ACN/MeOH mixtures as eluents with formic acid, acid acid and/or their ammonium salts as additives, temperatures between 10 and 25°C (except for -20°C for 3-hydroxybutyric acid) and a flow rate of 1.00 mL/min yielded full baseline resolution for all studied HCAs. Elution order for the HCA enantiomers was determined revealing different behaviors between the studied compounds.

9.3 Introduction

Short chain aliphatic hydroxycarboxylic acids (HCAs) are widely relevant compounds being amongst others part of metabolic pathways. The presence of the hydroxyl group along the alkyl chain often generates a stereogenic center which leads to the occurrence of two enantiomers (single stereogenic center) or several stereoisomers (more than one stereogenic center) with different chemical and biochemical properties. For this reason it is of utmost importance to strictly indicate which one of the enantiomers and stereoisomers, respectively, is used in a particular process. As a matter of consequence, proper methodologies for their separation, identification and quantification are required in areas such as biochemistry, clinical chemistry and quality control of products in the industry.

In the case of lactic acid (LA) [166,189,190], 2-hydroxybutyric acid (2-HBA) [191], 3-hydroxybutyric acid (3-HBA) [192], 2-hydroxyglutaric acid (2-HGA) [146,148,149,158], and glyceric acid (GlA) [193,194], alterations in the expected enantiomer ratio have been linked to some diseases. Their enantioselective analysis is consequently a major concern in biomarker studies and clinical analysis.

In various industries, e.g. food industry, quality control based on enantioselective analysis of certain enantiomers of HCAs is also critically important, for example in wine production, the course and progress of malolactic fermentation, a determining factor on the taste of wine, can be monitored by enantiomeric profiling of L-malic acid (L-MA) and L-LA [195]. D-LA is found in all wines in small quantities, while L-LA is only found in wines which have undergone malolactic acid fermentation. The enantiomer ratio consequently depends on the microbiological state.

Adulteration of commercial products is another important issue that can be sometimes monitored by the quantification of the corresponding enantiomers. For example, L-enantiomers of tartaric acid (TA) and MA, extracted from plants, are used as additives in certain products but in some cases they are replaced for synthetic racemic mixtures that are illegal or must be indicated on the label [196–198].

The enantioseparation of short chain HCAs is evidently challenging due to the difficulty to establish enough points of interactions between the chiral selector and the surface of the metabolite around its chiral center [102].

Different kinds of chiral selector and various analytical approaches have been tested to separate HCA enantiomers. Barbas and Saavedra published in 2002 a review with the main achievements obtained by capillary electrophoresis in different modes (ligand-exchange, macrocyclic antibiotics, cyclodextrins, ion-pair) to separate metabolites like LA, 2-HBA, MA and TA [102,199]. More recently, chiral separations by ligand exchange capillary electrophoresis have been also reported for MA, isocitric acid (ICA) and TA [196,197,200,201]. Capillary electrochromatography has been proposed recently for the separation of enantiomers of malic acid [198]. Such electrokinetic separation methods are not established in many laboratories and therefore HPLC methods are usually preferred.

In the case of liquid chromatography, different direct and indirect approaches have been reported for the chiral separation of HCAs. Indirect methods using derivatization with 1-(9-fluorenyl)ethyl chloroformate for LA and MA [202] or using (S)(+)-1-(2-pyrrolidinylmethyl)-pyrrolidine for LA and 3-HBA [192] are a few examples. Also derivatization with diacetyl-L-tartaric anhydride [160,203], or with *N*-(p-toluenesulfonyl)-L-phenylalanyl chloride [167] for chiral separations of D- and L-2-HGA have been described.

Ligand exchange is also a mechanism employed in LC for LA, 2-HBA, GlA, 2-HGA, MA and TA enantioseparation [204,205], however, due to copper ions in eluent cannot be hyphenated to MS [206]. Direct HPLC separations have been reported by using macrocyclic antibiotic chiral stationary phases (CSPs) for LA [207], 2-HGA [162] and GlA [193] or anion exchange-type quinine- and quinidine-derived CSPs for LA [179], 2-HGA [208] and 3-HBA [180], but in some of these cases full baseline resolution was not achieved.

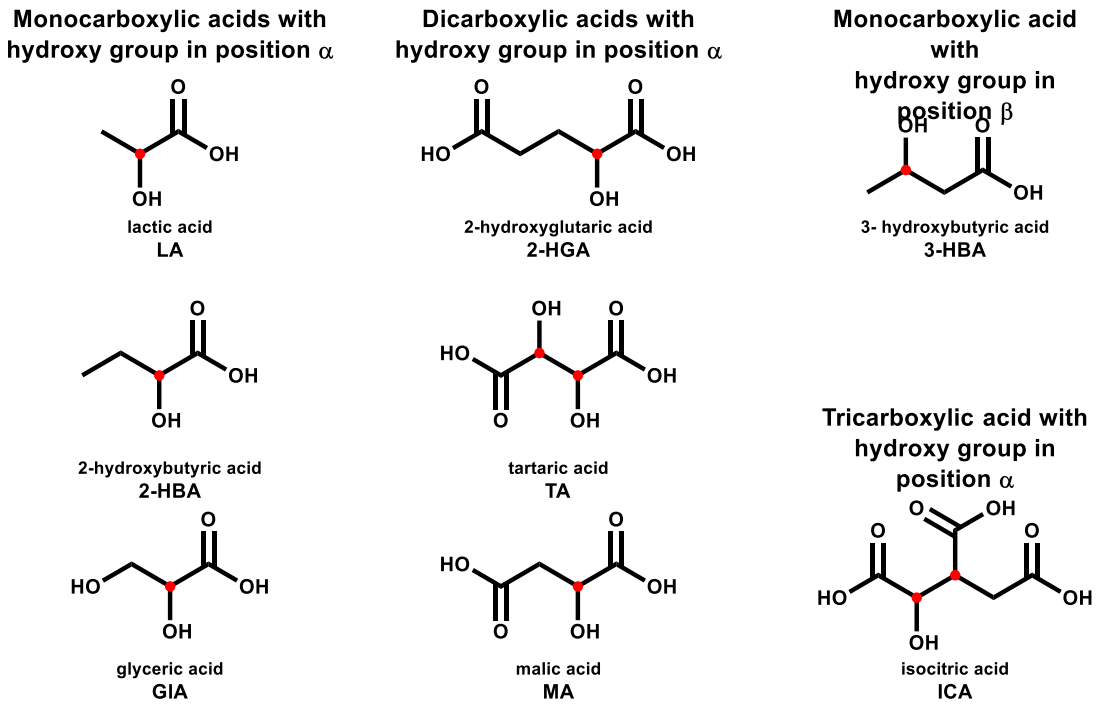

Figure 9.1. Structures of the studied aliphatic hydroxycarboxylic acids (HCAs)

In this study, seven α-hydroxycarboxylic acids and one β-hydroxycarboxylic acid (Figure 9.1) were selected in order to determine MS-compatible conditions for their full baseline resolution by employing four cinchona alkaloid-derived CSPs (Figure 9.2). It is supposed to be a first step towards enantioselective metabolomics of these important biological building blocks many of which are of clinical relevance. While in several of the above cited papers, it has been shown successful separations of the one or the other HCA, this work shows for the first time a systematic study and full baseline separation by direct HPLC enantiomer separation without derivatization of a wide range of HCAs of biological importance under MS-compatible conditions.

9.4 Experimental

9.4.1 Materials

All solvents used were of HPLC grade. Acetonitrile (ACN) was obtained from J.T. Baker (Deventer, The Netherlands) and methanol (MeOH) was purchased from Sigma-Aldrich (Steinheim, Germany). Formic acid (FA) was obtained by Carl Roth (Karlsruhe, Germany). Glacial acetic acid (AcOH), ammonia in methanol (NH_3) and ammonium acetate (NH_4OAc) were supplied from Sigma–Aldrich (Steinheim, Germany). Water was purified by a water filtration system from Elga Veolia (Paris, France).

The reagents DL-tartaric acid, D-tartaric acid, *threo*-D_sL_s-isocitric acid trisodium salt, D_s-*threo*-isocitric acid monopotassium salt, DL-malic acid disodium salt, L-malic acid disodium salt, DL-2-hydroxyglutaric acid sodium salt, L-2-hydroxyglutaric acid sodium salt, D-glyceric acid sodium salt, L-glyceric acid sodium salt, (*RS*)-2-hydroxybutyric acid sodium salt, (*S*)-2-hydroxybutyric acid, (*R*)-2-hydroxybutyric acid, DL-lactic acid sodium salt, L-lactic acid lithium salt, (*RS*)-3-hydroxybutyric acid sodium salt and (*R*)-3-hydroxybutyric acid were purchased from Sigma–Aldrich. Solutions 2.0 mg/mL of each racemic mixture and 1.0 mg/mL of each pure enantiomer were prepared in water. Also solutions with enantiomeric ratio 2:1 (m/m) were prepared by combining proper aliquots of solutions of racemic mixtures and single enantiomers.

The enantiomer elution order was assessed by injection of single enantiomer and/or non-racemic mixtures (2:1; m/m).

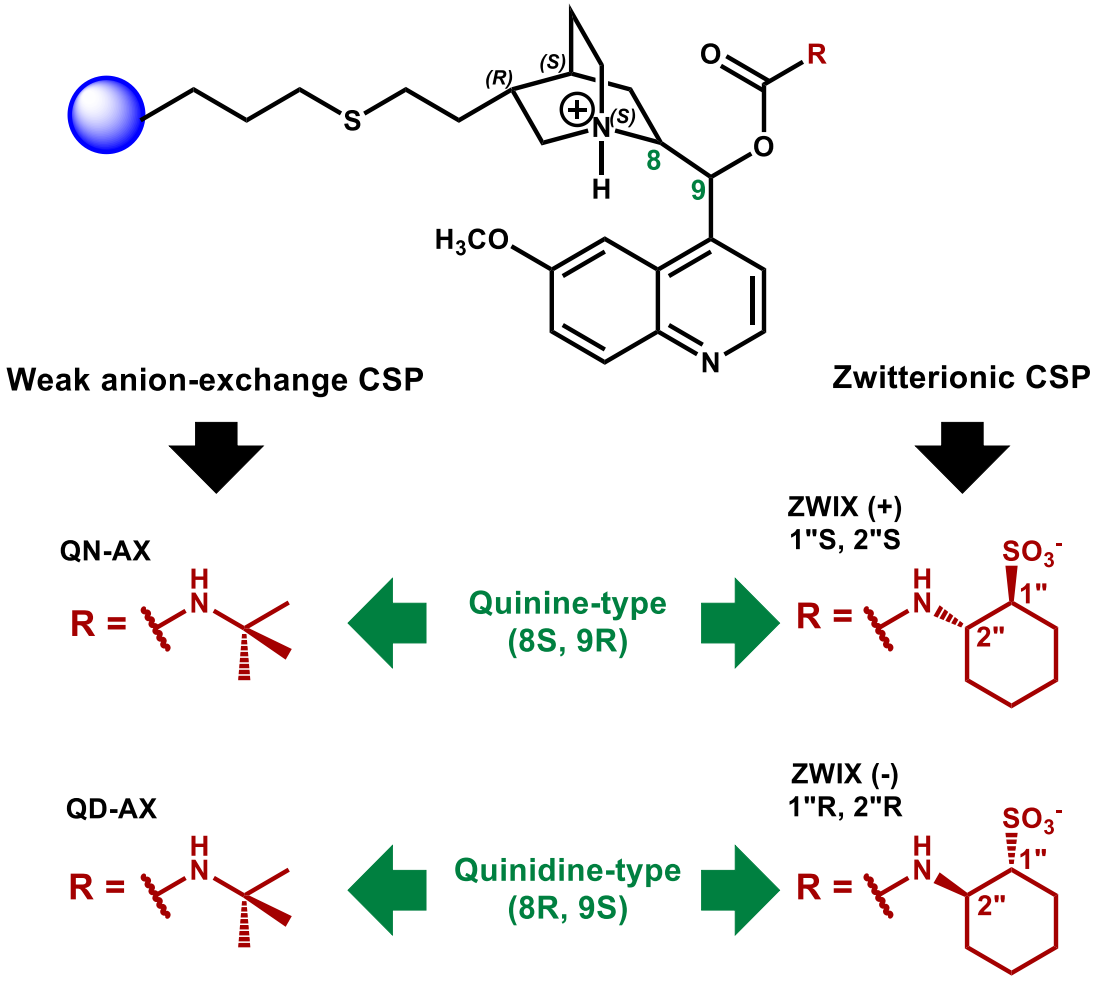

Figure 9.2. Chiral stationary phases tested in this study: Chiralpak QN-AX and QD-AX as well as Chiralpak ZWIX(+) and ZWIX(-)

9.4.2 Instrumentation and chromatographic method

LC experiments were carried out on a 1100 Series HPLC from Agilent Technologies (Waldbronn, Germany) equipped with a solvent degasser, a binary pump, an autosampler, a column

thermostat and a UV–VIS detector. UV signals were recorded at 220 nm. The HPLC system was connected to a Corona Charged Aerosol Detector, CAD from ESA Biosciences Inc., (Chelmsford, U.S.A.). The nitrogen flow of the CAD was adjusted to 35 psi. Data acquisition and analysis were done by using ChemStation software from Agilent Technologies.

Four different chiral stationary phases were employed in this study: a Chiralpak QD-AX (150 x 4 mm, 5 µm), a Chiralpak QN-AX (150 x 4 mm ID, 5 µm particle size), a Chiralpak ZWIX(+) column (150 x 4 mm ID, 3 µm particle size) and a Chiralpak ZWIX(-) column (150 x 4 mm ID, 3 µm particle size) from Chiral Technologies Europe (Illkirch, France). The void volumes of the columns were determined by injecting a solution of 10% (v/v) acetone in ACN with detection at 280 nm.

The columns were conditioned with the selected mobile phase at a flow rate of 1.0 mL/min for at least 30 min, before performing analysis. Column temperatures below 10 °C were achieved by using methanol-water baths cooled with liquid nitrogen.

9.5 Results and discussion

9.5.1 Enantioseparation of aliphatic HCAs on QN-AX and QD-AX columns

QN-AX and QD-AX are weak anion-exchange (WAX) columns employed mainly for the separation of chiral acidic compounds. Partial separation by using these columns was reported for 3-HBA [180] and baseline resolution was obtained for LA [179] and 2-HGA [208] previously. These three compounds along with other five HCAs were tested under different chromatographic conditions in order to achieve full baseline resolution for each of them by using compatible conditions for ESI-MS detection.

9.5.1.1 Elution conditions for HCAs

It was anticipated that HCAs with two and three carboxylic groups are compounds strongly retained on QD-AX and QN-AX CSPs and strong mobile phase conditions are required for their elution. Therefore, a mobile phase composed of MeOH/AcOH/NH_4OAc (98:2:0.5; v/v/m, condition A) was tested initially on QD-AX column for the elution of the eight HCAs. Results for the separation are summarized in Table 9.1 and Suppl. Figure 9.1a. As it can be seen, the retention times for these compounds range from 2.1 min (3-HBA) to 75.8 min (TA, second peak). Except for ICA and TA, the other six HCAs elute in less than 20 min. Baseline separations were obtained for the isomers of GlA, MA and TA. In the case of TA, it has to be pointed out that, in spite of the long retention time, high selectivity (α = 1.94) and high resolution (R_s = 7.76) were obtained. Only 3-HBA did not show even a partial separation for its enantiomers.

Similar conditions were tested on the QN-AX column and the results are also indicated in Table 9.1 and Suppl. Figure 9.1b. In this case, the retention times are slightly longer for most of the compounds except for ICA and TA, in which cases elution is not possible before 40 and 80 min, respectively. For the case of these 2 compounds a stronger mobile phase with 4% (v/v) acetic acid and 1% (m/v) ammoniun acetate (condition B) was used to elute the analytes (see Table 9.1, and Suppl. Figure 9.2).

Table 9.1. Resolution values and retention times (for second peak) obtained during enantioseparation of hydroxycarboxylic acids under different conditions

Column	Condition	3-HBA		LA		2-HBA		GlA		2-HGA		MA		ICA		TA	
		R_s	tR_2 [min]	R_s	tR_2 [min]	R_s	tR_2 [min]	R_s	tR_2 [min]	R_s	tR_2 [min]	R_s	tR_2 [min]	R_s	tR_2 [min]	R_s	tR_2 [min]
QD-AX	A	0.00	2.1	0.61	3.2	0.66	3.2	**1.70**	4.3	0.85	7.2	**2.74**	13.2	0.42	27.7	**7.76**	75.8
QN-AX	A	0.00	2.1	0.98	3.7	**1.63**	3.8	**2.37**	5.4	0.00	9.5	0.00	15.1		>45		>80
QN-AX	B													0.60	17.9	0.73	31.1
QD-AX	C	0.00	1.9	0.65	3.0	1.00	3.0	**2.24**	5.2	0.72	6.2	**2.08**	15.8				
QN-AX	C	0.00	1.9	**1.52**	3.6	**2.76**	3.7	**3.67**	7.0	0.60	8.3	0.00	18.8				
QD-AX	D									**1.53**	13.4						
QD-AX	E	0.00	2.9	1.30	9.4	**2.01**	9.5										
QN-AX	E	0.00	3.0	**3.24**	11.9	**4.82**	12.7										
QD-AX	F	0.60	10.3														
QN-AX	F	0.54	9.8														
QD-AX	G	0.76	16.7														
QD-AX	H	**1.52**	49.3														
ZWIX(+)	I	0.00	2.1	0.00	2.0	0.00	2.0	**2.60**	3.0	0.00	2.0	0.00	2.2	0.00	2.5	1.06	3.5
ZWIX(-)	I	0.00	2.0	0.00	2.0	0.00	2.0	**6.43**	4.4	0.00	2.1	1.14	3.0	**2.27**	4.4	**2.37**	7.3
ZWIX(-)	J	0.00	2.1	0.00	2.1	0.00	2.1	**7.05**	5.9	0.00	2.1	1.28	3.3	**2.50**	4.8	**2.19**	8.6
ZWIX(-)	K	0.00	2.1	0.00	2.1	0.00	2.1	**6.82**	6.7	0.00	2.3	**1.57**	4.0	**3.00**	6.3	**2.76**	12.6

A: mobile phase MeOH/AcOH/NH_4OAc (98:2:0.5; v/v/m), 25 °C, 1.0 mL/min, **B**: mobile phase MeOH/AcOH/NH_4OAc (96:4:1; v/v/m), 25 °C, 1.0 mL/min, **C**: mobile phase 100 % MeOH containing 90 mM FA and 15 mM NH_3, 25 °C, 1.0 mL/min, **D**: mobile phase 100 % MeOH containing 40 mM FA and 5 mM NH_3, 10 °C, 1.0 mL/min, **E**: mobile phase ACN/MeOH (50:50; v/v containing 15 mM FA, 25 °C, 1.0 mL/min, **F**: mobile phase ACN/MeOH (95:5; v/v) containing 5 mM FA, 25 °C, 1.0 mL/min, **G**: mobile phase ACN/MeOH (95:5; v/v) containing 2.5 mM FA, 10 °C, 1.0 mL/min, **H**: mobile phase ACN/MeOH (95:5; v/v) containing 17.4 mM AcOH, 1.0 mL/min, **I**: mobile phase ACN/MeOH (50:50; v/v) containing 60 mM FA, 25 °C, 1.0 mL/min, **J**: mobile phase ACN/MeOH (50:50; v/v) containing 60 mM FA, 10 °C, 1.0 mL/min, **K**: mobile phase ACN/MeOH (50:50; v/v) containing 30 mM FA, 10 °C, 1.0 mL/min

In general, it is possible to see that QD-AX exhibits a better resolution for the separation of HCAs which are more strongly retained whereas the QN-AX reveals a better separation for the HCAs which are more weakly retained.

According to these results and considering that the used mobile phases (conditions A and B) contains a high concentration of ammonium acetate not ideally suited for ESI-MS-analysis, a mobile phase with similar elution strength but lower salt (electrolytes) content was tested next. Formic acid (FA) and ammonia (NH_3) were used instead of acetic acid (AcOH) and ammonium

acetate (NH_4OAc). A mobile phase composed of 100 % MeOH containing 90 mM FA and 15 mM NH_3 (condition C) was tested on the QD-AX and QN-AX columns. Compared to the previous conditions on the same two columns, slight improvements in resolution were obtained for LA, 2-HBA and GlA but not for MA and 2-HGA (see Table 9.1 and Suppl. Figure 9.3). In the case of ICA and TA some problems occurred due to long retention times and lack of reproducibility of chromatographic runs with this mobile phase and for this reason their separation was resumed on the zwitterionic columns later.

Because the separation already obtained for MA on QD-AX and GlA on QN-AX (under condition C) were good enough these compounds were not considered for further experiments on the two WAX columns. Conditions for improving the separation of 2-HGA and the less retained acids (2-HBA, LA and 3-HBA) are evaluated in the next steps.

9.5.1.2 Separation conditions for enantiomers of 2-HGA

In the case of 2-HGA, a previous study [208] employing a QD-AX column allowed to obtain a baseline resolution by using a mobile phase composed of 100 % methanol containing 40 mM FA at 10 °C. However, this mobile phase is not sufficiently stable because of the fast decomposition of formic acid in methanol (yielding relatively quickly formic acid methyl ester under ambient temperature, as previously reported [209]). For this reason, a concentration of 5 mM ammonia (condition D) was incorporated into the mobile phase. With this addition of ammonia resolution was reduced until 1.53 but it is still baseline separation (see Table 9.1 and Suppl. Figure 9.4).

9.5.1.3 Separation conditions for enantiomers of 3-HBA, LA and 2-HBA

In an attempt to improve the resolution of the most weakly retained acids, part of methanol in the eluent was replaced with acetonitrile and the formic acid concentration was decreased providing a mobile phase composed of ACN/MeOH (50:50; v/v) containing 15 mM FA (condition E, note that in this case no problems with mobile phase stability were observed due to the presence of ACN in the methanolic eluent). No separation was obtained for 3-HBA but considerable improvement was achieved in resolution for the separation of 2-HBA and LA on QN-AX column (see Table 9.1 and Suppl. Figure 9.5).

9.5.1.4 Separation conditions for enantiomers of 3-HBA

Conditions already tested with QD-AX and QN-AX columns have not showed yet even a partial separation of 3-HBA. For this reason, a greater increase in acetonitrile percentage and greater decrease in formic acid concentration yielding a mobile phase of ACN/MeOH (95:5; v/v) containing 5 mM FA (condition F) were used, allowing to obtain a partial separation on both

columns. A slightly better resolution (R_s = 0.60) was obtained on QD-AX column (Table 9.1 and Suppl. Figure 9.6) and it was therefore employed for further experiments. In the next step, a systematic study (Suppl. Table 9.3) considering two acetonitrile-methanol ratios, three FA concentrations, two temperatures and two flow rates, allowed to find a maximum in resolution of 0.76 (mobile phase composed of ACN/MeOH (95:5; v/v), containing 2.5 mM FA, 10 °C, 1.0 mL/min, condition G) which is still far from baseline resolution. For this reason acetic acid was re-employed as additive because it has been seen that separation factors are in some cases better with this counterion. Moreover, due to the low retention of 3-HBA there is no need for elevated counterion concentrations in this case for its elution. A mobile phase composed of ACN/MeOH (95:5; v/v) containing 17.4 mM AcOH (condition H), at 10 °C and with a flow rate of 1.0 mL/min yielded a resolution of 1.00.

Finally, the effect of changing the temperature from 20°C to -20°C (using five different temperatures) was studied. It turned out to have a major effect on resolution, being eventually possible to reach a baseline resolution (R_s = 1.52) at -20 °C (see Table 9.1 and Suppl. Figure 9.7).

This temperature effect on separation factors was also analyzed in terms of the Van´t Hoff equation (eq. 1)

$$ln\alpha = -\frac{\Delta\Delta H^\circ}{RT} + \frac{\Delta\Delta S^\circ}{R} \quad (1)$$

wherein ΔΔ*H*° and ΔΔ*S*° are differential standard enthalpy and entropy changes between the two corresponding enantiomers, *R* is the universal gas constant, and *T* is the absolute temperature in *K* [210].

According to the experimental data applied to equation 1, values for ΔΔH° (-0.381 ± 0.006 kJ mol^{-1}) and ΔΔS° (-0.92 ± 0.02 J mol^{-1} K^{-1}) were obtained. They permit to conclude that the enantioseparation of (*R*)- and (*S*)-3-HBA on QD-AX column is an enthalpically driven process (Figure 9.3) [210].

9.5.2 Enantioseparation of hydroxycarboxylic acids on ZWIX(+) and ZWIX(-)

The zwitterionic chiral stationary phases ZWIX(+) and ZWIX(-) (Figure 9.2) behave also as weak anion exchangers for the separation of HCA enantiomers because the sulfonic acid moiety does not represent a binding site which provides attractive interactions with HCAs. In contrast, this interaction site represents an intramolecular counterion owing to repulsive electrostatic interactions. Hence, due to the presence of this sulfonic acid group on the structure of zwitterionic CSPs, the retention of the HCA is weaker and they required milder conditions for elution than on the corresponding anion exchange (AX) congeners.

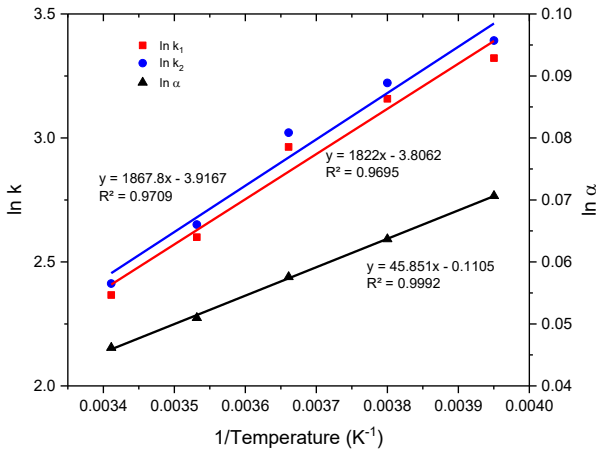

Figure 9.3. Temperature dependence of retention and separation factors as illustrated by van't Hoff plots. Mobile phase ACN/MeOH (95:5; v/v) containing 17.4 mM AcOH, 1.0 mL/min

Eluent gradients were initially used to determine proper conditions for the elution of all compounds. ACN/MeOH (50:50; v/v) containing 60 mM FA at 25 °C and 1.0 mL/min (condition I were selected and tested as isocratic conditions allowing the elution of all the HCAs in less than 10 min on both ZWIX(+) and ZWIX(-) (see Table 9.1 and Suppl. Figure 9.8). However, considerably better results were obtained with the ZWIX(-) column, which showed baseline resolution under these conditions for TA, ICA and GlA and almost baseline resolution for MA (R_s = 1.14) (see Table 9.1 and Suppl. Figure 9.8). In order to achieve full baseline resolution for these four compounds under the same conditions, temperature was decreased to 10°C (condition J) (see Suppl. Figure 9.9) and subsequently the FA concentration was reduced to 30 mM (condition K) (see Suppl. Figure 9.10). Thus, a resolution of 1.57 was obtained for MA (Figure 9.4f), whereas the other three mentioned acids kept good resolution making possible a separation of the four HCAs in less than 15 minutes on the ZWIX(-) column.

Figure 9.4 shows the best obtained separations of the eight studied HCAs from the different tested conditions with regard on obtaining full baseline resolution (Rs higher than 1.5) and shortest retention times (note, higher resolutions have been afforded for some HCAs with other conditions, yet at expense of longer run times; see Suppl. Material for full set of data).

9.5.3 Elution order of HCAs on studied CSPs

One important reported feature of quinine- and quinidine-derived CSPs is their pseudo-enantiomeric behavior which allows in most of the cases inversion of elution order by changing from QD-AX to QN-AX, or from ZWIX(+) to ZWIX(-), or vice versa [181,211]. It is also expected to have the same elution order for a certain pair of enantiomers on the corresponding AX and ZWIX

derived from the same cinchona alkaloid. This means that the columns QD-AX and ZWIX(-) should reveal the same elution orders because they are both derived from quinidine (QD) and the same situation should hold for QN-AX and ZWIX(+) which are both derived from quinine (QN).

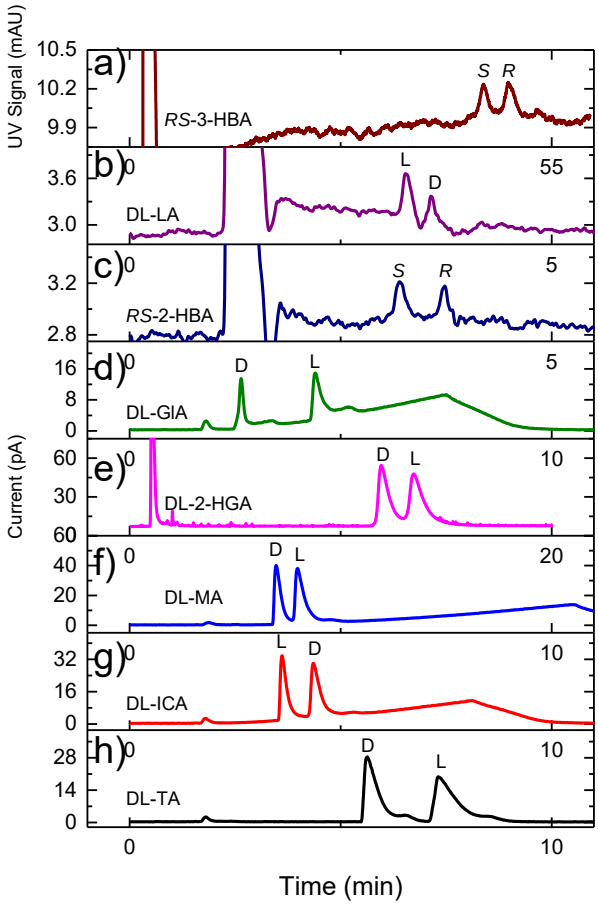

Figure 9.4. Chromatographic runs for the best separations of HCA enantiomers performed on different CSPs. a) *(RS)*-3-HBA on QD-AX; condition H at -20 °C, b) DL-LA on QN-AX; condition C, c) *(RS)*-2-HBA on QN-AX; condition C, d) DL-GlA on ZWIX(-); condition I, e) DL-2-HGA on QD-AX; condition D, f) DL-MA on ZWIX(-); condition K, g) DL-ICA on ZWIX(-); condition I, h) DL-TA on ZWIX(-); condition I (for details of experimental conditions see Table 9.1)

For the group of studied HCAs, elution order was determined on the columns for which partial or baseline separations were achieved, and this information is summarized in Table 9.2. Only for three HCAs (GlA, 2-HBA and TA) elution order could be determined on all four CSPs. Interestingly, their behaviors are different in each case. GlA follows the expected manner described above: the alkaloid moiety and its absolute configurations in position 8 and 9, respectively, are decisive for the elution order with stronger retention for the D-enantiomer on QN-AX and ZWIX(+) as well as the L-enantiomer on QD-AX and ZWIX(-) (Figure 9.5). For 2-HBA an inversion of elution order is observed by exchanging the QD-AX for QN-AX column, and vice versa, but not when

ZWIX(+) is exchanged for ZWIX(-) (Suppl. Figure 9.11). In the case of TA, there is no inversion of elution order obtained when QN-derived CSP is exchanged for QD-derived analog, neither when ZWIX(+) is exchanged for ZWIX(-) nor when QN-AX is exchanged for QD-AX columns. However, the elution order can be reversed by a change from the AX to the corresponding ZWIX column (Suppl. Figure 9.12).

Table 9.2. Elution orders for hydroxycarboxylic acids on studied chiral stationary phases

Compound	Configuration of the first eluted enantiomer on each column			
	QN-AX	**QD-AX**	**ZWIX(+)**	**ZWIX(-)**
3-HBA	R (D)	S (L)	R (D)	n.s.
LA	S (L)	R (D)	n.s.	S (L)
2-HBA	S (L)	R (D)	S (L)	S (L)
GlA	S (L)	R (D)	S (L)	R (D)
2-HGA	S (L)	R (D)	S (L)	n.s.
MA	n.s.	R (D)	n.s.	S (L)
ICA	1R,2S (D)	1R,2S (D)	1S,2R (L)	1S,2R (L)
TA	2R,3R (L)	2R,3R (L)	2S,3S (L)	2S,3S (L)

n.s.: no separation, TA (IUPAC name): 2,3-dihydroxybutanedioic acid, ICA (IUPAC name): 1-hydroxypropane-1,2,3-tricarboxylic acid

With respect to the other HCAs, elution order information could be determined only on two or three of the four CSPs. However, it can be seen that for example LA appears to behave like 2-HBA, and ICA and MA appear to behave like TA. In the case of TA, ICA and MA is interesting their similar behavior because all of them are oligocarboxylic acids (i.e. di- or tricarboxylic acids) with carboxylic groups in positions 1 and 4. In contrast, 2-HGA which was the other oligocarboxylic acid (dicarboxylic acid) studied, having carboxylic groups in position 1 and 5 has a behavior of elution order which is completely different. The above mentioned situations can be an important indication for completely different mechanisms of interaction between these HCAs and the chiral selector anchored on the corresponding CSPs.

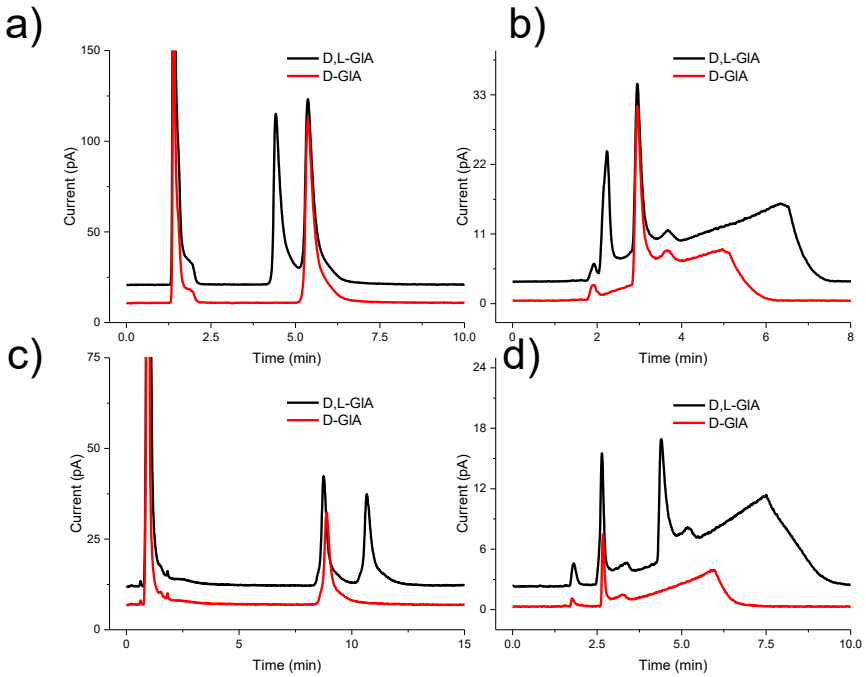

Figure 9.5. Chromatographic runs for a mixture of D- and L-GlA enantiomers or the D-GlA enantiomer on a) QN-AX column, b) ZWIX(+) column, c) QD-AX column and d) ZWIX(-) column.

9.6 Conclusions

MS-compatible conditions for the enantioseparation (full baseline resolution) of eight HCAs were determined in at least one of the four CSPs employed. Except for the case of 3-HBA, conditions for the chiral separation consist of ACN/MeOH mixtures as eluents containing FA and/or NH_3 as additives, temperatures between 10 and 25°C and a flow rate of 1.00 mL/min. In the case of 3-HBA enantiomers, acetic acid (17.4 mM) as additive and a temperature of -20 °C were required to obtain baseline resolution. When possible elution order was determined for the enantiomers revealing at least three different behaviors between the studied compounds, it means that no reversion of elution order by exchanging QD-AX and QN-AX columns, or ZWIX(+) and ZWIX(-) is possible with all these compounds, and it has to be analyzed in a case to case basis.

9.7 Acknowledgements

This work was supported by the “Struktur- und Innovationsfonds für die Forschung (SI-BW)” by the regional government of Baden-Württemberg (Ministry of Science, Research and Arts). C.C. is grateful for a DAAD doctoral fellowship (DAAD no. 57129429).

9.8 Supplementary material

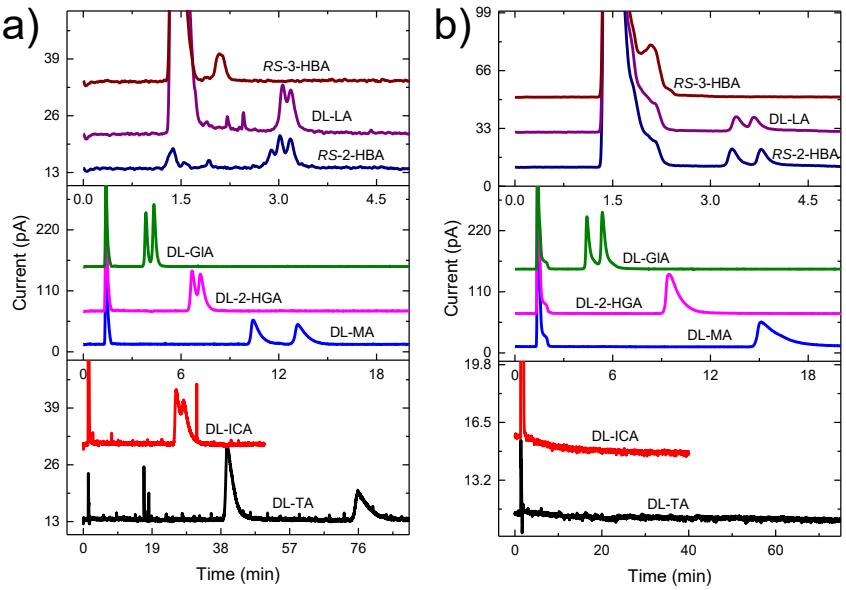

Suppl. Figure 9.1. Chromatographic runs for a mixture of HCA enantiomers on a) QD-AX column and b) QN-AX column. Mobile phase MeOH/AcOH/NH_4OAc (98:2:0.5; v/v/m), 25 °C, 1.0 mL/min

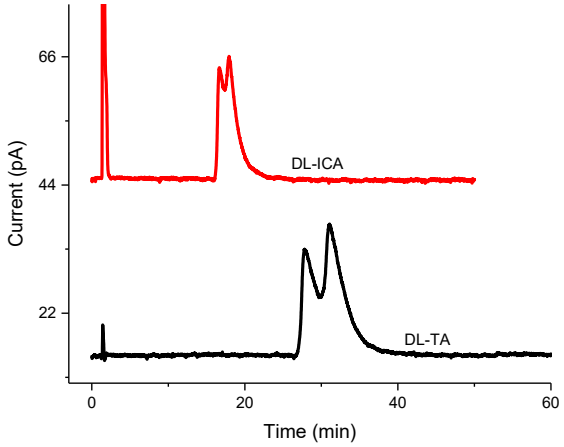

Suppl. Figure 9.2. Chromatographic runs for a mixture of D- and L-ICA enantiomers and D- and L-TA enantiomers on a QN-AX column. Mobile phase MeOH/AcOH/NH_4OAc (96:4:1; v/v/m), 25 °C, 1.0 mL/min

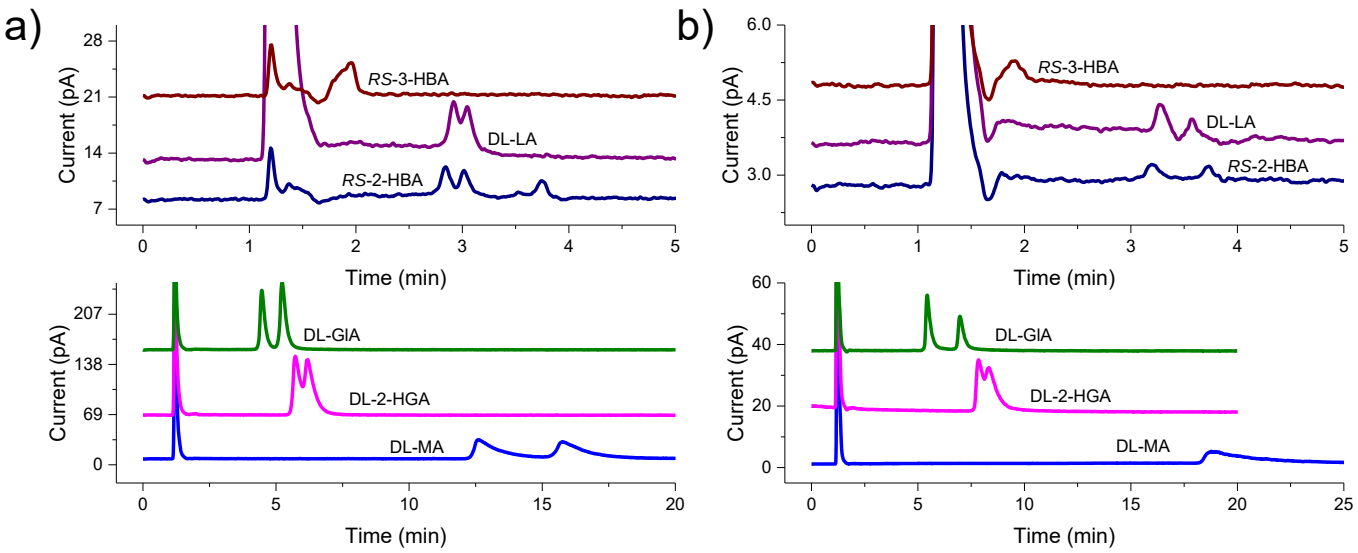

Suppl. Figure 9.3. Chromatographic runs for a mixture of HCA enantiomers on a) QD-AX column and b) QN-AX column. Mobile phase: 100 % MeOH containing 90 mM FA and 15 mM NH_3, 25 °C, 1.0 mL/min.

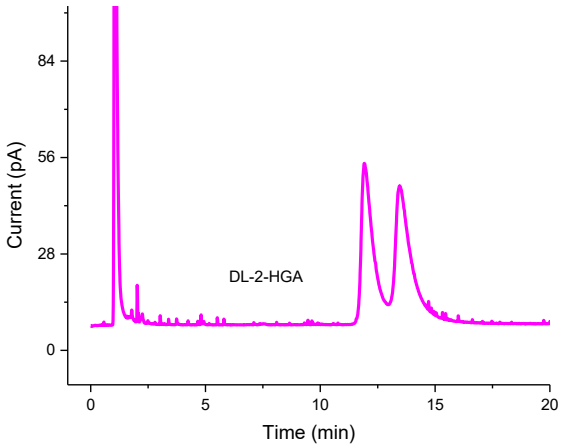

Suppl. Figure 9.4. Chromatographic runs for a mixture of D- and L-2-HGA on QD-AX column. Mobile phase: 100 % MeOH containing 40 mM FA and 5 mM NH_3, 10 °C, 1.0 mL/min.

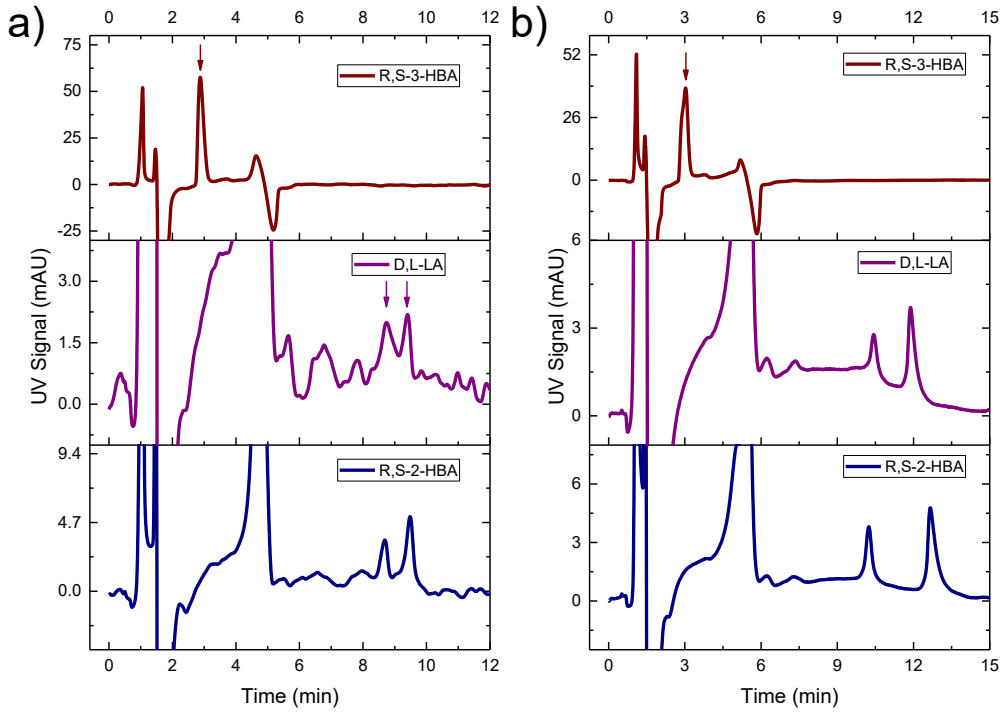

Suppl. Figure 9.5. Chromatographic runs for a mixture of less retained HCA enantiomers on a) QD-AX column and b) QN-AX column. Mobile phase ACN:MeOH 50:50 % v/v containing 15 mM FA, 25 °C, 1.0 mL/min

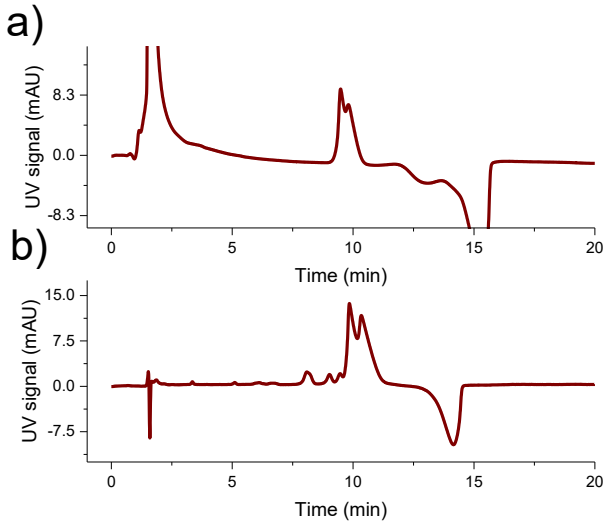

Suppl. Figure 9.6. Chromatographic runs for a mixture (*R*)- and (*S*)-3-HBA enantiomers on a) QN-AX column and b) QD-AX column. Mobile phase ACN/MeOH (95:5; v/v) containing 5 mM FA, 25 °C, 1.0 mL/min

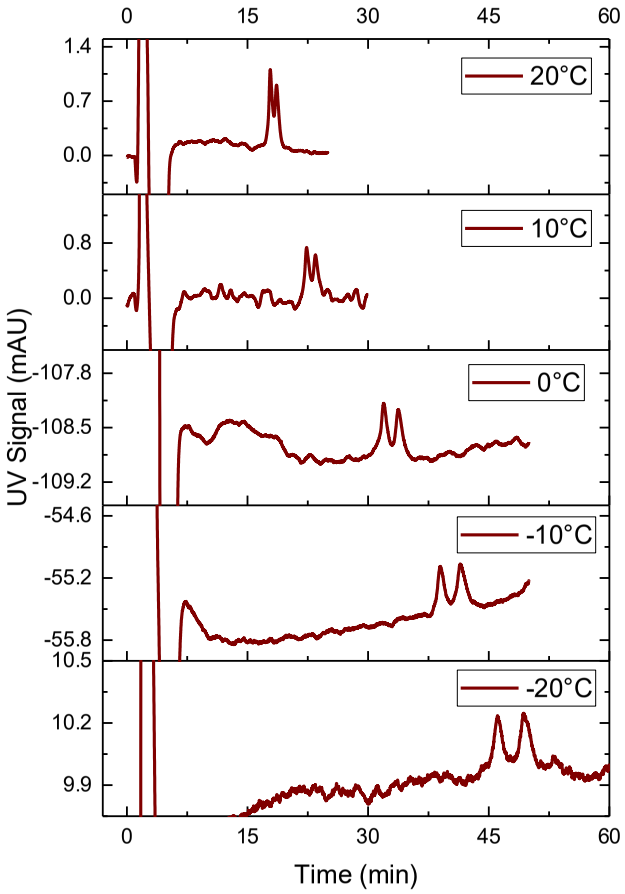

Suppl. Figure 9.7. Chromatographic runs for a mixture of (*R*)- and (*S*)-3-HBA at different temperatures from 20 (top) to -20 °C (bottom). Mobile phase ACN/MeOH (95:5; v/v) containing 17.4 mM AcOH, 1.0 mL/min

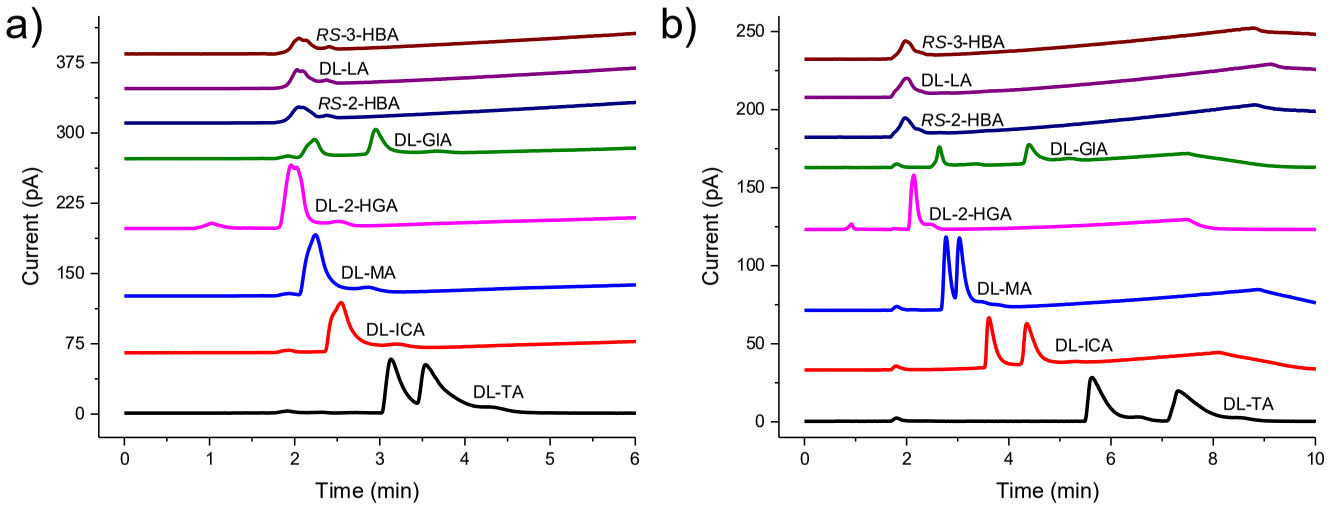

Suppl. Figure 9.8. Chromatographic runs for HCA enantiomers on a) ZWIX(+) column and b) ZWIX(-) column. Mobile phase ACN/MeOH (50:50; v/v) containing 60 mM FA, 25 °C, 1.0 mL/min

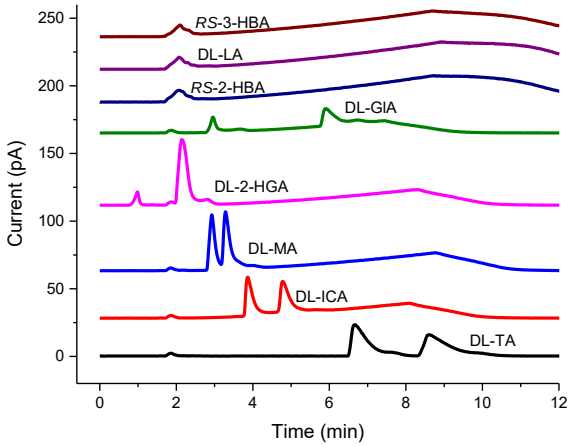

Suppl. Figure 9.9. Chromatographic runs for a mixture of HCA enantiomers on a) ZWIX(-) column. Mobile phase ACN/MeOH (50:50; v/v) containing 60 mM FA, 10 °C, 1.0 mL/min

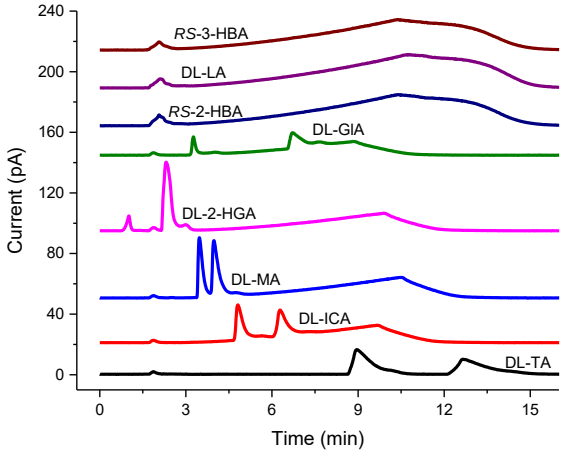

Suppl. Figure 9.10. Chromatographic runs for a mixture of HCA enantiomers on a) ZWIX(-) column. Mobile phase ACN/MeOH (50:50; v/v) containing 30 mM FA, 10 °C, 1.0 mL/min

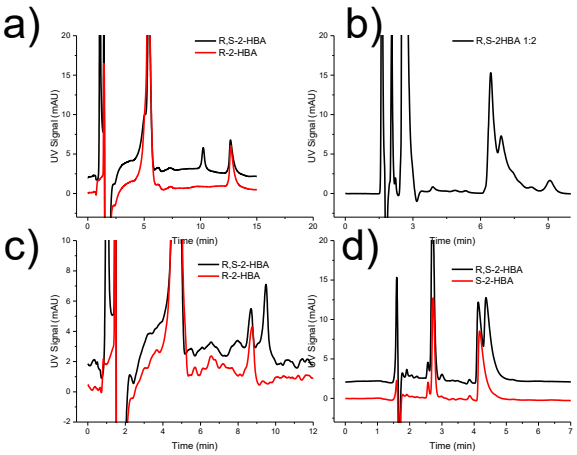

Suppl. Figure 9.11. Chromatographic runs for a mixture of (*R*)- and (*S*)-2-HBA enantiomers or single enantiomer on a) QN-AX column, b) ZWIX(+) column, c) QD-AX column and d) ZWIX(-) column.

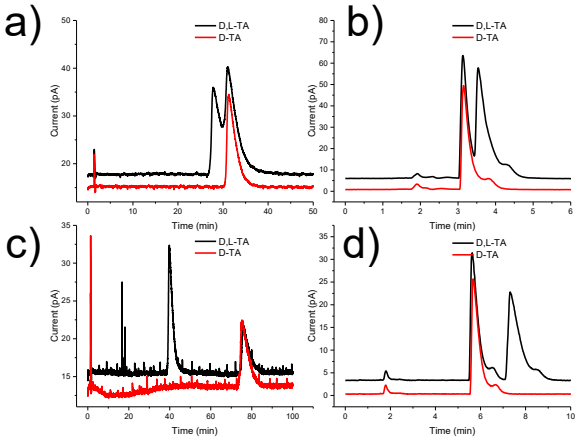

Suppl. Figure 9.12. Chromatographic runs for a mixture of D- and L-TA enantiomers or the D-TA enantiomer on a) QN-AX column, b) ZWIX(+) column, c) QD-AX column and d) ZWIX(-) column.

Suppl. Table 9.1. Chromatographic parameters obtained under different conditions for the separation of HCAs with QD-AX and QN-AX columns.

Column	Condition	Compound	tR_1 [min]	tR_2 [min]	k_1	k_2	α	N_1	N_2	R_S
QD-AX	A	D,L-TA	39.772	75.839	28.68	55.60	1.94	2237	2633	7.76
QD-AX	A	D,L-ICA	25.643	27.673	18.14	19.65	1.08	1247	260	0.42
QD-AX	A	D,L-MA	10.403	13.154	6.76	8.82	1.30	2245	2189	2.74
QD-AX	A	D,L-2-HGA	6.677	7.186	3.98	4.36	1.10	2399	1922	0.85
QD-AX	A	D,L-GlA	3.842	4.335	1.87	2.24	1.20	3266	3112	1.70
QD-AX	A	R,S-2-HBA	3.018	3.178	1.25	1.37	1.10	2023	3472	0.66
QD-AX	A	D,L-LA	3.060	3.184	1.28	1.38	1.07	4139	3541	0.61
QD-AX	A	R,S-3-HBA	2.090	2.090	0.56	0.56	1.00	946		0.00
QN-AX	A	D,L-MA	15.109	15.109	9.16	9.16	1.00	749		0.00
QN-AX	A	D,L-2-HGA	9.463	9.463	5.36	5.36	1.00	837		0.00
QN-AX	A	D,L-GlA	4.419	5.367	1.97	2.61	1.32	2237	2556	2.37
QN-AX	A	R,S-2-HBA	3.332	3.778	1.24	1.54	1.24	2414	3027	1.63
QN-AX	A	D,L-LA	3.396	3.669	1.28	1.47	1.14	2440	2732	0.98
QN-AX	A	R,S-3-HBA	2.082	2.082	0.40	0.40	1.00			0.00
QN-AX	B	D,L-TA	27.816	31.066	17.74	19.93	1.12	686	751	0.73
QN-AX	B	D,L-ICA	16.670	17.945	10.23	11.09	1.08	1541	815	0.60
QD-AX	C	D,L-MA	12.612	15.761	7.19	9.24	1.28	1244	1582	2.08
QD-AX	C	D,L-2-HGA	5.724	6.189	2.72	3.02	1.11	1553	1221	0.72
QD-AX	C	D,L-GlA	4.465	5.229	1.90	2.40	1.26	3301	3220	2.24
QD-AX	C	R,S-2-HBA	2.844	3.015	0.85	0.96	1.13	4311	5041	1.00
QD-AX	C	D,L-LA	2.918	3.045	0.90	0.98	1.09	3832	3692	0.65
QD-AX	C	R,S-3-HBA	1.949	1.949	0.27	0.27	1.00	369		0.00
QN-AX	C	D,L-MA	18.779	18.779	11.50	11.50	1.00	465		0.00
QN-AX	C	D,L-2-HGA	7.850	8.327	4.23	4.54	1.08	2247	1319	0.60
QN-AX	C	D,L-GlA	5.437	6.975	2.62	3.64	1.39	3387	3701	3.67
QN-AX	C	R,S-2-HBA	3.197	3.733	1.13	1.49	1.32	3354	7727	2.76
QN-AX	C	D,L-LA	3.375	3.570	1.25	1.38	1.10	3737	7240	1.52
QN-AX	C	R,S-3-HBA	1.913	1.913	0.27	0.27	1.00	291		0.00
QD-AX	D	D,L-2-HGA	11.918	13.446	6.59	7.56	1.15	2913	2373	1.53
QD-AX	E	R,S-2-HBA	8.689	9.488	4.91	5.45	1.11	7329	9602	2.01
QD-AX	E	D,L-LA	8.739	9.411	4.94	5.40	1.09	3232	8249	1.30
QD-AX	E	R,S-3-HBA	2.875	2.875	0.96	0.96	1.00	1146		0.00
QN-AX	E	R,S-2-HBA	10.240	12.660	6.16	7.85	1.27	9303	8161	4.82
QN-AX	E	D,L-LA	10.440	11.884	6.30	7.30	1.16	9906	10206	3.24
QN-AX	E	R,S-3-HBA	3.031	3.031	1.12	1.12	1.00	566		0.00
QD-AX	F	R,S-3-HBA	9.847	10.339	5.76	6.10	1.06	2935	2102	0.60
QN-AX	F	R,S-3-HBA	9.483	9.804	5.20	5.41	1.04	5615	3810	0.54
QD-AX	G	R,S-3-HBA	15.870	16.714	8.77	9.29	1.06	4861	2668	0.76
QD-AX	H at -20 °C	R,S-3-HBA	46.089	49.346	27.72	29.75	1.07	10288	6422	**1.52**
QD-AX	H at -10 °C	R,S-3-HBA	38.991	41.450	23.52	25.07	1.07	9224	6842	1.35
QD-AX	H at -0 °C	R,S-3-HBA	31.956	33.757	19.37	20.51	1.06	7764	7353	1.19
QD-AX	H at 10 °C	R,S-3-HBA	22.350	23.438	13.46	14.16	1.05	7419	6786	1.00
QD-AX	H at 20 °C	R,S-3-HBA	17.830	18.600	10.66	11.16	1.05	6995	4974	0.81

A: mobile phase MeOH/AcOH/NH_4OAC (98:2:0.5; v/v/m), 25 °C, 1.0 mL/min, **B**: mobile phase MeOH/AcOH/NH_4OAC (96:4:1; v/v/m), 25 °C, 1.0 mL/min, **C**: mobile phase 100 % MeOH containing 90 mM FA and 15 mM NH_3, 25 °C, 1.0 mL/min, **D**: mobile phase 100 % MeOH containing 40 mM FA and 5 mM NH_3, 10 °C, 1.0 mL/min, **E**: mobile phase ACN/MeOH (50:50; v/v) containing 15 mM FA, 25 °C, 1.0 mL/min **F**: mobile phase ACN/MeOH (95:5; v/v) containing 5 mM FA, 25 °C, 1.0 mL/min, **G**: mobile phase ACN/MeOH (95:5; v/v) containing 2.5 mM FA, 10 °C, 1.0 mL/min, **H**: mobile phase ACN/MeOH (95:5; v/v) containing 17.4 mM AcOH, 1.0 mL/min

Suppl. Table 9.2. Chromatographic parameters obtained under different conditions for the separation of HCAs with ZWIX(+) and ZWIX(-) columns.

Column	Condition	Compound	tR_1 [min]	tR_2 [min]	k_1	k_2	α	N_1	N_2	R_S
ZWIX(+)	I	D,L-TA	3.131	3.538	0.99	1.25	1.26	1506	1027	1.06
ZWIX(+)	I	D,L-ICA	2.545	2.545	0.62	0.62	1.00	624		0.00
ZWIX(+)	I	D,L-MA	2.245	2.245	0.43	0.43	1.00	577		0.00
ZWIX(+)	I	D,L-2-HGA	1.960	1.960	0.25	0.25	1.00	341		0.00
ZWIX(+)	I	D,L-GlA	2.234	2.952	0.42	0.88	2.08	904	2148	2.60
ZWIX(+)	I	R,S-2-HBA	2.047	2.047	0.30	0.30	1.00	372		0.00
ZWIX(+)	I	D,L-LA	2.029	2.029	0.29	0.29	1.00	571		0.00
ZWIX(+)	I	R,S-3-HBA	2.051	2.051	0.31	0.31	1.00	437		0.00
ZWIX(-)	I	D,L-TA	5.632	7.312	2.75	3.87	1.41	1635	1167	2.37
ZWIX(-)	I	D,L-ICA	3.613	4.354	1.41	1.90	1.35	2827	2172	2.27
ZWIX(-)	I	D,L-MA	2.772	3.035	0.85	1.02	1.21	2684	2396	1.14
ZWIX(-)	I	D,L-2-HGA	2.140	2.140	0.43	0.43	1.00	1550		0.00
ZWIX(-)	I	D,L-GlA	2.643	4.399	0.76	1.93	2.54	3201	2433	6.43
ZWIX(-)	I	R,S-2-HBA	1.968	1.968	0.31	0.31	1.00	284		0.00
ZWIX(-)	I	D,L-LA	1.997	1.997	0.33	0.33	1.00	251		0.00
ZWIX(-)	I	R,S-3-HBA	1.978	1.978	0.32	0.32	1.00	311		0.00
ZWIX(-)	J	D,L-TA	6.660	8.613	3.36	4.63	1.38	1414	1027	2.19
ZWIX(-)	J	D,L-ICA	3.871	4.781	1.53	2.13	1.39	2326	2257	2.50
ZWIX(-)	J	D,L-MA	2.928	3.286	0.91	1.15	1.26	1880	2121	1.28
ZWIX(-)	J	D,L-2-HGA	2.146	2.146	0.40	0.40	1.00	399		0.00
ZWIX(-)	J	D,L-GlA	2.955	5.894	0.93	2.85	3.06	2506	1572	7.05
ZWIX(-)	J	R,S-2-HBA	2.069	2.069	0.35	0.35	1.00	166		0.00
ZWIX(-)	J	D,L-LA	2.075	2.075	0.36	0.36	1.00	155		0.00
ZWIX(-)	J	R,S-3-HBA	2.102	2.102	0.37	0.37	1.00	161		0.00
ZWIX(-)	K	D,L-TA	8.952	12.647	4.84	7.25	1.50	1167	966	2.76
ZWIX(-)	K	D,L-ICA	4.811	6.285	2.14	3.10	1.45	2156	2011	3.00
ZWIX(-)	K	D,L-MA	3.470	3.980	1.26	1.60	1.26	2394	1900	1.57
ZWIX(-)	K	D,L-2-HGA	2.313	2.313	0.51	0.51	1.00	376		0.00
ZWIX(-)	K	D,L-GlA	3.263	6.708	1.13	3.38	2.99	3660	1144	6.82
ZWIX(-)	K	R,S-2-HBA	2.067	2.067	0.35	0.35	1.00	190		0.00
ZWIX(-)	K	D,L-LA	2.093	2.093	0.37	0.37	1.00	178		0.00
ZWIX(-)	K	R,S-3-HBA	2.066	2.066	0.35	0.35	1.00	210		0.00

I: mobile phase ACN/MeOH (50:50; v/v) containing 60 mM FA, 25 °C, 1.0 mL/min, **J**: mobile phase ACN/MeOH (50:50; v/v) containing 60 mM FA, 10 °C, 1.0 mL/min, K: mobile phase ACN/MeOH (50:50; v/v) containing 30 mM FA, 10 °C, 1.0 mL/min

Suppl. Table 9.3. Systematic study and resolution obtained during optimization of conditions for separation of (*R*)- and (*S*)-3-HBA.

Number of experiment	ACN-MeOH (v/v) Ratio	FA concentration (mM)	Temperature (°C)	Flow rate (mL/min)	R_s
1	95.0:5.0	2.5	10	0.5	**n.d.**
2	95.0:5.0	2.5	10	1.0	**0.76**
3	95.0:5.0	2.5	25	0.5	**n.d.**
4	95.0:5.0	2.5	25	1.0	**0.65**
5	95.0:5.0	5	10	0.5	**0.63**
6	95.0:5.0	5	10	1.0	**0.43**
7	95.0:5.0	5	25	0.5	**0.56**
8	95.0:5.0	5	25	1.0	**0.55**
9	95.0:5.0	10	10	0.5	**n.d.**
10	95.0:5.0	10	10	1.0	**n.d.**
11	95.0:5.0	10	25	0.5	**0.43**
12	95.0:5.0	10	25	1.0	**0.44**
13	97.5:2.5	2.5	10	0.5	**n.d.**
14	97.5:2.5	2.5	10	1.0	**0.61**
15	97.5:2.5	2.5	25	0.5	**n.d.**
16	97.5:2.5	2.5	25	1.0	**0.61**
17	97.5:2.5	5	10	0.5	**0.53**
18	97.5:2.5	5	10	1.0	**0.49**
19	97.5:2.5	5	25	0.5	**0.50**
20	97.5:2.5	5	25	1.0	**0.50**
21	97.5:2.5	10	10	0.5	**n.d.**
22	97.5:2.5	10	10	1.0	**n.d.**
23	97.5:2.5	10	25	0.5	**0.41**
24	97.5:2.5	10	25	1.0	**0.33**

n.d.: not determined

10 Publication V. Chiral separation of disease biomarkers

10.1 Title

Chiral separation of disease biomarkers with 2-hydroxycarboxylic acid structure

Carlos Calderón[1], Cristina Santi[1,2], Michael Lämmerhofer[1]*

[1]Institute of Pharmaceutical Sciences, Pharmaceutical (Bio-)Analysis, University of Tübingen, Auf der Morgenstelle 8, 72076 Tübingen, Germany

[2]Dipartimento di Chimica e Tecnologia del Farmaco, Università degli Studi di Perugia, Perugia, Italy

Reprinted with permission from Journal of Separation Science, Volume 41, Pages 1224-1231,

DOI: 10.1002/jssc.201701243

Copyright (2018) WILEY-VCH Verlag GmbH & Co. KGaA

10.2 Abstract

Chiral 2-hydroxycarboxylic acids are compounds which have been linked to particular diseases and are putative biomarkers with some diagnostic potential. The importance of identifying whether a particular enantiomer is related to certain diseases has been encouraged recently. However, in many cases it has not yet been elucidated whether there are stereochemical implications with respect to these biomarkers and whether their enantioselective analysis provides new insights and diagnostic potential. In this study 13 disease related chiral 2-hydrocarboxylic acids were studied for their chiral separation by HPLC on three cinchona alkaloid-derived chiral stationary phases. From a subgroup of eight 2-hydroxymonocarboxylic acids, baseline resolution could be achieved and inversion of elution order by exchanging *tert*-butylcarbamoyl quinidine chiral stationary phase (Chiralpak QD-AX) for the corresponding quinine analogue (Chiralpak QN-AX) is shown for seven of them. Furthermore, conditions for chiral separation of the 2-hydroxydicarboxylic acids, citramalic acid, 2-isopropylmalic acid and 2-hydroxyadipic acid are reported and compared to the previous reported conditions for 2-hydroxyglutaric acid and malic acid.

10.3 Introduction

Chiral 2-hydroxycarboxylic acids are compounds which are known for their relationship with particular human illnesses, especially but not only with inherited metabolic diseases. Lactic acid (LA) [190], 2-hydroxy-3-methylbutyric acid (2-H-3-MBA) [212,213], 2-hydroxy-3-methylpentanoic acid (2-H-3-MPA) [212,213], 2-hydroxyisocaproic acid (2-HICA) [212–214], 2-hydroxyadipic acid (2-HAA) [215] and also 2-hydroxyglutaric acid (2-HGA) [148,150,156] are related to certain types of organic acidurias. Increased amounts of 2-HICA have also been found in patients with Zellweger syndrome, a congenital disorder [216]. 2-Hydroxycaproic acid (2-HCA) showed to be the most significant substance observed in the cerebrospinal fluid of a patient with Nocardia infection, an uncommon cause of meningitis [217]. 2-HBA, in the plasma, has been pointed out as a good marker for early stage type II diabetes [218] and 2-isopropylmalic acid (2-IMA) has been described as a biomarker for asthma diagnosis [219]. Related to cancer, altered concentrations of LA have been found in tumors [220], and the enantiomer D-2-HGA has been described as an oncometabolite [158,165,221]. In other mammals, citramalic acid has been considered as a marker of several unusual chronic diseases developed in cheetahs (Acinonyx jubatus) [222].

In some of the mentioned cases, the occurrence and relevance of a particular enantiomer or the enantiomeric ratio has been indicated for their specific correlation with a disease or as a biomarker of disease. Struys [223], for example, described very well how critical is this indication

in the case of 2-HGA since L-2-HGA and D-2-HGA are related to different acidurias [156] and only D-2-HGA has been described as an oncometabolite [158].

Different studies have approached the enantioseparation of 2-hydroxycarboxylic acids. Some of them are ligand exchange CE [102,196,201], ligand exchange LC [224], GC analysis after derivatization [163], LC after derivatization [225], direct LC by using macrocyclic antibiotic chiral stationary phases (CSPs) [162,193,207] and quinine- or quinidine- derived CSPs [169,179,180,208,226,227], amongst others.

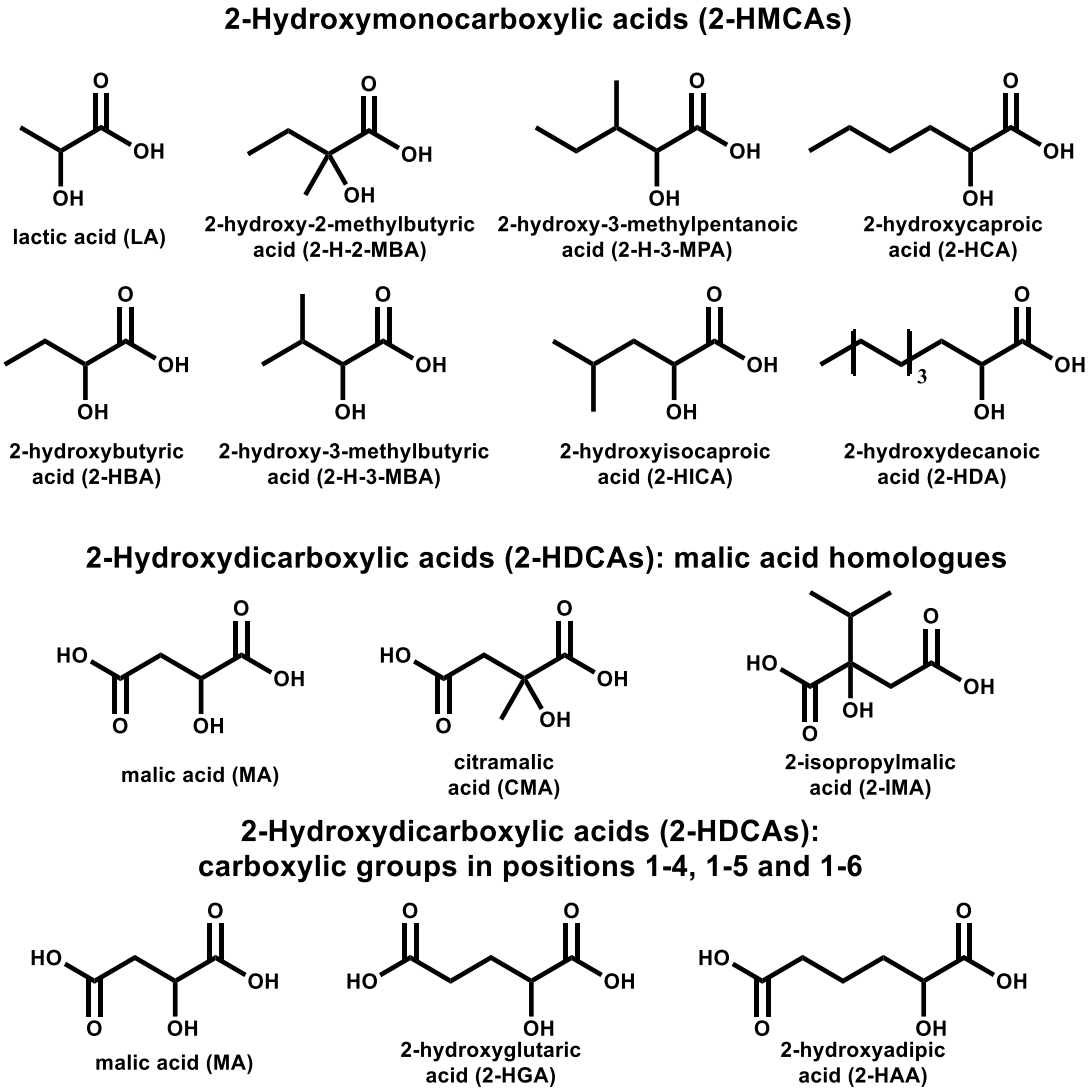

Figure 10.1. Structures of the studied 2-hydroxycarboxylic acids

In this study, a group of 13 potential biomarkers of disease with 2-hydroxycarboxylic acid structure (Figure 10.1) were tested on three cinchona alkaloid-derived CSPs (Figure 10.2) in order to determine MS-compatible conditions for their enantiomeric analysis. At the same time it was evaluated how certain modifications on the structure of 2-hydroxycarboxylic acids affect their retention and selectivity on the employed CSPs.

10.4 Experimental

10.4.1 Materials

The samples (*RS*)-2-hydroxybutyric acid sodium salt (RS-2-HBA), (*R*)-2-hydroxybutyric acid (R-2-HBA), (*RS*)-lactic acid sodium salt (RS-LA), (S)-lactic acid lithium salt (S-LA), (*RS*)-2-hydroxy-2-methylbutyric acid (RS-2-H-2-MBA), (*RS*)-2-hydroxy-3-methylbutyric acid (RS-2-H-3-MBA), (*S*)-2-hydroxy-3-methylbutyric acid (S-2-H-3-MBA), (*RS*)-2-hydroxycaproic acid (RS-2-HCA), (*RS*)-2-hydroxyisocaproic acid (RS-2-HICA), (*S*)-2-hydroxyisocaproic acid (S-2-HICA), (*RS*)-malic acid disodium salt (RS-MA), (*S*)-malic acid disodium salt (S-MA), (*RS*)-2-hydroxyglutaric acid sodium salt (RS-2-HGA), (*S*)-2-hydroxyglutaric acid sodium salt (S-2-HGA), (*RS*)-2-hydroxyadipic acid sodium salt (RS-2-HAA), (*RS*)-citramalic acid potassium salt (RS-CMA), (*R*)-citramalic acid sodium salt (R-CMA), (*RS*)-2-isopropylmalic acid (RS-2-IMA) were purchased from Sigma–Aldrich (Steinheim, Germany), (*RS*)-2-hydroxydecanoic acid (RS-2-HDA) was obtained from ABCR (Karlsruhe, Germany) and (*2RS,3RS*)-2-hydroxy-3-methylpentanoic acid (2RS,3RS-2-H-3-MPA) was purchased from Chemspace (Riga, Latvia).

Mobile phases were prepared with solvents of HPLC grade. Methanol (MeOH) was supplied by Sigma-Aldrich (Steinheim, Germany) and acetonitrile (ACN) was purchased from J.T. Baker (Deventer, The Netherlands). As additives, formic acid 98% (FA) was obtained by Carl Roth (Karlsruhe, Germany) and 4 M ammonia (NH_3) in methanol was purchased from Sigma–Aldrich (Steinheim, Germany). Water was obtained with a water filtration system from Elga Veolia (Paris, France).

10.4.2 Instrumentation and chromatographic method

LC experiments were carried out on two different instruments: Agilent 1100 Series G2445D LC/MSD Ion Trap (Waldbronn, Germany) and an Agilent 1100 Series HPLC equipped with a UV–VIS detector and connected to a Corona Veo Charged Aerosol Detector (CAD), from Thermo Fisher Scientific (Waltham, Massachusetts, U.S.A.). The nitrogen flow of the CAD was adjusted to 60 psi.

Data acquisition and analysis were done by using ChemStation software from Agilent Technologies.

For the MSD Ion Trap negative mode was employed with a nebulizer pressure of 80 psi, dry gas flow of 12 L/min and dry temperature of 325 °C. Presented chromatograms from MSD Ion Trap correspond to the EIC ($[M-H]^-$) of each studied 2-hydrocarboxylic acid with a mass tolerance of ± 0.5 Da.

Three chiral stationary phases from Chiral Technologies Europe (Illkirch, France) were employed: a Chiralpak QD-AX (150 x 4 mm, 5 µm), a Chiralpak QN-AX (150 x 4 mm ID, 5 µm particle size) and a Chiralpak ZWIX(-) column (150 x 4 mm ID, 3 µm particle size). 10% (v/v) acetone solution in ACN with detection at 280 nm was used for determining t_0 under each tested condition. Methanol-water bath cooled with liquid nitrogen was used when a column temperature lower than 0 °C was tested.

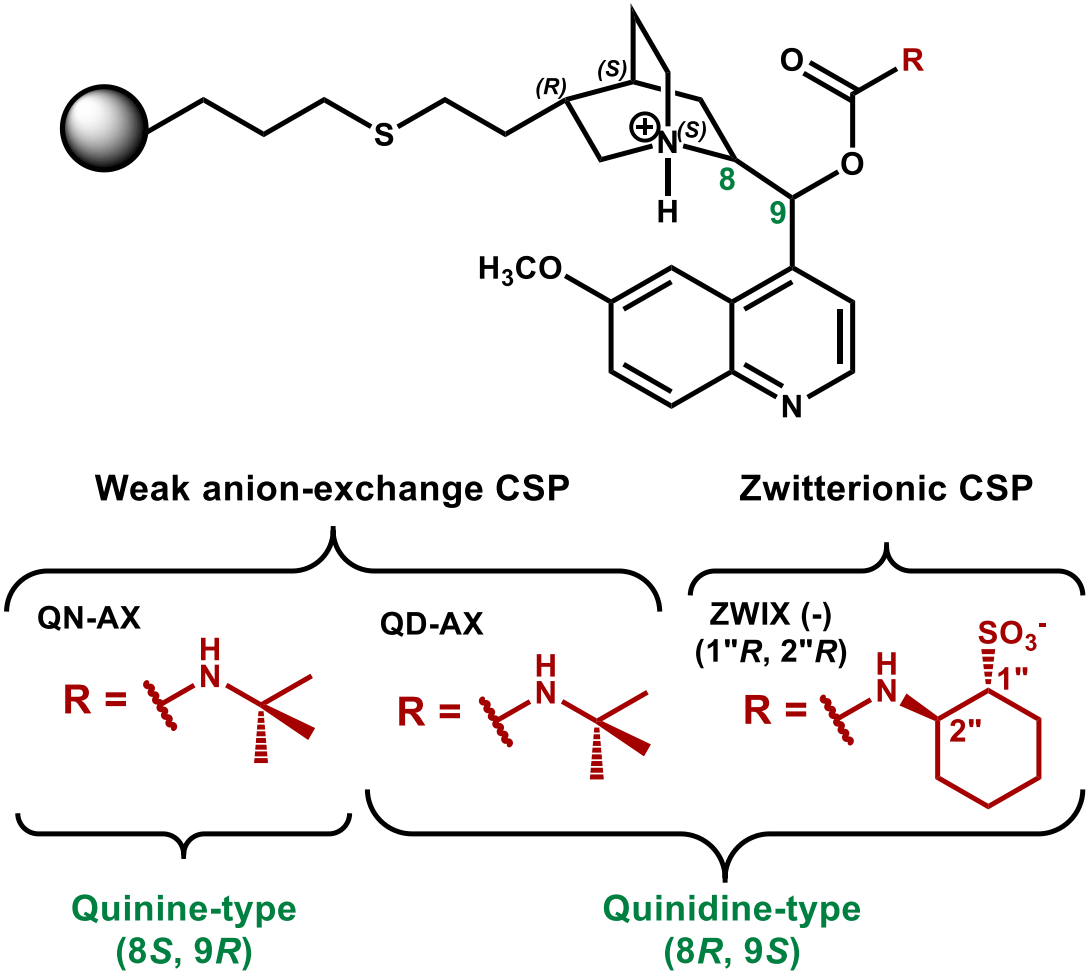

Figure 10.2. Chiral stationary phases tested in this study: Chiralpak QN-AX and QD-AX as well as Chiralpak ZWIX(-)

10.5 Results and discussion

In order to determine MS-compatible conditions for the chiral separation of the 13 putative disease biomarkers with 2-hydrocarboxylic acid structure, they were classified into three different groups (see Figure 10.1) according to their structural similarity. The groups are as follows: 1) 2-H-2-MBA, 2-H-3-MBA, 2-H-3-MPA, 2-HICA, 2-HCA and 2-HDA which are 2-hydroxy monocarboxylic acids (2-HMCA) similar to previously studied LA and 2-HBA [226], 2) CMA and 2-IMA which are homologues of MA and 3) 2-HAA, which was analyzed in comparison to 2-HGA and MA, another two dicarboxylic acids, to see the influence of the distance between the two carboxylic groups, since they are located in position 1-6, 1-5 and 1-4, respectively.

10.5.1 Enantioseparation of 2-hydroxy monocarboxylic acids on chiral weak anion-exchangers

Because of the similar structure of these 2-HMCA with the already studied LA and 2-HBA, weak anion-exchange (WAX) columns QD-AX and QN-AX (see Figure 10.2), well described in the literature [228], were employed for their separation. In comparison with previously reported conditions [209] for the separation of these two compounds a small amount of ammonia (ACN:MeOH 50:50 v/v containing 15 mM FA and 2.5 mM NH_3, at 1.0 mL/min and 10 °C) was added to the mobile phase in order to increase its stability.

Chromatograms for the chiral separation on QN-AX and QD-AX columns of the eight 2-HMCA are shown in Figure 10.3. The corresponding chromatographic data for the mentioned separations are summarized in Suppl. Table 10.1. As can be seen, in general better resolution can be obtained for the eight compounds on the QN-AX column, with which baseline resolution can be achieved for all compounds except 2-H-2-MBA.

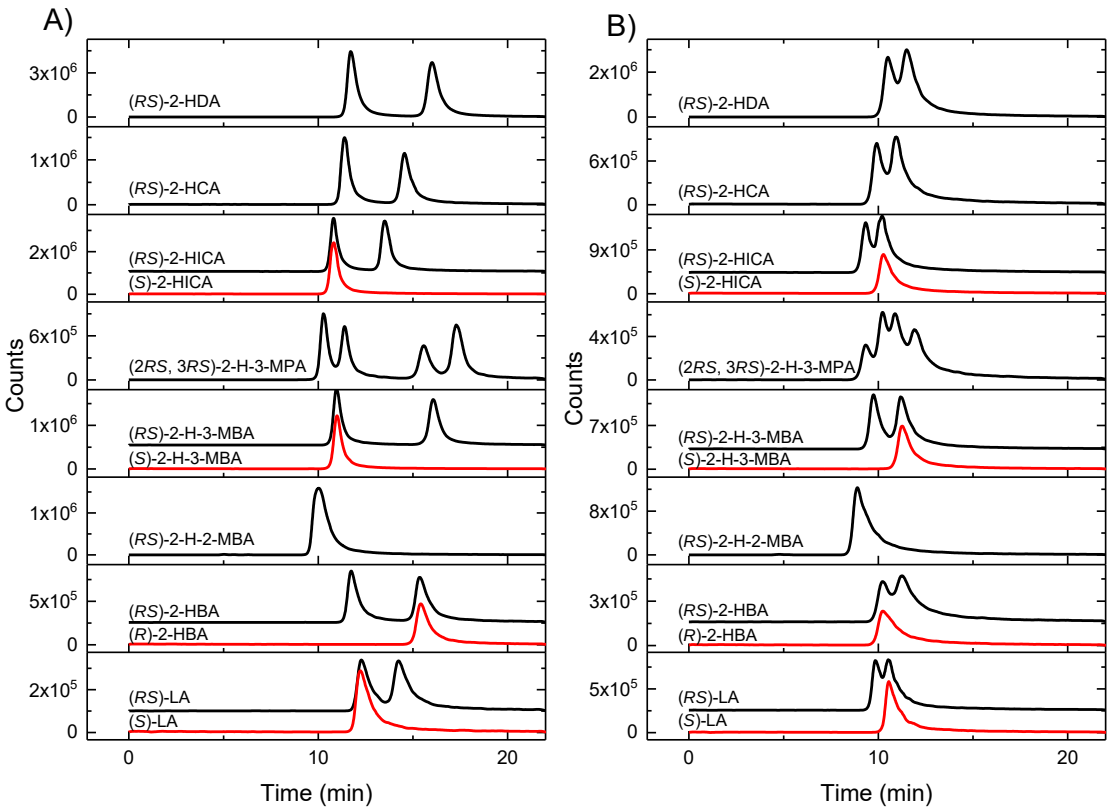

Figure 10.3. Chromatographic runs for a mixture and single enantiomers of 2-HMCA on A) QN-AX column and B) QD-AX column. Mobile phase ACN/MeOH (50:50; v/v) containing 15 mM FA and 2.5 mM NH3, 10 °C, 1.0 mL/min

In the case of 2-H-2-MBA, the presence of a methyl group at the stereogenic center of the α-carbon perturbs the chiral recognition and leads to loss of enantioselectivity (Suppl. Table 10.1: condition A). For this reason, the same mobile phase and flow rate were tested at -20°C [226]

(Suppl. Table 10.1: condition B). Partial separation (R_s 0.50) was achieved on the QN-AX column, but no separation on QD-AX. 2-H-3-MPA has two stereogenic centers and it is possible to observe the separation of all four stereoisomers on both columns (QN-AX and QD-AX). Based on the peak areas the two corresponding pairs of enantiomers elute as peaks 1 - 4, and 2 - 3 (wherein 1 is the compound with the shortest retention time and 4 is the compound with the longest retention time, see Suppl. Figure 10.2).

10.5.2 Elution orders for 2-hydroxy monocarboxylic acids

Availability of at least one pure enantiomer of the compounds LA, 2-HBA, 2-H-3-MBA and 2-HICA allowed determining the elution order of these compounds on QN-AX and QD-AX columns. The results are depicted in Figure 10.3. It can be seen that an elution order S<R occurs on the QN-AX column and the opposite R<S on the QD-AX column for the four compounds, confirming the possibility of inversion of the elution order by exchanging the two weak anion exchanger columns.

For the cases of 2-H-3-MPA, 2-HCA and 2-HDA no pure enantiomer was available and it was therefore not possible to assign the configurations of the eluted enantiomers. However, it was possible to confirm the inversion of the elution order between the QD-AX and QN-AX columns by collecting the eluted fractions of the peaks on the QN-AX column (identified from 1 to 2, or from 1-4 in case of 2-H-3-MPA) and injecting them on the QD-AX column (see Suppl. Figure 10.2, Suppl. Figure 10.3 and Suppl. Figure 10.4).

Since retention increases with acetonitrile-content in the mobile phase composed of MeOH/ACN and enantiomer resolution is lost upon addition of water to the mobile phase, it can be assumed that the hydroxyl group takes part in the interaction with the chiral selector and thus enantiomer recognition process. The reversal of the elution order upon changing from QN-AX to QD-AX may be based on this polar interaction with the selector's carbamate, although it could not be completely excluded that an elution order reversal would occur when hydrophobic and/or steric interactions of the hydroxy acids' alkyl residues are the secondary interactions supporting chiral recognition.

10.5.3 Case of CMA and 2-IMA: homologues of malic acid

For the enantiomeric separation of citramalic acid and 2-isopropylmalic acid similar chromatographic conditions as previously used for the separation of malic acid enantiomers were selected. Both weak anion exchanger column QD-AX and zwitterionic ion-exchanger column ZWIX (-) [169,229] showed to be effective for their chiral separations. However, stronger interaction of these compounds on the QD-AX column due to the second carboxylic acid

required higher amounts of FA and ammonia as additives which can be a problem while working with MS instruments. For this reason, further separations of citramalic acid (CMA) and 2-isopropylmalic acid (2-IMA) enantiomers were focusing on the use of the ZWIX (-) column. A mobile phase consisting of ACN:MeOH 50:50 v/v containing 30 mM FA at 1.0 mL/min and 10 °C was employed. The results of this experiment can be seen in Figure 10.4A for CMA and Suppl. Figure 10.5A for 2-IMA (Suppl. Table 10.1: condition C). It was possible to achieve baseline separation for CMA (R_s 1.96). The elution order is S<R (see Suppl. Figure 10.5B), similar as previously reported for MA [226].

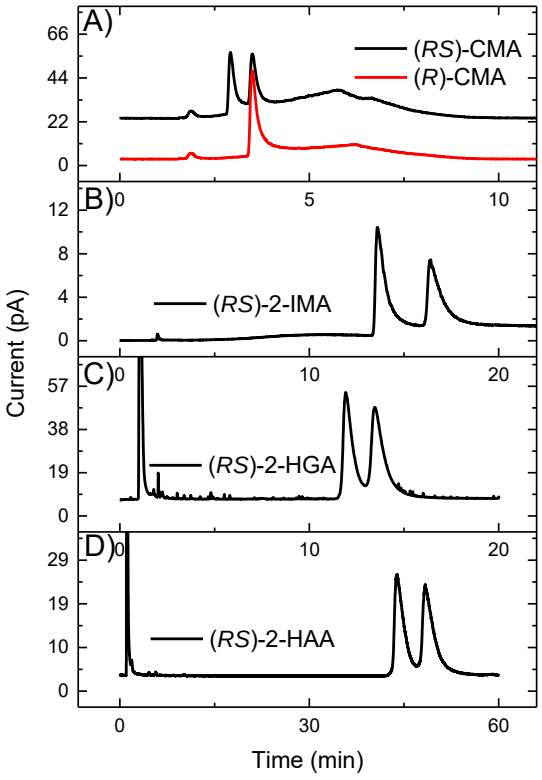

Figure 10.4. Chromatographic runs for the best achieved separations of 2-HDCA enantiomers performed on different CSPs. A) (RS)-CMA and (R)-CMA on ZWIX(−); condition C, B) (RS)-2-IMA on ZWIX(−); condition F, C) (RS)-2-HGA on QD-AX; eluent: MeOH 100% containing 40 mM of FA and 5 mM NH_3, at 1.0 mL/min and 10◦C and D) (RS)-2-HAA on QN-AX; condition A (for details of experimental conditions see Suppl. Table 10.1).

In the case of 2-IMA not even partial separation was achieved under these conditions. However, although a higher ACN concentration increased the retention at constant (30 mM) FA (see Suppl. Table 10.1: condition D), no separation was achieved in spite of reasonable retention factors. In sharp contrast, reduction of FA increased both retention and enantioselectivity (see Suppl. Table 10.1: condition E). Therefore, a mobile phase with milder conditions (ACN:MeOH 85:15 v/v containing 5 mM FA, at 1.0 mL/min and 10 °C) was tested, and a successful baseline separation

was achieved (see Suppl. Figure 10.5 and Suppl. Table 10.1: conditions C-F). This is a bit uncommon behavior because typically with chiral ion exchanger systems the counterion concentration has primarily influence on the retention but does not affect significantly enantioselectivity (due to parallel regression lines of log *k* vs log [*C*] curves for first and second eluted enantiomer). Here, it seems that enantioselectivity is only originating when the analyte is tightly bound to the chiral selector (different slopes of log *k* vs log [*C*] curves; see later). Relatively high *k* values are needed to develop enantioselectivity. Indeed, there is also a slightly positive effect of higher ACN content on enantioselectivity (conditions E vs F), yet the counterion effect is more dominating here.

10.5.4 Case of 2-HAA

The strategy to determine the conditions for chiral separation of 2-HAA (a 2-HDCA with carboxylic groups in positions 1-6) was based on the previously observed trends regarding mobile phase effects on retention factors and selectivities of 2-HGA (a 2-HDCA with carboxylic groups in positions 1-5) and of MA (a 2-HDCA with carboxylic groups in position 1-4). A mobile phase consisting of 100 % MeOH containing 90 mM FA and 15 mM NH_3, at 25 °C, with a flow rate of 1.0 mL/min was used for the elution of these compounds on the QD-AX column (see Suppl. Figure 10.6 and Suppl. Table 10.1: condition G). Significant differences of the retention factors indicate how determinant is the position of the two carboxylic groups (i.e. their distance from each other) on the interaction between these compounds and the quinidine- and quinine-derived stationary phases, respectively. In the case of 2-HAA the interaction of the second carboxylic group (distant from the stereogenic center) seems to be not as strong as in the case of MA and therefore its behavior is more or less similar to the cases of 2-HMCAs, except for its much stronger retention. For this reason 2-HAA was tested with the employed conditions for 2-HMCA on QD-AX and QN-AX columns (see Suppl. Table 10.1: condition A and Suppl. Figure 10.7(A-B)), showing, as in the case of the 2-HMCAs, better resolution (R_s 1.58) on the QN-AX column than on the QD-AX column. The increased retention can be explained by a simple retention model for ion-exchange, the stoichiometric displacement model. According to this model, one solute ion is stoichiometrically displaced from the ion-exchange site by one counterion *C* so that a linear relationship between log *k* and log [*C*] can be derived (eq. 1)

$$log\ k = log\ K_z - Z\ log[\ C]$$

wherein *k* is the retention factor, [*C*] the molar concentration of the counterion in the eluent, Z is the slope of the linear regression line, and log K_z the intercept. K_z is a system specific constant depending on specific surface area, charge density on the surface and the ion-exchange equilibrium constant with exponential contribution of *Z* [230]. *Z* is related to the quotient of the

effective charge number of the analyte and the counterion ($Z = z_{eff,i} / z_{eff,c}$). As can be seen from Figure 10.5, the slope of the log *k* vs log [*C*] dependency is nearly factor 2 larger for 2-HAA than 2-HCA. Since the effective charge number of the counterion is equal in both systems (the identical mobile phase was used), this can be explained by the differences in the effective charge number of the two analytes. Due to a second carboxylic group in 2-HAA, its effective charge number is almost factor 2 higher (ca. 1.5; note the pK_a of the second carboxylic group is lower). Only at very high counterion concentration their retention factors will be in the same range, otherwise the 2-HAA is significantly stronger retained due to a larger log K_z (exponential contribution of *Z* to the intercept) [230]. The chromatograms for these separations can be found in the Suppl. Figure 10.8.

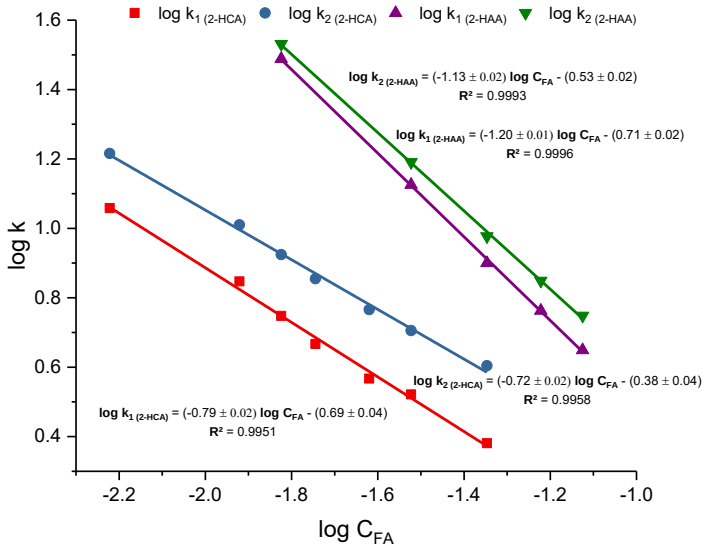

Figure 10.5. Effect of FA concentrations on retention of (RS)-2-HCA and (RS)-2-HAA in accordance to the stoichiometric displacement model. Column: QN-AX; Eluent: ACN:MeOH (50:50;v/v) with different concentrations of FA while keeping constant the FA:NH_3 ratio, at 1.0 mL/min and 10◦C.

The inversion of the elution order of the enantiomers of 2-HAA were also confirmed by collecting single peaks after elution on the QN-AX column and their injection on the QD-AX column (Suppl. Figure 10.7).

10.6 Concluding remarks

Thirteen 2-hydroxycarboxylic acids, the majority of them never tested on cinchona alkaloid based chiral stationary phases, were classified into three different groups, in order to determine MS-compatible conditions for their chiral separation. A first group of eight 2-HMCAs were studied on QN-AX and QD-AX columns, showing in all the cases better resolution on the QN-AX

column. Only for 2-H-2-MBA it was not possible to achieve baseline resolution with the studied conditions. The same elution order and an inversion of the elution order by exchanging QD-AX and QN-AX column was confirmed for LA, 2-HBA, 2-H-3-MBA and 2-HICA. Since authentic single enantiomer standards with known configuration were available, the configuration of the eluted enantiomer peaks could be assigned. Thus, this method can now be used for determination of the absolute configuration of respective samples with unknown stereoconfiguration. For 2-H-3-MPA (for both pairs of enantiomers), 2-HCA and 2-HDA the reversal of the elution order was confirmed. However, assignment of the absolute configurations is only possible for the latter two compounds by analogy considerations owing to a consistent chiral recognition mechanism.

In a second group, CMA and 2-IMA, analyzed as homologues of MA, were studied and conditions for their chiral separations were determined on ZWIX (-) column.

In the third group, 2-HAA was compared as a 2-HDCA with MA and 2-HGA. It was possible to observe how the presence of a second carboxylic group become less determinant in the interaction with the tested CSP when the distance of this second carboxylic group with respect to the first one is longer. Thereby, the strength of the interaction with the QD-AX CSP decreased with increasing distance of the carboxylic group from the stereogenic center and the first α–carboxylic group, respectively. MS-compatible conditions for the chiral separation of 2-HAA on QN-AX column are finally reported.

10.7 Conflict of interest statement

The authors declared no conflicts of interest.

10.8 Acknowledgements

C.C. is grateful to the DAAD for a doctoral fellowship (DAAD no. 57129429).

10.9 Supplementary material

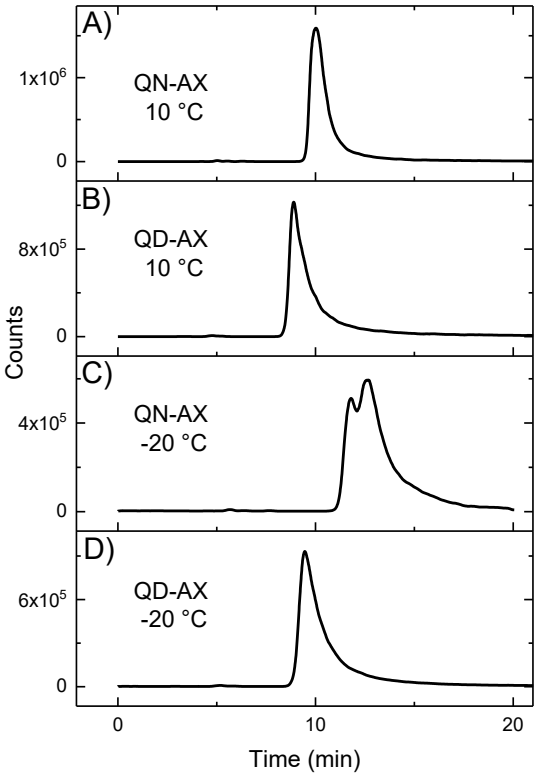

Suppl. Figure 10.1. Chromatographic runs for a mixture of (*R*)-and (*S*)-2-H-2-MBA enantiomers on A) QN-AX column at 10 °C, B) QD-AX column at 10 °C, C) QN-AX column at -20 °C and D) QD-AX column at -20 °C. Mobile phase ACN/MeOH (50:50; v/v) containing 15 mM FA and 2.5 mM NH_3, 1.0 mL/min

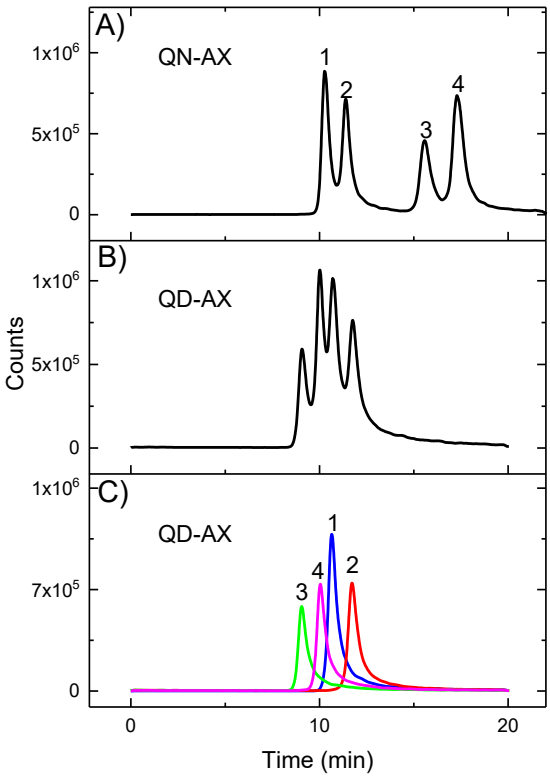

Suppl. Figure 10.2. Chromatographic runs for (2*RS*, 3*RS*)-2-H-3-MPA A) QN-AX column and B) QD-AX column. C) Chromatographic runs on QD-AX column of the peaks separately collected from elution on QN-AX column. Mobile phase ACN/MeOH (50:50; v/v) containing 15 mM FA and 2.5 mM NH_3, 10 °C, 1.0 mL/min

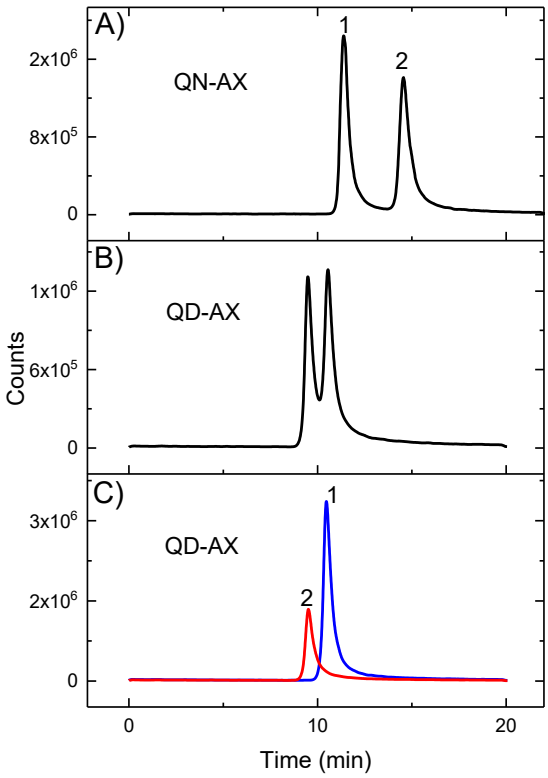

Suppl. Figure 10.3. Chromatographic runs for a mixture of (*R*)-and (*S*)-2-HCA enantiomers on A) QN-AX column and B) QD-AX column. C) Chromatographic runs on QD-AX column of the peaks separately collected from elution on QN-AX column. Mobile phase ACN/MeOH (50:50; v/v) containing 15 mM FA and 2.5 mM NH_3, 10 °C, 1.0 mL/min

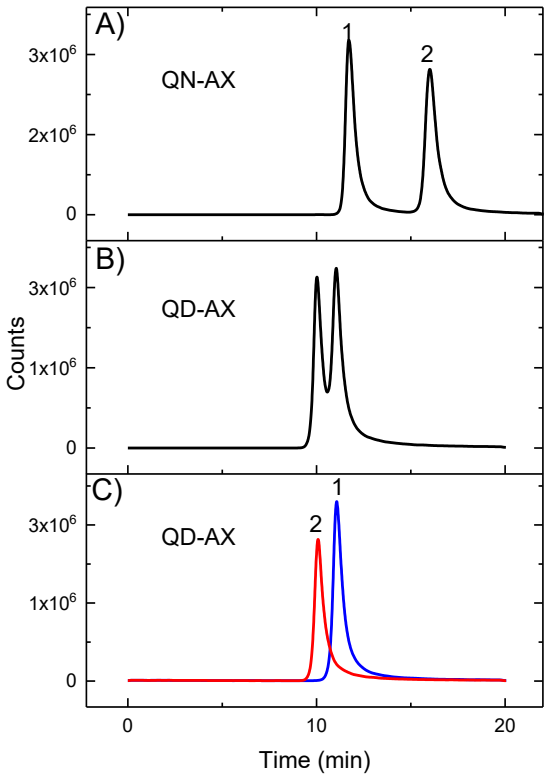

Suppl. Figure 10.4. Chromatographic runs for a mixture of (*R*)-and (*S*)-2-HDA enantiomers on A) QN-AX column and B) QD-AX column. C) Chromatographic runs on QD-AX column of the peaks separately collected from elution on QN-AX column. Mobile phase ACN/MeOH (50:50; v/v) containing 15 mM FA and 2.5 mM NH_3, 10 °C, 1.0 mL/min

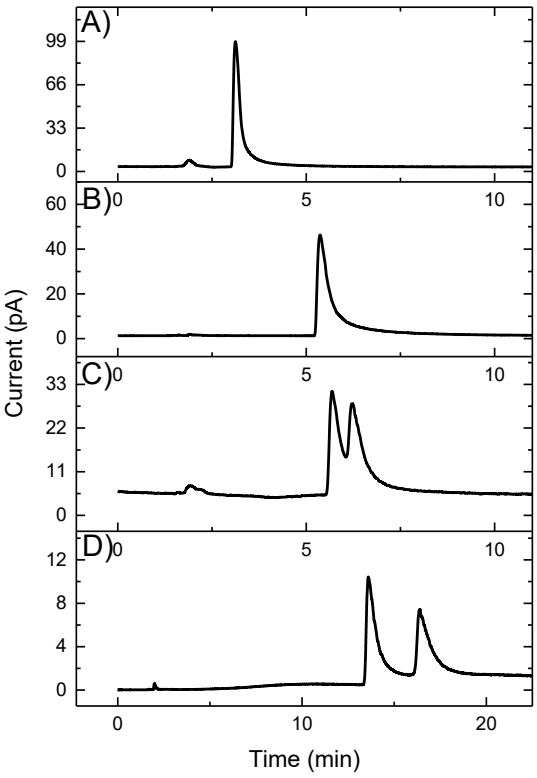

Suppl. Figure 10.5. Chromatographic runs for a racemic mixture of 2-HAA on ZWIX (-) column. Conditions: **A)** mobile phase ACN:MeOH, 50:50, v/v containing 30 mM FA, 10 °C, 1.0 mL/min B) mobile phase ACN/MeOH (85:15; v/v) containing 30 mM FA, 10 °C, 1.0 mL/min, C) mobile phase ACN/MeOH (50:50; v/v) containing 5 mM FA, 10 °C, 1.0 mL/min and D) ACN:MeOH, 85:15, v/v containing 5 mM FA, 10 °C, 1.0 mL/min

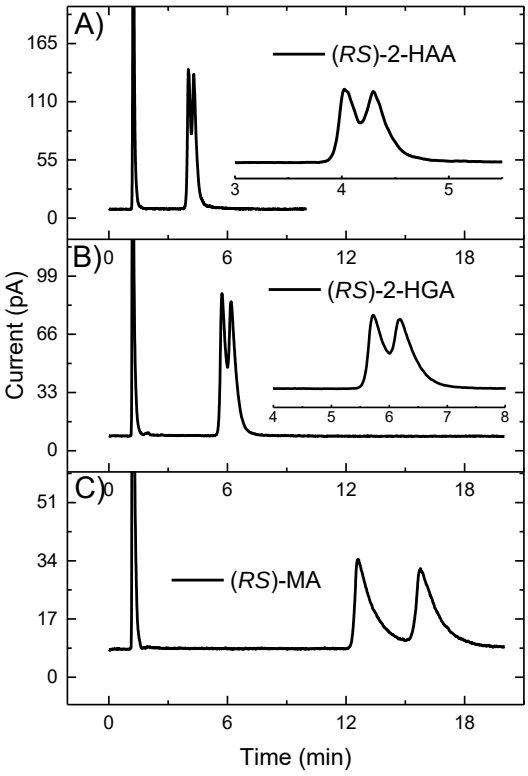

Suppl. Figure 10.6. Chromatographic runs for racemic mixtures of 2-HDCAs on QD-AX column A) (*RS*)-2-HAA, B) (*RS*)-2-HGA and C) (*RS*)-MA. Mobile phase, 100 % MeOH containing 90 mM FA and 15 mM NH_3, 25 °C, 1.0 mL/min.

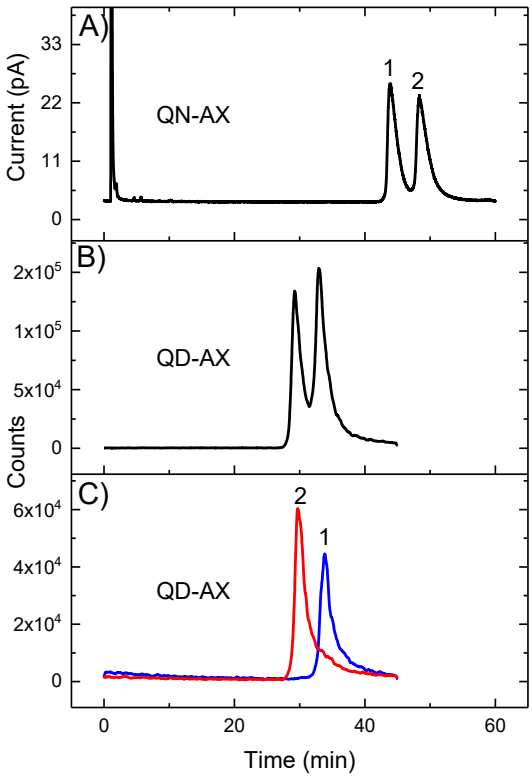

Suppl. Figure 10.7. Chromatographic runs for a mixture of (*R*)-and (*S*)-2-HAA enantiomers on A) QN-AX column and B) QD-AX column. C) Chromatographic runs on QD-AX column of the peaks collected from elution on QN-AX column. Mobile phase ACN/MeOH (50:50; v/v) containing 15 mM FA and 2.5 mM NH_3, 10 °C, 1.0 mL/min

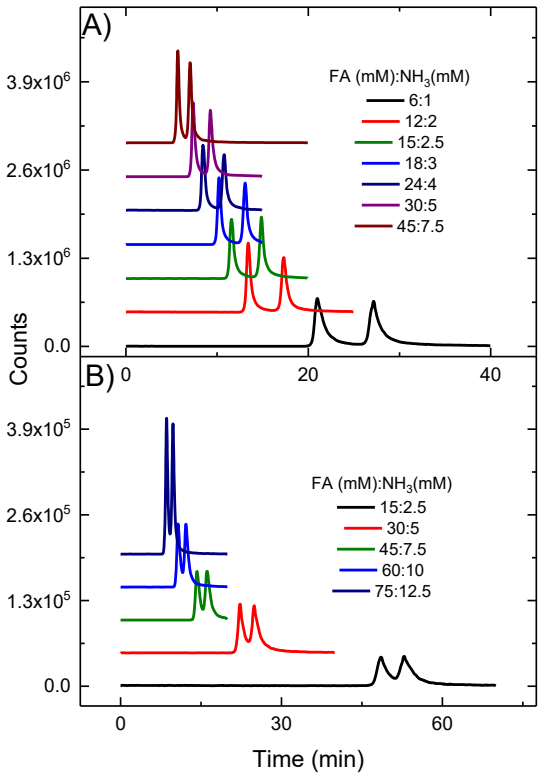

Suppl. Figure 10.8. Chromatographic runs showing the effect of FA concentrations on retention of (RS)-2-HCA and (RS)-2-HAA. Column: QN-AX; Eluent: ACN:MeOH (50:50;v/v) with different concentrations of FA while keeping constant the FA:NH_3 ratio, flow rate, 1.0 mL/min; column temperature, 10◦C.

Suppl. Table 10.1. Chromatographic parameters obtained under different conditions for the separation of HCAs with QD-AX, QN-AX and ZWIX (-) columns.

Column	Condition	Compound	tR_1 [min]	tR_2 [min]	k_1	k_2	α	N_1	N_2	R_S
QN-AX	A	(*RS*)-LA	11.913	14.181	6.91	8.41	1.22	930	974	1.32
QN-AX	A	(*RS*)-2-HBA	11.158	15.210	6.40	9.09	1.42	1065	1383	2.66
QN-AX	A	(*RS*)-2-H-2-MBA	9.324	9.324	5.19	5.19	1.00	273		0.00
QN-AX	A	(*RS*)-2-H-3-MBA	10.324	15.903	5.85	9.55	1.63	1336	1853	4.22
QN-AX	A	(2*RS*, 3*RS*)-2-H-3-MPA[1-2]	9.427	10.844	5.26	6.20	1.18	1267	1548	1.29
QN-AX	A	(2*RS*, 3*RS*)-2-H-3-MPA[2-3]	10.844	15.227	6.20	9.10	1.47	1548	2047	3.53
QN-AX	A	(2*RS*, 3*RS*)-2-H-3-MPA[3-4]	15.227	17.242	9.10	10.44	1.15	2047	2120	1.40
QN-AX	A	(*RS*)-2-HICA	10.121	13.293	5.72	7.82	1.37	1441	1630	2.62
QN-AX	A	(*RS*)-2-HCA	10.597	14.354	6.03	8.52	1.41	1162	1611	2.77
QN-AX	A	(*RS*)-2-HDA	10.792	15.745	6.16	9.45	1.53	979	1440	3.21
QD-AX	A	(*RS*)-2-HBA	9.689	11.053	5.30	6.19	1.17	455	255	0.59
QD-AX	A	(*RS*)-2-H-2-MBA	8.089	8.089	4.26	4.26	1.00	202		0.00
QD-AX	A	(*RS*)-2-H-3-MBA	9.116	11.060	4.93	6.19	1.26	575	562	1.13
QD-AX	A	(*RS*)-2-H-3-MPA[1-2]	8.516	9.685	4.54	5.30	1.17	673	727	0.84
QD-AX	A	(*RS*)-2-H-3-MPA[2-3]	9.685	10.622	5.30	5.91	1.12	727	601	0.58
QD-AX	A	(*RS*)-2-H-3-MPA[3-4]	10.622	12.003	5.91	6.80	1.15	601	503	0.70
QD-AX	A	(*RS*)-2-HICA	8.660	9.964	4.63	5.48	1.18	405	428	0.70
QD-AX	A	(*RS*)-2-HCA	9.131	10.622	4.94	5.91	1.20	369	434	0.75
QD-AX	A	(*RS*)-2-HDA	9.617	11.130	5.25	6.24	1.19	365	305	0.65
QD-AX	A	(*RS*)-LA	8.876	9.935	4.77	5.46	1.14	528	368	0.58
QN-AX	B	(*RS*)-2-H-2-MBA	10.347	11.822	5.03	5.89	1.17	434	150	0.50
QD-AX	B	(*RS*)-2-H-2-MBA	9.093	9.093	4.34	4.34	1.00	107		0.00
ZWIX(-)	C	(*RS*)-MA	2.873	3.196	0.89	1.11	1.24	1529	1309	0.98
ZWIX(-)	C	(*RS*)-CMA	2.918	3.492	0.92	1.30	1.41	1799	2134	1.96
ZWIX(-)	C	(*RS*)-2-IMA	3.121	3.121	1.06	1.06	1.00	1578		0.00
ZWIX(-)	D	(*RS*)-2-IMA	5.368	5.368	2.51	2.51	1.00	1775		0.00
ZWIX(-)	E	(*RS*)-2-IMA	5.685	6.222	2.75	3.11	1.13	1829	1448	0.89
ZWIX(-)	F	(*RS*)-2-IMA	13.597	16.407	7.54	9.30	1.23	3582	3228	2.68
QD-AX	G	(*RS*)-MA	12.612	15.761	7.19	9.24	1.28	1244	1582	2.06
QD-AX	G	(*RS*)-2-HGA	5.724	6.189	2.72	3.02	1.11	1553	1221	0.71
QD-AX	G	(*RS*)-2-HAA	4.023	4.294	1.71	1.89	1.11	1789	1950	0.69
QN-AX	A	(*RS*)-2-HAA	43.954	48.354	29.48	32.53	1.10	4576	4486	1.58
QD-AX	A	(*RS*)-2-HAA	28.277	32.611	17.39	20.20	1.16	1108	1230	1.20

A: mobile phase ACN/MeOH (50:50; v/v) containing 15 mM FA and 2.5 mM NH_3, 10 °C, 1.0 mL/min, **B**: mobile phase ACN/MeOH (50:50; v/v) containing 15 mM FA and 2.5 mM NH_3, -20 °C, 1.0 mL/min, **C**: mobile phase ACN/MeOH (50:50; v/v) containing 30 mM FA, 10 °C, 1.0 mL/min **D**: mobile phase ACN/MeOH (85:15; v/v) containing 30 mM FA, 10 °C, 1.0 mL/min, **E**: mobile phase ACN/MeOH (50:50; v/v) containing 5 mM FA, 10 °C, 1.0 mL/min, **F**: mobile phase ACN/MeOH (85:15; v/v) containing 5 mM FA, 10 °C, 1.0 mL/min, **G**: mobile phase 100 % MeOH containing 90 mM FA and 15 mM NH_3, 25 °C, 1.0 mL/min

For (2*RS*, 3*RS*)-2-H-3-MPA four peaks were observed, therefore (2*RS*, 3*RS*)-2-H-3-MPA[1-2] denotes chromatographic parameters between the first and second peak, (2*RS*, 3*RS*)-2-H-3-MPA[2-3] between the second and third one and (2*RS*, 3*RS*)-2-H-3-MPA[3-4] between third and fourth one.

CONCLUDING REMARKS

Lipidomics is a field, which has experienced a continuous growing during last twenty years. Despite the development reached until now, there are still important challenges remaining in each step of the workflow for lipidomics analysis. Sample preparation, sample measurement, data processing, identification and annotation of lipids are among them. In this dissertation, three main studies were developed addressing some of the most critical steps of lipidomics analysis.

In the first study, two novel extraction protocols, IPA:H_2O 90:10 v/v (IPA90) and IPA:H_2O 75:25 v/v (IPA75) were compared to two traditionally employed protocols known as Matyash and Bligh & Dyer. The method IPA90 showed good performance according to the evaluated parameters and represents a good alternative for extraction of lipids in LC-MS based lipidomics studies. Extraction with IPA90 showed similar recoveries for polar and apolar lipid classes to the Matyash protocol, better than Bligh & Dyer for most polar lipid classes and better than IPA75 for most apolar lipid classes. In terms of precision, the four extraction protocols showed similar results with an average CV % around 15 % for detected features. Furthermore, extractions with IPA:H_2O do not require a separation of phases (organic layer from aqueous layer) which reduces the time for processing each sample and makes easier the automation of protocols. Also, the use of isopropanol instead of chloroform (in Bligh & Dyer) or MTBE (in Matyash), as the main solvent for extraction, enables the use of plasticware instead of glassware for handling of samples which also reduces costs and simplifies the protocol.

In the second study, lipid profile of keratinocytes was analyzed in a pharmacolipidomic study with the natural compound betulin. Focus is this study was especially given to the annotation of identified lipids which in turn allowed an adequate comparison of the changes in the lipid profile of keratinocytes before and after treatment with betulin. The identification of lipids was done through a targeted data processing in which selected set of precursor and product ions was analyzed for each lipid class but also retention time for corresponding ionic species in positive and negative mode and retention time for species of the same lipid class were considered for the annotation. Spotting plots showing the elution pattern for species of the same lipid class depending on the number of carbons and unsaturations are given, and their use is here fully encouraged in each LC-MS studies as a measure to avoid misidentifications. Changes in about 70% of the identified lipid species, evidence the significant influence of betulin in treated keratinocytes. A more detailed view of these changes shows a down-regulation of cholesteryl esters and triacylglycerides and an up-regulation of acyl carnitines, ceramides and most of the glycerophospholipids classes. These findings open the door to more targeted approaches in

order to determine the relationships between the changes in lipid classes and the healing effects evidenced in keratinocytes.

In a third study (developed as publications III, IV and V), methodologies for chiral separation of a group of lipids described as short chain hydroxy fatty acids (SCHFA) were developed. Screening of different chiral stationary phases, bulk solvents, additives and temperature conditions were performed and baseline resolution conditions were achieved and reported for all studied SCHFA. This last study exemplifies the complexity in the different levels of annotation which must be considered when lipids are identified. Thus, recognition of different lipid species is based in this case on separation with chiral stationary phases, since MS analysis does not offer the possibility to differentiate between enantiomers.

REFERENCES

[1] X. Han, Lipidomics, John Wiley & Sons, Inc, Hoboken, NJ, USA, 2016. doi:10.1002/9781119085263.

[2] G.P. Moss, P.A.S. Smith, D. Tavernier, Glossary of class names of organic compounds and reactivity intermediates based on structure (IUPAC Recommendations 1995), Pure Appl. Chem. 67 (1995) 1307–1375. doi:10.1351/pac199567081307.

[3] E. Fahy, S. Subramaniam, H.A. Brown, C.K. Glass, A.H. Merrill, R.C. Murphy, C.R.H. Raetz, D.W. Russell, Y. Seyama, W. Shaw, T. Shimizu, F. Spener, G. van Meer, M.S. VanNieuwenhze, S.H. White, J.L. Witztum, E.A. Dennis, A comprehensive classification system for lipids, J. Lipid Res. 46 (2005) 839–862. doi:10.1194/jlr.E400004-JLR200.

[4] W.W. Christie, X. Han, Lipid analysis, Woodhead Publishing Limited, 2010. doi:10.1533/9780857097866.

[5] Y.H. Rustam, G.E. Reid, Analytical Challenges and Recent Advances in Mass Spectrometry Based Lipidomics, Anal. Chem. 90 (2018) 374–397. doi:10.1021/acs.analchem.7b04836.

[6] B. Brügger, Lipidomics: Analysis of the Lipid Composition of Cells and Subcellular Organelles by Electrospray Ionization Mass Spectrometry, Annu. Rev. Biochem. 83 (2014) 79–98. doi:10.1146/annurev-biochem-060713-035324.

[7] X. Han, Lipidomics for studying metabolism, Nat. Rev. Endocrinol. 12 (2016) 668–679. doi:10.1038/nrendo.2016.98.

[8] E. Fahy, S. Subramaniam, R.C. Murphy, M. Nishijima, C.R.H. Raetz, T. Shimizu, F. Spener, G. van Meer, M.J.O. Wakelam, E.A. Dennis, Update of the LIPID MAPS comprehensive classification system for lipids, J. Lipid Res. 50 (2009) S9–S14. doi:10.1194/jlr.R800095-JLR200.

[9] E. Fahy, D. Cotter, M. Sud, S. Subramaniam, Lipid classification, structures and tools, Biochim. Biophys. Acta - Mol. Cell Biol. Lipids. 1811 (2011) 637–647. doi:10.1016/j.bbalip.2011.06.009.

[10] G. Liebisch, J.A. Vizcaíno, H. Köfeler, M. Trötzmüller, W.J. Griffiths, G. Schmitz, F. Spener, M.J.O. Wakelam, Shorthand notation for lipid structures derived from mass spectrometry, J. Lipid Res. 54 (2013) 1523–1530. doi:10.1194/jlr.M033506.

[11] R.C. Murphy, Tandem Mass Spectrometry of Lipids, Royal Society of Chemistry, Cambridge, 2014. doi:10.1039/9781782626350.

[12] T. Cajka, O. Fiehn, Comprehensive analysis of lipids in biological systems by liquid chromatography-mass spectrometry, TrAC Trends Anal. Chem. 61 (2014) 192–206. doi:10.1016/j.trac.2014.04.017.

[13] M. Lange, Z. Ni, A. Criscuolo, M. Fedorova, Liquid Chromatography Techniques in Lipidomics Research, Chromatographia. 82 (2019) 77–100. doi:10.1007/s10337-018-3656-4.

[14] A. Hartmann, M. Ganzera, Supercritical Fluid Chromatography - Theoretical Background and Applications on Natural Products, Planta Med. 81 (2015) 1570–1581. doi:10.1055/s-0035-1545911.

[15] C. West, Current trends in supercritical fluid chromatography, Anal. Bioanal. Chem. 410 (2018) 6441–6457. doi:10.1007/s00216-018-1267-4.

[16] P. Donato, V. Inferrera, D. Sciarrone, L. Mondello, Supercritical fluid chromatography for lipid analysis in foodstuffs, J. Sep. Sci. 40 (2017) 361–382. doi:10.1002/jssc.201600936.

[17] T. Cajka, O. Fiehn, Increasing lipidomic coverage by selecting optimal mobile-phase modifiers in LC–MS of blood plasma, Metabolomics. 12 (2016) 34. doi:10.1007/s11306-015-0929-x.

[18] E. Cífková, R. Hájek, M. Lísa, M. Holčapek, Hydrophilic interaction liquid chromatography-mass spectrometry of (lyso)phosphatidic acids, (lyso)phosphatidylserines and other lipid classes, J. Chromatogr. A. 1439 (2016) 65–73. doi:10.1016/j.chroma.2016.01.064.

[19] A.K. Samhan-Arias, J. Ji, O.M. Demidova, L.J. Sparvero, W. Feng, V. Tyurin, Y.Y. Tyurina, M.W. Epperly, A.A. Shvedova, J.S. Greenberger, H. Bayir, V.E. Kagan, A.A. Amoscato, Oxidized phospholipids as biomarkers of tissue and cell damage with a focus on cardiolipin, Biochim. Biophys. Acta - Biomembr. 1818 (2012) 2413–2423. doi:10.1016/j.bbamem.2012.03.014.

[20] S. Al Hamimi, M. Sandahl, M. Armeni, C. Turner, P. Spégel, Screening of stationary phase selectivities for global lipid profiling by ultrahigh performance supercritical fluid chromatography, J. Chromatogr. A. 1548 (2018) 76–82. doi:10.1016/j.chroma.2018.03.024.

[21] Y.S. Ling, H.J. Liang, M.H. Lin, C.H. Tang, K.Y. Wu, M.L. Kuo, C.Y. Lin, Two-dimensional LC-MS/MS to enhance ceramide and phosphatidylcholine species profiling in mouse liver, Biomed. Chromatogr. 28 (2014) 1284–1293. doi:10.1002/bmc.3162.

[22] M. Holčapek, M. Ovčačíková, M. Lísa, E. Cífková, T. Hájek, Continuous comprehensive

two-dimensional liquid chromatography-electrospray ionization mass spectrometry of complex lipidomic samples, Anal. Bioanal. Chem. 407 (2015) 5033–5043. doi:10.1007/s00216-015-8528-2.

[23] S. Wang, L. Zhou, Z. Wang, X. Shi, G. Xu, Simultaneous metabolomics and lipidomics analysis based on novel heart-cutting two-dimensional liquid chromatography-mass spectrometry, Anal. Chim. Acta. 966 (2017) 34–40. doi:10.1016/j.aca.2017.03.004.

[24] R. Berkecz, F. Tömösi, T. Körmöczi, V. Szegedi, J. Horváth, T. Janáky, Comprehensive phospholipid and sphingomyelin profiling of different brain regions in mouse model of anxiety disorder using online two-dimensional (HILIC/RP)-LC/MS method, J. Pharm. Biomed. Anal. 149 (2018) 308–317. doi:10.1016/j.jpba.2017.10.043.

[25] E. Rampler, A. Criscuolo, M. Zeller, Y. El Abiead, H. Schoeny, G. Hermann, E. Sokol, K. Cook, D.A. Peake, B. Delanghe, G. Koellensperger, A Novel Lipidomics Workflow for Improved Human Plasma Identification and Quantification Using RPLC-MSn Methods and Isotope Dilution Strategies, Anal. Chem. 90 (2018) 6494–6501. doi:10.1021/acs.analchem.7b05382.

[26] P. Le Pogam, M. Doué, Y. Le Page, D. Habauzit, M. Zhadobov, R. Sauleau, Y. Le Dréan, D. Rondeau, Untargeted Metabolomics Reveal Lipid Alterations upon 2-Deoxyglucose Treatment in Human HaCaT Keratinocytes, J. Proteome Res. 17 (2018) 1146–1157. doi:10.1021/acs.jproteome.7b00805.

[27] T. Cajka, O. Fiehn, LC-MS-Based Lipidomics and Automated Identification of Lipids Using the LipidBlast In-Silico MS/MS Library, in: S.K. Bhattacharya (Ed.), Lipidomics Methods Protoc., Springer New York, New York, NY, 2017: pp. 149–170. doi:10.1007/978-1-4939-6996-8_14.

[28] H. Zhang, Y. Gao, J. Sun, S. Fan, X. Yao, X. Ran, C. Zheng, M. Huang, H. Bi, Optimization of lipid extraction and analytical protocols for UHPLC-ESI-HRMS-based lipidomic analysis of adherent mammalian cancer cells, Anal. Bioanal. Chem. 409 (2017) 5349–5358. doi:10.1007/s00216-017-0483-7.

[29] T. Yamada, T. Uchikata, S. Sakamoto, Y. Yokoi, E. Fukusaki, T. Bamba, Development of a lipid profiling system using reverse-phase liquid chromatography coupled to high-resolution mass spectrometry with rapid polarity switching and an automated lipid identification software, J. Chromatogr. A. 1292 (2013) 211–218. doi:10.1016/j.chroma.2013.01.078.

[30] K. Sandra, A. dos S. Pereira, G. Vanhoenacker, F. David, P. Sandra, Comprehensive blood

plasma lipidomics by liquid chromatography/quadrupole time-of-flight mass spectrometry, J. Chromatogr. A. 1217 (2010) 4087–4099. doi:10.1016/j.chroma.2010.02.039.

[31] M. Ovčačíková, M. Lísa, E. Cífková, M. Holčapek, Retention behavior of lipids in reversed-phase ultrahigh-performance liquid chromatography-electrospray ionization mass spectrometry, J. Chromatogr. A. 1450 (2016) 76–85. doi:10.1016/j.chroma.2016.04.082.

[32] A. Fauland, H. Köfeler, M. Trötzmüller, A. Knopf, J. Hartler, A. Eberl, C. Chitraju, E. Lankmayr, F. Spener, A comprehensive method for lipid profiling by liquid chromatography-ion cyclotron resonance mass spectrometry, J. Lipid Res. 52 (2011) 2314–2322. doi:10.1194/jlr.D016550.

[33] J.H. Gross, Mass Spectrometry, Springer Berlin Heidelberg, Berlin, Heidelberg, 2011. doi:10.1007/978-3-642-10711-5.

[34] G. Siuzdak, An introduction to mass spectrometry ionization: An excerpt from The Expanding Role of Mass Spectrometry in Biotechnology, J. Assoc. Lab. Autom. 9 (2004) 50–63. doi:10.1016/j.jala.2004.01.004.

[35] J. Wang, C. Wang, X. Han, Tutorial on lipidomics, Anal. Chim. Acta. 1061 (2019) 28–41. doi:10.1016/j.aca.2019.01.043.

[36] K.K. Murray, R.K. Boyd, M.N. Eberlin, G.J. Langley, L. Li, Y. Naito, Definitions of terms relating to mass spectrometry (IUPAC Recommendations 2013), Pure Appl. Chem. 85 (2013) 1515–1609. doi:10.1351/PAC-REC-06-04-06.

[37] J. Zhou, C. Liu, D. Si, B. Jia, L. Zhong, Y. Yin, Workflow development for targeted lipidomic quantification using parallel reaction monitoring on a quadrupole-time of flight mass spectrometry, Anal. Chim. Acta. 972 (2017) 62–72. doi:10.1016/j.aca.2017.04.008.

[38] D. Schwudke, G. Liebisch, R. Herzog, G. Schmitz, A. Shevchenko, Shotgun Lipidomics by Tandem Mass Spectrometry under Data-Dependent Acquisition Control, Methods Enzymol. 433 (2007) 175–191. doi:10.1016/S0076-6879(07)33010-3.

[39] R. Welti, X. Wang, Lipid species profiling: A high-throughput approach to identify lipid compositional changes and determine the function of genes involved in lipid metabolism and signaling, Curr. Opin. Plant Biol. 7 (2004) 337–344. doi:10.1016/j.pbi.2004.03.011.

[40] G. Liebisch, W. Drobnik, M. Reil, B. Trümbach, R. Arnecke, B. Olgemöller, A. Roscher, G. Schmitz, Quantitative measurement of different ceramide species from crude cellular extracts by electrospray ionization tandem mass spectrometry (ESI- MS/MS), J. Lipid Res.

40 (1999) 1539–1546.

[41] T.A. Lydic, J. V. Busik, W.J. Esselman, G.E. Reid, Complementary precursor ion and neutral loss scan mode tandem mass spectrometry for the analysis of glycerophosphatidylethanolamine lipids from whole rat retina, Anal. Bioanal. Chem. 394 (2009) 267–275. doi:10.1007/s00216-009-2717-9.

[42] T. Petta, L.A.B. Moraes, L.H. Faccioli, Versatility of tandem mass spectrometry for focused analysis of oxylipids, J. Mass Spectrom. 50 (2015) 879–890. doi:10.1002/jms.3595.

[43] S.H. Kim, H.E. Song, S.J. Kim, D.C. Woo, S. Chang, W.G. Choi, M.J. Kim, S.H. Back, H.J. Yoo, Quantitative structural characterization of phosphatidylinositol phosphates from biological samples, J. Lipid Res. 58 (2017) 469–478. doi:10.1194/jlr.D069989.

[44] K. Retra, O.B. Bleijerveld, R.A. van Gestel, A.G.M. Tielens, J.J. van Hellemond, J.F. Brouwers, A simple and universal method for the separation and identification of phospholipid molecular species, Rapid Commun. Mass Spectrom. 22 (2008) 1853–1862. doi:10.1002/rcm.3562.

[45] B. Peng, S.T. Weintraub, C. Coman, S. Ponnaiyan, R. Sharma, B. Tews, D. Winter, R. Ahrends, A Comprehensive High-Resolution Targeted Workflow for the Deep Profiling of Sphingolipids, Anal. Chem. 89 (2017) 12480–12487. doi:10.1021/acs.analchem.7b03576.

[46] Z. Wu, J.C. Shon, K.-H. Liu, Mass Spectrometry-based Lipidomics and Its Application to Biomedical Research, J. Lifestyle Med. 4 (2014) 17–33. doi:10.15280/jlm.2014.4.1.17.

[47] R. Bonner, G. Hopfgartner, SWATH data independent acquisition mass spectrometry for metabolomics, TrAC - Trends Anal. Chem. (2018). doi:10.1016/j.trac.2018.10.014.

[48] F. Gao, J. McDaniel, E.Y. Chen, H.E. Rockwell, C. Nguyen, M.D. Lynes, Y.H. Tseng, R. Sarangarajan, N.R. Narain, M.A. Kiebish, Adapted MS/MS ALL Shotgun Lipidomics Approach for Analysis of Cardiolipin Molecular Species, Lipids. 53 (2018) 133–142. doi:10.1002/lipd.12004.

[49] B. Simons, D. Kauhanen, T. Sylvänne, K. Tarasov, E. Duchoslav, K. Ekroos, Shotgun lipidomics by sequential precursor ion fragmentation on a hybrid quadrupole time-of-flight mass spectrometer, Metabolites. 2 (2012) 195–213. doi:10.3390/metabo2010195.

[50] J. Schlotterbeck, M. Cebo, A. Kolb, M. Lämmerhofer, Quantitative analysis of chemoresistance-inducing fatty acid in food supplements using UHPLC–ESI-MS/MS, Anal. Bioanal. Chem. 411 (2019) 479–491. doi:10.1007/s00216-018-1468-x.

[51] T. Hyötyläinen, M. Orešič, Optimizing the lipidomics workflow for clinical studies—

practical considerations, Anal. Bioanal. Chem. 407 (2015) 4973–4993. doi:10.1007/s00216-015-8633-2.

[52] R.C. Murphy, P.H. Axelsen, Mass spectrometric analysis of long-chain lipids, Mass Spectrom. Rev. 30 (2011) 579–599. doi:10.1002/mas.20284.

[53] F.-F. Hsu, J. Turk, Electrospray Ionization with Low-Energy Collisionally Activated Dissociation Tandem Mass Spectrometry of Complex Lipids, in: Mod. Methods Lipid Anal. by Liq. Chromatogr., AOCS Publishing, 2005. doi:10.1201/9781439822319.ch3.

[54] R.C. Murphy, J. Fiedler, J. Hevko, Analysis of Nonvolatile Lipids by Mass Spectrometry, Chem. Rev. 101 (2001) 479–526. doi:10.1021/cr9900883.

[55] F.F. Hsu, J. Turk, Electrospray ionization with low-energy collisionally activated dissociation tandem mass spectrometry of glycerophospholipids: Mechanisms of fragmentation and structural characterization, J. Chromatogr. B Anal. Technol. Biomed. Life Sci. 877 (2009) 2673–2695. doi:10.1016/j.jchromb.2009.02.033.

[56] F.-F. Hsu, J. Turk, Electrospray ionization with low-energy collisionally activated dissociation tandem mass spectrometry of glycerophospholipids: Mechanisms of fragmentation and structural characterization, J. Chromatogr. B. 877 (2009) 2673–2695. doi:10.1016/j.jchromb.2009.02.033.

[57] M. Pulfer, R.C. Murphy, Electrospray mass spectrometry of phospholipids, Mass Spectrom. Rev. 22 (2003) 332–364. doi:10.1002/mas.10061.

[58] S. Tumanov, J.J. Kamphorst, Recent advances in expanding the coverage of the lipidome, Curr. Opin. Biotechnol. 43 (2017) 127–133. doi:10.1016/j.copbio.2016.11.008.

[59] K. Kishimoto, R. Urade, T. Ogawa, T. Moriyama, Nondestructive quantification of neutral lipids by thin-layer chromatography and laser-fluorescent scanning: Suitable methods for “lipidome” analysis, Biochem. Biophys. Res. Commun. 281 (2001) 657–662. doi:10.1006/bbrc.2001.4404.

[60] T. Porta Siegel, K. Ekroos, S.R. Ellis, Reshaping Lipid Biochemistry by Pushing Barriers in Structural Lipidomics, Angew. Chemie - Int. Ed. (2019). doi:10.1002/anie.201812698.

[61] K. Jurowski, K. Kochan, J. Walczak, M. Barańska, W. Piekoszewski, B. Buszewski, Comprehensive review of trends and analytical strategies applied for biological samples preparation and storage in modern medical lipidomics: State of the art, TrAC Trends Anal. Chem. 86 (2017) 276–289. doi:10.1016/j.trac.2016.10.014.

[62] Y. Wu, L. Li, Sample normalization methods in quantitative metabolomics, J. Chromatogr.

A. 1430 (2015) 80–95. doi:10.1016/j.chroma.2015.12.007.

[63] W. Yang, Y. Chen, C. Xi, R. Zhang, Y. Song, Q. Zhan, X. Bi, Z. Abliz, Liquid chromatography-tandem mass spectrometry-based plasma metabonomics delineate the effect of metabolites' stability on reliability of potential biomarkers, Anal. Chem. 85 (2013) 2606–2610. doi:10.1021/ac303576b.

[64] B. Burla, M.M. Arita, M.M. Arita, A.K. Bendt, A. Cazenave-Gassiot, E.A. Dennis, K. Ekroos, X. Han, K. Ikeda, G. Liebisch, M.K. Lin, T.P. Loh, P.J. Meikle, M. Orešič, O. Quehenberger, A. Shevchenko, F. Torta, M.J.O. Wakelam, C.E. Wheelock, M.R. Wenk, MS-based lipidomics of human blood plasma: a community-initiated position paper to develop accepted guidelines, J. Lipid Res. 59 (2018) 2001–2017. doi:10.1194/jlr.S087163.

[65] G. Liebisch, K. Ekroos, M. Hermansson, C.S. Ejsing, Reporting of lipidomics data should be standardized, Biochim. Biophys. Acta - Mol. Cell Biol. Lipids. 1862 (2017) 747–751. doi:10.1016/j.bbalip.2017.02.013.

[66] S. Furse, M.R. Egmond, J.A. Killian, Isolation of lipids from biological samples, Mol. Membr. Biol. 32 (2015) 55–64. doi:10.3109/09687688.2015.1050468.

[67] J. Folch, M. Lees, G.H. Sloane Stanley, A simple method for the isolation and purification of total lipides from animal tissues., J. Biol. Chem. 226 (1957) 497–509. http://www.ncbi.nlm.nih.gov/pubmed/13671378.

[68] E.G. Bligh, W.J. Dyer, A rapid method of total lipid extraction and purification, Can. J. Biochem. Physiol. 37 (1959) 911–917. doi:10.1139/o59-099.

[69] A. Hara, N.S. Radin, Lipid extraction of tissues with a low-toxicity solvent, Anal. Biochem. 90 (1978) 420–426. doi:10.1016/0003-2697(78)90046-5.

[70] V. Matyash, G. Liebisch, T. V. Kurzchalia, A. Shevchenko, D. Schwudke, Lipid extraction by methyl- tert -butyl ether for high-throughput lipidomics, J. Lipid Res. 49 (2008) 1137–1146. doi:10.1194/jlr.D700041-JLR200.

[71] L. Löfgren, M. Ståhlman, G.-B. Forsberg, S. Saarinen, R. Nilsson, G.I. Hansson, The BUME method: a novel automated chloroform-free 96-well total lipid extraction method for blood plasma, J. Lipid Res. 53 (2012) 1690–1700. doi:10.1194/jlr.D023036.

[72] J.M. Weir, G. Wong, C.K. Barlow, M.A. Greeve, A. Kowalczyk, L. Almasy, A.G. Comuzzie, M.C. Mahaney, J.B.M. Jowett, J. Shaw, J.E. Curran, J. Blangero, P.J. Meikle, Plasma lipid profiling in a large population-based cohort, J. Lipid Res. 54 (2013) 2898–2908. doi:10.1194/jlr.P035808.

[73] P.J. Meikle, G. Wong, D. Tsorotes, C.K. Barlow, J.M. Weir, M.J. Christopher, G.L. MacIntosh, B. Goudey, L. Stern, A. Kowalczyk, I. Haviv, A.J. White, A.M. Dart, S.J. Duffy, G.L. Jennings, B.A. Kingwell, Plasma lipidomic analysis of stable and unstable coronary artery disease, Arterioscler. Thromb. Vasc. Biol. 31 (2011) 2723–2732. doi:10.1161/ATVBAHA.111.234096.

[74] Z.H. Alshehry, C.K. Barlow, J.M. Weir, Y. Zhou, M.J. McConville, P.J. Meikle, An efficient single phase method for the extraction of plasma lipids, Metabolites. 5 (2015) 389–403. doi:10.3390/metabo5020389.

[75] R.L. Shaner, J.C. Allegood, H. Park, E. Wang, S. Kelly, C.A. Haynes, M.C. Sullards, A.H. Merrill, Quantitative analysis of sphingolipids for lipidomics using triple quadrupole and quadrupole linear ion trap mass spectrometers, J. Lipid Res. 50 (2009) 1692–1707. doi:10.1194/jlr.D800051-JLR200.

[76] M.C. Sullards, Y. Liu, Y. Chen, A.H. Merrill, Analysis of mammalian sphingolipids by liquid chromatography tandem mass spectrometry (LC-MS/MS) and tissue imaging mass spectrometry (TIMS), Biochim. Biophys. Acta - Mol. Cell Biol. Lipids. 1811 (2011) 838–853. doi:10.1016/j.bbalip.2011.06.027.

[77] L. Yao, S.-L. Lee, T. Wang, J.A. Gerde, Comparison of lipid extraction from microalgae and soybeans with aqueous isopropanol, J. Am. Oil Chem. Soc. 90 (2013) 571–578. doi:10.1007/s11746-012-2197-5.

[78] L. Liu, L. Na, Y. Niu, F. Guo, Y. Li, C. Sun, An Ultrasonic Assisted Extraction Procedure to Free Fatty Acids from the Liver Samples of Mice, J. Chromatogr. Sci. 51 (2013) 376–382. doi:10.1093/chromsci/bms151.

[79] C.Z. Ulmer, Liquid Chromatography-Mass Spectrometry Metabolic and Lipidomic Sample Preparation Workflow for Suspension-Cultured Mammalian Cells using Jurkat T lymphocyte Cells, J. Proteomics Bioinform. 08 (2015) 1367–671. doi:10.4172/jpb.1000360.

[80] T.W.T. Rupasinghe, Lipidomics: Extraction Protocols for Biological Matrices, in: 2013: pp. 71–80. doi:10.1007/978-1-62703-577-4_6.

[81] C. Breil, M. Abert Vian, T. Zemb, W. Kunz, F. Chemat, “Bligh and Dyer” and Folch methods for solid–liquid–liquid extraction of lipids from microorganisms. Comprehension of solvatation mechanisms and towards substitution with alternative solvents, Int. J. Mol. Sci. 18 (2017) 708. doi:10.3390/ijms18040708.

[82] A. Reis, A. Rudnitskaya, G.J. Blackburn, N.M. Fauzi, A.R. Pitt, C.M. Spickett, A comparison

of five lipid extraction solvent systems for lipidomic studies of human LDL, J. Lipid Res. 54 (2013) 1812–1824. doi:10.1194/jlr.M034330.

[83] J. Sheng, R. Vannela, B.E. Rittmann, Evaluation of methods to extract and quantify lipids from Synechocystis PCC 6803, Bioresour. Technol. 102 (2011) 1697–1703. doi:10.1016/j.biortech.2010.08.007.

[84] R.M. Gathungu, P. Larrea, M.J. Sniatynski, V.R. Marur, J.A. Bowden, J.P. Koelmel, P. Starke-Reed, V.S. Hubbard, B.S. Kristal, Optimization of Electrospray Ionization Source Parameters for Lipidomics to Reduce Misannotation of In-Source Fragments as Precursor Ions, Anal. Chem. 90 (2018) 13523–13532. doi:10.1021/acs.analchem.8b03436.

[85] M. Wang, C. Wang, R.H. Han, X. Han, Novel advances in shotgun lipidomics for biology and medicine, Prog. Lipid Res. 61 (2016) 83–108. doi:10.1016/j.plipres.2015.12.002.

[86] C.S. Ejsing, J.L. Sampaio, V. Surendranath, E. Duchoslav, K. Ekroos, R.W. Klemm, K. Simons, A. Shevchenko, Global analysis of the yeast lipidome by quantitative shotgun mass spectrometry, Proc. Natl. Acad. Sci. U. S. A. 106 (2009) 2136–2141. doi:10.1073/pnas.0811700106.

[87] C.S. Ejsing, E. Duchoslav, J. Sampaio, K. Simons, R. Bonner, C. Thiele, K. Ekroos, A. Shevchenko, Automated identification and quantification of glycerophospholipid molecular species by multiple precursor ion scanning, Anal. Chem. 78 (2006) 6202–6214. doi:10.1021/ac060545x.

[88] M. Ståhlman, C.S. Ejsing, K. Tarasov, J. Perman, J. Borén, K. Ekroos, High-throughput shotgun lipidomics by quadrupole time-of-flight mass spectrometry, J. Chromatogr. B Anal. Technol. Biomed. Life Sci. 877 (2009) 2664–2672. doi:10.1016/j.jchromb.2009.02.037.

[89] D. Schwudke, K. Schuhmann, R. Herzog, S.R. Bornstein, A. Shevchenko, Shotgun lipidomics on high resolution mass spectrometers, Cold Spring Harb. Perspect. Biol. 3 (2011) 1–13. doi:10.1101/cshperspect.a004614.

[90] H.C. Köfeler, A. Fauland, G.N. Rechberger, M. Trötzmüller, Mass spectrometry based lipidomics: An overview of technological platforms, Metabolites. 2 (2012) 19–38. doi:10.3390/metabo2010019.

[91] J. Li, T. Vosegaard, Z. Guo, Applications of nuclear magnetic resonance in lipid analyses: An emerging powerful tool for lipidomics studies, Prog. Lipid Res. 68 (2017) 37–56. doi:10.1016/j.plipres.2017.09.003.

[92] K. Jurowski, K. Kochan, J. Walczak, M. Barańska, W. Piekoszewski, B. Buszewski, Analytical Techniques in Lipidomics: State of the Art, Crit. Rev. Anal. Chem. 47 (2017) 418–437. doi:10.1080/10408347.2017.1310613.

[93] E. Alexandri, R. Ahmed, H. Siddiqui, M.I. Choudhary, C.G. Tsiafoulis, I.P. Gerothanassis, High resolution NMR spectroscopy as a structural and analytical tool for unsaturated lipids in solution, Molecules. 22 (2017). doi:10.3390/molecules22101663.

[94] T. Hyötyläinen, L. Ahonen, P. Pöhö, M. Orešič, Lipidomics in biomedical research-practical considerations, Biochim. Biophys. Acta - Mol. Cell Biol. Lipids. (2016). doi:10.1016/j.bbalip.2017.04.002.

[95] Waters, An overview of the principles of MSE, the engine that drives MS performance, (2011).

[96] T. Kind, H. Tsugawa, T. Cajka, Y. Ma, Z. Lai, S.S. Mehta, G. Wohlgemuth, D.K. Barupal, M.R. Showalter, M. Arita, O. Fiehn, Identification of small molecules using accurate mass MS/MS search, Mass Spectrom. Rev. 37 (2018) 513–532. doi:10.1002/mas.21535.

[97] T. Kind, K. Liu, D.Y. Lee, B. DeFelice, J.K. Meissen, O. Fiehn, LipidBlast in silico tandem mass spectrometry database for lipid identification, Nat. Methods. 10 (2013) 755–758. doi:10.1038/nmeth.2551.

[98] K. Ekroos, Lipidomics, Wiley-VCH Verlag GmbH & Co. KGaA, Weinheim, Germany, 2012. doi:10.1002/9783527655946.

[99] E. Ryan, G.E. Reid, Chemical Derivatization and Ultrahigh Resolution and Accurate Mass Spectrometry Strategies for “shotgun” Lipidome Analysis, Acc. Chem. Res. 49 (2016) 1596–1604. doi:10.1021/acs.accounts.6b00030.

[100] J.K. Pauling, M. Hermansson, J. Hartler, K. Christiansen, S.F. Gallego, B. Peng, R. Ahrends, C.S. Ejsing, Proposal for a common nomenclature for fragment ions in mass spectra of lipids, PLoS One. 12 (2017) 1–21. doi:10.1371/journal.pone.0188394.

[101] F. Ianni, G. Saluti, R. Galarini, S. Fiorito, R. Sardella, B. Natalini, Enantioselective high-performance liquid chromatography analysis of oxygenated polyunsaturated fatty acids, Free Radic. Biol. Med. (2019) 1–20. doi:10.1016/j.freeradbiomed.2019.04.038.

[102] C. Barbas, L. Saavedra, Chiral analysis of aliphatic short chain organic acids by capillary electrophoresis, J. Sep. Sci. 25 (2002) 1190–1196. doi:10.1002/1615-9314(20021101)25:15/17<1190::AID-JSSC1190>3.0.CO;2-7.

[103] T. Cajka, O. Fiehn, Comprehensive analysis of lipids in biological systems by liquid

chromatography-mass spectrometry, TrAC Trends Anal. Chem. 61 (2014) 192–206. doi:10.1016/j.trac.2014.04.017.

[104] M. Holčapek, Lipidomics, Anal. Bioanal. Chem. 407 (2015) 4971–4972. doi:10.1007/s00216-015-8740-0.

[105] T.A. Lydic, J. V Busik, G.E. Reid, A monophasic extraction strategy for the simultaneous lipidome analysis of polar and nonpolar retina lipids, J. Lipid Res. 55 (2014) 1797–1809. doi:10.1194/jlr.D050302.

[106] R.E. Patterson, A.J. Ducrocq, D.J. McDougall, T.J. Garrett, R.A. Yost, Comparison of blood plasma sample preparation methods for combined LC–MS lipidomics and metabolomics, J. Chromatogr. B. 1002 (2015) 260–266. doi:10.1016/j.jchromb.2015.08.018.

[107] C.Z. Ulmer, R.A. Yost, T.J. Garrett, Global UHPLC/HRMS Lipidomics Workflow for the Analysis of Lymphocyte Suspension Cultures, in: 2017: pp. 175–185. doi:10.1007/978-1-4939-6946-3_13.

[108] M.H. Sarafian, M. Gaudin, M.R. Lewis, F.-P. Martin, E. Holmes, J.K. Nicholson, M.-E. Dumas, Objective Set of Criteria for Optimization of Sample Preparation Procedures for Ultra-High Throughput Untargeted Blood Plasma Lipid Profiling by Ultra Performance Liquid Chromatography–Mass Spectrometry, Anal. Chem. 86 (2014) 5766–5774. doi:10.1021/ac500317c.

[109] J. Sostare, R. Di Guida, J. Kirwan, K. Chalal, E. Palmer, W.B. Dunn, M.R. Viant, Comparison of modified Matyash method to conventional solvent systems for polar metabolite and lipid extractions, Anal. Chim. Acta. 1037 (2018) 301–315. doi:10.1016/j.aca.2018.03.019.

[110] C. Pizarro, I. Arenzana-Rámila, N. Pérez-del-Notario, P. Pérez-Matute, J.-M. González-Sáiz, Plasma Lipidomic Profiling Method Based on Ultrasound Extraction and Liquid Chromatography Mass Spectrometry, Anal. Chem. 85 (2013) 12085–12092. doi:10.1021/ac403181c.

[111] S.K. Jensen, Improved Bligh and Dyer extraction procedure, Lipid Technol. 20 (2008) 280–281. doi:10.1002/lite.200800074.

[112] M.L. Dória, Z. Cotrim, B. Macedo, C. Simões, P. Domingues, L. Helguero, M.R. Domingues, Lipidomic approach to identify patterns in phospholipid profiles and define class differences in mammary epithelial and breast cancer cells, Breast Cancer Res. Treat. 133 (2012) 635–648. doi:10.1007/s10549-011-1823-5.

[113] H. Tsugawa, T. Cajka, T. Kind, Y. Ma, B. Higgins, K. Ikeda, M. Kanazawa, J. VanderGheynst,

O. Fiehn, M. Arita, MS-DIAL: data-independent MS/MS deconvolution for comprehensive metabolome analysis, Nat. Methods. 12 (2015) 523–526. doi:10.1038/nmeth.3393.

[114] G. Hopfgartner, D. Tonoli, E. Varesio, High-resolution mass spectrometry for integrated qualitative and quantitative analysis of pharmaceuticals in biological matrices, Anal. Bioanal. Chem. 402 (2012) 2587–2596. doi:10.1007/s00216-011-5641-8.

[115] L.C. Gillet, P. Navarro, S. Tate, H. Röst, N. Selevsek, L. Reiter, R. Bonner, R. Aebersold, Targeted Data Extraction of the MS/MS Spectra Generated by Data-independent Acquisition: A New Concept for Consistent and Accurate Proteome Analysis, Mol. Cell. Proteomics. 11 (2012) O111.016717. doi:10.1074/mcp.O111.016717.

[116] Y. Zhang, A. Bilbao, T. Bruderer, J. Luban, C. Strambio-De-Castillia, F. Lisacek, G. Hopfgartner, E. Varesio, The Use of Variable Q1 Isolation Windows Improves Selectivity in LC–SWATH–MS Acquisition, J. Proteome Res. 14 (2015) 4359–4371. doi:10.1021/acs.jproteome.5b00543.

[117] P.A. Krasutsky, Birch bark research and development, Nat. Prod. Rep. 23 (2006) 919–942. doi:10.1039/b606816b.

[118] M.N. Laszczyk, Pentacyclic triterpenes of the lupane, oleanane and ursane group as tools in cancer therapy, Planta Med. 75 (2009) 1549–1560. doi:10.1055/s-0029-1186102.

[119] U. Woelfle, M.N. Laszczyk, M. Kraus, K. Leuner, A. Kersten, B. Simon-Haarhaus, A. Scheffler, S.F. Martin, W.E. Müller, D. Nashan, C.M. Schempp, Triterpenes promote keratinocyte differentiation in vitro, Ex vivo and in vivo: A role for the transient receptor potential canonical (subtype) 6, J. Invest. Dermatol. 130 (2010) 113–123. doi:10.1038/jid.2009.248.

[120] S. Ebeling, K. Naumann, S. Pollok, T. Wardecki, S. Vidal-Y-Sy, J.M. Nascimento, M. Boerries, G. Schmidt, J.M. Brandner, I. Merfort, From a traditional medicinal plant to a rational drug: understanding the clinically proven wound healing efficacy of birch bark extract., PLoS One. 9 (2014) e86147. doi:10.1371/journal.pone.0086147.

[121] T. Wardecki, P. Werner, M. Thomas, M.F. Templin, G. Schmidt, J.M. Brandner, I. Merfort, Influence of Birch Bark Triterpenes on Keratinocytes and Fibroblasts from Diabetic and Nondiabetic Donors, J. Nat. Prod. 79 (2016) 1112–1123. doi:10.1021/acs.jnatprod.6b00027.

[122] H.L. Ziegler, H. Franzyk, M. Sairafianpour, M. Tabatabai, M.D. Tehrani, K. Bagherzadeh, H. Hägerstrand, D. Stærk, J.W. Jaroszewski, Erythrocyte membrane modifying agents and the inhibition of Plasmodium falciparum growth: Structure-activity relationships for

betulinic acid analogues, Bioorganic Med. Chem. 12 (2004) 119–127. doi:10.1016/j.bmc.2003.10.010.

[123] K.R. Feingold, The outer frontier: the importance of lipid metabolism in the skin, J. Lipid Res. 50 (2009) S417–S422. doi:10.1194/jlr.R800039-JLR200.

[124] A. Pappas, Epidermal surface lipids, Dermatoendocrinol. 1 (2009) 72–76. doi:10.4161/derm.1.2.7811.

[125] Y. Uchida, W.M. Holleran, Omega-O-acylceramide, a lipid essential for mammalian survival, J. Dermatol. Sci. 51 (2008) 77–87. doi:10.1016/j.jdermsci.2008.01.002.

[126] F. Gruber, C. Kremslehner, M.-S. Narzt, The impact of recent advances in lipidomics and redox lipidomics on dermatological research, Free Radic. Biol. Med. (2019) 1–10. doi:10.1016/j.freeradbiomed.2019.04.019.

[127] K.C. Madison, P.W. Wertz, J.S. Strauss, D.T. Downing, Lipid Composition of Cultured Murine Keratinocytes, J. Invest. Dermatol. 87 (1986) 253–259. doi:10.1111/1523-1747.ep12696636.

[128] M. Ponec, A. Weerheim, J. Kempenaar, A.M. Mommaas, D.H. Nugteren, Lipid composition of cultured human keratinocytes in relation to their differentiation., J. Lipid Res. 29 (1988) 949–61. http://www.ncbi.nlm.nih.gov/pubmed/2457643.

[129] M.L. Williams, B.E. Brown, D.J. Monger, S. Grayson, P.M. Elias, Lipid content and metabolism of human keratinocyte cultures grown at the air-medium interface, J. Cell. Physiol. 136 (1988) 103–110. doi:10.1002/jcp.1041360113.

[130] N. Schurer, A. Kohne, V. Schliep, K. Barlag, G. Goerz, Lipid composition and synthesis of HaCaT cells, an immortalized human keratinocyte line, in comparison with normal human adult keratinocytes, Exp. Dermatol. 2 (1993) 179–185. doi:10.1111/j.1600-0625.1993.tb00030.x.

[131] A. Reich, D. Schwudke, M. Meurer, B. Lehmann, A. Shevchenko, Lipidome of narrow-band ultraviolet B irradiated keratinocytes shows apoptotic hallmarks, Exp. Dermatol. 19 (2010) 103–110. doi:10.1111/j.1600-0625.2009.01000.x.

[132] D.R. Santinha, M.L. Dória, B.M. Neves, E.A. Maciel, J. Martins, L. Helguero, P. Domingues, M.T. Cruz, M.R. Domingues, Prospective phospholipid markers for skin sensitization prediction in keratinocytes: A phospholipidomic approach, Arch. Biochem. Biophys. 533 (2013) 33–41. doi:10.1016/j.abb.2013.02.012.

[133] L.H. Kennedy, C.H. Sutter, S.L. Carrion, Q.T. Tran, S. Bodreddigari, E. Kensicki, R.P.

Mohney, T.R. Sutter, 2,3,7,8-Tetrachlorodibenzo-p-dioxin-mediated production of reactive oxygen species is an essential step in the mechanism of action to accelerate human keratinocyte differentiation, Toxicol. Sci. 132 (2013) 235–249. doi:10.1093/toxsci/kfs325.

[134] E. Maciel, B.M. Neves, D. Santinha, A. Reis, P. Domingues, M.T. Cruz, A.R. Pitt, C.M. Spickett, M.R.M. Domingues, Detection of phosphatidylserine with a modified polar head group in human keratinocytes exposed to the radical generator AAPH, Arch. Biochem. Biophys. 548 (2014) 38–45. doi:10.1016/j.abb.2014.02.002.

[135] C. Hu, R. van der Heijden, M. Wang, J. van der Greef, T. Hankemeier, G. Xu, Analytical strategies in lipidomics and applications in disease biomarker discovery, J. Chromatogr. B Anal. Technol. Biomed. Life Sci. 877 (2009) 2836–2846. doi:10.1016/j.jchromb.2009.01.038.

[136] A. Triebl, J. Hartler, M. Trötzmüller, H. C. Köfeler, Lipidomics: Prospects from a technological perspective, Biochim. Biophys. Acta - Mol. Cell Biol. Lipids. 1862 (2017) 740–746. doi:10.1016/j.bbalip.2017.03.004.

[137] C. Hu, C. Wang, L. He, X. Han, Novel strategies for enhancing shotgun lipidomics for comprehensive analysis of cellular lipidomes, TrAC Trends Anal. Chem. (2018). doi:10.1016/j.trac.2018.11.028.

[138] B. Peng, S. Geue, C. Coman, P. Münzer, D. Kopczynski, C. Has, N. Hoffmann, M.C. Manke, F. Lang, A. Sickmann, M. Gawaz, O. Borst, R. Ahrends, Identification of key lipids critical for platelet activation by comprehensive analysis of the platelet lipidome, Blood. 132 (2018) e1–e12. doi:10.1182/blood-2017-12-822890.

[139] Z. Ahmed, M. Mayr, S. Zeeshan, T. Dandekar, M.J. Mueller, A. Fekete, Lipid-Pro: A computational lipid identification solution for untargeted lipidomics on data-independent acquisition tandem mass spectrometry platforms, Bioinformatics. 31 (2015) 1150–1153. doi:10.1093/bioinformatics/btu796.

[140] C. Calderón, C. Sanwald, J. Schlotterbeck, B. Drotleff, M. Lämmerhofer, Comparison of simple monophasic versus classical biphasic extraction protocols for comprehensive UHPLC-MS/MS lipidomic analysis of Hela cells, Anal. Chim. Acta. 1048 (2019) 66–74. doi:10.1016/j.aca.2018.10.035.

[141] J.D. Storey, The positive false discovery rate: a Bayesian intepretation and the q-value, Ann. Stat. 3 (2003) 2013–2035. doi:10.1214/aos/1074290335.

[142] I.A. Butovich, Fatty acid composition of cholesteryl esters of human meibomian gland

secretions, Steroids. 75 (2010) 726–733. doi:10.1016/j.steroids.2010.04.011.

[143] K. Vávrová, A. Kováčik, L. Opálka, Ceramides in the skin barrier, Eur. Pharm. J. 64 (2017) 28–35. doi:10.1515/afpuc-2017-0004.

[144] Y. Mizutani, H. Sun, Y. Ohno, T. Sassa, T. Wakashima, M. Obara, K. Yuyama, A. Kihara, Y. Igarashi, Cooperative Synthesis of Ultra Long-Chain Fatty Acid and Ceramide during Keratinocyte Differentiation, PLoS One. 8 (2013) 2–9. doi:10.1371/journal.pone.0067317.

[145] R. Sandhoff, Very long chain sphingolipids: Tissue expression, function and synthesis, FEBS Lett. 584 (2010) 1907–1913. doi:10.1016/j.febslet.2009.12.032.

[146] J.A. Losman, W.G. Kaelin, What a difference a hydroxyl makes: mutant IDH, (R)-2-hydroxyglutarate, and cancer, Genes Dev. 27 (2013) 836–852. doi:10.1101/gad.217406.113.

[147] R.A. Chalmers, A.M. Lawson, O. Borud, Gas chromatographic and mass spectrometric studies on urinary organic acids in a patient with congenital lactic acidosis due to pyruvate decarboxylase deficiency, Clin. Chim. Acta. 77 (1977) 117–124. doi:10.1016/0009-8981(77)90018-3.

[148] R.A. Chalmers, A.M. Lawson, R.W.E. Watts, A.S. Tavill, J.P. Kamerling, E. Hey, D. Ogilvie, D-2-hydroxyglutaric aciduria: Case report and biochemical studies, J. Inherit. Metab. Dis. 3 (1980) 11–15. doi:10.1007/BF02312516.

[149] M. Duran, J.P. Kamerling, H.D. Bakker, A.H. van Gennip, S.K. Wadman, L-2-Hydroxyglutaric aciduria: an inborn error of metabolism?, J. Inherit. Metab. Dis. 3 (1980) 109–112. doi:10.1007/BF02312543.

[150] P.G. Barth, G.F. Hoffmann, J. Jaeken, W. Lehnert, F. Hanefeld, A.H. van Gennip, M. Duran, J. Valk, R.B. Schutgens, F.K. Trefz, L-2-hydroxyglutaric acidemia: a novel inherited neurometabolic disease., Ann. Neurol. 32 (1992) 66–71. doi:10.1002/ana.410320111.

[151] P.G. Barth, G.F. Hoffmann, J. Jaeken, R.J.A. Wanders, M. Duran, G.A. Jansen, C. Jakobs, W. Lehnert, F. Hanefeld, J. Valk, R.B.H. Schutgens, F.K. Trefz, H.-P. Hartung, N.A. Chamoles, Z. Sfaello, U. Caruso, L-2-Hydroxyglutaric acidaemia: Clinical and biochemical findings in 12 patients and preliminary report on L-2-hydroxyacid dehydrogenase, J. Inherit. Metab. Dis. 16 (1993) 753–761. doi:10.1007/BF00711907.

[152] B. Wilcken, J. Pitt, D. Heath, P. Walsh, G. Wilson, N. Buchanan, l-2-Hydroxyglutaric aciduria: Three Australian cases, J. Inherit. Metab. Dis. 16 (1993) 501–504.

doi:10.1007/BF00711665.

[153] K.M. Gibson, H.J. Ten Brink, S.M. Schor, R.M. Kok, A.H. Bootsma, G.F. Hoffman, C. Jakobs, Stable-Isotope Dilution Analysis of D- and L-2-Hydroxyglutaric Acid: Application to the Detection and Prenatal Diagosis of D- and L-2-Hydroxyglutaric Acidemias, Pediatr. Res. 34 (1993) 277–280. doi:10.1203/00006450-199309000-00007.

[154] M. Wajner, D. de M. Coelho, R. Ingrassia, A.B. de Oliveira, E.N.B. Busanello, K. Raymond, R. Flores Pires, C.F.M. de Souza, R. Giugliani, C.R. Vargas, Selective screening for organic acidemias by urine organic acid GC-MS analysis in Brazil: Fifteen-year experience, Clin. Chim. Acta. 400 (2009) 77–81. doi:10.1016/j.cca.2008.10.007.

[155] Z. Patay, J.C. Mills, U. Lobel, A. Lambert, A. Sablauer, D.W. Ellison, Cerebral Neoplasms in L-2 Hydroxyglutaric Aciduria: 3 New Cases and Meta-Analysis of Literature Data, Am. J. Neuroradiol. 33 (2012) 940–943. doi:10.3174/ajnr.A2869.

[156] M. Kranendijk, E.A. Struys, G.S. Salomons, M.S. Van der Knaap, C. Jakobs, Progress in understanding 2-hydroxyglutaric acidurias, J. Inherit. Metab. Dis. 35 (2012) 571–587. doi:10.1007/s10545-012-9462-5.

[157] M. Kranendijk, G.S. Salomons, K.M. Gibson, C. Aktuglu-Zeybek, S. Bekri, E. Christensen, J. Clarke, A. Hahn, S.H. Korman, V. Mejaski-Bosnjak, A. Superti-Furga, C. Vianey-Saban, M.S. van der Knaap, C. Jakobs, E. a. Struys, Development and implementation of a novel assay for L-2-hydroxyglutarate dehydrogenase (L-2-HGDH) in cell lysates: L-2-HGDH deficiency in 15 patients with L-2-hydroxyglutaric aciduria, J. Inherit. Metab. Dis. 32 (2009) 713–719. doi:10.1007/s10545-009-1282-x.

[158] L. Dang, D.W. White, S. Gross, B.D. Bennett, M.A. Bittinger, E.M. Driggers, V.R. Fantin, H.G. Jang, S. Jin, M.C. Keenan, K.M. Marks, R.M. Prins, P.S. Ward, K.E. Yen, L.M. Liau, J.D. Rabinowitz, L.C. Cantley, C.B. Thompson, M.G. Vander Heiden, S.M. Su, Cancer-associated IDH1 mutations produce 2-hydroxyglutarate, Nature. 462 (2009) 739–744. doi:10.1038/nature08617.

[159] R. Stefan, R. Nejem, J. van Staden, H. Aboul-Enein, Determination of D-2-hydroxyglutaric acid in urine samples using enantioselective, potentiometric membrane electrodes based on antibiotics, Sensors Actuators B Chem. 106 (2005) 791–795. doi:10.1016/j.snb.2004.09.031.

[160] E.A. Struys, Measurement of Urinary D- and L-2-Hydroxyglutarate Enantiomers by Stable-Isotope-Dilution Liquid Chromatography-Tandem Mass Spectrometry after Derivatization with Diacetyl-L-Tartaric Anhydride, Clin. Chem. 50 (2004) 1391–1395.

doi:10.1373/clinchem.2004.033399.

[161] H.J.C. das Neves, J.P. Noronha, H. Rufino, A new method for the chiral HRGC assay of L-2-hydroxyglutaric acid in urine, J. High Resolut. Chromatogr. 19 (1996) 161–164. doi:10.1002/jhrc.1240190308.

[162] M.S. Rashed, M. AlAmoudi, H.Y. Aboul-Enein, Chiral liquid chromatography tandem mass spectrometry in the determination of the configuration of 2-hydroxyglutaric acid in urine, Biomed. Chromatogr. 14 (2000) 317–320. doi:10.1002/1099-0801(200008)14:5<317::AID-BMC989>3.0.CO;2-V.

[163] K.-R. Kim, J. Lee, D. Ha, J.H. Kim, Configurational analysis of chiral acids as O-trifluoroacetylated (−)-menthyl esters by achiral dual-capillary column gas chromatography, J. Chromatogr. A. 891 (2000) 257–266. doi:10.1016/S0021-9673(00)00690-7.

[164] A.C. Muntau, W. Röschinger, A. Merkenschlager, M.S. Van Der Knaap, C. Jakobs, M. Duran, G.F. Hoffmann, A.A. Roscher, Combined D-2- and L-2-hydroxyglutaric aciduria with neonatal onset encephalopathy: A third biochemical variant of 2-hydroxyglutaric aciduria?, Neuropediatrics. 31 (2000) 137–140. doi:10.1055/s-2000-7497.

[165] S. Gross, R.A. Cairns, M.D. Minden, E.M. Driggers, M.A. Bittinger, H.G. Jang, M. Sasaki, S. Jin, D.P. Schenkein, S.M. Su, L. Dang, V.R. Fantin, T.W. Mak, Cancer-associated metabolite 2-hydroxyglutarate accumulates in acute myelogenous leukemia with isocitrate dehydrogenase 1 and 2 mutations, J. Exp. Med. 207 (2010) 339–344. doi:10.1084/jem.20092506.

[166] A. Kaunzinger, A. Rechner, T. Beck, A. Mosandl, A.C. Sewell, H. Böhles, Chiral compounds as indicators of inherited metabolic disease. Simultaneous stereodifferentiation of lactic-, 2-hydroxyglutaric- and glyceric acid by enantioselective cGC, Enantiomer. 1 (1996) 177–82.

[167] Q.-Y. Cheng, J. Xiong, W. Huang, Q. Ma, W. Ci, Y.-Q. Feng, B.-F. Yuan, Sensitive Determination of Onco-metabolites of D- and L-2-hydroxyglutarate Enantiomers by Chiral Derivatization Combined with Liquid Chromatography/Mass Spectrometry Analysis, Sci. Rep. 5 (2015) 15217. doi:10.1038/srep15217.

[168] W. V Wickenhagen, G.S. Salomons, K.M. Gibson, C. Jakobs, E.A. Struys, Measurement of D-2-hydroxyglutarate dehydrogenase activity in cell homogenates derived from D-2-hydroxyglutaric aciduria patients, J. Inherit. Metab. Dis. 32 (2009) 264–268. doi:10.1007/s10545-009-1104-1.

[169] C. V. Hoffmann, R. Pell, M. Lämmerhofer, W. Lindner, Synergistic effects on enantioselectivity of zwitterionic chiral stationary phases for separations of chiral acids, bases, and amino acids by HPLC, Anal. Chem. 80 (2008) 8780–8789. doi:10.1021/ac801384f.

[170] I. Ilisz, N. Grecsó, F. Fülöp, W. Lindner, A. Péter, High-performance liquid chromatographic enantioseparation of cationic 1,2,3,4-tetrahydroisoquinoline analogs on Cinchona alkaloid-based zwitterionic chiral stationary phases, Anal. Bioanal. Chem. 407 (2015) 961–972. doi:10.1007/s00216-014-8247-0.

[171] I. Ilisz, N. Grecsó, A. Misicka, D. Tymecka, L. Lázár, W. Lindner, A. Péter, Comparison of the Separation Performances of Cinchona Alkaloid-Based Zwitterionic Stationary Phases in the Enantioseparation of β2- and β3-Amino Acids, Molecules. 20 (2014) 70–87. doi:10.3390/molecules20010070.

[172] H. Sugimoto, M. Kakehi, F. Jinno, Method development for the determination of D- and L-isomers of leucine in human plasma by high-performance liquid chromatography tandem mass spectrometry and its application to animal plasma samples, Anal. Bioanal. Chem. 407 (2015) 7889–7898. doi:10.1007/s00216-015-8999-1.

[173] F. Ianni, R. Sardella, A. Carotti, B. Natalini, W. Lindner, M. Lämmerhofer, Quinine-Based Zwitterionic Chiral Stationary Phase as a Complementary Tool for Peptide Analysis: Mobile Phase Effects on Enantio- and Stereoselectivity of Underivatized Oligopeptides, Chirality. 28 (2016) 5–16. doi:10.1002/chir.22541.

[174] R. Sardella, M. Lämmerhofer, B. Natalini, W. Lindner, Enantioselective HPLC of potentially CNS-active acidic amino acids with a cinchona carbamate based chiral stationary phase, Chirality. 20 (2008) 571–576. doi:10.1002/chir.20529.

[175] R.J. Reischl, W. Lindner, Methoxyquinoline labeling—A new strategy for the enantioseparation of all chiral proteinogenic amino acids in 1-dimensional liquid chromatography using fluorescence and tandem mass spectrometric detection, J. Chromatogr. A. 1269 (2012) 262–269. doi:10.1016/j.chroma.2012.07.046.

[176] X. Xiong, W.R.G. Baeyens, H.Y. Aboul-Enein, J.R. Delanghe, T. Tu, J. Ouyang, Impact of amines as co-modifiers on the enantioseparation of various amino acid derivatives on a tert-butyl carbamoylated quinine-based chiral stationary phase, Talanta. 71 (2007) 573–581. doi:10.1016/j.talanta.2006.04.038.

[177] R. Pell, G. Schuster, M. Lämmerhofer, W. Lindner, Enantioseparation of chiral sulfonates by liquid chromatography and subcritical fluid chromatography, J. Sep. Sci. 35 (2012)

2521–2528. doi:10.1002/jssc.201200448.

[178] S. Schiesel, M. Lämmerhofer, A. Leitner, W. Lindner, Quantitative high-performance liquid chromatography–tandem mass spectrometry impurity profiling methods for the analysis of parenteral infusion solutions for amino acid supplementation containing L-alanyl-L-glutamine, J. Chromatogr. A. 1259 (2012) 111–120. doi:10.1016/j.chroma.2012.01.020.

[179] P. Franco, T. Zhang, A. Gargano, M. Mahut, M. Lammerhofer, W. Lindner, K.E.Y. Points, Enantiomer and topoisomer separation of acidic compounds on anion-exchanger chiral stationary phases by HPLC and SFC, LC GC Eur. 25 (2012) 600–610.

[180] F. Ianni, Z. Pataj, H. Gross, R. Sardella, B. Natalini, W. Lindner, M. Lämmerhofer, Direct enantioseparation of underivatized aliphatic 3-hydroxyalkanoic acids with a quinine-based zwitterionic chiral stationary phase, J. Chromatogr. A. 1363 (2014) 101–108. doi:10.1016/j.chroma.2014.03.060.

[181] M. Lämmerhofer, W. Lindner, Liquid chromatographic enantiomer separation and chiral recognition by cinchona alkaloid-derived enantioselective separation materials, Adv. Chromatogr. 46 (2008) 1–107.

[182] P. Franco, T. Zhang, Common approaches for efficient method development with immobilised polysaccharide-derived chiral stationary phases, J. Chromatogr. B Anal. Technol. Biomed. Life Sci. 875 (2008) 48–56. doi:10.1016/j.jchromb.2008.06.051.

[183] C. V. Hoffmann, R. Reischl, N.M. Maier, M. Lämmerhofer, W. Lindner, Investigations of mobile phase contributions to enantioselective anion- and zwitterion-exchange modes on quinine-based zwitterionic chiral stationary phases, J. Chromatogr. A. 1216 (2009) 1157–1166. doi:10.1016/j.chroma.2008.12.044.

[184] K. Gyimesi-Forrás, K. Akasaka, M. Lämmerhofer, N.M. Maier, T. Fujita, M. Watanabe, N. Harada, W. Lindner, Enantiomer separation of a powerful chiral auxiliary, 2-methoxy-2-(1-naphthyl)propionic acid by liquid chromatography using chiral anion exchanger-type stationary phases in polar-organic mode; investigation of molecular recognition aspects, Chirality. 17 (2005) S134–S142. doi:10.1002/chir.20123.

[185] C. V. Hoffmann, R. Reischl, N.M. Maier, M. Lämmerhofer, W. Lindner, Stationary phase-related investigations of quinine-based zwitterionic chiral stationary phases operated in anion-, cation-, and zwitterion-exchange modes, J. Chromatogr. A. 1216 (2009) 1147–1156. doi:10.1016/j.chroma.2008.12.045.

[186] I. Ilisz, Z. Gecse, Z. Pataj, F. Fülöp, G. Tóth, W. Lindner, A. Péter, Direct high-performance

liquid chromatographic enantioseparation of secondary amino acids on Cinchona alkaloid-based chiral zwitterionic stationary phases. Unusual temperature behavior, J. Chromatogr. A. 1363 (2014) 169–177. doi:10.1016/j.chroma.2014.06.087.

[187] I. Ilisz, Z. Pataj, Z. Gecse, Z. Szakonyi, F. Fülöp, W. Lindner, A. Péter, Unusual Temperature-Induced Retention Behavior of Constrained β-Amino Acid Enantiomers on the Zwitterionic Chiral Stationary Phases ZWIX(+) and ZWIX(-), Chirality. 26 (2014) 385–393. doi:10.1002/chir.22333.

[188] T. Fornstedt, P. Sajonz, G. Guiochon, Thermodynamic study of an unusual chiral separation. Propranolol enantiomers on an immobilized cellulase, J. Am. Chem. Soc. 119 (1997) 1254–1264. doi:10.1021/ja9631458.

[189] L. Saavedra, C. Barbas, Optimization of the separation lactic acid enantiomers in body fluids by capillary electrophoresis, J. Chromatogr. B Anal. Technol. Biomed. Life Sci. 766 (2002) 235–242. doi:10.1016/S0378-4347(01)00473-X.

[190] J.B. Ewaschuk, G.A. Zello, J.M. Naylor, D.R. Brocks, Metabolic acidosis: separation methods and biological relevance of organic acids and lactic acid enantiomers, J. Chromatogr. B-Analytical Technol. Biomed. Life Sci. 781 (2002) 39–56. doi:10.1016/s1570-0232(02)00500-7.

[191] W.E. Gall, K. Beebe, K.A. Lawton, K.-P. Adam, M.W. Mitchell, P.J. Nakhle, J.A. Ryals, M. V. Milburn, M. Nannipieri, S. Camastra, A. Natali, E. Ferrannini, α-Hydroxybutyrate Is an Early Biomarker of Insulin Resistance and Glucose Intolerance in a Nondiabetic Population, PLoS One. 5 (2010) e10883. doi:10.1371/journal.pone.0010883.

[192] H. Tsutsui, T. Mochizuki, T. Maeda, I. Noge, Y. Kitagawa, J.Z. Min, K. Todoroki, K. Inoue, T. Toyo, Simultaneous determination of DL-lactic acid and DL-3-hydroxybutyric acid enantiomers in saliva of diabetes mellitus patients by high-throughput LC-ESI-MS/MS, Anal. Bioanal. Chem. 404 (2012) 1925–1934. doi:10.1007/s00216-012-6320-0.

[193] M.S. Rashed, H.Y. Aboul-Enein, M. AlAmoudi, M. Jakob, L.Y. Al-Ahaideb, A. Abbad, S. Shabib, E. Al-Jishi, Chiral liquid chromatography tandem mass spectrometry in the determination of the configuration of glyceric acid in urine of patients with D-glyceric and L-glyceric acidurias, Biomed. Chromatogr. 16 (2002) 191–198. doi:10.1002/bmc.126.

[194] N.W. Dimer, P.F. Schuck, E.L. Streck, G.C. Ferreira, D-glyceric aciduria, An. Acad. Bras. Cienc. 87 (2015) 1409–1414. doi:10.1590/0001-3765201520150021.

[195] A.J. Buglass, S.H. Lee, Sequential Analysis of Malic Acid and Both Enantiomers of Lactic Acid in Wine Using a High-Performance Liquid Chromatographic Column-Switching

Procedure, J. Chromatogr. Sci. 39 (2001) 453–458. doi:10.1093/chromsci/39.11.453.

[196] R. Knob, J. Petr, J. Sevčík, V. Maier, Enantioseparation of tartaric acid by ligand-exchange capillary electrophoresis using contactless conductivity detection., J. Sep. Sci. 36 (2013) 3426–3431. doi:10.1002/jssc.201300507.

[197] M. Kamencev, N. Komarova, O. Morozova, Enantioseparation of Tartaric and Malic Acids in Wines by Ligand Exchange Capillary Electrophoresis Using Uncoated Fused Silica Capillary, Chromatographia. 79 (2016) 927–931. doi:10.1007/s10337-016-3099-8.

[198] C. Aydoğan, V. Karakoç, A. Denizli, Chiral ligand-exchange separation and determination of malic acid enantiomers in apple juice by open-tubular capillary electrochromatography, Food Chem. 187 (2015) 130–134. doi:10.1016/j.foodchem.2015.04.062.

[199] S. Kodama, A. Yamamoto, A. Matsunaga, Direct chiral resolution of aliphatic α-hydroxy acids using 2-hydroxypropyl-β-cyclodextrin in capillary electrophoresis, Analyst. 124 (1999) 55–59. doi:10.1039/a807351a.

[200] S. Kodama, A. Yamamoto, S. Aizawa, Y. Honda, K. Suzuki, T. Kemmei, A. Taga, Enantioseparation of α-hydroxy acids by chiral ligand exchange CE with a dual central metal ion system, Electrophoresis. 33 (2012) 2920–2924. doi:10.1002/elps.201200210.

[201] S. Kodama, S. Aizawa, A. Taga, A. Yamamoto, Y. Honda, K. Suzuki, T. Kemmei, K. Hayakawa, Determination of α-hydroxy acids and their enantiomers in fruit juices by ligand exchange CE with a dual central metal ion system, Electrophoresis. 34 (2013) 1327–1333. doi:10.1002/elps.201200645.

[202] B. Fransson, U. Ragnarsson, Separation of enantiomers of α-hydroxy acids by reversed-phase liquid chromatography after derivatization with 1-(9-fluorenyl)ethyl chloroformate, J. Chromatogr. A. 827 (1998) 31–36. doi:http://dx.doi.org/10.1016/S0021-9673(98)00770-5.

[203] V. Poinsignon, L. Mercier, K. Nakabayashi, M.D. David, A. Lalli, V. Penard- Lacronique, C. Quivoron, V. Saada, S. De Botton, S. Broutin, A. Paci, Quantitation of isocitrate dehydrogenase (IDH)-induced D and L enantiomers of 2-hydroxyglutaric acid in biological fluids by a fully validated liquid tandem mass spectrometry method, suitable for clinical applications, J. Chromatogr. B. 1022 (2016) 290–297. doi:10.1016/j.jchromb.2016.04.030.

[204] G. Galaverna, F. Pantò, A. Dossena, R. Marchelli, F. Bigi, Chiral separation of unmodified α-hydroxy acids by ligand exchange HPLC using chiral copper(II) complexes of (S)-

phenylalaninamide as additives to the eluent, Chirality. 7 (1995) 331–336. doi:10.1002/chir.530070504.

[205] Z. Chilmonczyk, H. Ksycinska, J. Cybulski, M. Rydzewski, A. Les, Direct separation of α-hydroxy acid enantiomers by ligand exchange chromatography, Chirality. 10 (1998) 821–830. doi:10.1002/(SICI)1520-636X(1998)10:9<821::AID-CHIR8>3.0.CO;2-C.

[206] I. Ilisz, A. Péter, W. Lindner, State-of-the-art enantioseparations of natural and unnatural amino acids by high-performance liquid chromatography, TrAC Trends Anal. Chem. 81 (2016) 11–22. doi:10.1016/j.trac.2016.01.016.

[207] D. Norton, B. Crow, M. Bishop, K. Kovalcik, J. George, J.A. Bralley, High performance liquid chromatography-tandem mass spectrometry (HPLC/MS/MS) assay for chiral separation of lactic acid enantiomers in urine using a teicoplanin based stationary phase, J. Chromatogr. B Anal. Technol. Biomed. Life Sci. 850 (2007) 190–198. doi:10.1016/j.jchromb.2006.11.020.

[208] C. Calderón, J. Horak, M. Lämmerhofer, Chiral separation of 2-hydroxyglutaric acid on cinchonan carbamate based weak chiral anion exchangers by high-performance liquid chromatography, J. Chromatogr. A. 1467 (2016) 239–245. doi:10.1016/j.chroma.2016.05.042.

[209] K. Snoble, N. Fox, S.M. Lorenz, A.R. Kemperman, J.T. Przybytek, Stability of Formic Acid in Methanol Solutions and the Implications for Use in LC-MS Gradient Elution Analysis, LCGC North Am. 26 (2010).

[210] N. Grecsó, E. Forró, F. Fülöp, A. Péter, I. Ilisz, W. Lindner, Combinatorial effects of the configuration of the cationic and the anionic chiral subunits of four zwitterionic chiral stationary phases leading to reversal of elution order of cyclic β3-amino acid enantiomers as ampholytic model compounds, J. Chromatogr. A. 1467 (2016) 178–187. doi:10.1016/j.chroma.2016.05.041.

[211] C. V. Hoffmann, M. Laemmerhofer, W. Lindner, Novel strong cation-exchange type chiral stationary phase for the enantiomer separation of chiral amines by high-performance liquid chromatography, J. Chromatogr. A. 1161 (2007) 242–251. doi:10.1016/j.chroma.2007.05.092.

[212] G.R. Villani, G. Gallo, E. Scolamiero, F. Salvatore, M. Ruoppolo, “Classical organic acidurias”: diagnosis and pathogenesis, Clin. Exp. Med. 17 (2017) 305–323. doi:10.1007/s10238-016-0435-0.

[213] O.A. Mamer, M.L. Reimer, On the mechanisms of the formation of L-alloisoleucine and

the 2-hydroxy-3-methylvaleric acid stereoisomers from L-isoleucine in maple syrup urine disease patients and in normal humans., J. Biol. Chem. 267 (1992) 22141–7. http://www.ncbi.nlm.nih.gov/pubmed/1429566.

[214] E. Haan, G. Brown, A. Bankier, D. Mitchell, S. Hunt, J. Blakey, G. Barnes, Severe illness caused by the products of bacterial metabolism in a child with a short gut, Eur. J. Pediatr. 144 (1985) 63–65. doi:10.1007/BF00491929.

[215] J. Hagen, H. te Brinke, R.J.A. Wanders, A.C. Knegt, E. Oussoren, A.J.M. Hoogeboom, G.J.G. Ruijter, D. Becker, K.O. Schwab, I. Franke, M. Duran, H.R. Waterham, J.O. Sass, S.M. Houten, Genetic basis of alpha-aminoadipic and alpha-ketoadipic aciduria, J. Inherit. Metab. Dis. 38 (2015) 873–879. doi:10.1007/s10545-015-9841-9.

[216] A. Muth, J. Jung, S. Bilke, A. Scharrer, A. Mosandl, A.C. Sewell, H. Böhles, Simultaneous enantioselective analysis of chiral urinary metabolites in patients with Zellweger syndrome, J. Chromatogr. B Anal. Technol. Biomed. Life Sci. 792 (2003) 269–277. doi:10.1016/S1570-0232(03)00285-X.

[217] J.B. Brooks, J. V Kasin, D.M. Fast, M.I. Daneshvar, Detection of metabolites by frequency-pulsed electron capture gas-liquid chromatography in serum and cerebrospinal fluid of a patient with Nocardia infection., J. Clin. Microbiol. 25 (1987) 445–8. http://www.ncbi.nlm.nih.gov/pubmed/3818936.

[218] X. Li, Z. Xu, X. Lu, X. Yang, P. Yin, H. Kong, Y. Yu, G. Xu, Comprehensive two-dimensional gas chromatography/time-of-flight mass spectrometry for metabonomics: Biomarker discovery for diabetes mellitus, Anal. Chim. Acta. 633 (2009) 257–262. doi:10.1016/j.aca.2008.11.058.

[219] W. Checkley, M.P. Deza, J. Klawitter, K.M. Romero, J. Klawitter, S.L. Pollard, R.A. Wise, U. Christians, N.N. Hansel, Identifying biomarkers for asthma diagnosis using targeted metabolomics approaches, Respir. Med. 121 (2016) 59–66. doi:10.1016/j.rmed.2016.10.011.

[220] S. Walenta, T. Schroeder, W. Mueller-Klieser, Lactate in solid malignant tumors: potential basis of a metabolic classification in clinical oncology., Curr. Med. Chem. 11 (2004) 2195–204. doi:10.2174/0929867043364711.

[221] M. Yang, T. Soga, P.J. Pollard, Oncometabolites: Linking altered metabolism with cancer, J. Clin. Invest. 123 (2013) 3652–3658. doi:10.1172/JCI67228.

[222] A.S.W. Tordiffe, M. van Reenen, F. Reyers, L.J. Mienie, Gas chromatography-mass spectrometry profiles of urinary organic acids in healthy captive cheetahs (Acinonyx

jubatus), J. Chromatogr. B Anal. Technol. Biomed. Life Sci. 1049–1050 (2017) 8–15. doi:10.1016/j.jchromb.2017.02.018.

[223] E.A. Struys, 2-Hydroxyglutarate is not a metabolite; D-2-hydroxyglutarate and L-2-hydroxyglutarate are!, Proc. Natl. Acad. Sci. 110 (2013) E4939–E4939. doi:10.1073/pnas.1318777110.

[224] M.H. Hyun, J.I. Kim, Y.J. Cho, S.C. Han, Liquid chromatographic resolution of racemic alpha-hydroxycarboxylic acids on ligand exchange chiral stationary phases, Chromatographia. 60 (2004) 275–280. doi:10.1365/s10337-004-0358-x.

[225] M.H. Hyun, M.H. Kang, S.C. Han, Liquid chromatographic resolution of 2-hydroxycarboxylic acids on a new chiral stationary phase derived from (S)-leucine, J. Chromatogr. A. 868 (2000) 31–39. doi:http://dx.doi.org/10.1016/S0021-9673(99)01140-1.

[226] C. Calderón, M. Lämmerhofer, Chiral separation of short chain aliphatic hydroxycarboxylic acids on cinchonan carbamate-based weak chiral anion exchangers and zwitterionic chiral ion exchangers, J. Chromatogr. A. 1487 (2017) 194–200. doi:10.1016/j.chroma.2017.01.060.

[227] S.L. Liu, T. Oyama, Y. Miyoshi, S.Y. Sheu, M. Mita, T. Ide, W. Lindner, K. Hamase, J.A. Lee, Establishment of a two-dimensional chiral HPLC system for the simultaneous detection of lactate and 3-hydroxybutyrate enantiomers in human clinical samples, J. Pharm. Biomed. Anal. 116 (2015) 80–85. doi:10.1016/j.jpba.2015.05.036.

[228] M. Lämmerhofer, W. Lindner, Quinine and quinidine derivatives as chiral selectors I. Brush type chiral stationary phases for high-performance liquid chromatography based on cinchonan carbamates and their application as chiral anion exchangers, J. Chromatogr. A. 741 (1996) 33–48. doi:10.1016/0021-9673(96)00137-9.

[229] G. Lajkó, T. Orosz, I. Ugrai, Z. Szakonyi, F. Fülöp, W. Lindner, A. Péter, I. Ilisz, Liquid chromatographic enantioseparation of limonene-based carbocyclic β-amino acids on zwitterionic Cinchona alkaloid-based chiral stationary phases, J. Sep. Sci. 40 (2017) 3196–3204. doi:10.1002/jssc.201700450.

[230] H. Hinterwirth, M. Lämmerhofer, B. Preinerstorfer, A. Gargano, R. Reischl, W. Bicker, O. Trapp, L. Brecker, W. Lindner, Selectivity issues in targeted metabolomics: Separation of phosphorylated carbohydrate isomers by mixed-mode hydrophilic interaction/weak anion exchange chromatography, J. Sep. Sci. 33 (2010) 3273–3282. doi:10.1002/jssc.201000412.

LIST OF FIGURES

Figure 1.1. Skeleton of the 8 lipid categories defined by Lipid MAPS. 2

Figure 1.2. Distributions of structures available in LMSD. 3

Figure 1.3. Structure of main glycerophospholipid classes 5

Figure 1.4. Common structures of sphingolipids 6

Figure 2.1. Use of different chromatographic and mass spectrometric systems in lipidomics analysis. 7

Figure 2.2. Elution profile of lipid extracts in four different LC configurations RPLC, NPLC, HILIC and SFC (in normal phase mode). 9

Figure 2.3. Peak spotting plot for LPCs identified in a previous publication according to the number of double bonds. 10

Figure 3.1. Schematic diagram of a mass spectrometer. 12

Figure 3.2. Ionization technique employed in MS, classified according to their application and estimated relative hardness of softness. 13

Figure 3.3. Schematic diagram of the principle of electrospray ionization. 13

Figure 3.4. Scheme for classification of MS experiments. 17

Figure 3.5. Corresponding spectra of different PIS and NLS experiments of a rat myocardial lipid extract. 20

Figure 3.6. Schematic representation of DIA experiments A) MS^{All}, B) MS^{E} and C) SWATH 22

Figure 3.7. Common fragments of acyl carnitines in positive mode 24

Figure 3.8. Typical product ions of TGs 25

Figure 3.9. Typical product ions of DGs 25

Figure 3.10. Acylium product ion of carboxylate in MGs 26

Figure 3.11. Loss of polar headgroups for $[M+H]^+$ ions of glycerophospholipids 27

Figure 3.12. Mechanism for formation of carboxylate anions from [M-H]- of phospholipids. .. 28

Figure 3.13. Mechanism for loss of neutral ketenes (RxCH=C=O) from [M-H]- of phospholipids 28

Figure 3.14. Mechanism for loss of R_xCOOH from [M-H]- of phospholipids. 28

Figure 3.15. Common fragments after CID of $[M+H]^+$ of ceramides 29

Figure 3.16. Common fragments after CID of $[M-H]^-$ of ceramides 29

Figure 3.17. Common fragments after CID of $[M+H]^+$ of hexosylceramides 30

Figure 3.18. Common fragment after CID of $[M+NH_4]^+$ of cholesteryl esters 30

Figure 4.1. Change in the level of LPCs, from plasma samples extracted at different time points after storage at 4 °C 32

Figure 4.2. Example of deconvolution in cases of chromatographic coelutions. 37

Figure 5.1. Hierarchy of lipid identification and characterization. 39

Figure 6.1. Representative TICs for samples extracted with four different EPs using A) ESI (+) and B) ESI (-) mode. 51

Figure 6.2. PCA plots for intensities of detected features. 52

Figure 6.3. Venn diagrams showing the distribution of detected features with each EP and their overlapping selectivities. 53

Figure 6.4. Relative lipid class recoveries of endogenous lipids obtained with different EPs and using IPA90 as a reference. 54

Figure 6.5. Recoveries of isotopically labeled internal standards after pre and post-extraction spiking 55

Figure 6.6. Distribution of CVs (%) obtained for precision evaluation of peak intensities of features detected in all four EPs. 56

Figure 7.1. Scheme for lipid identification process. 72

Figure 7.2. Mass percentage distribution of analyzed lipid classes in keratinocytes (Control group). 75

Figure 7.3. Heatmap for comparison of relative intensities of 440 lipids, identified in human immortalized keratinocytes 76

Figure 7.4. Volcano plot for 611 identified lipid species whose intensity was compared between betulin-treated keratinocytes versus control keratinocytes. 77

Figure 8.1. a) Enantiomers of 2-HG-, D-2-hydroxyglutaric acid and L-2-hydroxyglutaric acid, b) Chiral stationary phases tested in this study: Chiralpak QN-AX and QD-AX as well as Chiralpak ZWIX(+) and ZWIX(-) 98

Figure 8.2. Generic gradient elution screening runs for a mixture of D- and L-2-HG, and pure enantiomer L-2-HG using a) ZWIX (+) and ZWIX (-), b) QD-AX and c) QN-AX column. 99

Figure 8.3. Effect of ACN:MeOH ratios on the chromatographic parameters of the separation of D- and L-2-HG. 101

Figure 8.4. Chromatographic runs for a mixture of D- and L-2-HG with a) different types of alcohols, and b) different types of co-ions (ammonia, NH_3; DEA, diethylamine; TEA, triethylamine) in the mobile phase. 103

Figure 8.5. Effect of FA concentrations in accordance to the stoichiometric displacement model. 104

Figure 8.6. Temperature dependence of retention and separation factors as illustrated by Van't Hoff plots. 105

Figure 8.7. Plot of resolution versus inverse of retention time for second peak, obtained during different chromatographic runs. 106

Figure 9.1. Structures of the studied aliphatic hydroxycarboxylic acids (HCAs) 118

Figure 9.2. Chiral stationary phases tested in this study: Chiralpak QN-AX and QD-AX as well as Chiralpak ZWIX(+) and ZWIX(-) 119

Figure 9.3. Temperature dependence of retention and separation factors as illustrated by van't Hoff plots. 124

Figure 9.4. Chromatographic runs for the best separations of HCA enantiomers performed on different CSPs. 125

Figure 9.5. Chromatographic runs for a mixture of D- and L-GlA enantiomers or the D-GlA enantiomer on a) QN-AX column, b) ZWIX(+) column, c) QD-AX column and d) ZWIX(-) column. 127

Figure 10.1. Structures of the studied 2-hydroxycarboxylic acids 139

Figure 10.2. Chiral stationary phases tested in this study: Chiralpak QN-AX and QD-AX as well as Chiralpak ZWIX(-) 141

Figure 10.3. Chromatographic runs for a mixture and single enantiomers of 2-HMCA on A) QN-AX column and B) QD-AX column. 142

Figure 10.4. Chromatographic runs for the best achieved separations of 2-HDCA enantiomers performed on different CSPs. 144

Figure 10.5. Effect of FA concentrations on retention of (RS)-2-HCA and (RS)-2-HAA in accordance to the stoichiometric displacement model. 146

LIST OF SUPPLEMENTARY FIGURES

Suppl. Figure 6.1. Z values for selected features (based on their intensity) in QC samples through the run sequence in A) ESI (+) and B) ESI (-). 63

Suppl. Figure 6.2. Venn diagram showing the distribution of detected features with blanks for EPs of IPA75 using plasticware, IPA90 using plasticware and IPA 90 using glassware in ESI (+). 63

Suppl. Figure 6.3. Venn diagram showing the distribution of detected features with blanks for EPs of IPA75 using plasticware, IPA90 using plasticware and IPA 90 using glassware in ESI (-). 64

Suppl. Figure 7.1. Distribution of 611 identified lipids in QC samples according to their lipid class with number of identified lipids for each class. 86

Suppl. Figure 7.2. Venn diagram showing the number of lipids identified in each ion mode and the distribution MS data used for identification of lipids in QC samples of keratinocytes. 87

Suppl. Figure 7.3. Spot maps m/z versus retention time for specific adducts of lipid classes in TOF MS analyzed in the ESI (+) and ESI (-). 88

Suppl. Figure 7.4. Spot maps m/z versus retention time for specific adducts of lipid classes in TOF MS analysis either in the ESI (+) or ESI (-). 89

Suppl. Figure 7.5. Relative intensities of CEs identified in betulin and control groups. 90

Suppl. Figure 7.6. Distribution of coefficient of variations (CVs, %) for 1293 analyzed traces (of 610 identified lipid species) in each group of samples 90

Suppl. Figure 7.7. Chemical structure of betulin and related compounds betulinic acid, erythrodiol and lupeol 91

Suppl. Figure 7.8. Absolute intensities of some triterpenes signals observed in lipid extract of keratinocytes 92

Suppl. Figure 8.1. Generic gradient elution screening runs for a mixture of D- and L-2-HG, and pure enantiomer L-2-HG using different cinchona alkaloid-derived chiral ion-exchanger CSPs. 108

Suppl. Figure 8.2. a) Gradient profile and corresponding b) mixed polar modifier-acid additive gradient screening runs for a mixture of D- and L-2-HG, using ZWIX(+) and QD-AX columns. 108

Suppl. Figure 8.3. Chromatographic runs for a mixture of D- and L-2-HG at different ratios of ACN:MeOH. 109

Suppl. Figure 8.4. Effect of different types of alcohols on the chromatographic parameters. 109

Suppl. Figure 8.5. Chromatographic runs for a mixture of D- and L-2-HG at different ratios of ACN:H_2O. 110

Suppl. Figure 8.6. Effect of different types of co-ions (ammonia, NH_3; DEA, diethylamine; TEA, triethylamine) in the mobile phase on the chromatographic parameters. 110

Suppl. Figure 8.7. a) Chromatographic runs for a mixture of D- and L-2-HG at different FA concentrations using QD-AX column, b) corresponding resolution and selectivity plots and c) peak area and USP tailing plots. 110

Suppl. Figure 8.8. a) Chromatographic runs for a mixture of D- and L-2-HG, at different temperatures, b) corresponding plots of chromatographic parameters. 111

Suppl. Figure 8.9. a) Chromatographic runs for a mixture of D- and L-2-HG, at different flow rates, and b), c) corresponding plots of chromatographic parameters. 111

Suppl. Figure 9.1. Chromatographic runs for a mixture of HCA enantiomers on a) QD-AX column and b) QN-AX column. 128

Suppl. Figure 9.2. Chromatographic runs for a mixture of D- and L-ICA enantiomers and D- and L-TA enantiomers on a QN-AX column. 128

Suppl. Figure 9.3. Chromatographic runs for a mixture of HCA enantiomers on a) QD-AX column and b) QN-AX column. 129

Suppl. Figure 9.4. Chromatographic runs for a mixture of D- and L-2-HGA on QD-AX column. 129

Suppl. Figure 9.5. Chromatographic runs for a mixture of less retained HCA enantiomers on a) QD-AX column and b) QN-AX column. 130

Suppl. Figure 9.6. Chromatographic runs for a mixture (*R*)- and (*S*)-3-HBA enantiomers on a) QN-AX column and b) QD-AX column. 130

Suppl. Figure 9.7. Chromatographic runs for a mixture of (*R*)- and (*S*)-3-HBA at different temperatures from 20 (top) to -20 °C (bottom). 131

Suppl. Figure 9.8. Chromatographic runs for HCA enantiomers on a) ZWIX(+) column and b) ZWIX(-) column. 131

Suppl. Figure 9.9. Chromatographic runs for a mixture of HCA enantiomers on a) ZWIX(-) column. 132

Suppl. Figure 9.10. Chromatographic runs for a mixture of HCA enantiomers on a) ZWIX(-) column. 132

Suppl. Figure 9.11. Chromatographic runs for a mixture of (*R*)- and (*S*)-2-HBA enantiomers or single enantiomer on a) QN-AX column, b) ZWIX(+) column, c) QD-AX column and d) ZWIX(-) column. 133

Suppl. Figure 9.12. Chromatographic runs for a mixture of D- and L-TA enantiomers or the D-TA enantiomer on a) QN-AX column, b) ZWIX(+) column, c) QD-AX column and d) ZWIX(-) column. 133

Suppl. Figure 10.1. Chromatographic runs for a mixture of (*R*)-and (*S*)-2-H-2-MBA enantiomers on A) QN-AX column at 10 °C, B) QD-AX column at 10 °C, C) QN-AX column at -20 °C and D) QD-AX column at -20 °C..... 148

Suppl. Figure 10.2. Chromatographic runs for (2*RS*, 3*RS*)-2-H-3-MPA A) QN-AX column and B) QD-AX column. C) Chromatographic runs on QD-AX column of the peaks separately collected from elution on QN-AX column. 149

Suppl. Figure 10.3. Chromatographic runs for a mixture of (*R*)-and (*S*)-2-HCA enantiomers on A) QN-AX column and B) QD-AX column. C) Chromatographic runs on QD-AX column of the peaks separately collected from elution on QN-AX column. 150

Suppl. Figure 10.4. Chromatographic runs for a mixture of (*R*)-and (*S*)-2-HDA enantiomers on A) QN-AX column and B) QD-AX column. C) Chromatographic runs on QD-AX column of the peaks separately collected from elution on QN-AX column. 151

Suppl. Figure 10.5. Chromatographic runs for a racemic mixture of 2-HAA on ZWIX (-) column. 152

Suppl. Figure 10.6. Chromatographic runs for racemic mixtures of 2-HDCAs on QD-AX column A) (*RS*)-2-HAA, B) (*RS*)-2-HGA and C) (*RS*)-MA. 153

Suppl. Figure 10.7. Chromatographic runs for a mixture of (*R*)-and (*S*)-2-HAA enantiomers on A) QN-AX column and B) QD-AX column. C) Chromatographic runs on QD-AX column of the peaks collected from elution on QN-AX column. 154

Suppl. Figure 10.8. Chromatographic runs showing the effect of FA concentrations on retention of (RS)-2-HCA and (RS)-2-HAA. 155

LIST OF TABLES

Table 1.1. Summary of the Major Functions of Individual Lipid Classes 1

Table 1.2. Names and designations of most common fatty acids..... 4

Table 3.1. Comparison of the features of some common mass analyzers: 14

Table 3.2 Comparison of commonly used detectors: 16

Table 3.3 Comparison among scan modes in mass spectrometry:..... 18

Table 3.4. Example of some PIS and NLS experiments applied in ESI–MS/MS analysis of lipids.21

Table 3.5. Molecular species formed during electrospray ionization of lipids. 23

Table 6.1. Description of processed features with MS-Dial and Multiquant softwares 50

Table 9.1. Resolution values and retention times (for second peak) obtained during enantioseparation of hydroxycarboxylic acids under different conditions 121

Table 9.2. Elution orders for hydroxycarboxylic acids on studied chiral stationary phases 126

LIST OF SUPPLEMENTARY TABLES

Suppl. Table 6.1. Information about internal standards of the SPLASH™ Lipidomix® Mass Spec Standard (in MeOH) 58

Suppl. Table 6.2. m/z values of sodium acetate clusters used for external calibration of QTOF 58

Suppl. Table 6.3. Information about design of MS experiments..... 59

Suppl. Table 6.4. Parameters used for processing of data with MS-Dial in negative and positive mode..... 60

Suppl. Table 6.5. Relative recoveries of endogenous lipids extracted with $CHCl_3$, IPA75 and MTBE EPs respect to IPA90 EP. 61

Suppl. Table 6.6. Recoveries of isotopically labeled internal standards after pre-extraction and post-extraction spiking..... 62

Suppl. Table 6.7. Distribution of CVs (%) obtained for precision evaluation of peak intensities of features detected in all four EPs. 62

Suppl. Table 7.1. Information about internal standards of the SPLASH™ Lipidomix® Mass Spec Standard (in MeOH) 81

LIST OF SUPPLEMENTARY TABLES

Suppl. Table 7.2. m/z values of sodium acetate clusters used for external calibration of QTOF 81

Suppl. Table 7.3. Information about design of MS and MS/MS experiments 82

Suppl. Table 7.4. Selected precursor and fragments ions for identification of each lipid class in ESI (+) and ESI (-) 83

Suppl. Table 7.5. Parameter for integration of peaks in Multiquant 3.0 84

Suppl. Table 7.6. Quantitation method for each analyzed lipid class 84

Suppl. Table 7.7. Distribution of coefficient of variations (CVs, %) for 1293 analyzed traces (of 610 identified lipid species) in each group of samples (See Suppl. Figure 3.6) 85

Suppl. Table 7.8. List of detected peaks in extract of keratinocytes with a significant FC for comparison between betulin and control group, which were analyzed as betulin related metabolites 85

Suppl. Table 7.9. Retention times for standards of betulin and some other related compounds 86

Suppl. Table 8.1. Chromatographic parameters obtained for the separations of D- and L-2-HG in the counterion gradient elution screening runs on the four different CSPs. 112

Suppl. Table 8.2. Chromatographic parameters obtained during the mixed polar modifier-counterion gradient elution separation of D- and L-2-HG with QD-AX and ZWIX(+) column. . 112

Suppl. Table 8.3. Chromatographic parameters obtained for the separations of D- and L-2-HG at different ACN:MeOH ratios. 112

Suppl. Table 8.4. Chromatographic parameters obtained for the separation of D- and L-2-HG by employing different types of alcohol 113

Suppl. Table 8.5. Chromatographic parameters obtained for the separation of D- and L-2-HG by employing different types of amines as co-ions 113

Suppl. Table 8.6. Chromatographic parameters obtained for the separation of D- and L-2-HG at different concentrations of formic acid. 113

Suppl. Table 8.7. Chromatographic parameters obtained during the separation of D- and L-2-HG at different temperatures. 114

Suppl. Table 8.8. Chromatographic parameters obtained during the separation of D- and L-2-HG at different flow rates 114

Suppl. Table 9.1. Chromatographic parameters obtained under different conditions for the separation of HCAs with QD-AX and QN-AX columns. 134

Suppl. Table 9.2. Chromatographic parameters obtained under different conditions for the separation of HCAs with ZWIX(+) and ZWIX(-) columns..... 135

Suppl. Table 9.3. Systematic study and resolution obtained during optimization of conditions for separation of (*R*)- and (*S*)-3-HBA. 136

Suppl. Table 10.1. Chromatographic parameters obtained under different conditions for the separation of HCAs with QD-AX, QN-AX and ZWIX (-) columns. 156

CURRICULUM VITAE

Personal data:

Name: Carlos Eduardo Calderón Castro

Date of Birth: September, 24 th, 1985

Gender: Male

Place of birth: Cartago, Costa Rica

e-mail: carlos.calderon@uni-tuebingen.de, ccalcas@gmail.com

Formal education

Ph. D. Student in Pharmacy at Eberhard-Karls-University of Tuebingen, Tuebingen (2015-2019)

Magister Scientae in Chemistry (2009-2014) at University of Costa Rica, Costa Rica

Bachelor degree in chemistry (2003-2008) at University of Costa Rica, Costa Rica

Symposiums and courses:

- ***June 2019*** *48th International Symposium on High-Performance Liquid Phase Separations and Related Techniques (HPLC 2019), Milan, Italy*
- ***March 2019*** *International PhD Students/Postdoc Meeting of the German Pharmaceutical Society (DPhG), Darmstadt, Germany*
- ***October 2018*** *Lipidomics Forum 2018, Dortmund, Germany*
- ***September 2018*** *32nd International Symposium on Chromatography, Cannes, France*
- ***February 2018*** *Irseer Naturstofftage, Irsee, Germany*
- ***September 2017*** *23rd International Symposium on Separation Sciences (ISSS 2017), Viena, Austria.*
- ***September 2016*** *31st International Symposium on Chromatography (ISC 2016), Cork, Ireland*
- ***August 2016*** *Curso: Sommerschule: Chromatographie und Kopplung mit Massenspektrometrie, Leibnitz, Austria*
- ***April 2015*** *4th International Conference and Exhibition on Metabolomics & Systems Biology, Philadelphia, USA*
- **May- June 2013** Internship during 5 weeks in Department of Pharmaceutical Biology and Biotechnology, Albert Ludwigs University Freiburg, Germany. Internship dedicated to cytotoxicity tests for isolated compounds against cancer cell lines.
- ***August 2012*** *International Congress on Natural Products Research, New York, USA*
- ***February 2010*** *VIRUS-HOST: partners in pathogenicity, Costa Rica*
- ***February 2009*** *8^{avo} Simposio Latinoamericano de Química Analítica Ambiental y Sanitaria. Costa Rica*

Publications

1. *C. Calderón, L. Rubarth, M. Cebo, I. Merfort, M. Lämmerhofer, Lipid atlas of keratinocytes and betulin effects on its lipidome profiled by comprehensive UHPLC-MS/MS with data independent acquisition using targeted data processing, Proteomics. (2019).*
2. *C. Calderón, C. Sanwald, J. Schlotterbeck, B. Drotleff, M. Lämmerhofer, Comparison of simple monophasic versus classical biphasic extraction protocols for comprehensive UHPLC-MS/MS lipidomic analysis of Hela cells, Anal. Chim. Acta. 1048 (2019). doi:10.1016/j.aca.2018.10.035.*
3. *C. Calderón, C. Santi, M. Lämmerhofer, Chiral separation of disease biomarkers with 2-hydroxycarboxylic acid structure, J. Sep. Sci. 41 (2018) 1224–1231. doi:10.1002/jssc.201701243*
4. *C. Calderón, M. Lämmerhofer, Chiral separation of short chain aliphatic hydroxycarboxylic acids on cinchonan carbamate-based weak chiral anion exchangers and zwitterionic chiral ion exchangers, J. Chromatogr. A. 1487 (2017) 194–200. doi:10.1016/j.chroma.2017.01.060.*
5. *C. Calderón, J. Horak, M. Lämmerhofer, Chiral separation of 2-hydroxyglutaric acid on cinchonan carbamate based weak chiral anion exchangers by high-performance liquid chromatography, J. Chromatogr. A. 1467 (2016) 239–245. doi:10.1016/j.chroma.2016.05.042.*
6. *C. De Ford, C. Calderón, P. Sehgal, N.U. Fedosova, R. Murillo, C. Olesen, et al., Discovery of Tricyclic Clerodane Diterpenes as Sarco/Endoplasmic Reticulum Ca 2+ -ATPase Inhibitors and Structure–Activity Relationships, J. Nat. Prod. 78 (2015) 1262–1270. doi:10.1021/acs.jnatprod.5b00062.*
7. *C. Calderón, C. De Ford, V. Castro, I. Merfort, R. Murillo, Cytotoxic Clerodane Diterpenes from Zuelania guidonia., J. Nat. Prod. 77 (2014) 455–463. doi:10.1021/np400672g.*

Languages:

Spanish (native speaker)

English (C2)

German (B2)